MODELING CO-DYNAMICS OF COVID-19, HIV AND TB: OPTIMAL CONTROL, COST-EFFECTIVENESS, AND THE ROLE OF VACCINATION BEHAVIOR

Tesfaneh Debele Batu

A Dissertation Submitted to
The Department of Applied Mathematics
College of Applied Natural Science

Presented in Fulfillment of the Requirement for the Degree of
Doctor of Philosophy in Applied Mathematics

School of Post Graduate Studies
Adama Science and Technology University

November, 2024
Adama, Ethiopia

MODELING CO-DYNAMICS OF COVID-19, HIV AND TB: OPTIMAL CONTROL, COST-EFFECTIVENESS, AND THE ROLE OF VACCINATION BEHAVIOR

Tesfaneh Debele Batu
Supervisor: Dr. Legesse Lemecha Obsu
Co-Supervisor: Prof. Chernet Tuge Deressa

A Dissertation Submitted to
The Department of Applied Mathematics
College of Applied Natural Science

Presented in Fulfillment of the Requirement for the Degree of
Doctor of Philosophy in Applied Mathematics

School of Post Graduate Studies
Adama Science and Technology University

November, 2024
Adama, Ethiopia

APPROVAL PAGE

We hereby certify that the recommendations and suggestions made by the board of examiners are appropriately incorporated into the final version of the dissertation entitled "**Modeling Co-Dynamics of COVID-19, HIV and TB: Optimal Control, Cost-Effectiveness, and the Role of Vaccination Behavior**" by **Tesfaneh Debele Batu**.

Supervisor	Signature	Date
Co-Supervisor	Signature	Date

We, the undersigned, members of the Board of Examiners of the dissertation open defense by **Tesfaneh Debele Batu** have read and evaluated the dissertation entitled "**Modeling Co-Dynamics of COVID-19, HIV and TB: Optimal Control, Cost-Effectiveness, and the Role of Vaccination Behavior**" and examined the candidate during open defense. This is, therefore, to certify that the dissertation is accepted for partial fulfillment of the requirement of the degree of Doctor of Philosophy in Applied Mathematics.

Chairperson	Signature	Date
External examiner 1	Signature	Date
External examiner 2	Signature	Date
Internal examiner 1	Signature	Date
Internal examiner 2	Signature	Date

Finally, approval and acceptance of the dissertation is contingent upon submission of its final copy to the School of Postgraduate Studies (SPGS) through the candidate's Department Graduate Council (DGC) and College Graduate Committee (CGC).

Department Head	Signature	Date
College Dean	Signature	Date
Shool of Postgraduate Studies, Dean	Signature	Date

DECLARATION

I hereby declare that this dissertation entitled "**Modeling Co-Dynamics of COVID-19, HIV and TB: Optimal Control, Cost-Effectiveness, and the Role of Vaccination Behavior**" is my original work. That is, it has not been submitted for the award of any academic degree, diploma or certificate in any other university. All sources of materials used for this dissertation have been duly acknowledged through appropriate citations.

Name	Signature	Date

RECOMMENDATION OF SUPERVISORS

We, the supervisors of this dissertation, hereby certify that we have read and revised the dissertation entitled "**Modeling Co-Dynamics of COVID-19, HIV and TB: Optimal Control, Cost-Effectiveness, and the Role of Vaccination Behavior**" prepared under our guidance by **Tesfaneh Debele Batu** submitted in partial fulfillment of the requirements for the degree of Doctor of Philosophy in Applied Mathematics. Therefore, we recommend the submission of the dissertation to the department for further review and defense.

Supervisor	Signature	Date
Co-Supervisor	Signature	Date

ACKNOWLEDGMENTS

I am deeply grateful to the Lord Almighty, for without Him in my life, I would not be where I am today. I would like to extend my heartfelt thanks to my loving and supportive wife, Miss Kalkidan Feleke, and to my precious children, Enku and Inanu, for standing by me through the ups and downs of my journey. Words cannot fully express the value of your patience and unwavering love; you are truly a gift from God.

I also want to express my sincere appreciation to my capable and supportive supervisor, Dr. Legesse Lemecha, for agreeing to supervise me and for diligently guiding me throughout the process. Thank you for your patience in reviewing my dissertation and for providing constructive criticism that has significantly helped me grow. May God bless you and your family as you continue to support other students.

I am grateful to my co-supervisor, Prof. Chernet Tuge, for his support, guidance, and encouragement during the research process.

My thanks also go to ASTU and the Department of Applied Mathematics as a whole for providing me with valuable research experience.

I cannot overlook the love and encouragement from my parents. Your unconditional support and prayers during my studies have been instrumental, and I pray that the Lord rewards your kindness in Jesus' name (Amen).

Lastly, I would like to acknowledge my friends and postgraduate classmates for sharing their valuable time with me. Our interactions, from academic discussions to moments of socializing, have been truly enriching. God bless all of you.

TABLE OF CONTENTS

LIST OF TABLES

LIST OF FIGURES

ACRONYMS AND ABBREVIATIONS

AIDS	Acquired Immune Deficiency Syndrome
ART	Antiretroviral Therapy
COVID-19	Coronavirus Disease 2019
EPHI	Ethiopian Public Health Institute
HIV	Human Immunodeficiency Virus
MERS	Middle East Respiratory Syndrome
MERS-CoV	Middle East Respiratory Syndrome Coronavirus
ODE	Ordinary Differential Equation
OECD	Organisation for Economic Co-operation and Development
PLHIV	People Living with HIV
SARS	Severe Acute Respiratory Syndrome
SARS-CoV	Severe Acute Respiratory Syndrome Coronavirus
SARS-CoV-2	Severe Acute Respiratory Syndrome Coronavirus 2
TB	Tuberculosis
WHO	World Health Organization

ABSTRACT

Despite the availability of numerous treatments and preventive measures for Coronavirus Disease 2019 (COVID-19), Human Immunodeficiency Virus (HIV) and tuberculosis (TB), these diseases continue to pose significant public health concerns with far-reaching socioeconomic implications. This dissertation aims to identify effective and efficient control strategies to mitigate coinfections of COVID-19 and HIV, as well as the concurrent infections of COVID-19, HIV, and TB, using mathematical models. It provides models that govern the transmission dynamics of COVID-19, HIV/AIDS and TB. For the formulated models, we establish the invariant region, positivity, and boundedness of the solutions; determine the reproduction numbers of the sub-models and the co-infection model; and examine the existence and stability of the equilibria. Parametric estimation and curve fitting were performed using data from Ethiopia, and numerical simulations were employed to support and clarify the analytical findings, demonstrating the effects of various parameters on COVID-19, HIV and TB co-infection and illustrating how preventive efforts impact the co-infected population. The first model examines the transmission of COVID-19 and HIV, taking into account individuals with advanced HIV/AIDS and those at risk of death from both diseases. Numerical simulations highlight that factors such as increased infectiousness among HIV patients and low vaccination rates lead to higher co- infection rates, while increased COVID-19 vaccination and treatment reduce mortality. The second model evaluates four intervention strategies—HIV prevention, HIV treatment, COVID-19 vaccination, and COVID-19 treatment— with simulations showing reductions in co-infections. A cost-effectiveness analysis identifies the combined approach of vaccination and treatment as the most viable strategy. The third model addresses the broader co-infection scenario involving TB. The model emphasizes the importance of vaccination, though challenges like vaccine inefficacy, waning immunity, and low information coverage persist. Numerical simulations show that waning immunity and high reinfection rates can exacerbate co-infection peaks, but information-driven vaccination strategies significantly mitigate these effects. Collectively, these three models underscore the need for coordinated efforts in vaccination, treatment, and public health communication to address the challenges posed by COVID-19, HIV and TB co-infection. The models provide essential guidance for developing targeted interventions and public health strategies aimed at reducing co-infection cases and associated mortality while accounting for complex behavioral and epidemiological factors such as waning immunity and the role of information dissemination.

KEYWORDS: HIV, COVID-19, TB, Stability analysis, Reproduction number, Optimal control, Bifurcation, Co-infection, Cost-effectiveness Analysis, Mathematical model, Simulation

CHAPTER 1

INTRODUCTION

This chapter offers crucial background information on coronavirus disease (COVID-19), Tuberculosis (TB), acquired immune deficiency syndrome (AIDS), and the co-infection of these diseases. It emphasizes the vital role of mathematical modeling in understanding and addressing these health challenges. The chapter then clearly defines the research problem, outlines the specific objectives of the study, and underscores its significance. Finally, it provides a brief overview of the dissertation's structure, guiding through the subsequent chapters.

1.1 Background of the Study

Humanity has been compelled to confront mortality and morbidity because of non communicable and communicable diseases. A noncommunicable disease is a term used to describe a group of chronic medical disorders and diseases that cannot be transmitted from one person to another. Genetics, malnutrition, lifestyle, and the environment are all factors that contribute to the development of these disorders. They generally progress slowly and gradually, and symptoms tend to accumulate steadily over time. Although they are non-communicable, at a global level, 7 of the 10 leading causes of death in 2019 were noncommunicable diseases (WHO, 2021d). As of 13th April 2021, these seven causes accounted for 44% of all deaths or 80% of the top 10. However, all noncommunicable diseases together accounted for 74% of deaths globally in 2019.

Communicable diseases are caused by various microbes or pathogens, with the most common being different types of viruses and bacteria. Fungi and protozoa are also known pathogens responsible for various diseases. Diseases caused by these pathogens are termed 'communicable' as these pathogens can be easily transmitted from one infected person to another non-infected person. Two of the most prevalent infectious diseases globally are tuberculosis (TB) and AIDS. Tuberculosis, caused by Mycobacterium tuberculosis, primarily affects the lungs but can also affect other parts of the body. AIDS, caused by the human immunodeficiency virus (HIV), weakens the immune system and leads to a range of opportunistic infections and diseases. In December 2019, a newly discovered infectious disease called COVID-19 emerged in Wuhan, China. It is caused by the Severe Acute Respiratory Syndrome Coronavirus-2 (SARS-CoV-2) virus. Low income people are far more likely to die of communicable diseases than non-communicable disease. Despite the global decline, 8 of the top 10 causes of death in

2021 in low-income countries were communicable diseases, with COVID-19, tuberculosis, and HIV/AIDS ranking among the top 10 (WHO, 2021d).

1.1.1 Coronavirus Disease (COVID-19)

Coronaviruses have been known since the 1930s and received a wide notice when they were confirmed to be the cause of the SARS pandemic in China (Al-Ahdal, Mohammed et al., 2012). Originating from Southern China in the autumn of 2002, the virus spread to 29 countries or regions with a total of 8096 cases and 774 deaths before it was brought under control within 7 months with an incredible global public health effort (Executive Board, 113, 2004; WHO, 2003). Ten years later, another pathogenic coronavirus known as Middle East respiratory syndrome coronavirus (MERS-CoV) emerged in Saudi Arabia. Infection occurs through direct contact with an infected animal (camel) or person (Chathappady House et al., 2021). Although MERS did not spread easily from person to person, the virus spread to 27 countries in the Middle East, Europe, Asia, and North America, including the United States. As of May 31, 2019, MERS-CoV had infected 2,442 individuals and killed 842 worldwide (Donnelly, Christl A et al., 2019).

SARS-CoV-2 belongs to the family Coronaviridae and order Nidovirales. The family consists of two subfamilies, Coronavirinae and Torovirinae, and members of the subfamily Coronavirinae are subdivided into four genera: alpha, beta, gamma, and delta coronavirus (Shereen, Muhammad et al., 2020). SARS-CoV-2, MERS-CoV, and SARS-CoV belong to the beta coronavirus subfamily and are major pathogens that primarily target the human respiratory system. SARS-CoV-2 is more transmissible and spreads faster than SARS and MERS. (Du, Wenjun et al., 2020).

The COVID-19 pandemic is the latest phenomenon to have profoundly impacted the world's social, Economic and political activities. Although we are now in the endemic phase, the effects of the disease are ongoing. As of 12 May 2024, there have been approximately 7 million deaths out of 775,431,269 million infected people, and there are still millions of active COVID-19 cases (WHO, 2024b). Fever, cough, tiredness, and loss of taste or smell are the most common symptoms . Other common symptoms include sore throat, headache, diarrhea, a rash on the skin, discoloration of fingers and toes, and red or irritated eyes. Most patients with these symptoms recover without requiring special treatment. However, individuals experiencing symptoms such as difficulty breathing, shortness of breath, loss of speech or mobility, confusion, or chest pain may be at risk of potentially life-threatening complications and require immediate medical attention (Rajendran, Dinesh et al., 2020).

In their work, Karia, Rutu et al. (2020) and Mediawati, Ati Surya et al. (2020) argue the existence of two modes of coronavirus transmission, direct and indirect. The disease is transmit-

ted directly through contact with respiratory droplets in the infected person (generated through coughing and sneezing). These droplets can settle in the mouth or nasal mucosa and lungs of people with inhaled air. Indirect transmission occurs when individuals touch surfaces contaminated with the virus and touch their faces (e.g., eyes, nose, mouth) (Jin, Yuefei et al., 2020).

To prevent COVID-19, governments have started to apply bans under many social restrictions. Lock-downs were at the forefront of these restrictions. By spring 2020, more than half of global population experienced strict containment, the first such large-scale effort in history (OECD, 2020). Although lock-downs helped suppress the virus, as early evidence suggested, they severely impacted social and economic life, disproportionately affecting vulnerable groups like those in poverty, migrants, and refugees (Atalan, 2020; WHO, 2020). In addition to lock-downs, preventive measures such as mask-wearing, hand hygiene, quarantine, social distancing, and travel restrictions were enforced to reduce transmission (Bahrami, A. and Ferns, G., 2020). Quarantine, while effective, raised concerns about risks of household transmission (Hou, Lulu et al., 2021). The pandemic also accelerated unprecedented vaccine development and distribution efforts globally.

As of April 8, 2022, the WHO has provided a list of 10 COVID-19 vaccines that met the necessary criteria for safety and efficacy (WHO, 2024a). Despite single-dose vaccines, majority of these vaccines require at least 2 doses, and taking COVID-19 full-dose vaccination provides strong protection against serious illness, hospitalization, and death due to the COVID-19 disease. As of April 29, 2023, a total of 5,105,854,153 individuals were fully vaccinated with the last dose of the primary series globally (WHO, 2024b). However, apart from administration, the WHO states that even fully vaccinated individuals can still be infected with COVID-19 (WHO, 2024d). Several studies have shown that immunity from vaccination or natural infection decreases over time, increasing susceptibility to reinfection. There have been documented cases of reinfection (Flacco, Maria Elena et al., 2022; Klompas, 2021; Ren, Xiangying et al., 2022; Wang, Jingzhou et al., 2021; Weike Zhou et al., 2022), indicating that COVID-19 vaccines do not provide permanent immunity, and individuals can contract COVID-19 multiple times. In this case, COVID-19 vaccination behavior is crucial for public health strategies aimed at increasing vaccine uptake and achieving herd immunity. The dynamics of vaccine acceptance can be influenced by various factors, including individual beliefs and the broader context of misinformation (Joachim O. Osur et al., 2022).

Understanding how the number of COVID-19 cases influences vaccination behavior is crucial for public health strategies. High infection rates can increase individuals' perceived risk, prompting greater vaccine uptake, whereas lower case numbers may lead to complacency and hesitancy (Joachim O. Osur et al., 2022; Priya, Singh et al., 2024). In addition, misinforma-

tion surrounding infection data can intensify vaccine skepticism (Joachim O. Osur et al., 2022). Therefore, public health campaigns should leverage real-time infection data to craft targeted messages that emphasize vaccination's importance during surges, continuously monitor infection trends to develop adaptive strategies, and combat misinformation to enhance vaccine acceptance. Overall, recognizing these dynamics is essential for effectively promoting vaccination and managing community health.

1.1.2 Acquired Immune Deficiency Syndrome (AIDS)

AIDS is an infectious disease caused by infection with the human immunodeficiency virus (HIV), which was originally identified in 1981. HIV weakens the immune system by attacking cells($CD4^+$ T-cells) which play an important role in protecting the host from pathogens (Maartens, Gary et al., 2014). Once HIV destroys these cells, it becomes even more difficult for the body to fight off other infections. In other words, affected individuals become increasingly vulnerable to many normally harmless microorganisms, eventually leading to severe morbidity and mortality. Not only does HIV attack $CD4^+$ T-cells, but it also uses these cells to multiply the virus (Pan, Xiaoyu et al., 2013). With the advancement of HIV, the infection is usually called AIDS.

HIV is transmitted primarily via unprotected sexual intercourse, contaminated blood transfusions, hypodermic needles, and from mother to child during pregnancy, delivery, or breastfeeding (Morison, 2001). Heterosexual transmission remains the dominant mode of transmission and accounts for about 85% of all HIV infections (Simon, Viviana et al., 2006). HIV transmission depends on the infectiousness of the infected partner; higher viral loads during later stages of the disease associated with an increased probability of transmission (Centers for Disease Control and Prevention and others, 2018).

Over the past four decades, HIV/AIDS has emerged as one of the greatest single causes of death and suffering worldwide. A systematic analysis of the global burden of diseases study conducted in Vos, Theo et al. (2020) showed that HIV/AIDS was the eleventh leading cause of the global burden of diseases in 2019. HIV/AIDS is the ninth and second leading cause for the global burden of diseases in the age groups 10–24 and 25–49, respectively. This result shows HIV/AIDS remains a challenge to be confronted for people around the world. WHO global HIV program recognizes HIV as a major global public health issue, having claimed almost 36.3 million(27.2–47.8 million) lives so far (WHO, 2021c). According to this program estimates, in 2020, 37.7 million (30.2–45.1 million) people were living with HIV, 1.5 million(1–2 million) had become newly infected over the previous year, and 800000(480000–1 million) people died from HIV-related causes globally. Moreover, based on the number of PLHIV, the WHO global

HIV program estimate placed Africa region at the forefront with contributing more than two-thirds, 25.4 million(20.7 - 30.3 million) people, which also accounted for almost 60% (880000) of the global new HIV infections and 460000(320000 - 680000) deaths from HIV-related causes.

Even if HIV/AIDS is not permanently curable, the main methods used to fight are preventive mechanisms (which include: abstinence, faithfulness and protection) which mainly rely on the level of behavioral change in the population, and providing Antiretroviral Therapy (ART) for those infected (Maartens, Gary et al., 2014). ART treatment improves health, prolongs life, and substantially reduces the risk of HIV transmission (Centers for Disease Control and Prevention and others, 2018). Although ART treatment significantly improves health outcomes for PLHIV, the co-infection of tuberculosis (TB) can pose a significant threat to their survival. TB, a leading cause of death among PLHIV (Sharma, 2024), can accelerate disease progression and increase the risk of mortality, even in those receiving effective ART. The COVID-19 pandemic has further complicated this issue because it can intensify the symptoms of TB and HIV (Daniel Eike et al., 2022; Gupta Parakriti et al., 2024), making it more difficult to manage these infections.

1.1.3 Tuberculosis (TB)

Tuberculosis (TB) is caused by Mycobacterium tuberculosis, which spreads through airborne droplets when an infected person coughs, sneezes, or speaks. TB primarily affects the lungs but can also target other body parts, such as the kidneys, spine, and brain. Factors that increase susceptibility to TB include weakened immune systems, with HIV co-infection being the most prominent. People living with HIV are at a significantly higher risk of developing active TB due to their compromised immune defenses. Other risk factors include malnutrition, which weakens the body's immune response, and chronic conditions like diabetes, which increase vulnerability to TB infections WHO (2024c).

TB remains one of the deadliest infectious diseases worldwide. According to the World Health Organization (WHO), approximately 10.6 million people fell ill with tuberculosis (TB) worldwide and 1.3 million people died from TB in 2022, including 167,000 PLHIV WHO (2024c). Early detection and treatment, infection control, and vaccination are key to TB prevention. Screening high-risk individuals, providing quality healthcare, and promoting hygiene in healthcare settings and communities are also crucial.

1.1.4 Co-infections Involving COVID-19, HIV and TB

In addition to its various effects, the emergence of COVID-19 presents additional challenges for patients with underlying medical disorders. This occurs because individuals with underlying medical issues are more susceptible to COVID-19. There is evidence in several publications that

people with underlying medical conditions may be infected with COVID-19 (Ejaz, Hasan et al., 2020; Elezkurtaj, Sefer et al., 2021; Gatechompol, Sivaporn et al., 2021; González-Domenech et al., 2021a; Kanwugu, Osman N. and Adadi, Parise, 2021; Mirzaei, Hossein et al., 2021; Ssentongo, Paddy et al., 2021; Tolossa, Tadesse et al., 2021). In particular, individuals with comorbidities such as hypertension, diabetes, obesity, chronic obstructive pulmonary disease (COPD), asthma, cardiovascular diseases (CVD), liver diseases, malignancy, HIV, tuberculosis (TB), and renal diseases are at higher risk of developing SARS-CoV-2 infection (Ejaz, Hasan et al., 2020).

COVID-19 among people living with HIV

A new WHO report confirmed that HIV infection is was a significant independent risk factor for both severe/critical COVID-19 presentation at hospital admission and in-hospital mortality (WHO, 2021a). Recently, 5th August 2021, the WHO press release warned that HIV infection increases the risk of severe and critical COVID-19 (WHO, 2021b). They advertise as they are becoming more aware, and following the data it has been confirmed that PLHIV has an increased risk for severe COVID as well as hospitalizations. That is, once hospitalized, patients have a 30% increased risk of death. As of April 29, 2021, 24 countries had contributed clinical data on people PLHIV to the WHO Global COVID-19 Clinical Data Platform (WHO, 2021a). This global sample showed that 9.2% (15522 / 168649) of cases hospitalized with expected or proven COVID-19 were HIV positive, and 96.1% (14914/15522) of the PLHIV included in the analysis were from the WHO African region, with 94.6% (14682/15522) of cases reported from South Africa alone. From the global sample, the prevalence of HIV was identified to be a significant independent risk factor for severe or critical COVID-19 at hospitalization and in-hospital death.

Suwanwongse, Kulachanya and Shabarek, Nehad (2020) found that HIV/AIDS and COVID-19 co-infected individuals with a significantly lower $CD4^+$ T cell count had a much greater mortality rate (7 out of 9 patients) than COVID-19 patients without HIV. T lymphocytes were responsible primarily for the functions of antibody production (LeBien, T. W. and Tedder, T. F., 2008). Recent evidence reported in González-Domenech et al. (2021a); Yang, Rongrong et al. (2021) and Squillace, Nicola et al. (2021) shows that the lymphocyte counts of patients with COVID-19 and HIV co-infection were lower than those of the COVID-19 patients without HIV infection. This information raises speculation that the low level of $CD4^+$ T lymphocyte counts in the HIV co-infection group might be one of the reasons for the relatively weak ability to produce antibodies (Yang, Rongrong et al., 2021), which have consistently emerged as a risk factor for severe COVID-19 and HIV/AIDS co-infection.

Limited information is available regarding the treatment and outcome of SARS-CoV-2 infection among PLHIV (Gatechompol, Sivaporn et al., 2021). The WHO recommends that PLHIV should be a recognized priority category in the national COVID-19 vaccination policy, regardless of their CD4 count, because they appear to be at a higher risk of severe outcomes and death from COVID-19 compared to other people (WHO, 2021b). However, making these vaccines available to people around the world remains a challenge for the globe. Limited access to vaccines in low- and middle-income nations, particularly in Africa, where HIV is most prevalent, can be regarded as an indicator of challenges in vaccine distribution.

COVID-19 among peoples co-infected with HIV and TB

COVID-19 co-infection with HIV and TB is widespread, and patients with these infections have a greater risk of fatality than those without co-infection cases (Mishra, Ajay et al., 2020; Song, Wan-mei et al., 2021). The TB/COVID-19 Global Study Group's research details the impact of COVID-19 and TB co-infection (Group, 2022). Based on data from 34 countries, the study concluded that TB and COVID-19 are a "cursed duet" and require immediate attention. Furthermore, this suggests TB should be considered a risk factor for severe COVID-19 disease. In relation to individuals living with HIV/AIDS, viremia was significantly associated with the severity of COVID-19, and a CD4 T cell count of < 200 $cells/mm^3$ was a significant risk factor for severe COVID-19 (WHO, 2021a).

People infected with three different diseases, including the recently identified COVID-19, are expected to occur as co-infection cases are apparent. A number of studies have demonstrated that triple infections with COVID-19 are becoming more common (González-Domenech et al., 2021b; Guido, Giacomo et al., 2023; Kuate, Marius et al., 2022; Mishina et al., 2021; Rivas, Neyla et al., 2020; Tolossa, Tadesse et al., 2021; Zein, Abdulrahman R. et al., 2022). In particular, the authors in González-Domenech et al. (2021b); Guido, Giacomo et al. (2023); Kuate, Marius et al. (2022); Rivas, Neyla et al. (2020); Tolossa, Tadesse et al. (2021); Zein, Abdulrahman R. et al. (2022) present the triple infection cases of three diseases: HIV, TB, and COVID-19. This implies, when studying the intersection of HIV and COVID-19, it is crucial to also consider TB for several key reasons: high rates of HIV/TB co-infection, especially in Sub-Saharan African countries; increased susceptibility to COVID-19; increased risk of severe COVID-19 and mortality (Aniefiok John et al., 2023; Jacques Tamuzi et al., 2020).

By 2019, over one-third of individuals with HIV had also been diagnosed with TB, highlighting the significant overlap between these two diseases (Gelaw, Yalemzewod Assefa et al., 2019; World Health Organization, 2024d; Zeru, 2021). A patient diagnosed with three infec-

tions at the same time can create a complicated situation for clinical management and treatment. Individually, the risks of these infections are high; when they come together, the consequences can be even more dire (Jacques Tamuzi et al., 2020). This highlights the need to investigate the triple infection dynamics of COVID-19, TB, and HIV and devise diverse interventions.

1.1.5 The Role of Mathematical Modeling

COVID-19 disease propagation rules and predictions necessitate theoretical, quantitative, and simulation investigation. The investigation is intrinsically linked to a mathematical model developed for infectious diseases. Mathematical models have been a useful tool for providing various reasons for disease dynamics and designing practical control strategies. They often incorporate two types of control strategies: constant in time and variable in time. Control strategies that are constant in time are modeled using a constant parameter, and the goal is to determine the best parameter value for a given performance measure. Control strategies that vary in time, on the other hand, are modeled by including intervention strategies as a function of time to determine the optimum function for a given performance measure.

The mathematical theory used to derive optimal control strategies that vary in time is referred to as optimal control theory (Martcheva, 2015). Pontryagin and his collaborators have been well known in developing optimal control theory for ordinary differential equations (Pontryagin, 1987). The work of Pontryagin is characterized by introducing the adjoint function to attach the differential equation to the objective functional, which is an integral expression developed with terms of the state and control variables (Lenhart, S. and Workman, J. T., 2007). Now a days, optimal control theory has become an important tool because it allows the integration of more realistic control strategies in modeling the dynamics of infectious disease. Omame, Andrew et al. (2020); Tilahun (2019) and Omame, A. and Okuonghae, D. (2021), among others, incorporate both time-dependent and time-independent controls to describe the co-dynamics of diseases and suggest various techniques to mitigate the impact of co-infection on the host's health and the spread of diseases in society.

A cost-effectiveness analysis of the intervention strategy is another benefit of modeling studies that are usually conducted in studies that incorporate time-dependent control strategies. The results of a cost-effectiveness analysis can be particularly useful for identifying efficient strategies when resources are limited. In addition to other important findings, this dissertation presents concrete results for mitigating COVID-19 and HIV/AIDS co-infection through a mathematical modeling study that incorporates time-dependent control strategies and assesses their efficiency.

1.2 Statement of the Problem

The emergence of HIV in the late 20th century marked a pivotal moment in the realm of infectious diseases. The early years of the epidemic were characterized by a lack of understanding regarding transmission, prevention, and treatment, which exacerbated the crisis. By the late 1990s, antiretroviral therapy (ART) had transformed HIV from a terminal illness into a manageable chronic condition, significantly improving life expectancy and reducing new infections in some regions (Tseng, Alice et al., 2015). Despite advancements in HIV treatment, 15 million people still lack access to ART , posing risks to their immune systems and maintaining HIV's status as a global health concern. According to the World Health Organization, approximately 39.9 million people were living with HIV in 2019, and 630000 million people died of HIV (WHO, 2023). TB is a leading cause of mortality among PLHIV, contributing significantly to AIDS-related deaths. In addition, it is estimated that 1. 3 million new HIV infections were reported in the same year. Africa continues to bear the brunt of the epidemic, accounting for nearly two-thirds of all people living with HIV (WHO, 2023). In the Sub-Saharan region, the average prevalence of HIV among adults is estimated at 10%, highlighting the urgent need for targeted interventions.

The COVID-19 pandemic, which emerged in late 2019, had a profound global impact, leading the World Health Organization (WHO) to declare it a Public Health Emergency of International Concern in early 2020 (WHO, 2024b). The virus spread swiftly, overwhelming healthcare systems and resulting in millions of deaths worldwide. In response, countries implemented lockdowns and various measures to curb transmission, while global collaboration fostered the development of vaccines that substantially decreased both cases and mortality rates. By 2023, the WHO announced the end of the global health emergency, marking a significant milestone in the battle against COVID-19 (WHO, 2024b). However, the virus continues to pose a public health challenge, with millions of new infections and thousands of deaths still reported in 2024 (WHO, 2024b). The ongoing presence of COVID-19 cases highlights the necessity for continued vigilance and effective public health strategies.

COVID-19 presents a heightened risk for PLHIV, particularly those with low CD4 counts or untreated HIV (Suwanwongse, Kulachanya and Shabarek, Nehad, 2020). Recent studies have examined various aspects of COVID-19 within this population, including its incidence and severity. One study found that among 4,134 PLHIV, 342 tested positive for COVID-19 (Yunihastuti, Evy et al., 2022). Global data from the WHO, encompassing nearly 350,000 patients across 38 countries, revealed that PLHIV are at increased risk of experiencing severe illness and death from COVID-19 (Bertagnolio, Silvia et al., 2022). The findings indicate that PLHIV face a 38% higher risk of severe or fatal outcomes compared with individuals without HIV. Further-

more, comorbidities and co-infections — such as tuberculosis (TB), which are prevalent among PLHIV— intensify the severity of COVID-19. The overlapping challenges posed by HIV, TB, and COVID-19 highlight the need for a comprehensive public health strategy that integrates treatment and prevention efforts, including combining HIV care with COVID-19 vaccination initiatives (UNAIDS, 2024).

Significant challenges exist in COVID-19 vaccination among PLHIV, especially in regions with high HIV prevalence like Sub-Saharan Africa, primarily due to vaccine hesitancy and socioeconomic barriers. Govere-Hwenje, Sabina et al. (2022) emphasize the importance of thoroughly understanding vaccine acceptance within vulnerable populations, noting that hesitancy can compromise the success of vaccination campaigns. These findings highlight the urgent need for comprehensive strategies to overcome barriers to COVID-19 vaccine uptake among PLHIV.

Mathematical models of disease transmission can be valuable tools for predicting future outbreaks and informing precautionary measures, helping to protect vulnerable populations and maximize the number of lives saved. Several works have been published on the dynamics of COVID-19 and HIV co-infection that include different control strategies. The problem addressed by this dissertation revolves around the complex dynamics of co-infections involving COVID-19 and HIV, focusing on populations with advanced stages of HIV and those undergoing antiretroviral therapy (ART). Moreover, it examines the impact of vaccination behaviors and the prevalence of tuberculosis (TB) in PLHIV.

The existing models on co-infection dynamics, (Belela Samuel Kotola et al., 2023; Nainggolan, Jonner et al., 2023; Notice, Ringa et al., 2022; Otoo, Dominic et al., 2024; Teklu, S. W. and Kotola, B. S., 2023), often neglect critical factors such as reinfection, vaccination behavior including waning immunity, the role of HIV treatment(ART) in co-infection, and the cost-effectiveness of intervention strategies. Additionally, to our knowledge, no research has addressed the dynamics of triple infections involving COVID-19, HIV, and TB. The dissertation fills these gaps by developing new compartmental models that capture reinfection dynamics, vaccination behavior, and the cost-effectiveness of interventions. These models determine optimal strategies for reducing the burden of co-infections in resource-limited settings and to mitigate the heightened risk of mortality among co-infected individuals.

1.3 Objectives of the Study

1.3.1 General Objective

To develop and analyze a mathematical model that captures the co-dynamics of COVID-19, HIV, and TB, focusing on optimal control strategies, cost-effectiveness, and the influence of

vaccination behavior on disease transmission and outcomes.

1.3.2 Specific Objectives

The specific objectives of this study are to:

1. formulate a mathematical model for the co-dynamics of COVID-19 and HIV/AIDS.
2. investigate the epidemiological impact of COVID-19 and HIV/AIDS co-infection.
3. develop optimal control model for COVID-19 and HIV/AIDS co-infection.
4. evaluate the cost-effectiveness of control strategies for COVID-19 and HIV/AIDS co-infection.
5. develop a model for the co-dynamics of COVID-19, HIV, and TB with vaccination behavior.
6. assess the impact of vaccination behavior on the transmission dynamics of COVID-19, HIV and TB.

1.4 Significance of the Study

Analyzing the co-infection dynamics of COVID-19, HIV and TB diseases is essential for creating targeted interventions and improving public health strategies. By understanding how these diseases interact, we can identify risk factors and effective prevention measures, ultimately guiding resource allocation in combating all three diseases simultaneously. As a result, the dissertation makes a significant contribution to:

a) all those who want to know about the co-dynamics of COVID-19 HIV/AIDS and TB and their control strategies.

b) all who want to use analysis techniques in the field of epidemiology and control infectious diseases in medical field.

c) researchers who want the experience of using modern qualitative and quantitative approaches to investigate the dynamics of infectious disease.

d) mathematicians who want to conduct further studies on biological backgrounds and apply them to constructing construction of new-mathematical modeling.

e) policymakers and disease control agencies who want to set appropriate goals to evaluate the performance of infection-control plans.

1.5 Delimitation of the Study

Despite numerous global challenges, the dual threat of COVID-19, HIV/ AIDS and TB remains among the most critical. Therefore, our research focused on the co-dynamics of COVID-19, HIV/AIDS and TB diseases. This dissertation primarily considers deterministic models that use differential equations to model the distribution of infectious diseases in a populations. Moreover, Ethiopia is a country with a high prevalence of HIV/AIDS and TB cases; this, it is considered a valuable data source for calibrating the model, understanding disease dynamics, and evaluating intervention strategies.

1.6 The Organization of the Dissertation

Chapter 1 describes the biological background of COVID-19, HIV, and TB, and describes the role of mathematical models in epidemiology. The statement of the problem, objectives, significance of the study, delimitation and limitations of the dissertation are laid out and the introductory chapter is concluded with a description of the structure of the dissertation.

Chapter 2 comprises a literature review on the mathematical modeling of COVID-19, COVID-19 and HIV, and COVID-19 and TB co-infections.

Chapter 3 provides methodologies implemented in the research. Some mathematical tools that are used throughout the rest of this dissertation are highlighted. Methods of data collection and mathematical procedures are also presented.

Chapter 4 presents an in-depth analysis of the co-infection dynamics between COVID-19 and HIV/AIDS. It includes a stability analysis of the model, alongside a bifurcation analysis. Additionally, simulations are provided to validate the analytical findings and illustrate the influence of various model parameters.

Chapter 5 presents Optimal Control Strategies for HIV and COVID-19 Co-infection with a cost-effectiveness analysis. We solve the control problem analytically and run some numerical simulations to illustrate the behavior of the solution and identify the most economical prevention strategy.

In Chapter 6, a model is developed to explore the co-dynamics of COVID-19, HIV, and TB, taking into account information-dependent vaccination behavior and waning immunity. The qualitative behaviors of the model are thoroughly examined, shedding light on the role of various parameters, including key behavioral factors.

In the final chapter, Chapter 7, we summarize the dissertation work, present our conclusions, provide recommendations based on the main results, and outline future work.

CHAPTER 2

LITERATURE REVIEW

The earliest attempts to understand disease spread date back to the 18th century, with pioneers like Daniel Bernoulli (1760), who used mathematical principles to model the spread of smallpox and demonstrated the benefits of variolation or inoculation. In 1766, he published what is now considered the first epidemiological model (Martcheva, 2015). His work laid the groundwork for the mathematical analysis of disease transmission, although the field remained largely dormant until the early 20th century.

The modern era of epidemic modeling began in 1927 with the development of the SIR (Susceptible-Infectious-Recovered) model by William Kermack and Anderson McKendrick. Their compartmental model introduced the concept of dividing the population into groups based on disease status and using differential equations to describe transitions between these groups (William Ogilvie Kermack and À. G. Mckendrick, 1927). This model provided key insights into how infectious diseases spread and established the mathematical foundations of epidemic modeling. They have found a threshold for the invasion and persistence of disease in the population, which is now almost universally denoted by $\mathscr{R}_0$. Throughout the 20th century, the field expanded to include more complex models that accounted for factors like birth and death rates, latent periods, and heterogeneous populations. The advent of computers in the mid-20th century allowed researchers to simulate more complex models, such as malaria and HIV.

In the 21st century, epidemic modeling has become a critical tool for public health planning, especially during outbreaks of diseases like SARS, Swine Flu(H1N1), Ebola, and most recently, COVID-19. With advances in data availability, computational power, and understanding of disease biology, models now incorporate detailed population dynamics, vaccination strategies, and interventions. Epidemic modeling continues to evolve, with a growing emphasis on co-infection models, real-time prediction, and data-driven approaches to better inform public health responses.

2.1 Mathematical Models of HIV

Over the past three decades, there has been persistent research into controlling the transmission of HIV through numerous mathematical studies. Recent mathematical models of HIV have delved into different aspects of infection dynamics and treatment strategies. In a recent work, Abiodun, Oluwakemi et al. (2023) proposed a mathematical model to study the effects of coun-

seling and screening of unaware infective on the transmission dynamics of HIV/AIDS in the presence of highly active antiretroviral therapy (HAART). They extend the model to an optimal control problem to include various intervention techniques. The optimal control problem is numerically analyzed using an iterative method – forward-backwards sweep Runge-Kutta fourth-order numerical approximation methodology. The numerical simulation findings reveal that the most efficient strategy to limit HIV infection is to use the optimal combination of condoms on susceptible and on infection transmission rate, counseling and testing on unaware infective, and treatment on aware HIV/AIDS infective.

Xue, Ling et al. (2023) establishes a compartmental model to analyze HIV transmission dynamics and control strategies in China with the goal of meeting the United Nations' 90-90-90 goals by 2030. The study demonstrates the existence and stability of both disease-free and endemic equilibria, indicating the potential for controlling HIV spread. The research also includes the development of an optimal control model to show that the proposed strategies can effectively eradicate AIDS by 2030. These strategies encompass measures such as screening for latent individuals and enhancing education for those unaware of their infection status. The analysis reveals that the combination of screening and education is the most cost-effective control strategy. These findings offer guidance for implementing effective mitigation strategies, which are crucial for achieving the goals set by the Joint United Nations Preprogram on HIV/AIDS. The results highlight the importance of strategic planning and resource allocation in combating HIV in China.

In their work, Ajao, Saheed et al. (2023) presents a mathematical model to analyze the transmission dynamics and control of HIV infection, addressing challenges such as access to ART due to various societal issues. The study demonstrates that the disease-free equilibrium is globally asymptotically stable when the reproduction number is less than one. Conversely, a unique endemic equilibrium exists when this number exceeds one, indicating the potential for sustained HIV transmission. The model exhibits forward bifurcation, which is crucial for understanding how small changes in parameters can lead to significant shifts in disease dynamics. The model is calibrated using data on HIV/AIDS prevalence in Nigeria from 1990 to 2019, showing that it accurately represents real-world scenarios. Their numerical simulation results show that the fraction of detected individuals remaining in treatment significantly influences the population dynamics of latently infected individuals and those progressing to AIDS, highlighting the importance of effective treatment strategies.

In Zviiteyi Chazuka et al. (2024), a novel mathematical model was introduced to analyze HIV transmission dynamics, incorporating control strategies such as preexposure prophylaxis (PrEP), condom use, and antiretroviral treatment. The study established the model's basic prop-

erties and computed the reproduction number, indicating the potential for HIV transmission without control measures. Sensitivity analysis highlighted the importance of optimal control strategies, leading to the formulation of an optimal control model that effectively captures the dynamics of HIV transmission. The researchers utilized demographic and epidemiological data from South Africa to conduct numerical simulations and demonstrate significant community-level benefits from implementing a combination of control measures. Their findings suggest that implementing a combination of preexposure prophylaxis (PrEP), condom use, and antiretroviral treatment strategies can lead to significant community-level benefits, indicating that a multi-faceted approach may be more cost-effective than relying on a single strategy alone.

2.2 Mathematical Models of TB

Recent mathematical models on tuberculosis (TB) have provided insights into both its transmission dynamics and intervention strategies. For instance, Kitaro, Damtew et al (2023) proposed a mathematical model to investigate how chemoprophylaxis treatment affects the transmission of tuberculosis, particularly with a focus on drug-resistant strains. This model includes chemoprophylaxis for latent TB infections, emphasizing that early treatment is vital for preventing the progression to active TB. The study highlights the importance of optimizing both preventive and therapeutic strategies to reduce TB incidence, especially in areas with a high prevalence of latent TB.

Olayiwola, M. O. and Adedokun, K. A. (2023) utilized a novel SEITR mathematical model to investigate the impact of treatment on physical limitations in tuberculosis. The model underwent qualitative analysis to validate key aspects. The findings underscore the importance of fractional-order analysis in understanding the effectiveness of treatment strategies aimed at reducing tuberculosis prevalence. The study indicates that the time fractional dynamics of TB treatment are closely linked to its efficacy. The conceptual results reveal that non-local interactions between the disease and the treatment could provide more effective methods for eradicating tuberculosis in real-world situations.

Eka D.A.Ginting et al. (2024) explores the influence of treatment failure on tuberculosis control strategies, incorporating vaccination interventions through a deterministic compartmental epi- demiological model. The findings emphasize that the efficacy of vaccination is crucial, with higher quality and longer-lasting vaccines producing more significant effects. Moreover, while reinfection may not directly influence the reproduction number, it plays a pivotal role in determining whether tuberculosis persists or is eradicated. This study highlights the intricate interplay of factors in tuberculosis control strategies, offering vital insights for effective interventions and policy development.

These models play a vital role in understanding both the biological processes and epidemiological dynamics of TB, providing insights for more effective interventions.

2.3 Mathematical Models of COVID-19

Many researchers have proposed and analyze SEIR (Susceptible - Exposed - Infected - Recovered) type models with little variations to describe the dynamics of the COVID-19 outbreak as time progresses and investigate the effect of applying different strategies to control the disease (Getachew B. B. and Eshetu D. G., 2021; Mwalili, Samuel et al., 2020; Ndairou, Faical et al., 2020; Pal, D. et al., 2020; Prem, Kiesha et al., 2020; Yang, C. and Wang, J., 2020; Yavuz, Mehmet et al., 2021). These models used different compartmental structures to model the various aspects of COVID-19 dynamics. They were created with the intent of simulating the dynamics of infection in certain nations or regions based on the severity of the epidemic in such countries.

For instance, Pal, D. et al. (2020) constructed a mathematical model of COVID-19 transmission based on the SEIR model with a hospital-quarantined group. The SEIR model results by Prem, Kiesha et al. (2020) showed that the rapidity transmission of COVID-19 has been reduced due to the complete lock-down of the city for about two months until late April 2020. Ndairou, Faical et al. (2020) formulated a compartmental mathematical model for the spread of the COVID-19 disease with special focus on the admissibility of a super-spreader individual. Getachew B. B. and Eshetu D. G. (2021) proposed a model that takes into account the impact of quarantine and the presence of an asymptomatic population, while also integrating a time-independent control strategy. The authors argued that optimal control measures can effectively decrease the number of exposed, asymptomatic infective, and quarantined individuals by focusing on preventing the spread within the susceptible population.

The paper by Mumbu, A. J. and Hugo, A. K. (2020) proposed a mathematical model for studying its transmission dynamics in the presence of face mask-wearing and hospitalization services of the human population in Tanzania. They formulated and analyzed a mathematical model for COVID-19 transmission between humans with the Susceptible-Masked-Unmasked-Exposed-Infected-Hospitalized-Recovered (SMUEIHR) compartments for analyzing the significance of wearing masks and hospitalizing the detected infectious as preventive and supportive measures in reducing transmission rate to the susceptible group. They obtain $\mathscr{R}_0 = 0.698$ in the presence of face masks wearing and medication services or hospitalization as a preventive measure for its transmission, whereas $\mathscr{R}_0 = 3.8$ in their absence. That is, they proved the necessity of face masks wearing and hospitalization services to COVID-19 patients to contain the disease spread to the population.

Further, Ali, Mohsin et al. (2020) formulated a mathematical model that incorporates the role of asymptomatic individuals as well as the effects of quarantine and isolation of different population groups. They analyzed the model to suggest strategies for effective control of the epidemic. Their analysis showed that a high rate of quarantine along with isolation of infected individuals is needed to control the disease, which lends support to the lock-down measures adopted across the globe to help combat the outbreak.

Aldila, Dipo et al. (2020) showed how the estimated parameter from the incidence data in Jakarta might exhibit a backward bifurcation when the quality and size of the patients handled in the hospital getting worse. Oluyori, D. A. and Adebayo, H. O. (2020) proposed a model that take saturation effect both in the incidence and treatment rate in to account and shows that the effectiveness of the treatment response applied determines whether an endemic situation is imminent within the population. Moreover, the results for model show that the limitation of medical resources alone can be a cause for bi-stability behavior and backward bifurcation, similarly to what was studied in Mohd, M. H. and Sulayman, F. (2020).

A mathematical model proposed by Kassa, Semu M et al. (2020) takes the human learning behavior and the involvement in self-protective measures against an infectious disease into account. The proposed model works on adding new compartment S_e, representing the cohort of individuals who are involved in a self-protective action against the infection into the usual SEIR model and behavior change function(e) which is described as a function of the prevalence $\lambda(t)$ of the disease. The model analysis has showed that the asymptomatic infectious group of individuals may play a major role in the re-emergence of the disease in the future. Therefore, it is recommended that in the absence of vaccination, countries need to develop capacities to detect and isolate at least 30% of the asymptomatic infectious group of individuals while treating in isolation at least 50% of symptomatic patients to control the disease.

In Bo Yang et al. (2022), a mathematical model is developed to assess the impact of vaccination on COVID-19 transmission, emphasizing the critical role of the reproduction number, $\mathscr{R}_0$, in understanding disease dynamics. The study identifies conditions for the existence of endemic equilibria, demonstrating that two equilibria can occur even when $\mathscr{R}_0$ is less than one, leading to backward bifurcation, where COVID-19 can persist. Stability analysis and simulations show that increasing vaccine efficacy and vaccination rates can reduce infection peaks and delay their timing. However, the study emphasizes that vaccination alone is insufficient for rapid control, highlighting the need for a combined strategy of vaccination and non-pharmaceutical interventions, such as reducing contact rates and isolating infected individuals, for effective COVID-19 management.

Waheed, Ahmad et al. (2021) introduce a nonlinear model that incorporates vaccinated in-

dividuals to analyze COVID-19 transmission dynamics. They establish the existence, uniqueness, boundedness, and positivity of the model's solutions and derive a threshold parameter that governs the pandemic's progression. The application of LaSalle's invariance principle confirm the global stability of the model's equilibria. Numerical simulations using the Runge-Kutta and Non-Standard Finite Difference methods validate these theoretical findings. Their results highlight that widespread vaccination, particularly through mandatory measures, is crucial for achieving faster eradication of COVID-19 and underscore the role of public awareness.

2.4 Co-infection Models Involving HIV and TB

Numerous mathematical modeling studies have been carried out to understand the transmission dynamics of co-infections in HIV/AIDS. For instance, Awoke, Temesgen D. and Kassa, Semu M. (2018), Mayanja, Edison et al. (2020) and Melese, Z. T. and Alemneh, H. T. (2021) are some of the recent works that have been used to investigate the dynamics of co-infections in HIV/AIDS.

A TB-HIV/AIDS co-infection model that incorporates prevalence-dependent behavior change in the population and treatment for the infected (and infectious) class is formulated and analyzed by Awoke, Temesgen D. and Kassa, Semu M. (2018). The model has been mathematically analyzed both for the subsystem corresponding to the cases that each disease type is isolated and in the case when there is co-infection. An optimal control model that minimizes the aggregate cost of the infections is also included. The model considers both intervention categories, preventive as well as treatment, and numerical simulations are presented. In the analysis, it has been indicated that the effect of prevention as well as treating the infected ones with the available pharmaceutical means affects significantly the optimal control strategy and its outcome.

Mayanja, Edison et al. (2020) formulated and analyzed a mathematical model for the HIV-Hepatitis C Virus (HCV) co-infection dynamics in the absence of therapy. They carried out a sensitivity analysis to determine the relative importance of the different parameters influencing the HIV-HCV co-infection dynamics. Their findings reveal that, in the long run, there is a substantial number of individuals co-infected with HIV and latent HCV. Therefore, they recommend that HIV and latently HCV-infected individuals need to seek early treatment to slow down the progression of HIV to AIDS and latent HCV to advanced HCV.

The study by Melese, Z. T. and Alemneh, H. T. (2021) presented a transmission dynamics model for visceral leishmaniasis(VL)-HIV co-infection, using numerical experiments to assess the impact of key parameters on the spread and control of the diseases. Their findings highlight that increasing the VL recovery rate(ϕ_1) and the recovery rate for VL-HIV co-infection(ϕ_2) are crucial in reducing the number of infectious individuals. Additionally, reducing the reservoir

population(c_1) and the contact rate(β_h) significantly decreases the number of infected reservoirs, sand flies, and co-infected populations. They recommend that stakeholders prioritize these parameters with targeted prevention strategies to curb the spread of VL, HIV, and co-infection within the community.

2.5 COVID-19 and TB Co-infection Models

The occurrence of coinfections between COVID-19 and TB necessitates modeling studies aimed at identifying effective mitigation strategies for these diseases. For instance, Kassahun, G. M. and Legesse, L. O. (2022) developed a co-infection model for TB and COVID-19 that categorizes the population into seven compartments. An in-depth analysis was conducted to ensure the mathematical and biological soundness of the model. To facilitate further analysis, the co-infection model is divided into submodels for COVID-19 and TB. The reproduction numbers for each sub-model, denoted as R_0^C and R_0^T, were computed to investigate the stability of the model's equilibria. The stability analysis of the submodels indicates that both the disease-free and endemic equilibria are locally and globally stable when $R_0^C < 1$ and $R_0^T < 1$, and when $R_0^C > 1$ and $R_0^T > 1$, respectively. However, after calculating the reproduction number R_0 for the full model, the stability analysis reveals that the TB-COVID-19 free equilibrium is not globally asymptotically stable when $R_0 < 1$, suggesting the possibility of backward bifurcation. In addition to verifying analytical results, numerical simulations were performed to examine the influence of different parameters on the transmission dynamics of these diseases. The findings from the numerical simulations demonstrate that a significant reduction in contact rates, coupled with an increase in treatment, can effectively minimize the spread of the TB and COVID-19 co-infection.

Bandekar & Ghosh (2022) developed a TB-COVID-19 model that considers waning immunity for both diseases. The study includes stability and bifurcation analyses for the TB-only, COVID-19-only, and combined models, examining the effects of infection rates, waning immunity, and mask effectiveness on disease prevalence. A sensitivity analysis using a normalized forward sensitivity index and LHS-PRCC method highlights key parameters influencing disease spread. The research presents optimal control strategies for timely TB treatment and enhanced COVID-19 testing and isolation. The findings stress the importance of various control measures for effective disease management and emphasize that continued treatment for other conditions during a pandemic is crucial to prevent co-infection-related mortality and ensure timely care.

Kifle, Z. S. and Obsu, L. L. (2023) developed a mathematical model that effectively captures the dynamics of COVID-19 and TB co-infection, including exogenous reinfection. Their analysis revealed that the TB sub-model can experience backward bifurcation, indicating that simply

reducing R0 may not be sufficient to eliminate TB from the community. They demonstrated that the equilibria of the full TB-COVID-19 model are locally asymptotically stable, but not globally stable due to the potential for backward bifurcation. The incorporation of exogenous reinfection into the model was shown to significantly impact the dynamics, allowing for the possibility of disease persistence even when $\mathscr{R}_0$ is below one. They employed numerical simulations to demonstrate the effectiveness of optimal control strategies in reducing the disease burden, highlighting the importance of vaccination and treatment in managing co-infections. Their results emphasized the necessity for integrated health interventions to effectively control both COVID-19 and TB, as the dynamics of these diseases are interconnected and complex.

2.6 COVID-19 and HIV Co-infection Models

Recent mathematical modeling studies have explored the co-dynamics of COVID-19 and HIV, revealing important insights for public health strategies. Notice, Ringa et al. (2022) proposed a new mathematical model to assess the impact of COVID-19 on HIV/AIDS and vice versa. The model highlights the complexities of their interactions and the impact of various prevention and treatment strategies. They computed the reproduction number and used it to prove the local and global asymptotic stability of the sub-models' disease-free and endemic equilibria. Additionally, the model was fitted to a real COVID-19 dataset from South Africa. The work also incorporated time-dependent controls representing intervention measures such as COVID-19 and HIV prevention interventions, as well as COVID-19 treatment. The results suggest that HIV prevention measures can significantly reduce the burden of co-infections with COVID-19. Furthermore, the study highlighted that effective COVID-19 treatment could enhance the immune response in co-infected individuals, thereby reducing the incidence of opportunistic infections such as HIV/AIDS.

The authors in Ahmed. M. Elaiw et al. (2022) proposed a within-host SARS-CoV-2/HIV co-infection model consisting of eight ordinary differential equations. They demonstrated that when SARS-CoV-2/HIV co-infected patients have weak CD4+ T-cell immunity, there is increased production of productively infected epithelial cells and SARS-CoV-2 particles. This heightened production may lead to severe SARS-CoV-2 infection in HIV patients. Additionally, their findings suggest that reducing the severity of SARS-CoV-2 infection in HIV patients could be achieved by increasing the death rate of infected epithelial cells during the latency period.

In a study conducted by Teklu, S. W. and Kotola, B. S. (2023), ordinary differential equations were utilized to model the transmission dynamics of both COVID-19 and HIV. The model consisted of eight compartments that involved individuals protected from COVID-19 as well as HIV infections. Standard methods were employed to establish the model's existence, unique-

ness, and to calculate the reproduction numbers. The study's sensitivity analysis revealed that transmission rates were the most influential parameters in increasing the reproduction number. Conversely, protection and treatment rates were found to have a reverse impact when increased. Additionally, numerical simulations were carried out to demonstrate the impact of certain parameters on the transmission of single infections and co-infections. Based on the analytical and numerical findings, the authors concluded that implementing effective protection and treatment rates could significantly reduce and potentially eliminate the spread of HIV/AIDS-COVID-19 co-infections in the community.

In addition, Belela Samuel Kotola et al. (2023) proposed an expanded model compared to their previous work (Teklu, S. W. and Kotola, B. S., 2023) by dividing the HIV-infected and the COVID-19-HIV co-infected population into two compartments each: aware and unaware, and by introducing a vaccinated compartment. Furthermore, they extended their proposed model to an optimal control problem with four control strategies: HIV prevention, COVID-19 prevention through quarantine, COVID-19 treatment, and HIV treatment. Their analysis, using Center Manifold theory, revealed the existence of a backward bifurcation phenomenon whenever the effective reproduction number is less than one. They conducted numerical simulations to confirm the global stability of the endemic equilibrium when the reproduction number is greater than one. Furthermore, their findings showed that combining all available preventive and treatment measures is the most effective strategy for significantly minimizing the spread of HIV/AIDS and COVID-19 co-infection.

Furthermore, Nainggolan, Jonner et al. (2023) proposed a co-infection model that takes into account a subpopulation protected against HIV, comprising individuals who have received cellular immune antibody vaccines against the HIV virus. In their study, they conducted a sensitivity analysis of the reproduction number to identify the parameters that influence co-infection of COVID-19 and HIV/AIDS. Through elasticity index analysis, they determined that the most sensitive parameters are β_1 (the transmission rate of COVID-19), β_2 (the transmission rate of HIV/AIDS), and τ (the treatment rate in the HIV/AIDS subpopulation). They suggest that reducing contact rates through measures such as social distancing for COVID-19 and condom use for HIV/AIDS could help decrease the incidences of both COVID-19 and HIV/AIDS. Additionally, maximizing efforts to treat HIV/AIDS could yield significant results in reducing the burden of co-infections.

A study conducted by Otoo, Dominic et al. (2024) proposed a compartmental modeling approach to address the control measures for both COVID-19 and HIV. The study utilized a nonlinear differential equation with ten compartments to formulate the model. The equilibria of the co-dynamics model were demonstrated to be both locally and globally stable. The numerical

simulations presented in the study indicated that public education for susceptible populations and the treatment of COVID-19-infected individuals are the most effective strategies for controlling the spread of both diseases. These interventions resulted in a significant reduction in COVID-19 infections, an increase in the recovery rate, and a notable decrease in the overall infected population. These findings mark a crucial advancement in combating both diseases and underscore the significance of prioritizing public health education and COVID-19 treatment efforts.

2.7 Models of the Dynamics of Triple Infection: COVID-19, HIV and TB

Although there are several reports showing the triple infection cases with COVID-19 (Guido, Giacomo et al., 2023; Tanne, 2022; Tolossa, Tadesse et al., 2021), the mathematical modeling studies this condition remain almost none. A detailed mathematical model was created to study the simultaneous dynamics of COVID-19, dengue, and HIV by Omame, Andrew et al. (2023). This marks, in our view, the first study to tackle the intricate scenario of triple infection involving COVID-19, with a dedicated compartment for individuals infected with all three diseases. The study employs rigorous analytical methods to examine the model's dynamical properties, demonstrating the stability of equilibria through Lyapunov function candidates under certain conditions. Optimal intervention strategies were identified to mitigate the co-circulation of these diseases, and a control system was analyzed to determine the most effective approaches for minimizing infections. Simulation results revealed that strategies targeting COVID-19 and dengue significantly reduced both single and dual infection cases, while those focusing on COVID-19 and HIV prevention yielded substantial decreases in new infections. A third approach aimed at preventing COVID-19 and co-infections also led to a notable reduction in overall infection rates. Among the strategies, the combined COVID-19/HIV approach was found to be the most effective, preventing the highest number of new infections. The authors emphasize the importance of integrated, multi-disease prevention strategies, highlighting the potential of a COVID-19/HIV control approach to manage pandemics and associated co-infections efficiently.

2.8 Gaps in the Literature on Co-Dynamics of COVID-19, HIV and TB

Existing literature on COVID-19 co-infection models, as highlighted by (Ahmed. M. Elaiw et al., 2022; Belela Samuel Kotola et al., 2023; Nainggolan, Jonner et al., 2023; Notice, Ringa et al., 2022; Otoo, Dominic et al., 2024; Teklu, S. W. and Kotola, B. S., 2023) predominantly focused on dual infections, such as COVID-19-HIV, while neglecting the inclusion of tuberculosis (TB) as a critical co-factor. These studies have provided valuable insights into the interactions between COVID-19 and HIV, exploring optimal control strategies and the effects of antiretro-

viral therapy (ART). However, the exclusion of TB from these models limits their applicability, particularly in high-burden regions where HIV/TB co-infection is prevalent. The role of behavioral factors, such as information-dependent vaccination, has been insufficiently explored, particularly regard- ing their impact on the transmission dynamics and control measures for diseases with waning immunity, such as COVID-19. Additionally, cost-effectiveness analyses of interventions in a co-infection context are often neglected, which reduces the applicability of these models for policymaking. These gaps indicate the need for more comprehensive models that incorporate the dynamics of COVID-19, HIV, and TB infections, consider the interplay of behavioral factors, and evaluate the cost-effectiveness of integrated intervention strategies.

CHAPTER 3

RESEARCH METHODOLOGY

This section provides a complete summary of the research design. It outlines the theoretical models, data collection methods, analysis techniques, and mathematical procedures used. It serves as a foundation for understanding the research methodology and the derivation of findings.

3.1 Models Formulation

The model formulation was carefully crafted to align with the research objectives and leverage the most current biological understanding of the infection's pathogenesis and the disease's epidemiology. To establish a solid foundation, an extension of the SIR compartmental models was formulated, incorporating several key assumptions. The basic analysis of the models, including the existence and uniqueness of solutions, was conducted using established mathematical theories. Local and global stability analyses were performed by linearization and applying global stability results. Optimal control strategies were implemented and analyzed using Pontryagin's maximum principle (a first-order necessary optimality condition). Additionally, numerical simulations were employed as a valuable tool to validate the mathematical descriptions of the situation and generate predictions that could be compared with the recorded observations.

3.2 Source and Method of Data Collection

To support the dissertation's research objectives, a comprehensive review of secondary data sources was conducted. These sources included reputable institutions such as EPHI, international bodies like the WHO and World Bank, and peer-reviewed publications. The collected data were meticulously analyzed to ensure the calibration of the model. Python, a versatile programming language, was employed to fit the model to real-world data, ensuring its accuracy and relevance to the specific context of this dissertation.

The dissertation work involves the data of people infected with COVID-19, HIV/AIDS and TB diseases. It contains only general research work that does not involve any risk for development. Moreover, we were committed to following all ethical principles during this study in accordance with the rules and regulations of Adama Science and Technology University.

3.3 Method of Data Analysis

Data analysis plays a crucial role in accurately estimating model parameters, validating the model, and understanding the dynamics of the epidemic. By fitting the model to real-world data, such as time-series infection count data, data analysis ensures that the model predictions' align with observed trends, thereby improving its reliability for forecasting and intervention planning. Parametric estimation in this context was performed SciPy optimization tools from Python. The parameter estimation follows a structured procedure, starting by formulating a system of ordinary differential equations to represent the dynamics of the co-infection model. The parameters to be estimated are then identified. An optimization problem was set up using SciPy's optimize module, where $minimize()$ was used for the model in Chapter 4 and $leastsquares()$ for the model in Chapter 6. The selected function minimizes the error between the model output and data. The model is repeatedly solved using a numerical ODE solver (*odeint*) for different parameter values until the optimal set of parameters is found that best fits the observed data. The procedure was validated through residual analysis to ensure the robustness of the parameter estimates.

3.4 Mathematical Procedure

In this dissertation, we develop a compartmental model based on nonlinear systems of differential equations to describe the dynamics of the COVID-19 outbreak as time progresses. There are four substantial processes. First, we propose and analyze a mathematical model for COVID-19 and HIV/AIDS co-infection. Second, based on actual data, we estimate parameters to make reliable quantitative predictions. Third, we propose an optimal control model to determine the optimal strategy for the control of the diseases. Version 3 of Python and/or MATLAB is used to verify the theoretical analysis and examine the responsiveness of the optimum control inputs. The forward-backward sweep method, which combines the forward application of a fourth-order Runge-Kutta method for the original system with the backward application of a fourth-order Runge-Kutta method for the adjoint system, was employed to solve the optimal control problem numerically. Finally, a model that describes the transmission dynamics of COVID-19, HIV, and TB was introduced to further reduce the complex burden of these diseases. Parametric estimations are performed based on the Python optimization package, and are used for numerical simulation purposes.

CHAPTER 4

CO-INFECTION DYNAMICS OF COVID-19 AND HIV/AIDS

This chapter presents a comprehensive analysis of the co-infection dynamics between COVID-19 and HIV/AIDS through the development of a mathematical model. It begins with a detailed model formulation that captures the transmission dynamics of both diseases, followed by a qualitative analysis to ensure the model's mathematical soundness. The chapter then dives into the analysis of sub-models for COVID-19 and HIV/AIDS individually, providing insights into their respective transmission patterns and impacts on the population. The co-infection model analysis explores how control parameters, such as vaccination and treatment rates, influence the reproduction numbers and overall transmission. Parametric estimation is conducted based on real-world data, and numerical simulations are performed to identify the effects of various interventions on reducing co-infection rates and mortality among PLHIV.

4.1 Model Formulation

In formulating co-infection model, the total population at time t, denoted by $N(t)$, is categorized into different compartments based on their epidemiological state: susceptible(S), COVID-19 fully vaccinated (V), COVID-19 infected individuals (I_C), individuals recovered from COVID-19 (R), HIV infectious but asymptomatic (I_H), individuals with advanced HIV disease (I_A), HIV and COVID-19 infected (I_{HC}), HIV and COVID-19 co-infected with clinical signs of AIDS (I_{AC}) and people at high risk of death due to co-infection (D_{HC}).

The model is formulated based on the following assumptions:

- All individuals in the population are equally likely to come into contact with one another.
- The vaccination rate is constant over time.
- Immunity gained from vaccination lasts for life and does not decrease over time.
- Individuals can not be infected with COVID-19 and HIV at the same time.
- Vaccination against one COVID-19 provides no protection against the HIV in a co-infection scenario.
- The rate at which an HIV progresses (that is, from HIV infection to AIDS) is constant.

- The transmission rate remains constant and is not affected by time, behavioral changes, or public health interventions.

The flow through the compartmental subpopulations is described as follows. A fraction of $(1-\rho)\Lambda$ human population is recruited in the susceptible class, where ρ is the proportion of vaccinated population and Λ is a recruitment rate of susceptible population. The remaining human population, $\rho\Lambda$, joins the vaccinated class. Loss of immunity after $\frac{1}{\psi}$ period of time in recovered class raises susceptible class. Following effective contact with COVID-19 and HIV infected individual, a susceptible may acquire COVID-19 and HIV diseases at rate of λ_C and λ_H, respectively. The rate at which susceptible become COVID-19 infected from individuals with active COVID-19(λ_C), is $\lambda_C = \gamma_c \frac{I_C+I_{HC}+I_{AC}}{N-D_{HC}}$, where γ_c stands for the rate of transmission of the COVID-19 disease. Due to severe health conditions, it was assumed that individuals at high risk of death (D_{HC}) are under follow-up and do not involve in the transmission of both diseases. The rate at which susceptible individuals acquire HIV infection from individuals with active HIV(λ_H), is $\lambda_H = \gamma_h \frac{I_H+I_{HC}+\varepsilon(I_A+I_{AC})}{N-D_{HC}}$, where γ_h stands for the rate of transmission of the HIV disease. Higher viral loads in the later stages of the disease increase the HIV transmission probability. So, it was assumed that individuals in (I_{AC}) class has transmission rate $\beta\varepsilon$, where $\varepsilon \geq 1$ is a modification parameter for the assumption that a individuals with advanced HIV are more likely to transmit the disease. Natural death decreases susceptible and other subpopulations at a rate of μ. It is assumed that vaccination is applied only to healthy individuals, so only susceptible individuals get vaccinated at a rate of ξ. There are findings which argue that COVID-19 vaccinated individuals can become infected even though they have been vaccinated. For this purpose the infection of vaccinated individuals happens at a reduced transmission rate $\sigma\gamma_c$, where $0 \leq \sigma \leq 1$ is the reduction coefficient. Here, if $\sigma = 0$, vaccinated individuals cannot get infected, and the vaccine is perfect. If $\sigma = 1$, vaccinated individuals get infected like susceptible individuals, and immunization plays no protective role. The rate of change of the COVID-19 infected population is increased due to transfer from the susceptible and vaccinated classes at the rate of λ_C and $\sigma\lambda_C$ respectively. This population decreases as infectious individuals are recovered at the rate θ or die due to the disease at the rate of δ_c. The rate of change of the HIV infected population is generated at a rate of λ_H from the susceptible and vaccinated population. Interacting with a COVID-19 infected person at rate of λ_C reduces the number of population in I_H class. Members of I_A transferred from I_H class at a rate of ω become infected with COVID-19 at a rate $\kappa\lambda_C$. Modification parameter $\kappa \geq 1$ accounts for the fact that there is an increased risk of getting COVID-19 for someone already infected with HIV, due to the vulnerability of the immune system. Moreover, they may lost their life due to HIV at the rate of δ_h. The number of populations in I_{HC} and I_{AC} classes, following the burden of the co-infection, transferred to D_{HC} family at a rate η_1 and η_2, and recovered from COVID-19 at a rate α and

φ, respectively. Co-infected individuals risked to death may lost their life at a rate δ_{hc}. The description of the remaining parameters can be seen from Table 4.3. Bringing the aforementioned assumptions together leads to the set of nonlinear ordinary differential equations given in (4.1). The schematic representation of model (4.1) is illustrated in Figure 4.1. It schematically represents the epidemiology of COVID-19 and HIV/AIDS co-infection. Circles are used to depict different diseases stages, and arrows show how people advance from one stage to the next.

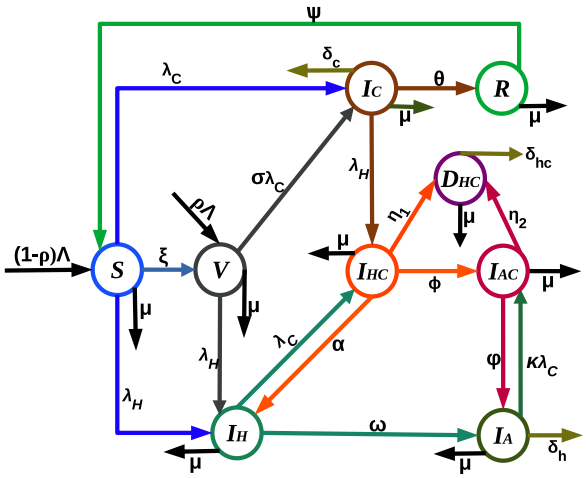

Figure 4.1: Model flow diagram for the co-infection model

The following system of differential equations describe the co-infection dynamics of COVID-19 and HIV/AIDS.

$$\begin{cases} S' = (1-\rho)\Lambda + \psi R - (D_1 + \lambda_C + \lambda_H)S, \\ V' = \rho\Lambda + \xi S - (\mu + \sigma\lambda_C + \lambda_H)V, \\ I_C' = \lambda_C S + \sigma\lambda_C V - (D_2 + \lambda_H)I_C, \\ R' = \theta I_C - D_3 R, \\ I_H' = (S+V)\lambda_H + \alpha I_{HC} - (D_4 + \lambda_C)I_H, \\ I_A' = \omega I_H + \varphi I_{AC} - (D_5 + \kappa\lambda_C)I_A, \\ I_{HC}' = \lambda_C I_H + \lambda_H I_C - D_6 I_{HC}, \\ I_{AC}' = \phi I_{HC} + \kappa\lambda_C I_A - D_7 I_{AC}, \\ D_{HC}' = \eta_1 I_{HC} + \eta_2 I_{AC} - D_8 D_{HC}, \end{cases} \tag{4.1}$$

where $D_1 = \mu + \xi$, $D_2 = \theta + \mu + \delta_c$, $D_3 = \mu + \psi$, $D_4 = \omega + \mu$, $D_5 = \mu + \delta_h$, $D_6 = \alpha + \phi + \mu + \eta_1$, $D_7 = \varphi + \mu + \eta_2$ and $D_8 = \delta_{hc} + \mu$.

4.2 Model Analysis

4.2.1 Invariant set, Positivity and Boundedness of Solutions

Since model system (4.1) involves a human population, all solutions must be positive and bounded and these solutions are realized in a positively invariant region. The positivity of the solutions and the positively invariant region were investigated through Theorem 4.2.1 under the presumption that all parameters are positive.

Theorem 4.2.1. *The solutions of system* (4.1) *with positive initial data remain positive for all* $t > 0$. *Furthermore, the biologically feasible region*

$$\Theta = \{(S,V,I_C,R,I_H,I_A,I_{HC},I_{AC},D_{HC}) \in \mathbb{R}^9 : 0 \leq N \leq \Lambda/\mu\}$$

is positively invariant and attracting for system (4.1).

Proof. Equations in (4.1) point inward on the boundary $\mathbb{R}^9_+ \setminus \{\mathbf{0}\}$. For instance if $S = 0$, then

$$\frac{dS}{dt} = (1-\rho)\Lambda + \psi R > 0.$$

From the second equation of (4.1), if $V = 0$, we have

$$\frac{dV}{dt} = (1-\rho)\Lambda + \psi R > 0.$$

Applying the same procedure, we can show that the remaining state variables are also positive $\forall t > 0$.

Furthermore, adding all the equations of the model system (4.1), total human populations satisfy the following equation,

$$\frac{dN}{dt} \leq \Lambda - \mu N.$$

Integrating both sides from 0 to t, we have

$$N(t) - N(0) \leq -\mu \int_0^t \left(N(s) - \frac{\Lambda}{\mu} \right) ds.$$

If $0 \leq N(0) \leq \frac{\Lambda}{\mu}$, from Gronwall inequality, we can deduce that

$$0 \leq N \leq \Lambda/\mu.$$

Therefore, all solutions in $\mathbb{R}^9_+$ are drawn to the region Θ. □

The implication of Theorem 4.2.1 is that the model equations (4.1) is epidemiologically meaningful, as it proved that all the state variables are non-negative and bounded. That is, no solution path can leave through any boundary of Θ and it is sufficient to consider the dynamics of the model (4.1) in Θ. In this region, the model is considered to be mathematically and epidemiologically well posed.

4.2.2 HIV/AIDS Sub-model Analysis

The HIV/AIDS sub-model, obtained when I_C, R, I_{HC}, I_{AC} and D_{HC} are all zero, is given by:

$$\begin{cases} S' = (1-\rho)\Lambda - (D_1 + \lambda_H)S, \\ V' = \rho\Lambda + \xi S - (\mu + \lambda_H)V, \\ I_H' = (S+V)\lambda_H - D_4 I_H, \\ I_A' = \omega I_H - D_5 I_A, \end{cases} \tag{4.2}$$

where $\lambda_H = \gamma_h \frac{I_H + \varepsilon I_A}{N}$.

Equilibria and reproduction number

Qualitative analysis of the steady-state solutions (equilibria) of (4.2) is performed to investigate the long-term behavior of the disease. This behavior depends largely on the equilibrium points, that is, time-independent solutions of the system. Since these solutions do not depend on time, we set $S'(t) = V'(t) = I_H'(t) = I_A'(t) = 0$. That is,

$$\begin{aligned} (1-\rho)\Lambda - (D_1 + \lambda_H)S &= 0 \\ \rho\Lambda + \xi S - (\mu + \lambda_H)V &= 0 \\ (S+V)\lambda_H - D_4 I_H &= 0 \\ \omega I_H - D_5 I_A &= 0 \end{aligned} \tag{4.3}$$

The disease free equilibrium (DFE), the state where the population is completely free from HIV infection, is obtained by setting I_H and I_A equals to zero and solving for S and V from (4.3). Thus, from the first and second equation of (4.3), we have

$$\begin{aligned} (1-\rho)\Lambda - D_1 S &= 0 \\ \rho\Lambda + \xi S - \mu V &= 0 \end{aligned}$$

Which imply, $S = \frac{\Lambda(1-\rho)}{D_1}$ and $V = \frac{\Lambda(\rho\mu+\xi)}{\mu D_1}$. Hence, the HIV/AIDS-free equilibrium, denoted by E_h^0, is given by,

$$E_h^0 = \left(\frac{\Lambda(1-\rho)}{D_1}, \frac{\Lambda(\rho\mu+\xi)}{\mu D_1}, 0, 0\right).$$

The reproduction number for the HIV/AIDS sub-model was established by applying the next-generation matrix method outlined in Appendix A.2 on system (4.2). The disease (infected) compartments of (4.2) are I_H and I_A and the non-disease (noninfected) compartments are S and V. Taking the infected compartments with their dynamics we have,

$$\mathcal{F} = \begin{pmatrix} (S+V)\lambda_H \\ 0 \end{pmatrix} \quad \text{and} \quad \mathcal{V} = \begin{pmatrix} D_4 I_H \\ D_5 I_A - \omega I_H \end{pmatrix}.$$

The Jacobian matrix of $\mathcal{F}$ and $\mathcal{V}$, denoted by F and V, at E_h^0 is given by

$$F = \begin{pmatrix} \gamma_h & \varepsilon\gamma_h \\ 0 & 0 \end{pmatrix} \quad \text{and} \quad V = \begin{pmatrix} D_4 & 0 \\ -\omega & D_5 \end{pmatrix}.$$

Hence, we have

$$FV^{-1} = \begin{pmatrix} \frac{\gamma_h}{D_4}\left(1+\frac{\omega\varepsilon}{D_5}\right) & \frac{\varepsilon\gamma_h}{D_5} \\ 0 & 0 \end{pmatrix}.$$

The corresponding eigenvalues are $\frac{\gamma_h}{D_4}\left(1+\frac{\omega\varepsilon}{D_5}\right)$ and 0. The basic reproduction number of HIV/AIDS sub-model, denoted by $\mathcal{R}_{0h}$, is given by

$$\mathcal{R}_{0h} = \frac{\gamma_h}{D_4}\left(1+\frac{\omega\varepsilon}{D_5}\right).$$

Theorem 4.2.2. *The HIV/AIDS-free equilibrium E_h^0 is locally asymptotically stable whenever $\mathcal{R}_{0h} < 1$ and unstable if $\mathcal{R}_{0h} > 1$.*

Proof. The Jacobian of system (4.2) at the HIV/AIDS-free equilibrium E_h^0 is

$$\begin{pmatrix} -D_1 & 0 & \frac{\mu(\rho-1)\gamma_h}{D_1} & \frac{\mu(\rho-1)\varepsilon\gamma_h}{D_1} \\ \xi & -\mu & -\frac{\gamma_h(\mu\rho+\xi)}{D_1} & -\frac{\varepsilon\gamma_h(\mu\rho+\xi)}{D_1} \\ 0 & 0 & \gamma_h - D_4 & \varepsilon\gamma_h \\ 0 & 0 & \omega & -D_5 \end{pmatrix}.$$

It is easy to see that $-\mu$ and $-D_1$ are negative eigenvalues. The remaining two eigenvalues are

the eigenvalues of the 2×2 matrix

$$\begin{pmatrix} \gamma_h - D_4 & \varepsilon\gamma_h \\ \omega & -D_5 \end{pmatrix}.$$

The characteristic equation takes the form

$$\ell^2 + a_1\ell + a_2 = 0\,, \tag{4.4}$$

where $a_1 = \left(D_5 + D_4\left(1 - \frac{\gamma_h}{D_4}\right)\right)$ and $a_2 = D_4D_5(1 - \mathscr{R}_{0h})$.

The stability of E_h^0 relies on the sign of the roots of equation (4.4). By Routh-Hurwitz condition (see Theorem A.1.4 from Appendix A.1), equation (4.4) has negative real part if $a_1 > 0$ and $a_2 > 0$. For $\mathscr{R}_{0h} < 1$, it is easy to see that the condition $a_1, a_2 > 0$ are satisfied. Therefore, E_h^0 is locally asymptotically stable whenever $\mathscr{R}_{0h} < 1$. If $\mathscr{R}_{0h} > 1$, $a_2 > 0$ and Descartes rule of sign (Wang, 2004) implies (4.4) has a real positive solution. Which implies the disease-free equilibrium E_h^0 is unstable for $\mathscr{R}_{0h} > 1$. □

The biological implication of *Theorem* 4.2.2 is that a sufficiently small flow of HIV/AIDS infected individuals will not generate an outbreak of the disease unless $\mathscr{R}_{0h} > 1$.

Theorem 4.2.3. *E_h^0 is globally asymptotically stable for $\mathscr{R}_{0h} < 1$.*

Proof. Consider the Lyapunov function given by,

$$L = \frac{1}{D_4}\left(1 + \frac{\omega\varepsilon}{D_5}\right) I_H + \frac{\varepsilon}{D_5} A.$$

$L = 0$ for $I_H,\ I_A = 0$ and $L > 0$ for $I_H,\ I_A \neq 0$. Furthermore,

$$\begin{aligned} L' =& \frac{1}{D_4}\left(1 + \frac{\omega\varepsilon}{D_5}\right) I_H' + \frac{\varepsilon}{D_5} A' \\ =& \frac{1}{D_4}\left(1 + \frac{\omega\varepsilon}{D_5}\right)\left(\frac{(S+V)}{N}\gamma_h(I_H + \varepsilon I_A) - D_4 I_H\right) + \frac{\varepsilon}{D_5}(\omega I_H - D_5 I_A) \\ \leq& (\mathscr{R}_{0h} - 1)(I_H + \varepsilon I_A) \end{aligned}$$

Thus, $L' < 0$ for $\mathscr{R}_{0h} < 1$ and $L' = 0$ for $\mathscr{R}_{0h} = 1$ or $I_H = 0$. It follows that, if $I_H = 0$, then $S \to \frac{\Lambda(1-\rho)}{D_1}$ and $V \to \frac{\Lambda(\rho\mu+\xi)}{\mu D_1}$ as $t \to \infty$. That is, $\{E_h^0\}$ is the largest invariant set such that $L' = 0$. Following Theorem A.1.6 (see Appendix A.1), we can conclude that $\{E_h^0\}$ is globally asymptotically stable. That is, when $\mathscr{R}_{0h} < 1$, all solutions of (4.2) converge to the disease-free equilibrium E_h^0. □

The epidemiological implication of this *Theorem* 4.2.3 is that independent of the initially available sub-populations in model (4.2), HIV/AIDS infected individuals will not lead to the large outbreaks and disease will die out in the long run. That is, the HIV/AIDS infected population vanishes in time.

Theorem 4.2.4. *The HIV/AIDS sub-model* (4.2) *has a unique endemic equilibrium if and only if* $\mathscr{R}_{0h} > 1$.

Proof. The endemic equilibrium of HIV/AIDS sub-model, $E_H^* = (S^*, V^*, I_H^*, I_A^*)$, is given by

$$S^* = \frac{(1-\rho)\Lambda}{D_1 + \lambda_H^*},\ V^* = \frac{\rho\Lambda + \xi S^*}{\mu + \lambda_H^*},\ I_A^* = \frac{\omega}{D_5} I_H^*,\ I_H^* = \frac{(S^* + V^*)\lambda_H^*}{D_4} \tag{4.5}$$

Substituting (4.5) into λ_H^*, we obtain

$$\lambda_H^* \left(\lambda_H^* - \frac{D_4 D_5 (\mathscr{R}_{0h} - 1)}{\omega + D_5} \right) = 0. \tag{4.6}$$

From (4.6), $\lambda_H^* = \frac{D_4 D_5 (\mathscr{R}_{0h} - 1)}{\omega + D_5}$ is used to establish the endemic equilibrium E_H^*. It is clear that $\lambda_H^* > 0$ if and only if $\mathscr{R}_{0h} > 1$. Thus, HIV/AIDS sub-model (4.2) has a unique positive solution whenever $\mathscr{R}_{0h} > 1$. Furthermore, $\mathscr{R}_{0h} < 1$ implies that the force of infection λ_H^* is negative (which is biologically meaningless). In this instance, the model does not have a positive equilibrium. Epidemiologically, this result implies that once the disease invades the population, the epidemic persists, and the number of population in S, V, I_H and I_A eventually approach the numbers S^*, V^*, I_H^* and I_A^*, respectively. □

4.2.3 COVID-19 Sub-model Analysis

Setting $I_H = 0$, $I_A = 0$, $I_{HC} = 0$, $I_{AC} = 0$, $D_{HC} = 0$ for (4.1), we obtain the COVID-19 sub-model which is given by:

$$\begin{cases} S' = (1-\rho)\Lambda + \psi R - (D_1 + \lambda_C) S, \\ V' = \rho\Lambda + \xi S - (\mu + \sigma\lambda_C) V, \\ I_C' = \lambda_C S + \sigma\lambda_C V - D_2 I_C, \\ R' = \theta I_C - D_3 R, \end{cases} \tag{4.7}$$

where the force of infection of the COVID-19 sub model (4.1) is $\lambda_C = \gamma_c \frac{I_C}{N}$.

Equilibria and reproduction number

Setting $I_C' = 0$ in (4.7) and using the same method as in Section 4.2.2, we obtain the COVID-19 free equilibrium which is denoted by E_c^0. It follows that,

$$E_c^0 = \left(\frac{\Lambda(1-\rho)}{D_1}, \frac{\Lambda(\rho\mu+\xi)}{\mu D_1}, 0, 0 \right).$$

By implementing the next-generation matrix method outlined in Appendix A.2 and considering I_C as the infected compartment, while treating S, V, and R as non-infected compartments, the reproduction number for the COVID-19 sub-model($\mathscr{R}_{0c}$) is calculated to be

$$\mathscr{R}_{0c} = \frac{(1-\rho)\mu\gamma_c}{D_1 D_2} + \frac{\sigma(\rho\mu+\xi)\gamma_c}{D_1 D_2}.$$

The reproduction number tells us how many secondary cases will one infected individual produce in an entirely susceptible population of hosts. In other words, it tells the number of infected people that are generated by the introduction of a single infected person into a susceptible population. The epidemiological interpretations of each term in $\mathscr{R}_{0c}$ are presented in the following way:

- The first term in $\mathscr{R}_{0c}$, given by $\frac{(1-\rho)\mu\gamma_c}{D_1 D_2}$, gives the number of secondary infections of susceptible individuals that an infected individual with COVID-19 can produce in a disease-free population.
- The second term in $\mathscr{R}_{0c}$, given by $\frac{\sigma(\rho\mu+\xi)\gamma_c}{D_1 D_2}$, gives the number of secondary infections of vaccinated individuals that a COVID-19 infected individual can produce in a disease-free population.

In the absence of vaccination, when $\sigma = 0$ and $\xi = 0$, $\mathscr{R}_{0c}$ is given by

$$\mathscr{R}_{0c}^* = \mathscr{R}_{0c} = \frac{\gamma_c}{D_2}.$$

Biologically, $\mathscr{R}_{0c}^*$ represents the number of secondary infections caused by one infected individual during the mean course of infection $(1/D_2)$ in a completely susceptible population.

The controlled reproduction $\mathscr{R}_{0c}$ can be written as

$$\mathscr{R}_{0c} = \left(\frac{(1-\rho)\mu + (\rho\mu+\xi)\sigma}{D_1} \right) \mathscr{R}_{0c}^*.$$

Which implies,

$$\frac{\partial \mathscr{R}_{0c}}{\partial \xi} = -\frac{(1-\rho)(1-\sigma)\mu}{D_1}\mathscr{R}^*_{0c} < 0, \quad \lim_{\xi\to\infty} \mathscr{R}_{0c} = \sigma\mathscr{R}^*_{0c} \quad \text{and} \quad \mathscr{R}_{0c} < \mathscr{R}^*_{0c}.$$

That is,

$$\sigma\mathscr{R}^*_{0c} < \mathscr{R}_{0c} < \mathscr{R}^*_{0c}.$$

If $\mathscr{R}^*_{0c} < 1$, then $\mathscr{R}_{0c} < 1$. This shows that vaccination coverage plays an important role in controlling the COVID-19 disease. However, for $\mathscr{R}^*_{0c} > 1$

$$\sigma\mathscr{R}^*_{0c} < 1 \quad \text{if and only if} \quad \sigma > \frac{1}{\mathscr{R}^*_{0c}}.$$

Thus, when $\mathscr{R}^*_{0c} > 1$ elimination of COVID-19 from the population relies on the vaccine efficacy, not on the vaccine coverage. For $\mathscr{R}_{0c} = 1$, that is, for $\sigma\mathscr{R}^*_{0c} < 1$, there exists a critical proportion of vaccination that will achieve eradication. Thus, the critical vaccination proportion for eradication of the disease, ξ^C, is given by

$$\xi^C = \frac{\mu(1-\mathscr{R}^*_{0c})}{\sigma\mathscr{R}^*_{0c} - 1}.$$

Theorem 4.2.5. *The COVID-19-free equilibrium E^0_c is locally asymptotically stable whenever $\mathscr{R}_{0c} < 1$ and unstable if $\mathscr{R}_{0c} > 1$.*

Proof. Jacobian of (4.7) at E^0_c, denoted by $\mathcal{J}$, is

$$\mathcal{J} = \begin{pmatrix} -D_1 & 0 & -\frac{\mu(1-\rho)\gamma_c}{D_1} & \psi \\ \xi & -\mu & -\frac{\sigma\gamma_c(\mu\rho+\xi)}{D_1} & 0 \\ 0 & 0 & -D_2(1-\mathscr{R}_{0c}) & 0 \\ 0 & 0 & \theta & -D_3 \end{pmatrix}.$$

The eigenvalues of $\mathcal{J}$ are: $-\mu$, $-D_1$ and $-D_2(1-\mathscr{R}_{0c})$. We can see that all eigenvalues are negative provided that $\mathscr{R}_{0c} < 1$. Therefore, we can conclude that E^0_c is locally asymptotically stable whenever $\mathscr{R}_{0c} < 1$. □

The epidemiological implication of Theorem 4.2.5 is that COVID-19 transmission control can be achieved by setting parameter values so that $\mathscr{R}_{0c} < 1$ if the initial size of the subpopulations involved in (4.7) is in the basin of attraction of E^0_c. Thus, a sufficiently small flow of infectious individuals will not generate an outbreak and the disease can be eliminated from

the community. On the other hand, if $\mathscr{R}_{0c} > 1$, the entire population will get infected quickly because a single infected person can spread COVID-19 to several people.

The endemic equilibrium point is represented by $E_c^* = (S^*, V^*, I_C^*, R^*)$ and it is obtained by equating system (4.7) to zero and solving for state variables. Indeed, we come up with the following equilibrium points,

$$S^* = \frac{(1-\rho)\Lambda + \psi R^*}{D_1 + \lambda_C^*}, \quad V^* = \frac{\rho\Lambda + \xi S^*}{\mu + \sigma\lambda_C^*}, \quad I_C^* = \frac{(S^* + \sigma V^*)\lambda_C^*}{D_2} \text{ and } R^* = \frac{\theta I_C^*}{D_3}. \tag{4.8}$$

Substituting (4.8) into λ_C^* implies that the endemic equilibrium of the model (4.7) meets the following equation.

$$\lambda_C^*(K\lambda_C^{*^2} + L\lambda_C^* + M) = 0,$$

where

$$\begin{aligned} K =& \sigma(\theta + D_3), \\ L =& \frac{D_1 D_2 \mathscr{R}_{0c}(\theta + D_3)}{\gamma_c} + \rho(1-\sigma)(D_2 D_3 - \theta\psi) + \sigma D_2 D_3 - \sigma\gamma_c D_3 \text{ and} \\ M =& D_1 D_2 D_3 (1 - \mathscr{R}_{0c}). \end{aligned}$$

The COVID-19-free equilibrium E_c^0 is obtained for $\lambda_C^* = 0$. The endemic equilibrium corresponds to the solution of

$$K\lambda_C^{*^2} + L\lambda_C^* + M = 0. \tag{4.9}$$

The endemic equilibrium is obtained by substituting the solution of (4.9) in S^*, V^*, I^* and R^*. If $\mathscr{R}_{0c} > 1$(or $M < 0$), then (4.9) has a unique positive root $\lambda_C^* = \frac{-L+\sqrt{\Delta}}{2K}$, where $\Delta = L^2 - 4KM > 0$. If $\mathscr{R}_0 = 1$(or $M = 0$), then (4.9) has a unique positive solution $\lambda_C^* = \frac{-L}{2K}$, provided that $L < 0$. Here, if $L = 0$, then $\lambda_C^* = 0$, which in turn gives E_c^0, and if $L > 0$, then $\lambda_C^* < 0$ and this does not make sense in epidemiology. For $\mathscr{R}_{0c} < 1$(or $M > 0$) and $\Delta > 0$, we consider two cases:

case1: If $L > 0$, then $\lambda_C^* < 0$, that is (4.9) had no positive solution.

case2: If $L < 0$, that is if $L < -2\sqrt{KM} < 0$, then (4.9) had two endemic equilibria.

Considering these different cases for the solution of (4.9), a theorem is established as follows.

Theorem 4.2.6. *The sub-model* (4.7) *has*

1. *a unique endemic equilibrium if*

   (a) $M < 0$ *if and only if* $\mathscr{R}_{0c} > 1$*;*

(b) $L < 0$ *and* $M = 0$ *or* $L^2 - 4KM = 0$*;*

2. *two endemic equilibria if* $M > 0,\ L < 0$ *and* $L^2 - 4KM > 0$*;*

3. *no endemic equilibrium otherwise.*

When the $\mathscr{R}_{0c} < 1$, the second case of Theorem 4.2.6 suggests the probability of backward bifurcation where a stable COVID-19-free and a stable endemic equilibrium coexist.

Backward bifurcation analysis

Backward bifurcation analysis of COVID-19 sub-model (4.7) was carried out by employing the center manifold theory (see Appendix A.3). We modify variables in the following manner to implement the center manifold theory.

$$x_1 = S,\ x_2 = V,\ x_3 = I_C,\ x_4 = R,\ \text{so that}\ ,\ N = x_1 + x_2 + x_3 + x_4\ \text{ and }\ \lambda_C = \frac{\gamma_c x_3}{N}.$$

Moreover, with $x = (x_1,\ x_2,\ x_3,\ x_4)^T$, system (4.7) can be expressed as $x' = (f_1,\ f_2,\ f_3,\ f_4)^T$. That is also,

$$\begin{cases} \frac{dx_1}{dt} = f_1 = (1-\rho)\Lambda + \psi x_4 - (D_1 + \lambda_C)\, x_1, \\ \frac{dx_2}{dt} = f_2 = \rho\Lambda + \xi x_1 - (\mu + \sigma\lambda_C) x_2, \\ \frac{dx_3}{dt} = f_3 = \lambda_C x_1 + \sigma\lambda_C x_2 - D_2 x_3, \\ \frac{dx_4}{dt} = f_4 = \theta x_3 - D_3 x_4. \end{cases} \tag{4.10}$$

The Jacobian of the system (4.10) at E_c^0 is given by,

$$\begin{pmatrix} -D_1 & 0 & -\frac{\gamma_c \mu(1-\rho)}{D_1} & \psi \\ \xi & -\mu & -\frac{\gamma_c \sigma(\mu\rho+\xi)}{D_1} & 0 \\ 0 & 0 & \frac{\gamma_c((1-\rho)\mu+\sigma(\rho\mu+\xi))}{D_1} - D_2 & 0 \\ 0 & 0 & \theta & -D_3 \end{pmatrix}. \tag{4.11}$$

Choosing γ_c as the bifurcation parameter and setting $\mathscr{R}_{0c} = 1$ gives

$$\gamma_c^* = \gamma_c = \frac{D_1 D_2}{((1-\rho)\mu + \sigma(\rho\mu + \xi))}.$$

For $\gamma_c = \gamma_c^*$, equation (4.11) has eigenvalues $-\mu - \xi$, $-\mu$, $-D_3$ and 0. We, therefore, apply the Center Manifold Theorem to analyze the dynamics of (4.10) about $\gamma_c = \gamma_c^*$.

The right-eigenvector $\mathbf{w} = (w_1,\ w_2,\ w_3,\ w_4)^T$ related to zero eigenvalue of (4.11) is

$$w_4 = \frac{\theta w_3}{D_3},\ \ w_1 = \frac{1}{D_1}\left(w_4\psi - \frac{\gamma_c\mu(1-\rho)w_3}{D_1}\right)$$
$$w_2 = \frac{1}{\mu}\left(\xi w_1 - \frac{\gamma_c\sigma w_3(\mu\rho+\xi)}{D_1}\right),\ \ w_3 > 0.$$

Similarly, the left-eigenvector $\mathbf{u} = (u_1,\ u_2,\ u_3,\ u_4)^T$ associated with the zero eigenvalue becomes

$$u_1 = 0,\ u_2 = 0,\ u_3 > 0,\ u_4 = 0.$$

There is no need to calculate the derivatives of f_1, f_2 and f_4. They are zero since u_1, u_2 and u_3 are all zero. From the derivatives of f_3, coefficients a and b defined in Appendix A.3 are computed as follows:

$$\begin{aligned}
a &= \sum_{k,i,j=1}^{4} v_k w_i w_j \frac{\partial^2 f_k}{\partial x_i \partial x_j}(E_c^0, \gamma_c^*) \\
&= \sum_{i,j=1}^{4}\left[v_3 w_i w_j \frac{\partial^2 f_3}{\partial x_i \partial x_j}(E_c^0, \gamma_c^*)\right] \\
&= \frac{2\gamma_c^*\mu v_3 w_3^2}{D_1 D_3 \Lambda}\left[\sigma\gamma_c^* D_3 - \left(\rho(1-\sigma)(D_2D_3 - \theta\psi) + \sigma D_2 D_3 + \frac{D_1 D_2(\theta + D_3)}{\gamma_c^*}\right)\right] \quad \text{and} \\
b &= \sum_{k,j=1}^{4} v_k w_j \frac{\partial^2 f_k}{\partial x_j \partial \beta}(E_c^0, \gamma_c^*) = \sum_{i=1}^{4} v_3 w_i \frac{\partial^2 f_3}{\partial x_i \partial \beta}(E_c^0, \gamma_c^*) = \frac{D_2 v_3 w_3}{\gamma_c^*}
\end{aligned}$$

From this result, we can observe that the COVID-19 sub-model exhibits backward bifurcation whenever $a > 0$. If the vaccine is perfect and there is no reinfection possibility for vaccinated individuals, that is, if $\sigma = 0$, the value of a becomes negative, which implies system (4.7) has a trans-critical bifurcation. The epidemiological significance of backward bifurcation is that, besides making $\mathscr{R}_{oc} < 1$, it needs more action to reduce COVID-19 disease transmission through the population. Figure 4.2 show the phenomenon of backward bifurcation as evidence of the COVID-19 sub-model analysis. A stable equilibrium is represented by a solid line and an unstable one by a dashed line. It confirms the analytical result, which show that endemic equilibrium exists when $\mathscr{R}_{oc} < 1$.

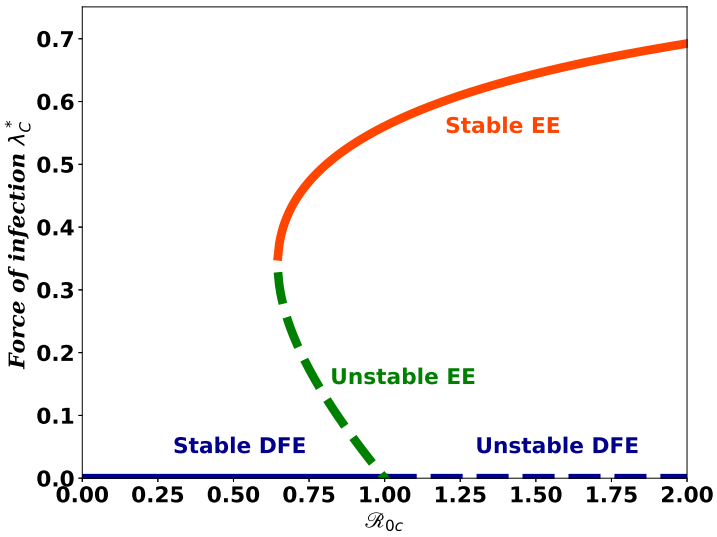

Figure 4.2: Backward bifurcation diagram for COVID-19 sub-model

4.2.4 Co-infection Model Analysis

Following the same procedure as in Section 4.2.2, the co-infection free equilibrium of model (4.1), denoted by E^0, can be obtained as

$$E^0 = \left(\frac{\Lambda(1-\rho)}{D_1}, \frac{\Lambda(\rho\mu+\xi)}{\mu D_1}, 0, 0, 0, 0, 0, 0, 0 \right).$$

The next generation matrix approach, established in Van den Driessche, P. and Watmough, J. (2002) (see Appendix A.2), is used to determine the reproduction number as follows. The rate of appearance of new infection and rate of transfer from one compartment to another in the infectious classes gives the following:

$$\mathcal{F} = \begin{pmatrix} (S+\sigma V)\lambda_C \\ (S+V)\lambda_H \\ 0 \\ \lambda_C I_H + \lambda_H I_C \\ \kappa\lambda_C \\ 0 \end{pmatrix} \text{ and } \mathcal{V} = \begin{pmatrix} (D_2+\lambda_H)I_C \\ (D_4+\lambda_C)I_H - \alpha I_{HC} \\ (\kappa\lambda_C + D_5)I_A + \omega I_H + \varphi I_{HC} \\ D_6 I_{HC_A} \\ D_7 I_{AC} - \phi I_{HC} \\ D_8 D_{HC} - \eta_1 I_{HC} - \eta_2 I_{AC} \end{pmatrix}.$$

The Jacobian of $\mathcal{F}$ and $\mathcal{V}$ at disease-free equilibrium E^0 are given as follows,

$$F = \begin{pmatrix} \frac{\gamma_c((1-\rho)\mu+\sigma(\mu\rho+\xi))}{D_1} & 0 & 0 & \frac{\gamma_c((1-\rho)\mu+\sigma(\mu\rho+\xi)+)}{D_1} & \frac{\gamma_c((1-\rho)\mu+\sigma(\mu\rho+\xi))}{D_1} & 0 \\ 0 & \gamma_h & \varepsilon\gamma_h & \gamma_h & \varepsilon\gamma_h & 0 \\ 0 & 0 & 0 & 0 & 0 & 0 \\ 0 & 0 & 0 & 0 & 0 & 0 \\ 0 & 0 & 0 & 0 & 0 & 0 \\ 0 & 0 & 0 & 0 & 0 & 0 \end{pmatrix} \text{ and}$$

$$V = \begin{pmatrix} D_2 & 0 & 0 & 0 & 0 & 0 \\ 0 & D_4 & 0 & -\alpha & 0 & 0 \\ 0 & -\omega & D_5 & 0 & -\varphi & 0 \\ 0 & 0 & 0 & D_6 & 0 & 0 \\ 0 & 0 & 0 & -\phi & D_7 & 0 \\ 0 & 0 & 0 & -\eta_1 & -\eta_2 & D_8 \end{pmatrix}.$$

Which implies,

$$FV^{-1} = \begin{pmatrix} \mathscr{R}_{0c} & 0 & 0 & \frac{D_2\mathscr{R}_{0c}(D_7+\phi)}{D_6D_7} & \frac{D_2\mathscr{R}_{0c}}{D_7} & 0 \\ 0 & \mathscr{R}_{0h} & \frac{\varepsilon\gamma_h}{D_5} & \frac{\gamma_h(\alpha D_7(D_5+\omega\varepsilon)+D_4(D_5(D_7+\varepsilon\phi)+\varphi\varepsilon\phi))}{D_4D_5D_6D_7} & \frac{\varepsilon(D_5+\varphi)\gamma_h}{D_5D_7} & 0 \\ 0 & 0 & 0 & 0 & 0 & 0 \\ 0 & 0 & 0 & 0 & 0 & 0 \\ 0 & 0 & 0 & 0 & 0 & 0 \\ 0 & 0 & 0 & 0 & 0 & 0 \end{pmatrix}$$

The reproduction number, $\mathscr{R}_0$, for the COVID-19-HIV/AIDS co-infection model is the maximum of eigenvalues of the next generation matrix, FV^{-1}. That is, $\mathscr{R}_0 = max\{0, \mathscr{R}_{0c}, \mathscr{R}_{0h}\}$. Thus,

$$\mathscr{R}_0 = max\{\mathscr{R}_{0c}, \mathscr{R}_{0h}\}.$$

This implies that the dynamics of COVID-19 and HIV/AIDS co-infection will be dominated by the disease with the bigger reproduction number. From Theorem 2 of Van den Driessche, P. and Watmough, J. (2002), the following theorem is deduced.

Theorem 4.2.7. *The disease-free equilibrium E^0 is locally asymptotically stable if $\mathscr{R}_0 < 1$ and unstable if $\mathscr{R}_0 > 1$.*

To investigate the global stability of E^0 we apply the approach in Chavez, C Castillo et al.

(2002). First, we write system (4.1) in the form

$$\begin{aligned}\frac{d\mathbf{X}}{dt} &= F(\mathbf{X},\mathbf{I})\\ \frac{d\mathbf{I}}{dt} &= G(\mathbf{X},\mathbf{I}),\ G(\mathbf{X},\mathbf{0}) = \mathbf{0}\end{aligned}$$

where $\mathbf{X} = (S,V,R)$ and $\mathbf{I} = (I_C, I_H, I_A, I_{HC}, I_{AC}, D_{HC})$ denotes uninfected and infected population respectively. $U_0 = (\mathbf{X}^*, \mathbf{0})$ denotes the disease-free equilibrium of system (4.1). Furthermore, suppose

$H1:$ For $\frac{d\mathbf{X}}{dt} = F(\mathbf{X},\mathbf{0})$, $\mathbf{X}^*$ is globally asymptotically stable,

$H2:$ $G(\mathbf{X},\mathbf{I}) = A\mathbf{I} - \hat{G}(\mathbf{X},\mathbf{I})$, $\hat{G}(\mathbf{X},\mathbf{I}) \geq 0$ for $(\mathbf{X},\mathbf{I}) \in \Theta$, where $A = D_{\mathbf{I}}G(\mathbf{X}^*,\mathbf{0})$ is an M-matrix (the off-diagonal elements of A are nonnegative).

Theorem 4.2.8. *The disease-free equilibrium $U_0 = (\mathbf{X}^*,\mathbf{0})$ is a globally asymptotic stable equilibrium of (4.1) provided that $\mathscr{R}_0 < 1$ and that assumptions (H1) and (H2) are satisfied.*

Proof. Writing system (4.1) for investigating H1 and H2, we have

$$F(\mathbf{X},\mathbf{0}) = \begin{pmatrix}(1-\rho)\Lambda + \psi R - D_1 S\\ \rho\Lambda + \xi S - \mu V\\ -D_3 R\end{pmatrix},$$

$$A = \begin{pmatrix}-D_2(1-\mathscr{R}_0) & 0 & 0 & D_2\mathscr{R}_0 & D_2\mathscr{R}_0 & 0\\ 0 & \gamma_h - D_4 & \varepsilon\gamma_h & \alpha+\gamma_h & \varepsilon\gamma_h & 0\\ 0 & \omega & -D_5 & 0 & \varphi & 0\\ 0 & 0 & 0 & -D_6 & 0 & 0\\ 0 & 0 & 0 & \phi & -D_7 & 0\\ 0 & 0 & 0 & \eta_1 & \eta_2 & -D_8\end{pmatrix}$$

and

$$\hat{G}(\mathbf{X},\mathbf{I}) = \begin{pmatrix}\left(D_2\mathscr{R}_{oc} - \frac{(S+\sigma V)\gamma_c}{N}\right)(I_C + I_{HC} + I_{AC}) + \lambda_H I_C\\ \gamma_h\left(1 - \frac{S+V}{N}\right)(I_H + I_{HC} + I_{AC}) + \lambda_C I_H\\ \kappa\lambda_C I_A\\ -\lambda_C I_H - \lambda_H I_C\\ -\kappa\lambda_C I_A\\ 0\end{pmatrix}.$$

The matrix A is M-matrix, but all rows of $\hat{G}(\mathbf{X},\mathbf{I})$ are not non negative for all $(\mathbf{X},\mathbf{I}) \in \Theta$. So assumption H2 is not satisfied. Hence, the disease-free equilibrium E^0 may not be globally stable, and backward bifurcation may occur in the system (4.1). That is, the co-infection may persist even if the dominant reproduction number ($\mathscr{R}_0$) is less than unity. However, if maximum protection is provided against the COVID-19 and HIV/AIDS co-infection, that is, if the third and fourth rows of $\hat{G}(\mathbf{X},\mathbf{I})$ are positive, then global stability of disease free equilibrium may be achieved. That is to say, if incidences of co-infection are kept to an absolute minimum, efforts made to fight COVID-19 and HIV/AIDS may become successful.

□

4.2.5 Effects of Control Parameters and Transmission Rate on $\mathscr{R}_{0c}$ and $\mathscr{R}_{0h}$

In this section, the impact of some parameters on reproduction numbers is analyzed qualitatively. Effects of the control parameter, ξ and θ, and transmission rates, γ_c, analysis are performed by evaluating the partial derivatives of the reproduction numbers with respect to these parameters. We can see that

$$\frac{\partial \mathscr{R}_{0c}}{\partial \xi} = -\frac{\mu(1-\rho)(1-\sigma)\gamma_c}{D_1^2 D_2} < 0, \qquad \frac{\partial \mathscr{R}_{0c}}{\partial \theta} = -\frac{\gamma_c((1-\rho)\mu+\sigma(\mu\rho+\xi))}{D_1 D_2^2} < 0,$$
$$\frac{\partial \mathscr{R}_{0c}}{\partial \gamma_c} = \frac{((1-\rho)\mu+\sigma(\rho\mu+\xi))}{D_1 D_2} > 0, \qquad \frac{\partial \mathscr{R}_{0h}}{\partial \gamma_h} = \frac{1}{D_4}\left(1+\frac{\omega\varepsilon}{D_5}\right) > 0.$$

The reproduction number $\mathscr{R}_{0c}$ is a decreasing function with respect to the control parameters, ξ and θ. That means, for every value of ξ and θ, the vaccination of susceptible individuals and treating COVID-19-infected individuals step-down $\mathscr{R}_{0c}$ (see Figure 4.3) and therefore reduce the COVID-19 and HIV/AIDS co-infection cases. On the other hand, $\mathscr{R}_{0c}(\gamma_c)$ and $\mathscr{R}_{0h}(\gamma_h)$ are increasing functions for any γ_c and γ_h, respectively.

4.3 Parametric Estimation

Ethiopia is considered in estimating some model parameters. The scarcity of data on HIV and COVID-19 co-infection makes the fitting on real COVID-19 data only. The total number of people who have contracted COVID-19 each month since March 2020, when the disease first appeared in Ethiopia, was compiled from EPHI (2022a). Table 4.1 displays this data.

To fit the model to the actual data, the Python library's scipy function scipy.optimize.curve_fit(), an algorithm based on a Levenburg-Marquardt method to fit functions to data, is employed. Indeed, the required Python libraries were imported and the function that is to be fitted to the

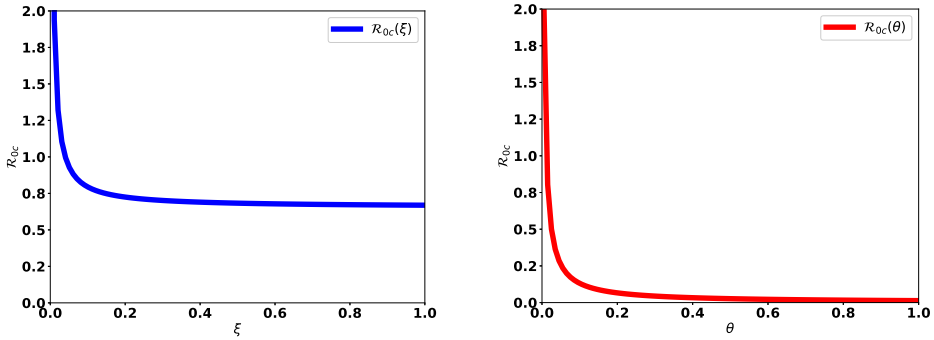

(a) Effects of COVID-19 vaccination rate(ξ) (b) Effects of COVID-19 treatment rate(θ)

Figure 4.3: $\mathscr{R}_{0c}$ for different values of vaccination and treatment rates.

existing data was defined. That is, system (4.1) with initial values was written as

$$\mathbf{x}' = g(t, \mathbf{x}, \mathbf{p}), \quad \mathbf{x}(\mathbf{t_0}) = \mathbf{x_0}, \tag{4.12}$$

where $\mathbf{p}$ is a vector of parameters for the model that need to be found and $\mathbf{x}$ is the vector of state variables.

The aim of the parametric estimation was to determine the parameter vector $\mathbf{p}$ so that the sum of the square of residuals

$$\sum_{i=1}^{n} (\mathbf{x_i} - \tilde{\mathbf{x}}_\mathbf{i})^2 \tag{4.13}$$

is as small as possible, where $\tilde{\mathbf{x}}_\mathbf{i}$ is the real data and $\mathbf{x_i} = \mathbf{x}(t_i, \mathbf{p})$ is a solution to (4.12) at time t_i for a given $\mathbf{p}$. In this regard, the curve_fit function returns the tuple of optimal parameters, in the sense that minimizing equation (4.13) subject to (4.12). The details of procedures for using scipy in fitting data are given in scipy.org (2021).

Data for the total population and the life expectancy of Ethiopia for the year 2021 were obtained from World Bank (2022). The total population and life expectancy are estimated to be $120,283,026$ and 65 years, respectively. It follows that $\mu = \frac{1}{(65\times 12)}$ per month and $\Lambda = \mu \times N = 154209$ people per month. On March 31, 2020, 25 people were found to be COVID-19 infected and 2 people were recovered from COVID-19. Since no vaccine was available and no co-infection was reported in the first month of the outbreak, we set the values of V, I_{HC}, I_{AC}, and D_{HC} to 0. For simulation purposes, the initial values for I_H and I_A are assumed as in Table 4.2. Furthermore, $S(0)$ is obtained by subtracting these initial values from the total population. These values were used to perform the relevant simulations and obtain the values of the parameters in Table 4.3 that were fitted to the real data. The solution curve in comparison to COVID-19 data

Table 4.1: COVID-19 cases in Ethiopia from March, 2020, to April 2023.

Months	Cases			
	2020	2021	2022	2023
January	- -	137650	465158	499531
February	- -	159072	468727	499981
March	25	206589	469758	500564
April	130	257442	470568	500834
May	950	271514	472743	- -
June	5846	276174	488724	- -
July	17530	280365	492237	- -
August	52131	308134	493190	- -
September	75368	345674	493579	- -
October	96169	365167	493960	- -
November	110074	371536	494578	- -
December	124264	420342	498001	- -

Table 4.2: Initial values for state variables

Variables	S	V	I_C	R	I_H	I_A	I_{HC}	I_{AC}	D_{HC}
Values	119663000	0	25	2	413333	206666	0	0	0

is shown in Figure 4.4.

4.4 Numerical Simulations and Results

Numerical simulations confirm the results of the qualitative analysis of the sub-models and the co-infection model. The impact of parameters on the expansion and control of COVID-19, HIV/AIDS and their co-infection were assessed. With some exceptions, initial conditions in Table 4.2 and values of parameters in Table 4.3 are employed to attain simulations.

The numerical simulation of the stability analysis of disease-free equilibria established in Theorem 4.2.3, and Theorem 4.2.7 are depicted in Figures 4.5 and 4.6, respectively. These figures are used to show how the models, the HIV/AIDS sub-model and co-infection, behave about the disease-free equilibria. The parameter values $\gamma_h = 0.00502$ and $\omega = 0.15$, so that $\mathscr{R}_{0h} = 0.459473$, with different initial conditions, are used to show the global stability of HIV/AIDS-free equilibrium (see Figure 4.5). On the other hand, $\gamma_c = 1.2$ and $\gamma_h = 0.008$, so $\mathscr{R}_0 = 0.791337$, are used to show the local stability of disease-free equilibrium of the full model. The Python script detailed in Appendix B.2 is utilized for generating these figures.

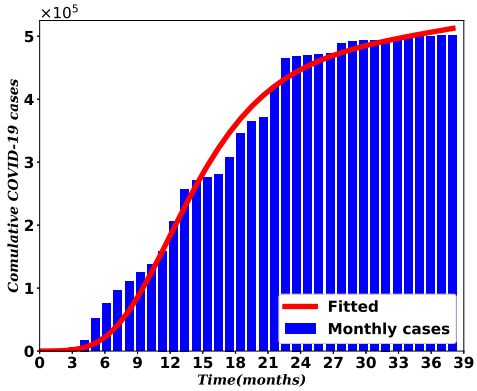

Figure 4.4: Model fit to real data

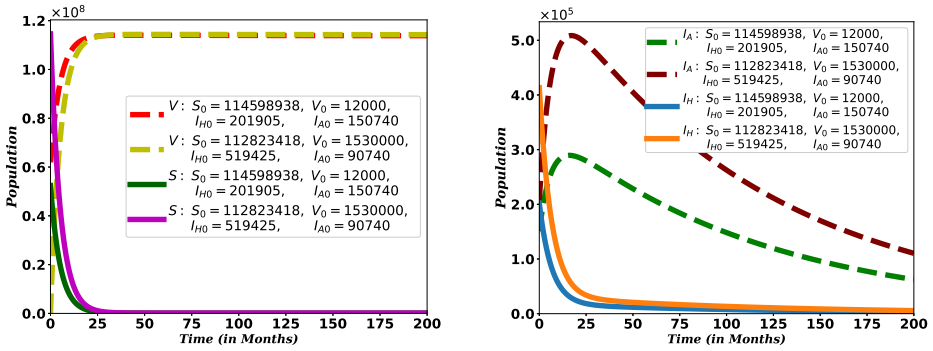

(a) Susceptible and Vaccinated

(b) HIV infected

Figure 4.5: Global stability of HIV-free equilibrium for HIV sub-model.

4.4.1 Transmission Rates Versus Co-infection Cases

Figure 4.7 show the contribution of HIV and COVID-19 to the population in D_{HC}. From Figure 4.7a, we can see that it is essential to bring down COVID-19 transmission rates to reduce the potential for death from the burden of both diseases, HIV and COVID-19.

In Figure 4.8, various transmission rates are used to illustrate how they affect the number of co-infected populations. These sub-figures show that as transmission rates decrease, the value of the graphs decreases. That is, a decrease in γ_c from 0.8 to 0.7 and γ_h from 0.095 to 0.075, decreases the co-infection cases significantly.

4.4.2 HIV Transmissibility and Immunosuppression

An increase in viral load in HIV/AIDS patients increases their ability to transmit the disease to uninfected people and makes them vulnerable to other diseases (Centers for Disease Control

Table 4.3: Values of parameters in Equation 4.1.

Parameters	Description	Values	Source
γ_c	Transmission rate of COVID-19	1.93768	Fitted
η_1	Risk of death rate for I_{HC}	0.02486	Fitted
γ_h	Effective transmission rate of HIV	0.011	Assumed
α	Recovery rate from COVID-19 for I_{HC}	0.1	Fitted
ρ	Ratio of vaccinated population	0.25	Assumed
δ_h	HIV induced death rate	0.016	(EPHI, 2022b)
ψ	COVID-19 reinfection rate	0.0048	Fitted
η_2	Risk of death rate for I_{AC}	0.0274	Fitted
ξ	COVID-19 vaccination rate	0.1935	Assumed
ω	HIV progression rate for I_H population	0.07	(Hussaini, N. et al., 2016)
σ	COVID-19 vaccine inefficacy	0.01	Assumed
φ	Recovery rate from COVID-19 for I_{AC}	0.0003	Fitted
θ	Recovery rate from COVID-19 for I_C	0.0121	Fitted
κ	Modification parameter	1.22	Assumed
ε	Modification parameter	1.385	Assumed
δ_{hc}	Co-infection induced death rate	0.03851	Fitted
δ_c	COVID-19 induced death rate	0.01511	Fitted
ϕ	HIV progression rate for I_{HC} population	0.00067	Assumed

and Prevention and others, 2018). Increased HIV transmissibility and exposure to COVID-19 may also increase the number of co-infections. Figures 4.9 and 4.10 confirm this phenomenon. From these figures, it can be seen that COVID-19 and HIV/AIDS co-infection increase with increased HIV transmissibility.

Moreover, in Figures 4.10a to 4.10c it is shown that HIV/AIDS immunosuppression increases the number of co-infection cases. That is, as the value of κ increases, the population in I_{HC}, I_{AC} and D_{HC} also increases. One way or another, it can be understood that HIV/AIDS viral load is directly related to the likelihood of contracting COVID-19, which may contribute to the risk of co-infection-related deaths (see Figure 4.10c). This implies that slowing the progression of the HIV/AIDS virus is important and critical to reducing the impact of COVID-19 and HIV/AIDS.

4.4.3 COVID-19 Treatment and Vaccine to Minimize Co-infection Cases and Risk of Death Among PLHIV

The impact of COVID-19 vaccine on the number of co-infected populations is illustrated in Figures 4.11 and 4.12. The sub-figures show that, as the value of the vaccination rate (ξ) of COVID-19 is increases, the number of co-infected populations decreases, which means the

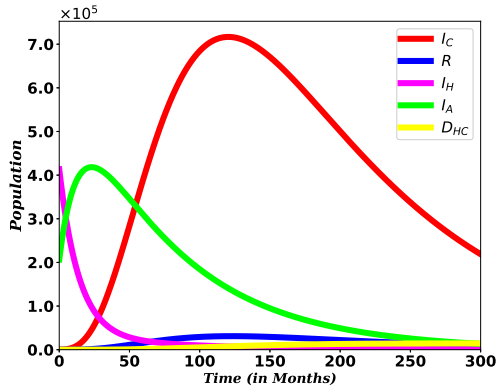

(a) R, I_C, I_H, I_A and D_{HC}

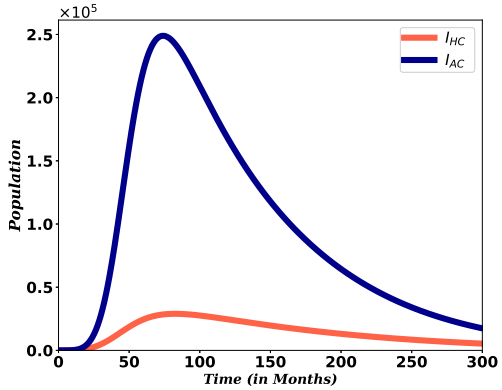

(b) I_{HC} and I_{AC}

Figure 4.6: Local stability of disease-free equilibrium E^0

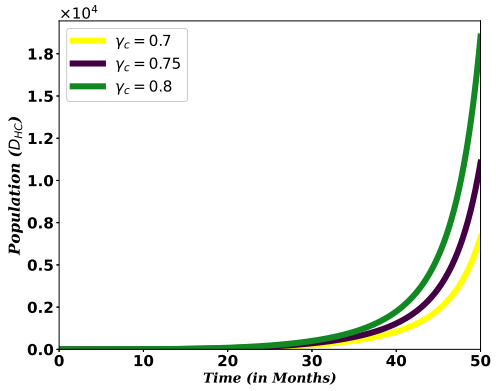

(a) D_{HC} for different values of γ_c

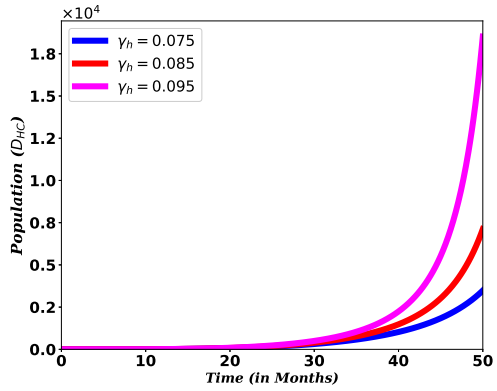

(b) D_{HC} for different values of γ_h

Figure 4.7: Simulation of D_{HC} for different values of transmissions rates γ_c and γ_h.

expansion of COVID-19 and HIV/AIDS co-infection will decrease.

For PLHIV, efforts such as vaccination minimize the chance of contracting COVID-19 disease, which might be one of the reasons for the relatively weak ability to produce antibodies and lower lymphocyte counts (Squillace, Nicola et al., 2021). Treating co-infected individuals plays a vital role in reducing the number of deaths among HIV/AIDS patients. Simulations in Figure 4.13 reveals that treating co-infected individuals have a reverse impact on increasing the death risk among PLHIV infected with COVID-19. This indicates COVID-19 diagnosis and treatment for HIV/AIDS infected people should be strengthened since it can lower fatalities from co-infection, especially when these people are vulnerable to the disease.

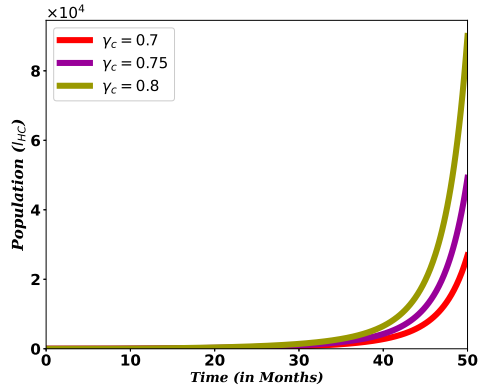

(a) I_{HC} for different values of γ_c

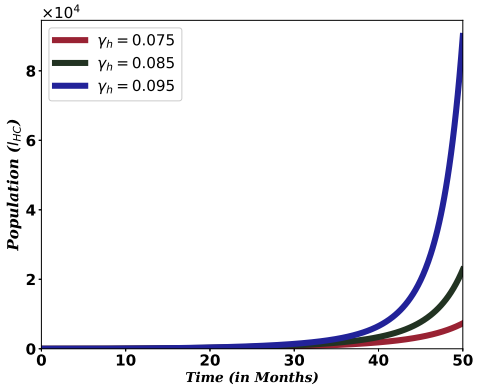

(b) I_{HC} for different values of γ_h

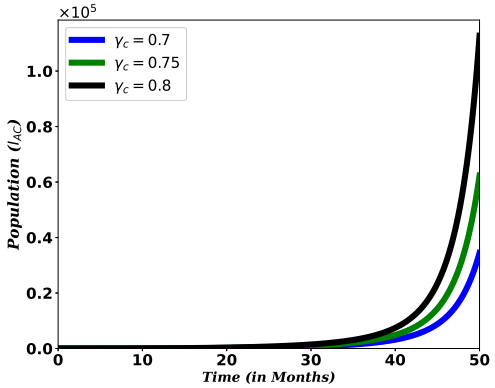

(c) I_{AC} for different values of γ_c

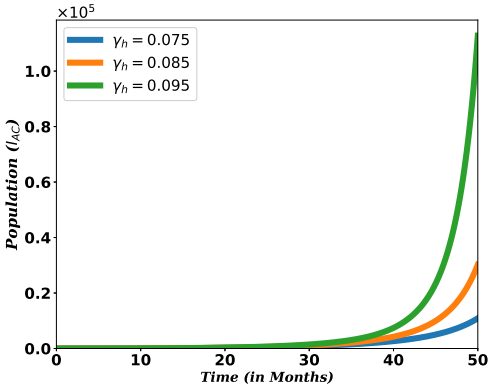

(d) I_{AC} for different values of γ_h

Figure 4.8: Simulation of I_{HC} and I_{AC} for different values of transmission rates γ_c and γ_h.

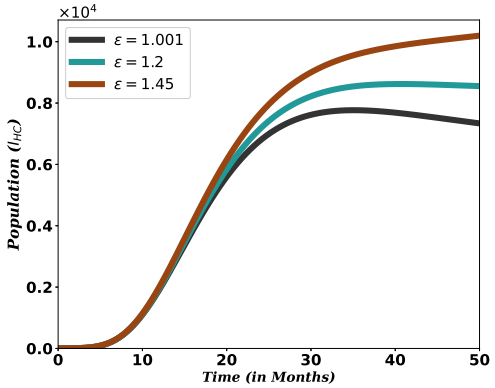

(a) Effect of ε on I_{HC}

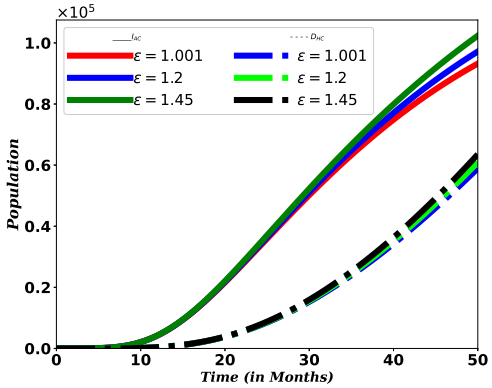

(b) Effect of ε on I_{AC}

Figure 4.9: Effects of ε on the number co-infection.

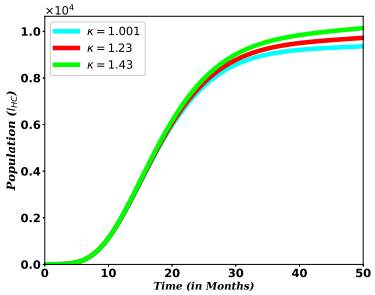

(a) Effect of κ on I_{HC}

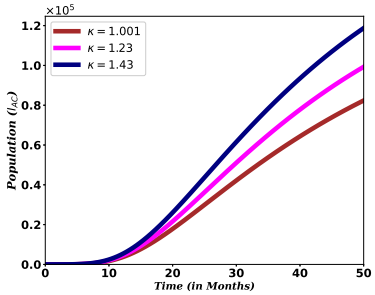

(b) Effect of κ on I_{AC}

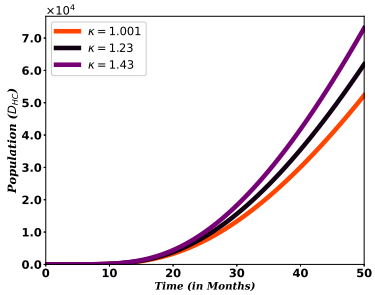

(c) Effect of κ on D_{HC}

Figure 4.10: Effects of κ on the number co-infection.

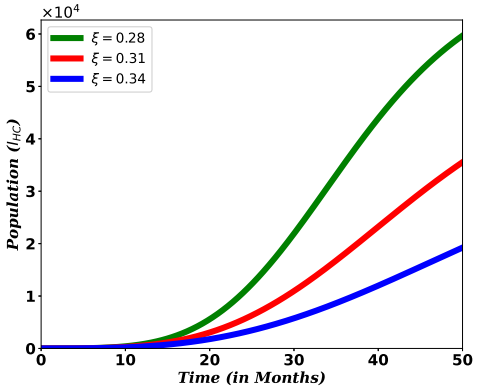

(a) Effect of vaccine on I_{HC}

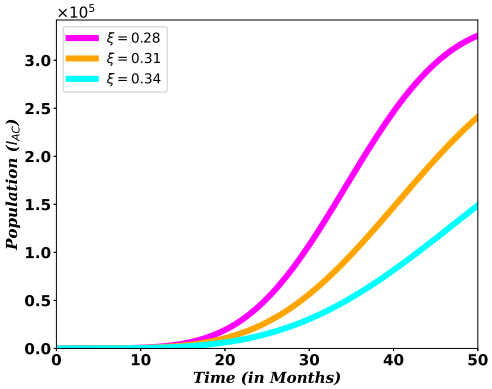

(b) Effect of vaccine on I_{AC}

Figure 4.11: Effects of COVID-19 vaccination I_{HC} and I_{AC} population.

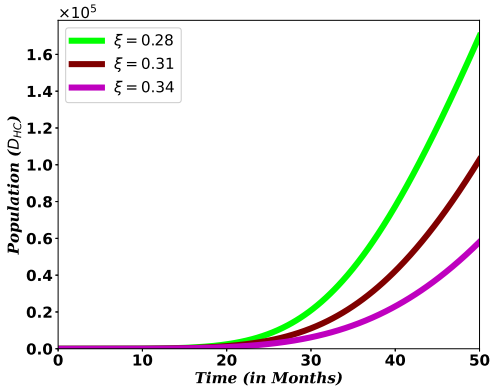

(a) Effect of vaccine(ξ)

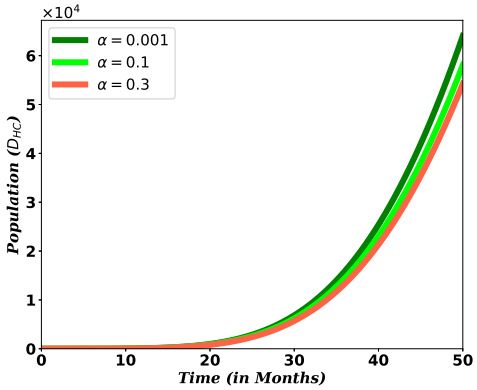

(b) Effect of treatment(α)

Figure 4.12: Effect of COVID-19 vaccination and treatment on D_{HC} population.

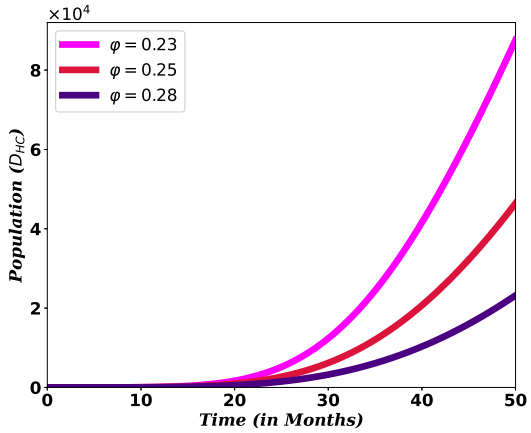

(a) Effect of treatment(φ)

Figure 4.13: Effect of COVID-19 treatment, for individuals in I_{AC} class, on D_{HC}.

CHAPTER 5

OPTIMAL CONTROL STRATEGIES FOR HIV AND COVID-19 CO-INFECTION: A COST-EFFECTIVENESS ANALYSIS

This chapter focuses on modeling the dynamics of co-infections involving COVID-19 and HIV. It begins with the formulation of a mathematical model that captures the transmission and progression of these diseases within a population. The analysis includes examining sub-models, the COVID-19 only and HIV only models, as well as their co-infection. The chapter further explores the impact of HIV on the endemic characteristics of COVID-19. Numerical simulations are used to illustrate the model's dynamics and the effectiveness of control measures. Lastly, the chapter discusses the cost-effectiveness of various control strategies, ranging from single to combined interventions, evaluating their impact on managing the co-infections.

5.1 Model Formulation

The HIV-COVID-19 co-infection model is structured by categorizing the total population into nine mutually exclusive compartments: susceptible (S), HIV-positive (H), HIV-positive individuals undergoing treatment (H^t), COVID-19-vaccinated (V_c), COVID-19-infected (C), individuals with both COVID-19 and HIV infections (H_c), individuals receiving HIV treatment who contract COVID-19 (H_c^t), recovered from COVID-19 (C^r) and individuals at risk of death due to co-infection (D_{hc}). Recruitment, denoted by the rate ψ, and immunity loss to the COVID-19 virus, with a rate of η_c, contribute to an increase in the susceptible population. Individuals susceptible to both COVID-19 and HIV can contract these diseases at rates represented by $\chi_C = \pi_c \frac{C+H_c+H_c^t}{N-D_{hc}}$, and $\chi_H = \pi_h \frac{H+H^t+H_c+H_c^t}{N-D_{hc}}$, respectively, from those actively infected with COVID-19 and HIV. Here, standard incidence functions are used to produce a more precise representation of frequency-dependent transmissions, such as HIV/AIDS, because the average number of sexual contacts per individual is relatively constant (Li, Michael Y, 2018; Martcheva, 2015; Samares, Pal et al., 2006). Furthermore, it is understood that the spread of COVID-19 might reach a threshold where adding more susceptible individuals does not significantly increase the rate of new infections due to variables such as self-protective measures (Manfredi, P. and D'Onofrio, A., 2013) and immunization (Ben Ashby and Alex Best, 2021; Ogidi, Odangowei Inetiminebiet al., 2021). This approach acknowledges that the number of contacts an individual has does not increase proportionally with population size, preventing overestimation of transmission in large populations (Samares, Pal et al., 2006). Presumably, individuals at risk

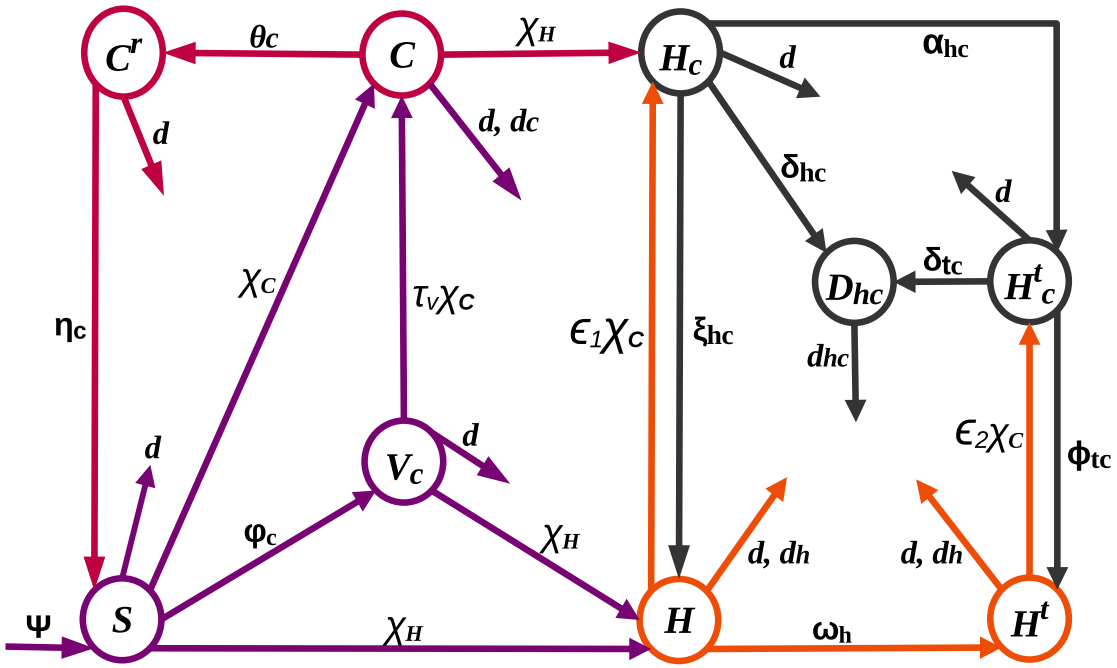

Figure 5.1: The HIV and COVID-19 co-infection model flow diagram.

of co-infection-related death (D_{hc}) receive specialized care and are excluded from the transmission of both diseases. The parameters π_h and π_c denote transmission probabilities for HIV and COVID-19 infections, respectively. Individuals who receive the COVID-19 vaccine transferred to the vaccinated class at a rate of φ_c. It is assumed that COVID-19 infection occurs at a reduced rate $\tau_v\chi_c$ among those who are vaccinated, where τ_v signifies vaccine inefficacy: $\tau_v = 0$ implies a perfect vaccine, rendering vaccinated individuals immune, while $\tau_v = 1$ indicates that vaccinated individuals face the same risk as the unvaccinated. On the other hand, individuals in the H and H^t classes, due to compromised immunity, experience increased rates of $\varepsilon_1\chi_c$ and $\varepsilon_2\chi_c$, for contracting COVID-19 (Danwang, Celestin et al., 2022; Höft, Maxine A. et al., 2024), where ε_1 and ε_2 are modification parameters. The H^t class expands at a rate of ω_h as individuals in the H class undergo treatment. Both H and H^t classes may experience HIV-related mortality at a rate of d_h. The rate of recovery from COVID-19 differ for individuals in the C, H_c and H_c^t classes, denoted by θ_c, ξ_{hc} and ϕ_{tc}, respectively. Individuals in the C class face mortality at a rate of d_c, while those in the H_c and H_c^t classes, becoming susceptible to death (Höft, Maxine A. et al., 2024), are added to D_{hc} at rates of δ_{hc} and δ_{tc}, respectively, before succumbing to the burden of co-infection at a rate of d_{hc}. Figure 5.1 illustrates the dynamic changes within these compartments.

Given the aforementioned assumptions and descriptions, we hereby formulate the following systems of nonlinear differential equations:

$$\begin{cases} S' = \psi - (\beta_1 + \chi_C + \chi_H)\, S + \eta_c C^r, \\ V_c' = \varphi_c S - (\tau_v \chi_C + \chi_H + d) V_c, \\ C' = \chi_C S + \tau_v \chi_C V_c - (\beta_2 + \chi_H) C, \\ C^{r\prime} = \theta_c C - \beta_3 C^r, \\ H' = (S + V_c)\chi_H + \xi_{hc} H_c - (\beta_4 + \varepsilon_1 \chi_C) H, \\ H^{t\prime} = \omega_h H + \phi_{tc} H_c^t - (\beta_5 + \varepsilon_2 \chi_C) H^t, \\ H_c' = \varepsilon_1 \chi_C H + \chi_H C - \beta_6 H_c, \\ H_c^{t\prime} = \varepsilon_2 \chi_C H^t + \alpha_{hc} H_c - \beta_7 H_c^t, \\ D_{hc}' = \delta_{hc} H_c + \delta_{tc} H_c^t - \beta_8 D_{hc}, \end{cases} \tag{5.1}$$

where $\beta_1 = \varphi_c + d$, $\beta_2 = d_c + d + \theta_c$, $\beta_3 = d + \eta_c$, $\beta_4 = \omega_h + d + d_h$, $\beta_5 = d_h + d$, $\beta_6 = d + \alpha_{hc} + \xi_{hc} + \delta_{hc}$, $\beta_7 = d + \phi_{tc} + \delta_{tc}$, and $\beta_8 = d_{hc} + d$.

The initial conditions of the equations of the model (5.1) are as follows:

$$\begin{cases} S(0) = S_0,\ V_c(0) = V_{c0},\ C(0) = C_0,\ C^r(0) = C_0^r,\ H(0) = H_0,\ H^t(0) = H_0^t,\ H_c(0) = H_{c0}, \\ H_c^t(0) = H_{c0}^t,\ D_{hc}(0) = D_{hc0}. \end{cases} \tag{5.2}$$

5.2 Model Analysis

This section outlines the qualitative properties of (5.1). This includes the existence and uniqueness of positive and bounded solutions and the stability of equilibria.

5.2.1 Invariant Set, Positivity and Boundedness of Solutions

The positivity and boundedness of solutions are established in the following theorem.

Theorem 5.2.1. *Assuming that all initial conditions in (5.2) are positive, the solutions of the system (5.1) remain positive for all $t > 0$. Furthermore, the set*

$$\Upsilon = \{(S, V_c, C, C^r, H, H^t, H_c, H_c^t, D_{hc}) \in \mathbb{R}^9 : 0 \leq N \leq \psi/d\}$$

is a positively invariant region and serves as an attracting set for system (5.1).

Table 5.1: A description of the parameters in Equation (5.1).

Parameters	Description	Values	Source
ψ	Rate of recruitment	5070	Assumed
ϕ_{tc}	Recovery rate for H_c^t from COVID-19	0.0578	Assumed
τ_v	COVID-19 vaccine inefficacy	0.01	Assumed
π_h	Transmission rate for HIV	0.01	(Ayele, Tigabu et al., 2021)
ε_2	Modification parameter	1.2	Assumed
α_{hc}	Recovery rate of H_c from COVID-19	0.08068	Assumed
φ_c	Rate of vaccination	0.01041	Assumed
θ_c	The recovery rate of the C class	0.18219	(Deressa & Duressa, 2021)
ε_1	Modification parameter	1.25	Assumed
η_c	Rate of immunity loss for COVID-19	0.033	Assumed
d_h	HIV-related mortality rate	0.00133	(UNAIDS, 2023)
π_c	Transmission rate for COVID-19	1	(Deressa & Duressa, 2021)
d_c	COVID-19 induced death rate	0.00011	(Deressa & Duressa, 2021)
δ_{hc}	Transfer rate from H_c to D_{hc} class	0.00983	Assumed
δ_{tc}	Transfer rate from H_c^t to D_{hc} class	0.000161	Assumed
ξ_{hc}	Recovery rate for H_c from COVID-19	0.004	Assumed
d_{hc}	Co-infection-related mortality rate	0.004392	Assumed
d	Natural death rate	4×10^{-5}	(Kassahun et al., 2022)
ω_h	Transfer rate from H to T class	0.006561	Assumed

Proof. It follows from the first equation of system (5.1) that, $\frac{dS}{dt}\big|_{S=0} = \psi + \eta_c C^r > 0$. We can see that $S(t)$ remains positive $\forall t > 0$. Which implies, the solution cannot exit Υ by crossing the boundary $S = 0$. Similarly, it is easy to show that $V_c, C, C^r, H, H^t, H_c, H_c^t, D_{hc} > 0$, for all $t > 0$. Furthermore, $N(t)$ satisfy $\frac{dN}{dt} \leq \psi - dN$. Thus, we can deduce that $0 \leq N \leq \psi/d$. Hence, all solutions in $\mathbb{R}_+^9$ are attracted to the region Υ. By Lemma 1 from Williams, Chukwu et al. (2020), we can deduce that Υ is an invariant and positively defined set. □

Theorem 5.2.1 confirm the epidemiological soundness of model (5.1), establishing the positivity and boundedness of all state variables. In other words, no solution path can extend beyond the boundaries of Υ, rendering it adequate to focus on the dynamics of system (5.1) within the confines of Υ. As the right-hand side of (5.1) is locally Lipschitz, the existence of solutions follows from the Picard-Lindelöf Theorem (see Theorem A.1.2 from Appendix A.1). Therefore, we establish the following theorem.

Theorem 5.2.2. *Solutions to system* (5.1) *exist and are unique for all* $t \geq 0$.

From Theorem 5.2.1 and Theorem 5.2.2 we can deduce that model (5.1) is epidemiologically meaningful and mathematically well-posed.

5.2.2 COVID-19 Sub-model Analysis

Setting $H = H^t = H_c = H_c^t = D_{hc} = 0$ yields the following sub-model of COVID-19:

$$\begin{cases} S' = \psi - (\beta_1 + \chi_C)\, S + \eta_c C^r, \\ V_c' = \varphi_c S - (\tau_v \chi_C + d) V_c, \\ C' = \chi_C S + \tau_v \chi_C V_c - \beta_2 C, \\ C^{r\prime} = \theta_c C - \beta_3 C^r, \end{cases} \tag{5.3}$$

where $\chi_C = \pi_c \frac{C}{N}$.

Following the same procedure as in Section 4.2.2, the COVID-19 free equilibrium ($\mathcal{E}_c^0$) is determined as $\mathcal{E}_c^0 = \left(\frac{\psi}{\beta_1}, \frac{\varphi_c \psi}{d\beta_1}, 0, 0\right)$ and the COVID-19 sub-model's reproduction number($\mathcal{R}_\emptyset^c$) is determined as $\mathcal{R}_\emptyset^c = \frac{(d+\varphi_c\tau_v)\pi_c}{\beta_1\beta_2}$. In simpler terms, the epidemiological interpretation of the first and second terms of $\mathcal{R}_\emptyset^c$ is that they represent the number of secondary infections that can be produced by one COVID-19 infected individual in susceptible and vaccinated class, respectively. Without vaccination, when $\varphi_c, \tau_v = 0$, $\mathcal{R}_\emptyset^c$ is given by $\mathcal{R}_\emptyset^c = \widehat{\mathcal{R}}_\emptyset^c = \frac{\pi_c}{\beta_2}$. and $\mathcal{R}_\emptyset^c$ can be expressed as $\mathcal{R}_\emptyset^c = \frac{(d+\varphi_c\tau_v)\mathcal{R}_\emptyset^{c*}}{\beta_1}$. This implies that the critical vaccination proportion that will lead to COVID-19 eradication is $\frac{d(1-\mathcal{R}_\emptyset^{c*})}{1-\tau_v\mathcal{R}_\emptyset^{c*}}$, which can be obtained by letting $\mathcal{R}_\emptyset^c = 1$ and solving for φ_c.

Theorem 5.2.3. *$\mathcal{E}_c^0$ is locally asymptotically stable, whenever $\mathcal{R}_\emptyset^c < 1$.*

Proof. The Jacobian of system (5.3) at $\mathcal{E}_0^c$ is

$$\begin{pmatrix} -\beta_1 & 0 & -\frac{\pi_c d}{\varphi_c + d} & \eta_c \\ \varphi_c & -d & -\frac{\pi_c \varphi_c \tau_v}{\varphi_c + d} & 0 \\ 0 & 0 & \frac{\pi_c(\varphi_c\tau_v + d)}{\varphi_c + d} - \beta_2 & 0 \\ 0 & 0 & \theta_c & -\beta_3 \end{pmatrix}. \tag{5.4}$$

We can see that, whenever $\mathcal{R}_\emptyset^c < 1$, the eigenvalues of matrix (5.4) are all negative. This means that when $\mathcal{R}_\emptyset^c < 1$, an outbreak cannot be caused by COVID-19-infected individuals and the disease can be eliminated. □

The endemic equilibrium point $\mathcal{E}_c = (S^*, V_c^*, C^*, C^{r*})$, is computed as:

$$\begin{aligned}
S^* &= \frac{\beta_2\beta_3\psi(\tau_v\chi_C + d)}{\tau_v\left[\beta_2\beta_3 - \eta_c\theta_c\right]\chi_C^2 + \left[(\tau_v\varphi_c + d)\left(\beta_2\beta_3 - \eta_c\theta_c\right) + \tau_v\beta_2\beta_3 d\right]\chi_C + \beta_1\beta_2\beta_3 d} \\
V_c^* &= \frac{\varphi_c\beta_2\beta_3\psi}{\tau_v\left[\beta_2\beta_3 - \eta_c\theta_c\right]\chi_C^2 + \left[(\tau_v\varphi_c + d)\left(\beta_2\beta_3 - \eta_c\theta_c\right) + \tau_v\beta_2\beta_3 d\right]\chi_C + \beta_1\beta_2\beta_3 d} \\
C^* &= \frac{\beta_3\psi\chi_C(\tau_v\chi_C + \varphi_c\tau_v + d)}{\tau_v\left[\beta_2\beta_3 - \eta_c\theta_c\right]\chi_C^2 + \left[(\tau_v\varphi_c + d)\left(\beta_2\beta_3 - \eta_c\theta_c\right) + \tau_v\beta_2\beta_3 d\right]\chi_C + \beta_1\beta_2\beta_3 d} \\
C^{r*} &= \frac{\psi\theta_c\chi_C(\tau_v\chi_C + \varphi_c\tau_v + d)}{\tau_v\left[\beta_2\beta_3 - \eta_c\theta_c\right]\chi_C^2 + \left[(\tau_v\varphi_c + d)\left(\beta_2\beta_3 - \eta_c\theta_c\right) + \tau_v\beta_2\beta_3 d\right]\chi_C + \beta_1\beta_2\beta_3 d}
\end{aligned} \tag{5.5}$$

Substituting S^*, V_c^*, C^* and C^{r*} of (5.5) into $\chi_C^* = \frac{\pi_c C^*}{S^* + V_c^* + C^* + C^{r*}}$ yields $\chi_C^*(q_2{\chi_C^*}^2 + q_1\chi_C^* + q_0) = 0$, where $q_0 = \beta_1\beta_2\beta_3(1 - \mathcal{R}_0^c)$, $q_1 = \tau_v\beta_2\beta_3 + (d + \tau_v\varphi_c)(\beta_3 + \theta_c) - \pi_c\tau_v\beta_3$ and $q_2 = \tau_v(\beta_3 + \theta_c)$. For $\chi_C^* = 0$, we obtain the disease free equilibrium $\mathcal{E}_0^c$. Thus, the endemic equilibrium satisfies the following equation:

$$q_2{\chi_C^*}^2 + q_1\chi_C^* + q_0 = 0. \tag{5.6}$$

The solution of χ_C^* is given by $\chi_C^* = \frac{-q_1 \pm \sqrt{q_1^2 - 4q_0q_2}}{2q_2}$. To assess the potential for an endemic equilibrium in (5.3), we explore two distinct scenarios, emphasizing positive real solutions while excluding the possibility of negative and complex solutions in (5.6). Consequently, we observe that Equation (5.6):

1. possesses a unique positive solution if $\mathcal{R}_0^c > 1$ and
2. exhibits two positive solutions if $\mathcal{R}_0^c < 1$ and $q_1 < 0$.

The second condition indicates the backward bifurcation phenomenon, the co-existence of a stable endemic and COVID-19-free equilibria, even if $\mathcal{R}_0^c < 1$. For $\tau_v = 0$ and/or $\varphi_c = 0$, we obtain $q_1 > 0$, implying that the imperfect vaccine can cause the backward bifurcation.

5.2.3 HIV Sub-model Analysis

Setting the state variables related to COVID-19 and co-infection equal to zero, $C = C^r = H_c = H_c^t = D_{hc} = 0$, gives the following HIV-only sub-model:

$$\begin{cases}
S' = \psi - (\beta_1 + \chi_H)S, \\
V_c' = \varphi_c S - (\chi_H + d)V_c, \\
H' = (S + V_c)\chi_H - \beta_4 H, \\
H^{t\prime} = \omega_h H - \beta_5 H^t,
\end{cases} \tag{5.7}$$

where $\chi_H = \pi_h \frac{H+H^t}{N}$.

To identify equilibrium points, HIV-free and endemic, we set the right hand side of (5.7) equal to 0. Thus, HIV-free equilibrium($\mathcal{E}_h^0$), obtained when $H = H^t = 0$, is given by $\mathcal{E}_h^0 = \left(\frac{\psi}{\beta_1}, \frac{\varphi_c \psi}{d\beta_1}, 0, 0\right)$.

The next generation matrix result in Appendix A.2 is employed to find the reproduction numbers of the sub- and co-infection models. Thus, the reproduction number($\mathcal{R}_\emptyset^h$) of the HIV-only sub-model (5.7) is determined as

$$\mathcal{R}_\emptyset^h = \frac{\pi_h}{\beta_5} \tag{5.8}$$

Theorem 5.2.4. *$\mathcal{E}_h^0$, whenever $\mathcal{R}_\emptyset^h < 1$, is locally asymptotically stable.*

Proof. The Jacobian of (5.7) becomes,

$$\begin{pmatrix} -\beta_1 & 0 & -\frac{d\pi_h}{\beta_1} & -\frac{d\pi_h}{\beta_1} \\ \varphi_c & -d & -\frac{\varphi_c \pi_h}{\beta_1} & -\frac{\varphi_c \pi_h}{\beta_1} \\ 0 & 0 & \pi_h - \beta_4 & \pi_h \\ 0 & 0 & \omega_h & -\beta_5 \end{pmatrix}$$

It is evident that $-d, -\beta_1$ and $-\beta_6$ are all negative. Two other eigenvalues are found in the matrix

$$\begin{pmatrix} \pi_h - \beta_4 & \pi_h \\ \omega_h & -\beta_5 \end{pmatrix}$$

Accordingly, the characteristic polynomial becomes $P(\lambda) = \lambda^2 + (\beta_4 + \beta_5 - \pi_h)\lambda + \beta_4\beta_5(1 - \mathcal{R}_\emptyset^h)$. The local stability of $\mathcal{E}_h^0$ is determined by the sign of the roots of $P(\lambda) = 0$. When $\mathcal{R}_\emptyset^h < 1$, the Routh-Hurwitz criterion leads us to the conclusion that all roots of $P(\lambda) = 0$ are negative, establishing the local asymptotic stability of $\mathcal{E}_h^0$. Conversely, if $\mathcal{R}_\emptyset^h > 1$, the disease-free equilibrium becomes unstable due to the presence of a positive eigenvalue. □

The epidemiological interpretation of the local stability of a disease-free equilibrium suggests that an epidemic is unlikely to occur, and there exists a potential for eliminating the disease from the population, especially when the flow of infectious individuals is relatively small. Specifically, Theorem 5.2.4 implies the feasibility of controlling HIV transmission by reducing $\mathcal{R}_\emptyset^h$ below one.

If $\mathcal{R}_0^h > 1$, we obtain the endemic equilibrium point $\mathcal{E}_h = (S^*, V_c^*, H^*, H^{t*})$, where

$$S^* = \frac{\psi}{\beta_1 + \beta_5(\mathcal{R}_0^H - 1)},\ V^* = \frac{\varphi_c \psi}{\left[\beta_1 + \beta_5(\mathcal{R}_0^h - 1)\right]\left[d + \beta_5(\mathcal{R}_0^h - 1)\right]},$$
$$H^{t*} = \frac{\omega_h \psi(\mathcal{R}_0^h - 1)}{\beta_4\left[d + \beta_5(\mathcal{R}_0^h - 1)\right]} \text{ and } H^* = \frac{\beta_5 \psi(\mathcal{R}_0^h - 1)}{\beta_4\left[d + \beta_5(\mathcal{R}_0^h - 1)\right]}.$$

Consequently, we can say that HIV persists in the population for $\mathcal{R}_0^h > 1$. However, for $\mathcal{R}_0^H < 1$, we can see that $H^*, H^{t*} < 0$, which is biologically meaningless. Therefore, the theorem presented below has been established.

Theorem 5.2.5. *Model (5.7), whenever $\mathcal{R}_0^h > 1$, has a unique endemic equilibrium.*

5.2.4 Co-infection Model Analysis

The disease-free equilibrium, $\mathcal{E}^0$, is given by $\mathcal{E}^0 = \left(\frac{\psi}{\beta_1}, \frac{\varphi_c \psi}{\beta_1 d}, 0, 0, 0, 0, 0, 0, 0, 0, 0\right)$. The reproduction number($\mathcal{R}_0$) for the COVID-19 and HIV co-infection model is obtained as $\mathcal{R}_0 = max\{\mathcal{R}_0^c,\ \mathcal{R}_0^h\}$. Furthermore, the subsequent theorem is established by employing Theorem 2 introduced in Van den Driessche, P. and Watmough, J. (2002).

Theorem 5.2.6. *$\mathcal{E}^0$ is unstable if $\mathcal{R}_0 > 1$ and locally asymptotically stable if $\mathcal{R}_0 < 1$.*

To assess the global stability of $\mathcal{E}^0$, we employ the method described in Chavez, C Castillo et al. (2002). By adopting the notation from Chavez, C Castillo et al. (2002) as in Section 4.2.4 and rephrasing system (5.1) as Equation (3.1) of Chavez, C Castillo et al. (2002), we obtain

$$\hat{G}(\mathbf{X}, \mathbf{I}) = \begin{pmatrix} \pi_c(C + H_c + H_c^t)\left(\frac{S(0)}{N(0)} - \frac{S}{N} + \tau_v\left(\frac{V_c(0)}{N(0)} - \frac{V_c}{N}\right)\right) + \chi_H C \\ \pi_h(H + H^t + H_c + H_c^t)\left(1 - \frac{S+V_c+C^r}{N}\right) + \chi_C H \\ \chi_C H^t \\ -\chi_C H - \chi_H C \\ -\chi_C H^t \\ 0 \end{pmatrix}$$

where $\mathbf{I} = (C, H, H^t, H_c, H_c^t, D_{hc})$ and $\mathbf{X} = (S, V_c, C^r)$ denotes infected and uninfected population respectively.

The fourth and fifth rows of $\hat{G}(\mathbf{X}, \mathbf{I})$ are less than zero. So, the assumption H2 in Chavez, C Castillo et al. (2002) is not satisfied. This suggests that $\mathcal{E}^0$ might not be globally asymptotically stable. That is, system (5.1) exhibits backward bifurcation, as proved by the following theorem.

Theorem 5.2.7. *System (5.1) undergoes a backward bifurcation at $\mathcal{R}_0 = 1$ when*

$$\tau_v(1-\tau_v)\varphi_c\beta_2 - (\tau_v\varphi_c + d)^2\left(1+\frac{\theta_c}{\beta_3}\right) > 0.$$

Proof. The central manifold approach outlined in Castillo-Chavez, C. and Song, Baojun (2004) (see Appendix A.3) is used to show existence of backward bifurcation in system (5.1). Thus, the following change of variables is introduced: $\tilde{z}_1 = S$, $\tilde{z}_2 = V_c$, $\tilde{z}_3 = C$, $\tilde{z}_4 = C^r$, $\tilde{z}_5 = H$, $\tilde{z}_6 = H^t$, $\tilde{z}_7 = H_c$, $\tilde{z}_8 = H_c^t$, and $\tilde{z}_9 = D_{hc}$. So that, $N = \sum_{j=1}^{9}\tilde{z}_j$, $\chi_C = \pi_h\frac{\tilde{z}_3+\tilde{z}_7+\tilde{z}_8}{N-\tilde{z}_9}$ and $\chi_H = \pi_h\frac{\tilde{z}_5+\tilde{z}_6+\tilde{z}_7+\tilde{z}_8}{N-\tilde{z}_9}$.

Moreover,

$$\tilde{\mathbf{z}}' = \mathbf{p} = (p_1,\ p_2,\ p_3,\ p_4,\ p_5,\ p_6,\ p_7,\ p_8,\ p_9)^T \tag{5.9}$$

is used to express system (5.1) with $\tilde{\mathbf{z}} = (\tilde{z}_1,\ \tilde{z}_2,\ \tilde{z}_3,\ \tilde{z}_4,\ \tilde{z}_5,\ \tilde{z}_6,\ \tilde{z}_7,\ \tilde{z}_8,\ \tilde{z}_9)^T$.

Suppose $\mathcal{R}_0 = max\{\mathcal{R}_0^c,\ \mathcal{R}_0^h\} = \mathcal{R}_0^c$. After selecting π_c as the bifurcation parameter and setting $\mathcal{R}_0^c = 1$, we get $\pi_c = \pi_c^* = \frac{\beta_1\beta_2}{\tau_v\varphi_c+d}$. At $\mathcal{E}^0$, the Jacobian of the system (5.9) for $\pi_c = \pi_c^*$ has a simple zero eigenvalue, but the real part of all other eigenvalues are negative. Consequently, we used the notion in Castillo-Chavez, C. and Song, Baojun (2004) and performed the following calculations.

For zero eigenvalue, we have the right-eigenvector $(w_1, w_2, w_3, w_4, w_5, w_6, w_7, w_8, w_9)^T$ and left-eigenvector $(v_1, v_2, v_3, v_4, v_5, v_6, v_7, v_8, v_9)$, where

$$w_1 = \frac{w_3}{\beta_1}\left(\frac{\theta_c\eta_c}{\beta_3} - \frac{\pi_c^* d}{\beta_1}\right), w_2 = \frac{\varphi_c}{d}\left(w_1 - \frac{\tau_v\pi_c^* w_3}{\beta_1}\right), w_3 > 0, w_4 = \frac{w_3\theta_c}{\beta_3}, v_3 > 0,$$
$$v_7 = \frac{\beta_2(\alpha_{hc}+\beta_7)v_3}{\beta_6\beta_7},\ v_8 = \frac{\beta_2 v_3}{\beta_7} \text{ and } w_5, w_6, w_7, w_8, w_9, v_1, v_2, v_4, v_5, v_6, v_9 = 0.$$

The values of a and b are calculated as follows:

$$\begin{aligned}
a &= \sum_{k,i,j=1}^{9} v_k w_i w_j \frac{\partial^2\tilde{p}_k}{\partial\tilde{z}_i\partial\tilde{z}_j}(\mathcal{E}^0, \pi_c^*) \\
&= \sum_{i,j=1}^{9}\left[v_3 w_i w_j \frac{\partial^2\tilde{p}_3}{\partial\tilde{z}_i\partial\tilde{z}_j}(\mathcal{E}^0,\pi_c^*) + v_7 w_i w_j \frac{\partial^2\tilde{p}_7}{\partial\tilde{z}_i\partial\tilde{z}_j}(\mathcal{E}^0,\pi_c^*) + v_8 w_i w_j \frac{\partial^2\tilde{p}_8}{\partial\tilde{z}_i\partial\tilde{z}_j}(\mathcal{E}^0,\pi_c^*)\right] \\
&= \frac{2d\beta_2 v_3 w_3^2}{\psi(\tau_v\varphi_c+d)^2}\left(\tau_v(1-\tau_v)\varphi_c\beta_2 - (\tau_v\varphi_c+d)^2\left(1+\frac{\theta_c}{\beta_3}\right)\right)
\end{aligned}$$

and

$$
\begin{aligned}
b &= \sum_{k,j=1}^{9} v_k w_j \frac{\partial^2 \tilde{p}_k}{\partial \tilde{z}_j \partial \pi_c}(\mathcal{E}^0, \pi_c^*) \\
&= \sum_{i,j=1}^{9} \left[v_3 w_i w_j \frac{\partial^2 \tilde{p}_3}{\partial \tilde{z}_i \partial \pi_c}(\mathcal{E}^0, \pi_c^*) + v_7 w_i w_j \frac{\partial^2 \tilde{p}_7}{\partial \tilde{z}_i \partial \pi_c}(\mathcal{E}^0, \pi_c^*) + v_8 w_i w_j \frac{\partial^2 \tilde{p}_8}{\partial \tilde{z}_i \partial \pi_c}(\mathcal{E}^0, \pi_c^*) \right] \\
&= \frac{v_3 w_3 (\tau_v \varphi_c + d)}{\beta_1} > 0.
\end{aligned}
$$

The coefficient b remains positive. Therefore, at $\mathcal{R}_0 = 1$, backward bifurcation is exhibited, when $a > 0$. It is obvious that $a < 0$ when the vaccination is perfect($\tau_v = 0$). Hence, as per Theorem 4.1 in Castillo-Chavez, C. and Song, Baojun (2004), system (5.1) will experience a trans-critical bifurcation at $\mathcal{R}_0$. This indicates that the backward bifurcation characteristic of the co-infection model (5.1) emerges from an imperfect vaccine, a common cause for backward bifurcation (Gumel, 2012). □

5.2.5 The Influence of HIV on the Endemic Chapter of COVID-19

Even though the World Health Organization has classified COVID-19 as a persistent health challenge, no longer deeming it a public health emergency of international concern (WHO, 2024b), it continues to pose a significant threat to global health. This section will focus on investigating the contribution of HIV to the transmission of COVID-19. Hence, we write d in (5.8) in terms of $\mathcal{R}_0^h$ to express $\mathcal{R}_0^c$ in terms of $\mathcal{R}_0^h$. That is, $d = \frac{\pi_h - \mathcal{R}_0^h d_h}{\mathcal{R}_0^h}$. Upon replacing this d value in $\mathcal{R}_0^c$, we obtain $\mathcal{R}_0^c = \frac{\mathcal{R}_0^h \pi_c \left(\pi_h + \mathcal{R}_0^h (\varphi_c \tau_v - d_h)\right)}{\left(\pi_h + \mathcal{R}_0^h (\varphi_c - d_h)\right)\left(\mathcal{R}_0^h (d_c - d_h + \theta_c) + \pi_h\right)}$. Which implies,

$$
\frac{\partial \mathcal{R}_0^c}{\partial \mathcal{R}_0^h} = \frac{(\pi_h - \mathcal{R}_0^h (d_h + \varphi_c \tau_v))^2 + (1 - \tau_v)\varphi_c {\mathcal{R}_0^h}^2 (\varphi_c \tau_v - \theta_c - d_c)}{\left(\pi_h + \mathcal{R}_0^h (\varphi_c - d_h)\right)^2 \left(\mathcal{R}_0^h (d_c - d_h + \theta_c) + \pi_h\right)^2}.
$$

In the community, when $\frac{\partial \mathcal{R}_0^c}{\partial \mathcal{R}_0^h} > 0$ (that is when $\frac{(\pi_h - \mathcal{R}_0^h (d_h + \varphi_c \tau_v))^2 + (1 - \tau_v)\tau_v {\varphi_c}^2 {\mathcal{R}_0^h}^2}{\varphi_c (1 - \tau_v)(\theta_c + d_c) {\mathcal{R}_0^h}^2} > 1$), there is a corresponding rise in COVID cases as the number of HIV cases increases. The positive correlation between the two implies that targeted interventions and health campaigns within communities where both HIV and COVID-19 are prevalent are necessary to combat the transmission of these infections.

5.2.6 Uncertainty and Sensitivity Analysis

Sensitivity analysis determines the contribution of each parameter value to the reproduction number. It is well known that there are uncertainties related to the estimation of some param-

eter values. An uncertainty analysis, using Latin Hypercube Sampling(LHS), is carried out to account for the effect of such uncertainties. We perform a Latin Hypercube Sampling (LHS) on the parameters that appear in the expression for reproduction numbers. It is worth mentioning that the LHS, which is a stratified sampling technique without replacement, enables the assessment of parameter variations across simultaneous uncertainty ranges for each parameter of the model. For the sensitivity analysis, a Partial Rank Correlation Coefficient (PRCC) was computed between the values of the parameters in the response function and those derived from the sensitivity analysis. We carried out a total of 1000 simulations per LHS run. Figure 5.2 shows the different parameters and their PRCC's.

Figure 5.2a shows the Partial Rank Correlation Coefficients (PRCC) of parameters with respect to the basic reproduction number $\mathcal{R}_0^c$. The parameter π_c has the highest positive PRCC, indicating that it significantly increases $\mathcal{R}_0^c$, making it the most influential factor for infection spread. Parameters τ_v has moderate positive effects on $\mathcal{R}_0^c$. Parameters φ_c and θ_c show negative correlations, suggesting they have relevant impact in reducing $\mathcal{R}_0^c$. Figure 5.2b shows the Partial Rank Correlation Coefficients (PRCC) between the basic reproduction number $\mathcal{R}_0^h$ and four key parameters: π_h, d, d_h, and ω_h. The positive PRCC value for π_h indicates a strong positive correlation, meaning that as π_h increases, $\mathcal{R}_0^h$ tends to increase significantly. On the other hand ω_h have negative correlations with $\mathcal{R}_0^h$, suggesting that increasing these parameters leads to a decrease in the reproduction number. Therefore, control strategies should prioritize reducing π_c and π_h, while also increasing θ_c, φ_c and ω_h for effective disease management.

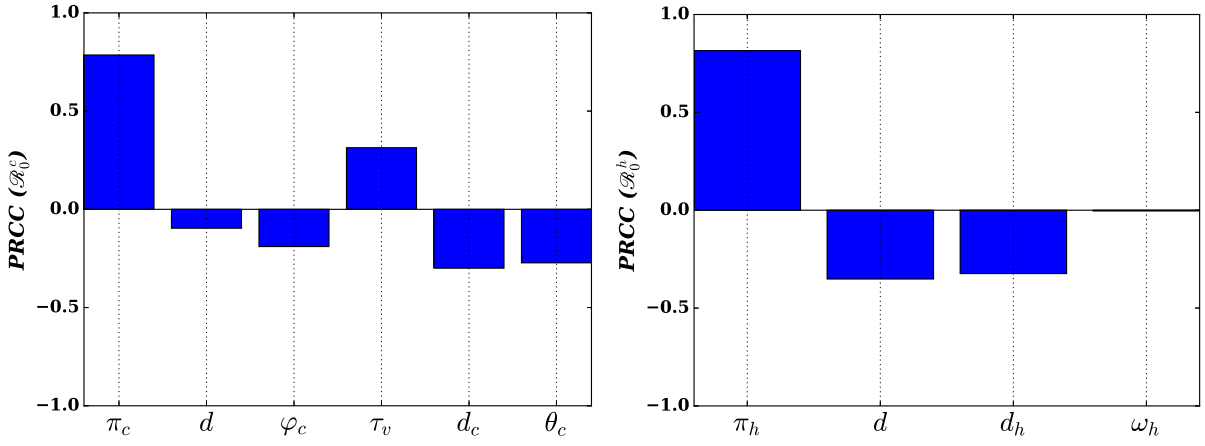

(a) PRCC values when $\mathcal{R}_0^c$ is the responce function

(b) PRCC values when $\mathcal{R}_0^h$ is the responce function

Figure 5.2: Sensitivity and uncertainty analysis results.

5.3 Model Extension to Include Optimal Control

This section introduces four Lebesgue measurable control functions of time to model (5.1). The following is a description of these control functions:

$u_1(t)$: steps made to promote and supply the COVID-19 vaccination,

$u_2(t)$: initiatives aimed at preventing the spread of HIV,

$u_3(t)$: measures taken to reduce the COVID-19 burden through treatment and

$u_4(t)$: the use of antiretroviral therapy (ART) for HIV patients.

To make things simple, we will define $x = (S, V_c, C, C^r, H, H^t, H_c, H_c^t)$ and $u = (u_1, u_2, u_3, u_4)$.

Upon including u_1, u_2, u_3, and u_4 into (5.1), we derive the optimal control model as follows:

$$\begin{cases} S' = \psi - (\beta_1 + u_1 + \chi_C + (1-u_2)\chi_H)\, S + \eta_c C^r, \\ V_c' = (\varphi_c + u_1)S - (\tau_v \chi_C + (1-u_2)\chi_H + d)V_c, \\ C' = \chi_C S + \tau_v \chi_C V_c - (\beta_2 + u_3 + (1-u_2)\chi_H)C, \\ C^{r\prime} = (u_3 + \theta_c)C - \beta_3 C^r, \\ H' = (1-u_2)(S+V_c)\chi_H + (u_3 + \xi_{hc})H_c - (\beta_4 + u_4 + \varepsilon_1 \chi_C)H, \\ H^{t\prime} = (u_4 + \omega_h)H + (u_3 + \phi_{tc})H_c^t - (\beta_5 + \varepsilon_2 \chi_C)H^t, \\ H_c' = \varepsilon_1 \chi_C H + (1-u_2)\chi_H C - (\beta_6 + u_3 + u_4)H_c, \\ H_c^{t\prime} = \varepsilon_2 \chi_C H^t + (u_4 + \alpha_{hc})H_c - (\beta_7 + u_3)H_c^t, \\ D_{hc}' = \delta_{hc} H_c + \delta_{tc} H_c^t - \beta_8 D_{hc}, \end{cases} \tag{5.10}$$

subject to (5.2).

The controls u_1 and u_3 in (5.10) were added to the existing parameters to increase the vaccination rates as well as the rate of recovery of COVID-19, respectively. Moreover, adding u_4 represents an increase in HIV treatment efforts. Furthermore, using u_2 as a multiplicative effect represents a proportional reduction in HIV transmission rates. The aim of introducing u_1, u_2, u_3 and u_4 in (5.1) is to identify the most cost-effective intervention strategy to reduce HIV and COVID-19 co-infection cases. To accomplish this, the following objective function is established.

$$J(u) = \int_0^{t_f} F(t, x, u)\, dt, \tag{5.11}$$

where $F(t,x,u) = a_1C + a_2H + a_3H^t + a_4H_c + a_5H_c^t + a_6D_{hc} + \frac{1}{2}\sum_{j=1}^{4} B_j u_j^2$ and t_f is the final time.

The state variables, along with the balancing weight parameters a_1, a_2, a_3, a_4, a_5 and a_6 in F, are employed to minimize the number of co-infected individuals over a specific duration. The non-linear expression $B_i u_i^2$, consistent with previous works (Deressa & Duressa, 2021; Mekonnen, Kassahun et al., 2022), represents the expenses associated with treatment and prevention, reflecting the inherently non-linear nature of costs. Thus, our goal is to determine the optimal control $u^* = (u_1^*, u_2^*, u_3^*, u_4^*)$ so that, given system (5.10) with initial conditions (5.2),

$$J(u_1^*, u_2^*, u_3^*, u_4^*) = \min_{u \in \mathcal{U}} J(u), \tag{5.12}$$

where $\mathcal{U} = \{u |\ 0 \leq u_j(t) \leq 1, j = 1,2,3,4,\ \text{for } 0 \leq t \leq t_f\}$ is the set of admissible control functions.

To achieve this, we first verify that (5.10) has solutions, and then we use Pontryagin's Maximum Principle (see Theorem A.4.1 from Appendix A.4) to characterize the optimal controls.

5.3.1 Existence of Control Problem

Theorem 5.3.1. *There exists an optimal control to problem to* (5.12).

Proof. The existence of solutions to an optimal control problem (5.12) is established using Theorem 4.1 and Corollary 4.1 from Fleming, Wendell H and Rishel, Raymond W (2012). Thus, we must meet the conditions mentioned further down:

A1: The set of state variables and controls are non-empty.

A2: The set $\mathcal{U}$ is convex and closed.

A3: $F(t,x,u)$ is convex on $\mathcal{U}$.

A4: System (5.1) can be expressed as $h(t,x,u) = r(t,x) + s(t,x)u^T$

A5: h is continuous and there exist $K > 0$ such that

(i) $|h(t,x,u)| \leq K(1 + |x| + |u|)$,

(ii) $|h(t,x,u) - h(t,x,u)| \leq K|x_1 - x|(1 + |u|)$, for all $u \in \mathcal{U},\ 0 \leq t \leq T_f$.

A6: $F(t,x,u) \geq c_1 |u|^{c_2} - c_3,\ c_1 > 0,\ c_2 > 1$.

Let's examine each of these conditions one by one now.

A1: For the set of control variables, without at least one effective control, we cannot have optimal controls. Furthermore, we can figure out that there is a unique solution that passes through the initial condition (5.2) because the right-hand side of system (4.1) is locally lipshizian (see Theorem A.1.2 from Appendix B.2).

A2: Let $u,\ v \in \mathcal{U}$. Then $\sigma u + (1-\sigma)v \geq 0,\ (1-\sigma)v \leq (1-\sigma)$ and $\sigma u \leq \sigma$, where $0 < \sigma < 1$. Which implies $0 \leq \sigma u + (1-\sigma)v \leq 1$. Hence $\mathcal{U}$ is Convex and closed.

A3: To show the convexity of t F , we need to prove that:

$$LHS = \sigma F(t,x,u) + (1-\sigma)F(t,x,v) - F(t,x,\sigma u + (1-\sigma)v) \geq 0, \text{for } u,\ v \in \mathcal{U} \text{ and } 0 < \sigma < 1.$$

Thus,

$$\begin{aligned} LHS =& \frac{\sigma}{2}\sum_{i=1}^{5} B_i u_i^2 + \frac{(1-\sigma)}{2}\sum_{i=1}^{4} B_i v_i^2 - \frac{1}{2}\sum_{i=1}^{4} B_i(\sigma u_i + (1-\sigma)v_i)^2 \\ =& \frac{\sigma(1-\sigma)}{2}\sum_{i=1}^{4} B_i(u_i^2 - 2u_i v_i + v_i^2) \\ =& \frac{\sigma(1-\sigma)}{2}\sum_{i=1}^{4} B_i(u_i - v_i)^2 \geq 0 \end{aligned}$$

A4: System (4.1) can be written as,

$$h(t,x,u) = r(t,x) + s(t,x)\ u^T,$$

where,

$$r = \begin{pmatrix} S\psi - (\beta_1 + \chi_C + \chi_H)S + \eta_c C^r \\ \varphi_c S - (\tau_v \chi_C + \chi_H + d)V_c \\ \chi_C S + \tau_v \chi_C V_c - (\beta_2 + \chi_H)C \\ \theta_c C - (\beta_3 + \chi_H)C^r \\ \chi_H(S + V_c) + \xi_{hc} H_c - (\beta_4 + \varepsilon_1 \chi_C)H \\ \omega_h H + \phi_{tc} H_c^t - (\beta_5 + \varepsilon_2 \chi_C)H^t \\ \chi_C H + \chi_H C - \beta_6 H_c \\ \chi_C H^t + \alpha_{hc} H_c - \beta_7 H_c^t \\ \delta_{hc} H_c + \delta_{tc} H_c^t - \beta_8 D_{hc} \end{pmatrix}, \quad s = \begin{pmatrix} -S & \chi_H S & 0 & 0 \\ S & \chi_H V_c & 0 & 0 \\ 0 & \chi_H C & -C & 0 \\ 0 & 0 & C & 0 \\ 0 & -\chi_H(V_c + S) & H_c & -H \\ 0 & 0 & H_c^t & H \\ 0 & -\chi_H C & -H_c & -H_c \\ 0 & 0 & -H_c^t & H_c \\ 0 & 0 & 0 & 0 \end{pmatrix}$$

A5: Since $S, V_c, C, C^r, H, H^t, H_c$ and H_c^t are bounded, there exists a constant K such that

$$|h(t,0,0)| \leq K,\ |h_x(t,x,u)| \leq K(1+|u|),\ |h_u(t,x,u)| \leq K. \tag{5.13}$$

Applying mean vale theorem and using (5.13) we have

$$\left|\frac{h(t,x_1,u)-h(t,x,u)}{x_1-x}\right| = |h_x(t,x,u)|,\ \left|\frac{h(t,x,0)-h(t,0,0)}{x}\right| = |h_x(t,x,0)| \text{ and}$$
$$\left|\frac{g(t,x,u)-g(t,x,0)}{u}\right| = |g_u(t,x,u)|.$$

Which implies, $|h(t,x_1,u)-h(t,x,u)| \leq K|x_1-x|(1+|u|)$, $|h(t,x,0)| \leq K(1+|x|)$ and $|h(t,x,u)| \leq K(1+|x|+|u|)$, respectively. Thus, condition A5 has met.

A6:

$$\begin{aligned}
F(t,x,u) &\geq \frac{B_1}{2}u_1^2+\frac{B_2}{2}u_2^2+\frac{B_3}{2}u_3^2+\frac{B_4}{2}u_4^2\\
&\geq \frac{B_1}{2}u_1^2+\frac{B_2}{2}u_2^2+\frac{B_3}{2}u_3^2+\frac{B_4}{2}u_4^2-\frac{B_4}{2}\\
&\geq \max\left(\frac{B_1}{2},\frac{B_2}{2},\frac{B_3}{2},\frac{B_4}{2}\right)\left(u_1^2+u_2^2+u_3^2+u_4^2\right)-\frac{B_4}{2}\\
&= \max\left(\frac{B_1}{2},\frac{B_2}{2},\frac{B_3}{2},\frac{B_4}{2}\right)|(u_1,u_2,u_3,u_4)|^2-\frac{B_4}{2}
\end{aligned}$$

Therefore, $F(t,x,u) \geq c_1|u|^{c_2}-c_3$, where $c_1 = \max\left(\frac{B_1}{2},\frac{B_2}{2},\frac{B_3}{2},\frac{B_4}{2}\right) > 0$, $c_2 = 2 > 1$ and $c_3 = \frac{B_4}{2}$.

Hence, since all of the aforementioned conditions are met, there are optimal control variables ${u_1}^*, u_2^*, u_3^*$, and u_4^* that satisfy (5.12) . □

5.3.2 Necessary Conditions

To use Pontryagin's Minimum Principle, first, we transform the optimal control problem (5.12) into a point-wise Hamiltonian, G, minimization problem:

$$G = F(t,x,u)+\sum_{j=1}^{9} l_j \tilde{f}_j(t,x,u),$$

where l_j, also known as the adjoint variables, are piecewise differentiable functions that need to be found, and $\tilde{f}_j$ represents the right-hand side of the ith equation of system (5.10).

Theorem 5.3.2. *Suppose* $\hat{x}_1 = S, \hat{x}_2 = V_c, \hat{x}_3 = C, \hat{x}_4 = C^r, \hat{x}_5 = H, \hat{x}_6 = H^t, \hat{x}_7 = H_c, \hat{x}_8 = H_c^t$ *and* $\hat{x}_9 = D_{hc}$ *be optimal state solutions and* u^* *be the corresponding control set for the optimal control problem* (5.10) *and* (5.11)*. Then the adjoint variables satisfy*

$$\frac{dl_j}{dt} = -\frac{\partial G}{\partial \hat{x}_j} \tag{5.14}$$

with transversality conditions $l_j(t_f) = 0$*, for* $j = 1, 2, 3, ..., 9$*. Furthermore, the control set* u^* *is characterized by*

$$\begin{aligned}
u_1^* &= \max\left\{0, \min\left\{1, \frac{(l_1 - l_2)S}{B_1}\right\}\right\}, \\
u_2^* &= \max\left\{0, \min\left\{1, \frac{\chi_H\left((l_5 - l_1)S + (l_5 - l_2)V_c\right) + C(l_7 - l_3)}{B_2}\right\}\right\}, \\
u_3^* &= \max\left\{0, \min\left\{1, \frac{(l_7 - l_5)H_c + C(l_3 - l_4) + (l_8 - l_6)H_c^t}{B_3}\right\}\right\}, \\
u_4^* &= \min\left\{0, \min\left\{1, \frac{(l_7 - l_8)H_c + H(l_5 - l_6)}{B_4}\right\}\right\}.
\end{aligned} \tag{5.15}$$

Proof: By differentiating the Hamiltonian with respect to the state variables, we derive the following differential equation governing the adjoint variables.

$$\begin{aligned}
\frac{dl_1}{dt} =& \left((\chi_C + Q_1)L_1 + \beta_1 + u_1\right)l_1 - \left(\frac{(\tau_v\chi_C + Q_1)V_c}{N} + \varphi_c + u_1\right)l_2 - \left(\frac{Q_1 C}{N} + \left(1 - \frac{Q_3}{N}\right)\chi_C\right)l_3 \\
&- \left(\frac{\varepsilon_1\chi_C H}{N} + Q_1\left(1 - \frac{Q_2}{N}\right)\right)l_5 - \frac{\varepsilon_2\chi_C H^t l_6}{N} + \frac{(Q_1 C + \varepsilon_1\chi_C H)l_7}{N} + \frac{l_8\varepsilon_2\chi_C H^t}{N} \\
\frac{dl_2}{dt} =& -\frac{l_1(\chi_C + Q_1)S}{N} + l_2(L_2(\tau_v\chi_C + Q_1) + d) - l_3\left(\chi_C\left(\tau_v - \frac{Q_3}{N}\right) + \frac{Q_1 C}{N}\right) \\
&- l_5\left(\frac{\varepsilon_1\chi_C H}{N} + Q_1\left(1 - \frac{Q_2}{N}\right)\right) - \frac{l_6\varepsilon_2\chi_C H^t}{N} + l_7\left(\frac{Q_1 C}{N} + \frac{\varepsilon_1\chi_C H}{N}\right) + \frac{l_8\varepsilon_2\chi_C H^t}{N} \\
\frac{dl_3}{dt} =& l_1 S\left(Q_4 - \frac{Q_1}{N}\right) + l_2 V_c\left(\tau_v Q_4 - \frac{Q_1}{N}\right) + l_3(Q_1 L_3 - Q_3 Q_4 + \beta_2 + u_3) - (u_3 + \theta_c)l_4 \\
&+ l_5\left(\frac{Q_1 Q_2}{N} + \varepsilon_1 Q_4 H\right) + \varepsilon_2 Q_4 l_6 H^t - l_7(Q_1 L_3 + \varepsilon_1 Q_4 H) - \varepsilon_2 Q_4 l_8 H^t - a_1 \\
\frac{dl_4}{dt} =& -l_1\left(\frac{(\chi_C + Q_1)S}{N} + \eta_c\right) - \frac{l_2 V_c(Q_1 + \tau_v\chi_C)}{N} - l_3\left(\frac{Q_1 C}{N} - \frac{\chi_C Q_3}{N}\right) + \beta_3 l_4 \\
&- l_5\left(\frac{\varepsilon_1\chi_C H}{N} - \frac{Q_1 Q_2}{N}\right) - \frac{l_6\varepsilon_2\chi_C H^t}{N} + l_7\left(\frac{Q_1 C}{N} + \frac{\varepsilon_1\chi_C H}{N}\right) + \frac{l_8\varepsilon_2\chi_C H^t}{N} \\
\frac{dl_5}{dt} =& l_1 S\left(Q_5 - \frac{\chi_C}{N}\right) + l_2 V_c\left(Q_5 - \frac{\tau_v\chi_C}{N}\right) + l_3\left(\frac{\chi_C Q_3}{N} + Q_5 C\right) + l_5(\varepsilon_1\chi_C L_4 - Q_2 Q_5 + \beta_4 + u_4)
\end{aligned}$$

$$
\begin{aligned}
&-l_6\left(\frac{\varepsilon_2\chi_c H^t}{N}+\omega_h+u_4\right)-l_7\left(\varepsilon_1\chi_c L_4+Q_5C\right)+\frac{\varepsilon_2\chi_c l_8 H^t}{N}-a_2\\
\frac{dl_6}{dt}=&l_1S\left(Q_5-\frac{\chi_c}{N}\right)+l_2V_c\left(Q_5-\frac{\tau_v\chi_c}{N}\right)+l_3\left(\frac{\chi_c Q_3}{N}+Q_5C\right)-l_5\left(\frac{\varepsilon_1\chi_c H}{N}+Q_2Q_5\right)\\
&+l_6\left(\varepsilon_2\chi_c L_5+\beta_5\right)-l_7\left(Q_5C-\frac{\chi_c H}{N}\right)-l_8\varepsilon_2\chi_c L_5-a_3\\
\frac{dl_7}{dt}=&\left(Q_4+Q_5\right)l_1S+l_2V_c\left(\tau_vQ_4+Q_5\right)-l_3\left(Q_3Q_4-Q_5C\right)-l_5\left(-\varepsilon_1Q_4H+Q_2Q_5+u_3+\xi_{hc}\right)\\
&+\varepsilon_2Q_4l_6H^t-l_7\left(Q_5C+\varepsilon_1Q_4H-\beta_6-u_3-u_4\right)-l_8\left(\varepsilon_2Q_4H^t+u_4+\alpha_{hc}\right)-l_9\delta_{hc}-a_4\\
\frac{dl_8}{dt}=&\left(Q_4+Q_5\right)l_1S+l_2V_c\left(\tau_vQ_4+Q_5\right)-l_3\left(Q_3Q_4-CQ_5\right)+l_5\left(\varepsilon_1Q_4H-Q_2Q_5\right)\\
&-l_6\left(-\varepsilon_2Q_4H^t+u_3+\phi_{tc}\right)-l_7\left(Q_5C+\varepsilon_1Q_4H\right)-l_8\left(\varepsilon_2Q_4H^t-\beta_7-u_3\right)-l_9\delta_{tc}-a_5\\
\frac{dl_9}{dt}=&\beta_8l_9-a_6
\end{aligned}
$$

where

$$
\begin{aligned}
Q_1=&(1-u_2)\chi_H, Q_2=S+V_c, Q_3=S+\tau_vV_c, Q_4=\frac{\pi_c-Q_1}{N}, Q_5=\frac{(1-u_2)\pi_h-Q_2}{N},\\
&L_1=\left(1-\frac{S}{N}\right),\ L_2=\left(1-\frac{V_c}{N}\right),\ L_3=\left(1-\frac{C}{N}\right),\ L_4=\left(1-\frac{H}{N}\right)\text{ and }L_5=\left(1-\frac{H^t}{N}\right).
\end{aligned}
$$

The characterization in (5.15) is obtained by solving u_j^* from $\frac{\partial G}{\partial u_j}=0$, where $j=1,2,3,...,9$, and applying standard control arguments involving bounds on the controls.

5.4 Numerical Simulations and Results

This section presents numerical simulations to validate the qualitative analysis results of system (5.1) and to illustrate the contribution of optimal control strategies on cases of COVID-19 and HIV co-infection. For this study, the total population and life expectancy of Ethiopia in 2021 have been taken into account. The estimated total population were $N=120,283,026$ with a life expectancy of 65 years (World Bank, 2022). Consequently, $d=\frac{1}{(65\times365)}$ per day and $\psi=d\times N=5070$ people per day. We employed parameter values from existing research, and where data were unavailable, we estimated certain parameters within acceptable ranges. Table 5.1 presents the parameter values used in the numerical simulations. For the numerical simulations, the following initial conditions were applied: $S(0)=120269406$, $V_c(0)=8000$, $C(0)=800$, $C^r(0)=1200$, $H(0)=1500$, $H^t(0)=1800$, $H_c(0)=150$, $H_c^t(0)=120$, and $D_{hc}(0)=50$.

5.4.1 Simulations of the Co-infection Model

Figure 5.3b illustrates that even when $\mathcal{R}_0^c$ is less than 1, the state variables tend to converge toward positive values. This suggests that the COVID-19 sub-model exhibits a backward bifurcation phenomenon. Figure 5.3a indicates that the backward bifurcation occurs at $\mathcal{R}_0^c = 1$. For $\mathcal{R}_0^c < 1$, two endemic equilibria (stable and unstable) coexist with a stable disease-free equilibrium in the vicinity of $\mathcal{R}_0^c = 1$. The occurrence of a backward bifurcation is epidemiologically significant as it demonstrates that the condition of $\mathcal{R}_0^c < 1$ is necessary but not sufficient for disease control. This implies that eradicating COVID-19 can be challenging when a backward bifurcation phenomenon is present in the dynamics of disease transmission.

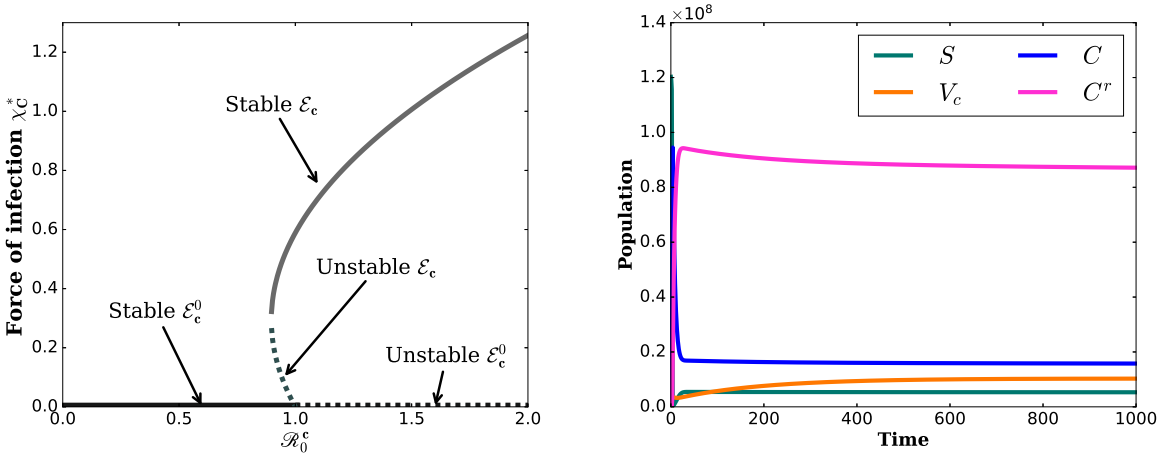

(a) Bifurcation diagram.

(b) State variables.

Figure 5.3: Backward bifurcation diagram and endemic equilibrium when $\mathcal{R}_0^c = 0.35$.

5.4.2 Simulations of the Optimal Control Model

The optimal control problem (5.10) is analyzed iteratively using the Runge-Kutta forward-backward sweep numerical approximation method described in Appendix A.4. In line with this approach, first, a fourth-order Runge-Kutta method is employed to solve the state variable solutions forward in time with an initial guess for the control variables. Then, the solutions of the state variables are used to solve (5.14) backward in time. Once the state and adjoint solutions are solved, the control is updated with these new values. These procedures are repeated until the solutions converge. In performing numerical simulation associated with the optimal control problem, the following set of values of costs are considered: $B_1 = 30$, $B_2 = 20$, $B_3 = 50$ and $B_4 = 150$. The weighted coefficients are further assumed to be $a_1 = 100$, $a_2 = 100$, $a_3 = 50$, $a_4 = 120$, $a_5 = 80$ and $a_6 = 150$. The intention of setting a high weight coefficient value for D_{hc} is to minimize the loss of lives from HIV and COVID-19 infections. To examine the outcome of

control strategies, we consider four different scenarios:

Scenario 1: use of single control strategy,

Scenario 2: implementing a combination of two control strategies,

Scenario 3: implementing a combination of three control strategies and

Scenario 4: implementing a combination of all control strategies.

Numerical results for all four scenarios are presented for the final time period of $t_f = 120$. In the following section, we will take a closer look at each scenario.

Scenario 1: Use of single control strategy

Here, the following strategies are taken into account:

Strategy A: Vaccination only ($u_1 \neq 0$)

Strategy B: Prevention for HIV only ($u_2 \neq 0$)

Strategy C: Treatment for COVID-19 only ($u_3 \neq 0$)

Strategy D: Treatment for HIV only ($u_4 \neq 0$)

The effectiveness of the control strategies and their impact profiles are depicted in Figure 5.4. In Figure 5.4a, it is evident that COVID-19 and HIV treatment options significantly reduce the population in the H_c compartment compared to other strategies. The highest peak value in Figure 5.4b is attributed to an increase in HIV treatment efforts. However, this figure reveals the inverse outcome of COVID-19 treatment on the population in H_c^t. Figures 5.4c and 5.4h demonstrate that the treatment of COVID-19 is more crucial than other options in reducing the risk of mortality from co-infection. The calculations leading to Figures 5.4h and 5.4i are provided in Section 5.5.1. Overall, these figures illustrate that, in terms of consistently reducing the number of deaths, COVID-19 appears to contribute more effectively. In summary, the COVID-19 treatment approach seems to play a more significant role in consistently lowering the number of deaths.

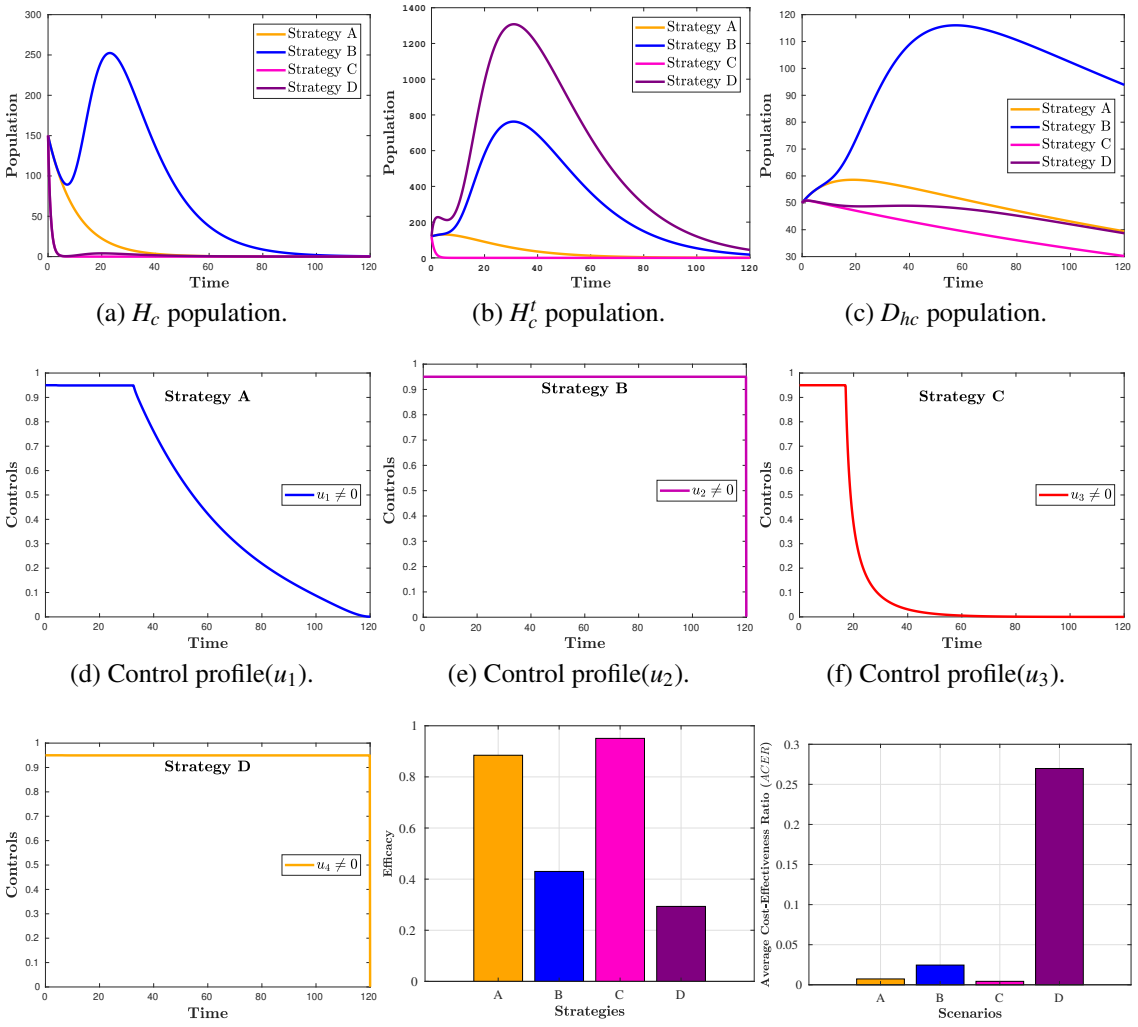

(a) H_c population. (b) H_c^t population. (c) D_{hc} population.

(d) Control profile(u_1). (e) Control profile(u_2). (f) Control profile(u_3).

(g) Control profile(u_4). (h) Efficacy in scenario 1. (i) Cost-effectiveness in scenario 1.

Figure 5.4: A simulation showing how Scenario 1's strategies affect the outcome.

Scenario 2: Use of combinations of two controls

This section examines the following combinations of two strategies.

Strategy E: COVID-19 vaccination and HIV prevention ($u_1, u_2 \neq 0$)

Strategy F: Vaccination and treatment for COVID-19 ($u_1, u_3 \neq 0$)

Strategy G: COVID-19 vaccination and treatment for HIV ($u_1, u_4 \neq 0$)

Strategy H: Treatment for COVID-19 and prevention for HIV ($u_2, u_3 \neq 0$)

Strategy I: Prevention and treatment for HIV ($u_2, u_4 \neq 0$)

Strategy J: Treatment for COVID-19 and HIV ($u_3, u_4 \neq 0$)

Figure 5.5 presents the simulation results for a combination of two control strategies. The figure indicates that the combinations of u_1 and u_3, u_2 and u_3, and u_3 and u_4 have resulted in the lowest number of co-infection cases and the lowest risk of mortality. This observation is reinforced by Figure 5.5j, which provides a detailed illustration of the effectiveness of each of the six measures, as discussed further in Section 5.5.2. Moreover, if these measures are to be implemented, u_2 and u_4 should remain at their maximum level until the intervention is over, as depicted in Figures 5.5d to 5.5i. In contrast, the control efforts u_1 and u_3 can gradually decrease from their maximum after a certain number of days.

Scenario 3: Use of combinations of three controls

To investigate the impact of three control strategies, the following combinations are taken into account:

Strategy K: Combination of u_1, u_2 and u_3 ($u_4 = 0$)

Strategy L: Combination of u_1, u_2 and u_4 ($u_3 = 0$)

Strategy M: Combination of u_1, u_3 and u_4 ($u_2 = 0$)

Strategy N: Combination of u_2, u_3 and u_4 ($u_1 = 0$)

Figure 5.6 shows that a combination of three interventions is more successful in reducing the number of HIV and COVID-19 cases than using simply one or a hybrid of two strategies. Moreover, from this figure, we can see that H_c and D_{hc} populations appear to be reduced in almost the same manner in all four triple control strategies. The effectiveness of each of these strategies is demonstrated in Figure 5.6h, which was constructed using the information from Section 5.5.3. The corresponding control profiles are depicted in Figures Figures 5.6d to 5.6g.

Scenario 4: Use of a combination of four control

This section refers to:

Strategy O: Combination of u_1, u_2, u_3 and u_4.

Figure 5.7 reveals what happens when all control strategies are put into practice. This figure clearly indicates that applying all control measures is the most effective way to reduce the co-infection cases among all the intervention techniques included in this work.

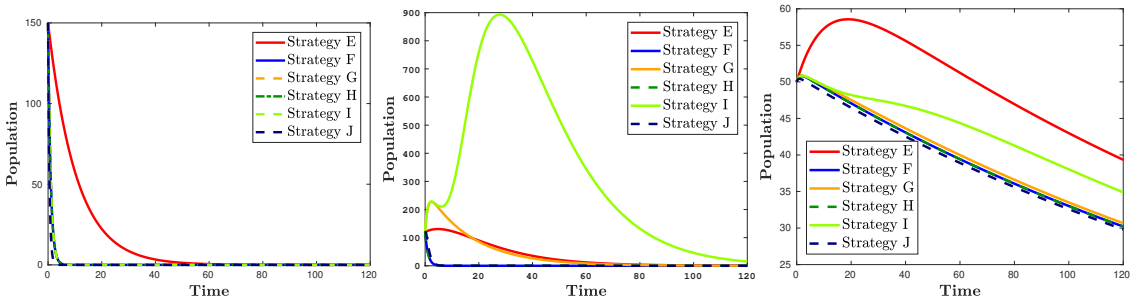

(a) H_c population. (b) H_c^t population. (c) D_{hc} population.

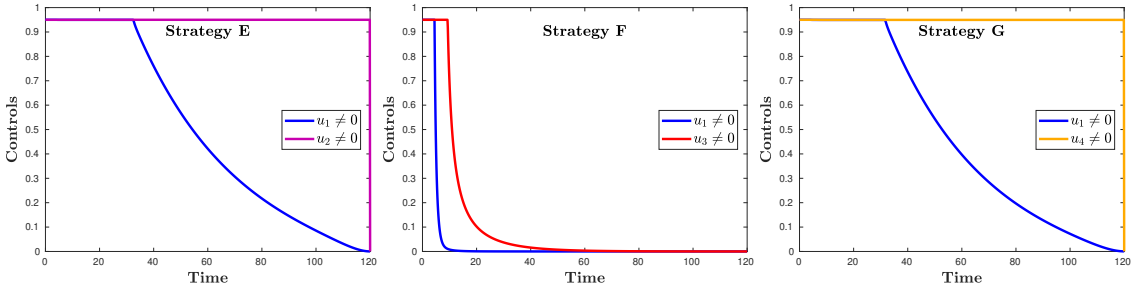

(d) Control profiles: u_1 and u_2. (e) Control profiles: u_1 and u_3. (f) Control profiles: u_1 and u_4.

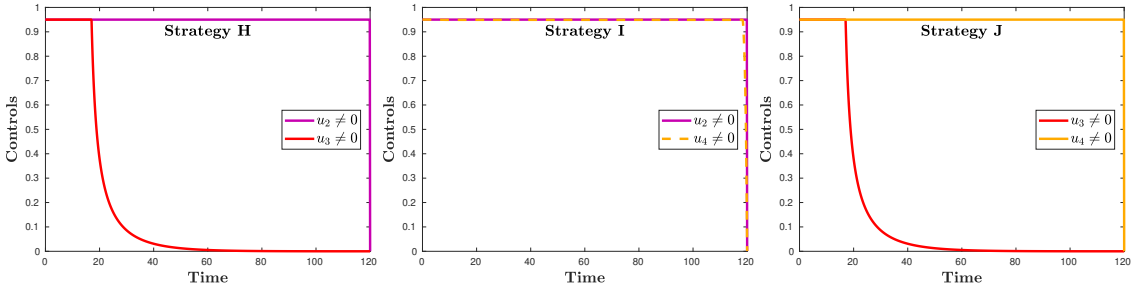

(g) Control profiles: u_2 and u_3. (h) Control profiles: u_2 and u_4. (i) Control profiles: u_3 and u_4.

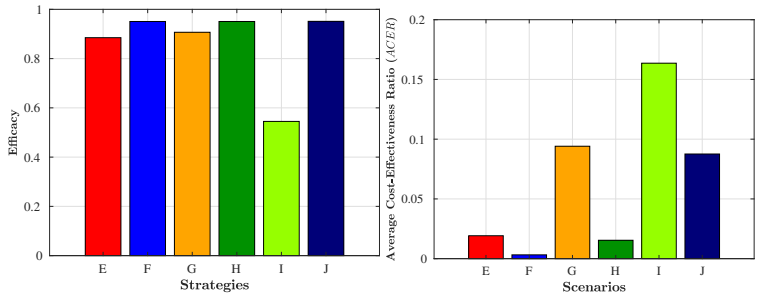

(j) Efficacy in scenario 2. (k) Cost-effectiveness in scenario 2.

Figure 5.5: Simulation showing the effect strategies in Scenario 2.

5.5 Cost-Effectiveness Analysis

In managing infectious diseases it is important to identify an effective strategy that emphasizes favorable results while efficiently allocating resources. Effectiveness refers to the capacity

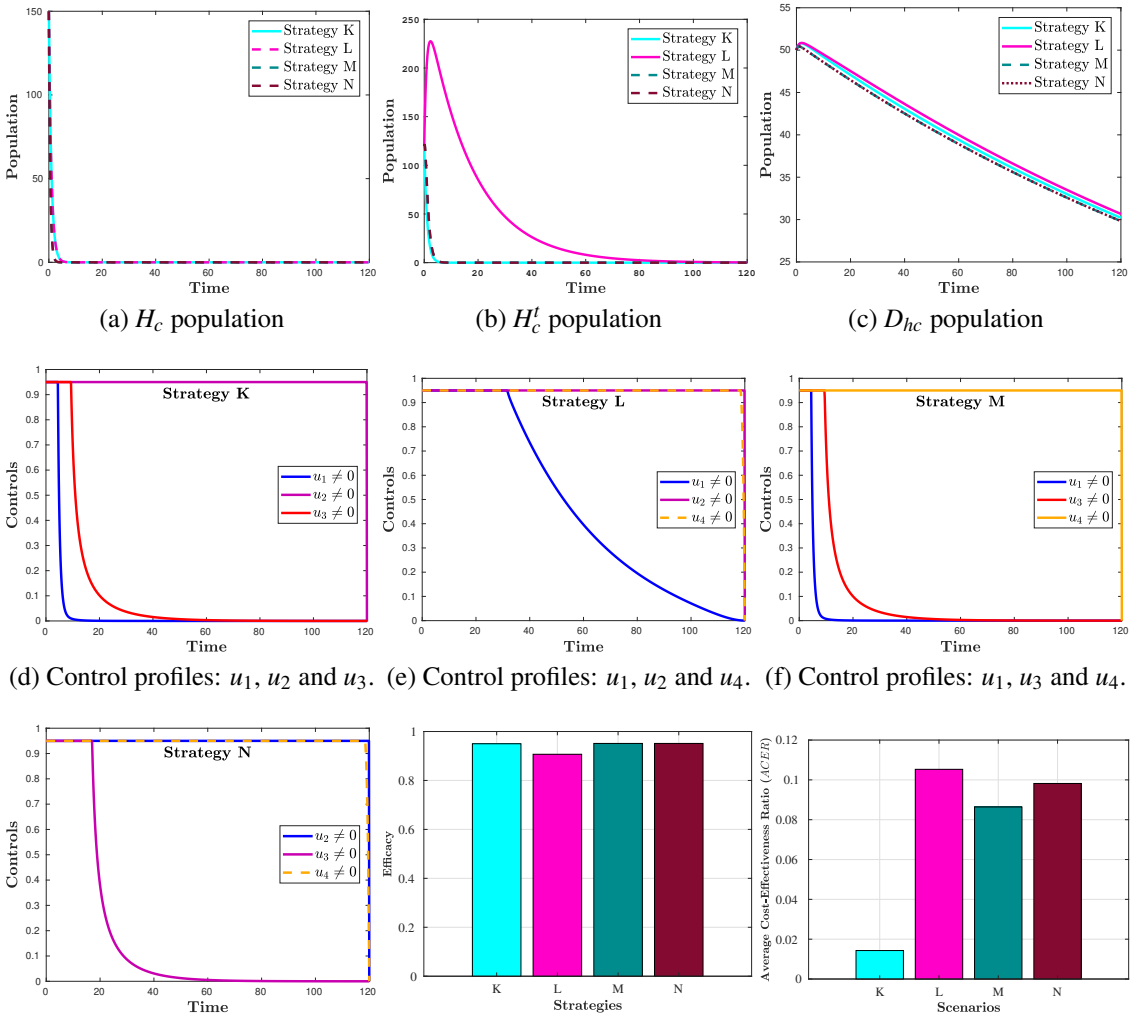

(a) H_c population (b) H_c^t population (c) D_{hc} population

(d) Control profiles: u_1, u_2 and u_3. (e) Control profiles: u_1, u_2 and u_4. (f) Control profiles: u_1, u_3 and u_4.

(g) Control profiles: u_2, u_3 and u_4. (h) Efficacy in scenario 3. (i) Cost-effectiveness in scenario 3.

Figure 5.6: Simulation showing the effect strategies in Scenario 3

to effectively control and mitigate the impact of diseases. For a variety of reasons, including financial constraints, it may not be feasible to rank the most effective options first, whereas the least expensive alternative may not have the desired effect. To create sustainable prevention strategies that maximize resources and promote the best possible health outcomes, it is imperative to strike a balance between effectiveness and costs. Cost-effectiveness aids in locating the optimal balance. Cost-effectiveness refers to resource allocation that maximizes the return on investment for the interventions made. Cost-effectiveness analysis, particularly in low-resource settings like Ethiopia, can guide the efficient allocation of limited healthcare resources. It supports decision-makers in prioritizing interventions that provide the greatest health benefits for the lowest cost. This approach strengthens the practical relevance by ensuring sustainable, impactful disease control strategies. Identifying effective and cost-effective strategies among the

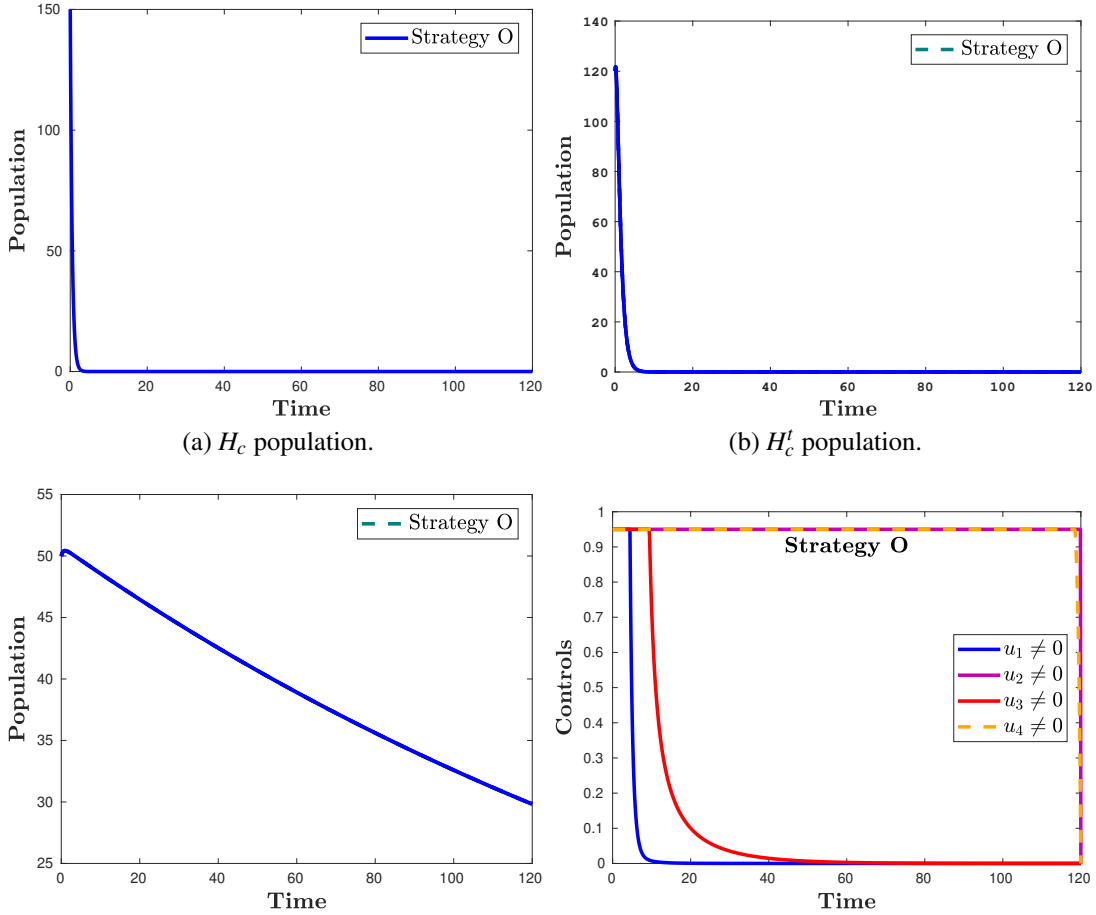

(a) H_c population.

(b) H_c^t population.

(c) D_{hc} population.

(d) Control profiles: u_1, u_2, u_3 and u_4.

Figure 5.7: Simulation showing the effect strategy O.

options provided in this study is the main objective of this section. Determining the most efficient and economical control strategy requires more analysis than simply comparing Figures 5.4 to 5.6, which shows the number of infected people at the end of the implementation of each strategy. The definitions and methodologies outlined in Darmawati, Darmawati et al. (2022) and Rodrigues, Paula et al. (2014) were used to conduct an efficacy and cost-effective analysis. Consequently, effectiveness ($\widetilde{E}$) is defined as the proportion of averted co-infection cases to the total number of possible co-infection cases without intervention. That is,

$$\widetilde{E} = \frac{\text{Total averted co-infection cases } (T_{av})}{\text{The aggregate of co-infected in the course of } T \text{ period}} \tag{5.16}$$

The difference between the total number of individuals before and after the control techniques were implemented was used to calculate the overall number of co-infections avoided. In terms of effectiveness, the highest $\widetilde{E}$ value is said to be the most effective, whereas the lowest $\widetilde{E}$ value is said to be the least effective.

The infection-averted ratio (*IAR*), average cost-effectiveness ratio (*ACER*), and incremental cost-effectiveness ratio (*ICER*) are the three methods most frequently used in cost-effectiveness analyses. For this study, we considered the ACER and ICER methods. The following is the definition of ACER:

$$ACER = \frac{\text{Total cost invested in a particular strategy } (T_{cost})}{\text{The aggregate of co-infections averted by the strategy } (T_{av})}.$$

The total cost was calculated using the cost function $\int_0^T \sum_{i=1}^4 Q_i u_i(t)dt$. The ACER method evaluates the cost-effectiveness of a single intervention strategy by comparing it with the option of taking no action. This cost-effectiveness analysis method indicates that the best option is the one with the minimum ACER value.

The Incremental Cost-Effectiveness Ratio (ICER) is a method that enables the comparison of the health and cost benefits of two different interventions, which are vying for the same limited resources. When applying the ICER approach, it is important to compare two competing intervention strategies incrementally, with one intervention being compared to the next-less effective intervention. As a result, the control strategies are ranked according to the number of co-infections averted to examine the ICER of the strategies provided in scenarios 1, 2, 3, and 4, as shown in Table 5.2. Taking into account strategies m and n as two competing control measures, ICER is described as,

$$ICER = \frac{\text{Change in total costs invested in strategies } m \text{ and } n}{\text{Change in the total number of co-infections averted in strategies } m \text{ and } n}.$$

5.5.1 Cost-effectiveness Analysis of Scenario 1: Single Control Strategy

We employ (5.16) to calculate the effectiveness of the interventions. From Table 5.3, we can observe that Strategy C is the most effective among the strategies implemented in Scenario 2. Using ACER and ICER, we now look into the most economical approach. Following the definition and analysis of ACER, strategy D has the maximum ACER value, followed by strategies B, A, and C (see Table 5.3, fifth column). Consequently, this method suggests that Strategy C is the most economical in Scenario 1. Using the averted co-infection rank from Table 5.2, the ICER results, which is shown in Table 5.3, are calculated as follows:

$$ICER(D) = \frac{8111.4 - 0}{30069 - 0} = 0.2698$$
$$ICER(B) = \frac{1082.7 - 8111.4}{44101 - 30069} = -0.50091$$

Table 5.2: Prevented co-infections and total cost of control strategies.

Strategy	T_{av}	T_{cost}
Scenario 1: Single control strategies		
Strategy D ($u_4 \neq 0$)	30069	8111.4
Strategy B ($u_2 \neq 0$)	44101	1082.7
Strategy A ($u_1 \neq 0$)	90713	661.3473
Strategy C ($u_3 \neq 0$)	97478	422.4568
Scenario 2: Double control strategies		
Strategy I ($u_2 \neq 0, u_4 \neq 0$)	55886	9141.1
Strategy E ($u_1 \neq 0, u_2 \neq 0$)	90741	1743.4
Strategy G ($u_1 \neq 0, u_4 \neq 0$)	92990	8753.2
Strategy F ($u_1 \neq 0, u_3 \neq 0$)	97478	309.0571
Strategy H ($u_2 \neq 0, u_3 \neq 0$)	97478	1504.9
Strategy J ($u_3 \neq 0, u_4 \neq 0$)	97542	8540.9
Scenario 3: Triple control strategies		
Strategy L ($u_1 \neq 0, u_2 \neq 0, u_4 \neq 0$)	93005	9794.5
Strategy K ($u_1 \neq 0, u_2 \neq 0, u_3 \neq 0$)	97478	1392.7
Strategy M ($u_1 \neq 0, u_3 \neq 0, u_4 \neq 0$)	97542	8429.2
Strategy N ($u_2 \neq 0, u_3 \neq 0, u_4 \neq 0$)	97542	9579.2
Scenario 4: Four control strategies		
Strategy O ($u_1, u_2, u_4 \neq 0$)	97542	9467.6

$$ICER(A) = \frac{661.3473 - 1082.7}{90713 - 44101} = -0.00904$$
$$ICER(C) = \frac{422.4568 - 661.3473}{97478 - 9071390713} = -0.03531$$

When we compare $ICER(D)$ and $ICER(A)$, we find that approach A saves 0.2788 dollars in comparison to strategy D. Thus strategy D is more costly than strategy A. Thus, in the next ICER computations, approach D is omitted. We will now carry on comparing the remaining three strategies.

$$ICER(B) = \frac{1082.7 - 0}{44101 - 0} = 0.02455$$
$$ICER(A) = \frac{661.3473 - 1082.7}{90713 - 44101} = -0.00904$$
$$ICER(C) = \frac{422.4568 - 661.3473}{97478 - 9071390713} = -0.03531$$

Table 5.3: The T_{av}, T_{cost}, $\widetilde{E}$, ACER and ICER for the intervention strategies in Scenario 1.

Strategy	T_{av}	T_{cost}	$\widetilde{E}$	ACER	ICER
Strategy D $(u_4 \neq 0)$	30069	8111.4	0.2933	0.2698	0.2698
Strategy B $(u_2 \neq 0)$	44101	1082.7	0.4301	0.0246	-0.50091
Strategy A $(u_1 \neq 0)$	90713	661.3473	0.8847	0.0073	-0.00904
Strategy C $(u_3 \neq 0)$	97478	422.4568	0.9507	0.0043	-0.03531

Upon examining the results, we can see that Strategy B is more expensive than Strategy A. Therefore Strategy is ruled out since it is less cost-effective than Strategy A. The incremental cost-effectiveness ratio of strategies A and C are recalculated in the following manner:

$$ICER(A) = \frac{661.3473 - 0}{90713 - 0} = 0.00729$$
$$ICER(C) = \frac{422.4568 - 661.3473}{97478 - 9071390713} = -0.03531$$

Using strategy C results in a 0.0426 savings compared to strategy A. Therefore, of the four solutions in Scenario 1, strategy C is the most economical. This supports the outcome derived from the ACER analysis.

5.5.2 Cost-effectiveness Analysis of Scenario 2: Combination of Two Control Strategies

Although Strategy J is successful in preventing co-infections, based on the *ACER* value, the most economical approach among the options in scenario 2 is Strategy F, as shown in the fifth and sixth columns of Table 5.4. The ICER of the strategies in scenario 2 is determined using the

Table 5.4: The T_{av}, T_{cost}, $\widetilde{E}$, ACER and ICER for the intervention strategies in Scenario 2.

Strategy	T_{av}	T_{cost}	$\widetilde{E}$	ACER	ICER
Strategy I $(u_2 \neq 0, u_4 \neq 0)$	55886	9141.1	0.545	0.1636	0.163567
Strategy E $(u_1 \neq 0, u_2 \neq 0)$	90741	1743.4	0.885	0.0192	-0.21224
Strategy G $(u_1 \neq 0, u_4 \neq 0)$	92990	8753.2	0.9069	0.0941	3.11685
Strategy F $(u_1 \neq 0, u_3 \neq 0)$	97478	309.06	0.9507	0.0032	-1.88149
Strategy H $(u_2 \neq 0, u_3 \neq 0)$	97478	1504.9	0.9507	0.0154	—
Strategy J $(u_3 \neq 0, u_4 \neq 0)$	97542	8540.9	0.9513	0.0876	109.9375

rank of avoided co-infections shown in Table 5.4.

$$ICER(I) = \frac{9141.1 - 0}{55886 - 0} = 0.163567$$
$$ICER(E) = \frac{1743.4 - 9141}{90741 - 55886} = -0.21224$$

$$ICER(G) = \frac{8753.2 - 1743.4}{92990 - 90741} = 3.11685$$
$$ICER(F) = \frac{309.06 - 8753.2}{97478 - 92990} = -1.88149$$
$$ICER(J) = \frac{8540.9 - 1509}{97542 - 97478} = 109.9375$$

It should be noted that $ICER(H)$ is not determined in this case because Strategies F and H prevent the same number of co-infections. The remaining results, displayed in Table 5.4, indicate that ICER(G) is less than ICER(J). This implies that, because Strategy J is more expensive than Strategy G, it should be disregarded from the Scenario 2 options, even though it is more successful in preventing co-infections. Comparing the remaining strategies(E, F, G, H and I), we can infer that Strategy G is pricier than Strategy I. Hence, it is also ruled out from further analysis. The ICER for each of the strategies I, E, and F is then computed as follows.

$$ICER(I) = \frac{9141.1 - 0}{55886 - 0} = 0.163567$$
$$ICER(E) = \frac{1743.4 - 9141}{90741 - 55886} = -0.21224$$
$$ICER(F) = \frac{309.06 - 1743.4}{97478 - 90741} = -0.21291$$

Comparing strategies E and I, it is evident that Strategy I dominates Strategy E. Consequently, Strategy I is omitted from the competitors in scenario 2. Next, as iterated below, the ICER is recalculated for Strategies E, and F.

$$ICER(E) = \frac{1743.4}{90741} = 0.0192$$
$$ICER(F) = \frac{309.06 - 1743.4}{97478 - 90741} = -0.21291$$

The incremental cost-effectiveness ratio (ICER) values obtained for Strategy F indicate that Strategy E is overpriced and ineffective as compared to Strategy F. Afterwards, Strategy E cannot be considered cost-effective in scenario 2. Consequently, we will continue to find a more cost-effective strategy from strategies F and H. It can be seen that although strategies F and H are the same in T_{av}, strategy F has a cost advantage over strategy H of $1,054.9 - 309.06 = 1195.84$. This affirms the cost-effectiveness of Strategy F. Based on this, we can conclude that Strategy F(promoting and delivering COVID-19 vaccines and treatments) is an economical approach offered in Scenario 2.

5.5.3 Cost-effectiveness Analysis of Scenario 3: Combination of Three Control Strategies

In Scenario 3, the effectiveness analysis shows that Strategies M and N are the most effective interventions (see Table 5.5). We performed an average cost-effectiveness ratio (ACER) analysis to determine the cost of applying the interventions and their effectiveness. From Table 5.5, we observe that Strategy K has the lowest ACER value. This value implies that Strategy K is an economical approach that can be implemented. To support this conclusion, we conducted an ICER analysis. The incremental cost-effectiveness ratio shown in Table 5.5 is calculated in the following manner:

$$
\begin{aligned}
ICER(L) &= \frac{9794.5-0}{93005-0} = 0.10531 \\
ICER(K) &= \frac{1392.7-9794.5}{97478-93005} = -1.87834 \\
ICER(M) &= \frac{8429.2-1392.7}{97542-97478} = 109.94531
\end{aligned}
$$

Note that because both Strategies M and N have the same T_{av} values, they prevent the same number of co-infections, $ICER(N)$ is not computed here. A comparison of Strategies L and M shows that Strategy M strongly prevails over Strategy L. As a result, strategy M is excluded from further ICER analyses. We now compare Strategies L, K, and N.

$$
\begin{aligned}
ICER(L) &= \frac{9794.5-0}{93005-0} = 0.10531 \\
ICER(K) &= \frac{1392.7-9794.5}{97478-93005} = -1.87834 \\
ICER(N) &= \frac{9579.2-1392.7}{97542-97478} = 127.9141
\end{aligned}
$$

Looking at the $ICER$ values, we observe that Strategy N is overpriced than Strategy L. Therefore, Strategy N is ruled out. Further evidence that Strategy K is more affordable than Strategy L comes from comparing $ICER(L)$ with $ICER(K)$, which indicates a cost advantage of 1.9836 for Strategy K over L. Therefore, Strategy K(administering vaccines and treatments for COVID-19 and taking steps to prevent the spread of HIV) is the most economical among the four alternatives presented in Scenario 3.

5.5.4 Cost-effectiveness Analysis of All Scenarios

The effectiveness, ACER, and ICER analyses of the implementation of all control strategies ($u_1, u_2, u_3, u_4 \neq 0$) are presented in Table 5.6. By comparing the effectiveness and costs of various strategies, we successfully identified the most efficient and cost-effective solutions for

Table 5.5: The T_{av}, T_{cost}, $\widetilde{E}$, ACER and ICER for the interventions in Scenario 3.

Strategy	T_{av}	T_{cost}	$\widetilde{E}$	ACER	ICER
Strategy L $(u_1 \neq 0, u_2 \neq 0, u_4 \neq 0)$	93005	9794.5	0.907	0.1053	0.10531
Strategy K $(u_1 \neq 0, u_2 \neq 0, u_3 \neq 0)$	97478	1392.7	0.9507	0.0143	-1.87834
Strategy M $(u_1 \neq 0, u_3 \neq 0, u_4 \neq 0)$	97542	8429.2	0.9513	0.0864	109.94531
Strategy N $(u_2 \neq 0, u_3 \neq 0, u_4 \neq 0)$	97542	9579.2	0.9513	0.0982	—

Table 5.6: The T_{av}, T_{cost}, $\widetilde{E}$, ACER and ICER for the intervention strategies in Scenario 4.

Strategy	T_{av}	T_{cost}	$\widetilde{E}$	ACER	ICER
Strategy O $(u_i \neq 0, i = 1,2,3,4)$	97542	9467.6	0.9513	0.0971	0.0971

scenarios 1, 2, 3, and 4. Now, to identify the optimal approaches across all situations, we evaluate the most efficient strategies from each scenario and compare them. Table 5.7 displays the most cost-effective strategies for each scenario, which are ranked on the basis of the number of co-infections they have prevented. This table clarifies that Strategy O is the most effective in preventing co-infection cases, as it successfully averted the highest number of co-infections compared to other strategies. Furthermore, according to the values indicated in the fifth column, Strategy F is the most economical approach among the given strategies across all scenarios. The ICER analyses further validate this conclusion and they are conducted in the following manner:

$$ICER(C) = \frac{422.4568 - 0}{97478 - 0} = 0.0043$$
$$ICER(O) = \frac{946.6 - 422.4568}{97542 - 97478} = 141.33$$

It is important to note that $ICER(F)$ and $ICER(K)$ cannot be calculated as both strategies have prevented the same number of cases, as indicated in Table 5.7. Accordingly, it is easy to see that Strategy O carries weight over Strategy C. As a result of this, strategy O is deemed unsuitable and therefore eliminated as an option. Comparing Strategies C, F, and K is still necessary. Despite preventing the same number of occurrences, Strategy F is the most economical, saving $422.4568 - 30906 = 113.4$ compared to Strategy C and $1392.7 - 309.2 = 1083.642$ in contrast with Strategy K. That is, Strategy F(promoting and delivering COVID-19 vaccines and treatments) is the most cost-effective among all the strategies provided in this work to tackle the challenges posed by HIV and COVID-19 co-infection, as shown in Figure 5.8. The letters at the top of the bars in Figure 5.8 represent strategies in the scenario. Therefore, it is recommended to prioritize these strategies for mitigating the impact of these diseases.

Table 5.7: Incremental cost-effectiveness ratio for scenarios 1 to 4.

Strategy	T_{av}	T_{cost}	$\widetilde{E}$	ACER	ICER
Strategy C $(u_3 \neq 0)$	97478	422.4568	0.9507	0.0043	0.0043
Strategy F $(u_1 \neq 0, u_3 \neq 0)$	97478	309.06	0.9507	0.0032	—
Strategy K $(u_1 \neq 0, u_2 \neq 0, u_3 \neq 0)$	97478	1392.7	0.9507	0.0143	—
Strategy O $(u_i \neq 0, i = 1,2,3,4)$	97542	9467.6	0.9513	0.0971	141.33

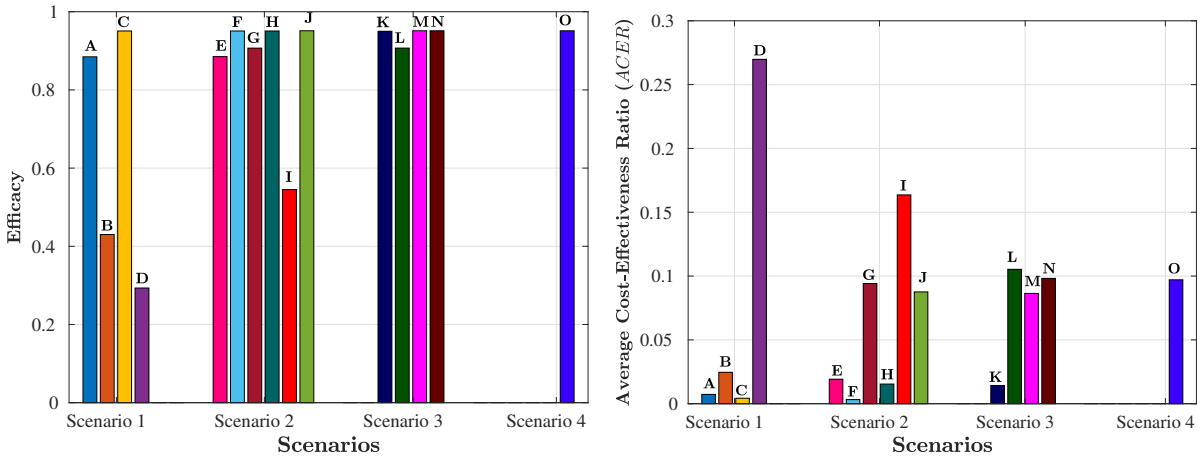

(a) Efficacy of the four scenarios.

(b) Cost-effectiveness of the four scenarios.

Figure 5.8: An overview of all scenarios and their comparative analysis.

CHAPTER 6

CO-DYNAMICS OF COVID-19, HIV and TB WITH INFORMATION-DEPENDENT VACCINATION BEHAVIOR AND WANING IMMUNITY

This chapter delves deeper into the dynamics of triple infections, specifically focusing on COVID-19, TB, and HIV. It begins with the introduction of the co-dynamics model, which integrates the interaction between these diseases. The information-dependent model is also discussed, considering how information and awareness influence disease transmission. A thorough model analysis is conducted, covering the positivity and boundedness of solutions, and extending to the examination of individual diseases and co-infection models. Special emphasis is given to the combined dynamics of the three diseases. The chapter also covers parametric estimation for model fitting and numerical simulations, which highlight key aspects such as the influence of HIV and TB on the persistence of COVID-19. Additionally, it explores the effects of reinfection and the role of behavioral parameters on disease outcomes.

6.1 The Co-dynamics Model

The model divides the total population $N(t)$ into nine disjoint compartments: susceptible (S), COVID-19 vaccinated (V_c), COVID-19 infected (I_c), TB infected(I_t), HIV infected(I_h), COVID-19 and TB co-infected(C_{ct}), COVID-19 and/or TB recovered(R_{ct}), COVID-19 and HIV co-infected(C_{ch}), TB and HIV co-infected(C_{th}) and COVID-19-HIV and TB co-infected(A). It incorporates disease-specific transmission, recovery, and mortality rates to effectively represent the interactions between COVID-19, TB, and HIV. It also captures the differences in how each disease spreads, progresses, and responds to vaccination, as well as the potential for reinfection. The recovery and re-susceptibility rates are tailored to the characteristics of each disease: COVID-19 features short-term immunity with partial protection after recovery, whereas TB and HIV have chronic courses, with HIV being considered incurable. Additionally, the model includes a transmission reduction factor for COVID-19-vaccinated individuals and recognizes the waning immunity associated with the disease.

In the model formulation, it is assumed that there is a homogeneous mixing of individuals in the population where all individuals are equally likely to catch the infection if exposed to the disease. However, contracting two or three infections simultaneously is not considered. Accordingly, susceptible individuals that increase at the recruitment rate χ may contract COVID-19, TB,

and HIV diseases at the rates of $\zeta_c = \frac{\pi_c(I_c+C_{ct}+C_{ch}+A)}{N}$, $\zeta_t = \frac{\pi_t(I_t+C_{ct}+A)}{N}$, and $\zeta_h = \frac{\pi_h(I_h+C_{ch}+A)}{N}$, respectively. The parameters π_c, π_t, and π_h represent the effective contact rates for COVID-19, TB, and HIV, respectively. Here, standard incidence functions are used to produce a more precise representation of frequency-dependent transmissions, such as HIV/AIDS, because the average number of sexual contacts per individual is relatively constant (Samares, Pal et al., 2006). Furthermore, it is understood that the spread of COVID-19 and TB might reach a threshold where adding more susceptible individuals does not significantly increase the rate of new infections due to variables such as self-protective measures (Manfredi, P. and D'Onofrio, A., 2013) and immunization (Ben Ashby and Alex Best, 2021; Ogidi, Odangowei Inetiminebiet al., 2021). This approach acknowledges that the number of contacts an individual has does not increase proportionally with population size, preventing overestimation of transmission in large populations (Samares, Pal et al., 2006). It is assumed that vaccination, which has a waning rate φ_c, is applied only to healthy individuals, so only susceptible individuals get vaccinated at a rate of ν. While COVID-19 vaccines are safe, effective, and life-saving, they do not offer complete protection to every vaccinated individual (WHO, 2024d). Furthermore, there is still a possibility of contracting COVID-19 even after being vaccinated (Flacco, Maria Elena et al., 2022; Klompas, 2021). The infection of vaccinated individuals happens at a reduced transmission rate $\sigma_c\zeta_c$, where $0 \leq \sigma_c \leq 1$ is the reduction coefficient. Here, if $\sigma_c = 0$, vaccinated individuals cannot get infected, and the vaccine is perfect. If $\sigma_c = 1$, vaccinated individuals get infected like susceptible individuals, and immunization plays no protective role. The recovered class R_{ct} receives inflows from I_c, I_t and C_{ct} at rates θ_c, θ_t, and θ_{ct}, respectively. However, a proportion of γ_c from R_{ct} become susceptible again for COVID-19 only. This assumption is taken into account because COVID-19 has a short period of recovery and loss of immunity when compared to TB. Individuals in C_{th} and A recover from TB at rates of η_t and α_t , respectively. Individuals in C_{ch} and A recover from COVID-19 at rates of φ_c and ω_c , respectively. Individuals in C_{ch} recover from COVID-19 at the rate of ϕ_c. Because HIV cannot be cured, individuals in an HIV-infected compartment are assumed to be uncured. The natural death rate μ_d reduces the number of people in each compartment. Furthermore, the disease-induced mortality rates δ_c, δ_t, δ_h, δ_{ct}, δ_{ch}, δ_{th}, and δ_a reduce the number of population in I_c, I_t, I_h, C_{ct}, C_{ch}, C_{th}, and A, respectively. Figure 6.1 illustrates the flow diagram depicting the co-dynamics of COVID-19, HIV and TB.

Bringing the aforementioned assumptions together leads to the set of nonlinear ordinary

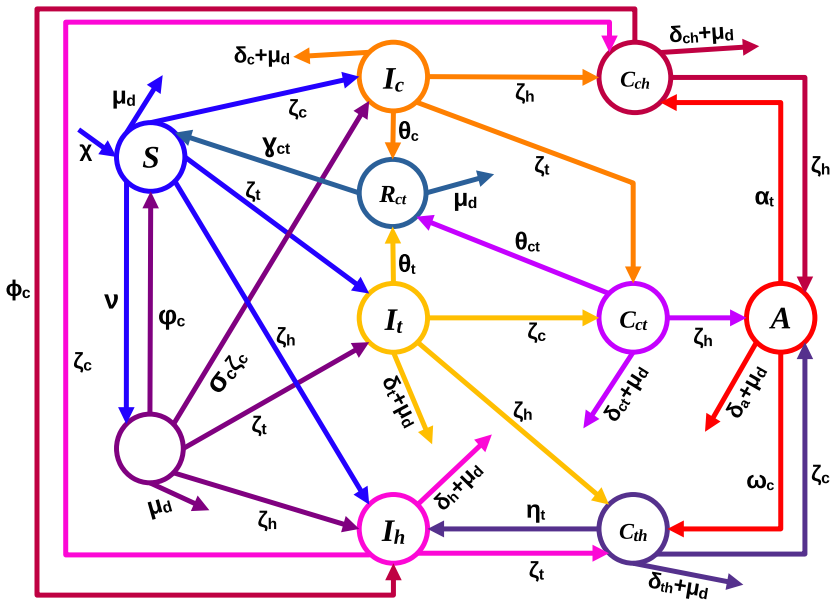

Figure 6.1: Flow diagram for model Equation (6.1).

differential equations given in equation(6.1).

$$\begin{cases} S' = \chi - (\nu + \zeta_c + \zeta_t + \zeta_h + \mu_d)S + \varphi_c V_c + \gamma_c R_{ct} \\ V_c' = \nu S - (\sigma_c\zeta_c + \zeta_t + \zeta_h + \varphi_c + \mu_d)V_c \\ I_c' = \zeta_c S + \sigma_c\zeta_c V_c - (\delta_c + \theta_c + \zeta_t + \zeta_h + \mu_d)I_c \\ I_t' = \zeta_t S + \zeta_t V_c - (\delta_t + \theta_t + \zeta_c + \zeta_h + \mu_d)I_t \\ C_{ct}' = \zeta_c I_t + \zeta_t I_c - (\delta_{ct} + \zeta_h + \theta_{ct} + \mu_d)C_{ct} \\ R_{ct}' = \theta_c I_c + \theta_t I_t + \theta_{ct} C_{ct} - (\gamma_c + \mu_d)R_{ct} \\ I_h' = \zeta_h S + \zeta_h V_c + \eta_t C_{th} + \phi_c C_{ch} - (\delta_h + \zeta_c + \zeta_t + \mu_d)I_h \\ C_{ch}' = \zeta_c I_h + \zeta_h I_c + \alpha_t A - (\delta_{ch} + \zeta_t + \mu_d + \phi_c)C_{ch} \\ C_{th}' = \zeta_t I_h + \zeta_h I_t + \omega_c A - (\delta_{th} + \eta_t + \zeta_c + \mu_d)C_{th} \\ A' = \zeta_c C_{th} + \zeta_t C_{ch} + \zeta_h C_{ct} - (\delta_a + \alpha_t + \mu_d + \omega_c)A \end{cases} \tag{6.1}$$

6.2 The Information-dependent Model

In this section, we leverage the concept of information-dependent epidemic models to transform the parameter ν in equation (6.1) into a function that takes into account the level of information accessible within the community. These information may be availed currently or on the past information they have on the spread of the disease. Following the approach of information-

dependent models (Manfredi, P. and D'Onofrio, A., 2013), the information on the status of the disease in the community is described using the information index $M(t)$. The information index function M, which summarizes the information about the current and past values of the disease , is described by the distributed delay:

$$M(t) = \int_{-\infty}^{t} g(I_c(\tau), I_{ct}(\tau), I_{ch}(\tau), A(\tau)) a e^{-a(t-\tau)} d\tau, \tag{6.2}$$

where the function g describes the role played by the COVID-19 infectious size in the information dynamics and is assumed to be dependent on the prevalence, specifically on the compartments I_c, I_{ct}, I_{ch}, and A. Thus, we assume that $g = \kappa I$, where $I = I_c + I_{ct} + I_{ch} + A$. The parameter $\kappa \in (0,1)$ represents the level of information coverage. It acts as a combination of two contrasting factors: disease under-reporting and the extent of media coverage about the disease, which tends to heighten public concern (Buonomo, 2020). The delay kernel, $ae^{-a(t-\tau)}$, in (6.2) represents the weight given to past history of the disease. The parameter a takes the meaning of the inverse of the average time delay of the collected information on the disease.

From (6.2), using linear chain trick (Norman and MacDonald, 2008), we obtain the differential equation that governs the dynamics of M as

$$M' = a(kI - M) \tag{6.3}$$

Furthermore, the vaccination rate is described by the following information-dependent function:

$$\nu(M) = \nu_0 + \nu_1(M), \tag{6.4}$$

where the constant $0 < \nu_0 < 1$ represents the fraction of the population that chooses to get vaccinated regardless of rumors and information about the status of the disease in the population, while $\nu_1(M) = \frac{hDM}{1+DM}$, where $h = \nu_{max} - \nu_0$, $\nu_{max} > \nu_0$, represents the fraction of the population whose vaccination choice is influenced by the information. The parameter ν_{max} represents the maximum level of vaccine adoption in situations with a high perceived risk. The parameter D which determines the reactivity of ν_1, reflects the effectiveness of the information campaign in promoting vaccination. Figure 6.2, simulated for parameter values $\nu_0 = 0.012, \nu_{\max} = 0.08$ and $D = 10$, depicts the information-dependent vaccination rate function $\nu(M)$. The blue curve shows how the vaccination rate ν varies with the information level M, initially increasing linearly and then saturating. The red dashed line indicates the maximum vaccination rate $\nu_{\max}$, while the green dashed line marks the threshold information level $\frac{1}{D}$ which results in half of the maximum and baseline vaccinations. At low information levels ($M \ll \frac{1}{D}$), the rate approxi-

mates $\nu \approx hDM + \nu_0$, showing a linear increase plus the baseline ν_0. At high information levels ($M \gg \frac{1}{D}$), the rate approaches $v \approx \nu_{\max}$, indicating saturation where further information has a diminishing effect. The baseline ν_0 ensures a non-zero vaccination rate even with low information dissemination. Using a function $\nu(M)$ to model information-dependent vaccination rates in offers a realistic representation of how vaccination rates increase with information levels and eventually saturate, capturing the diminishing returns of information dissemination. Incorporat-

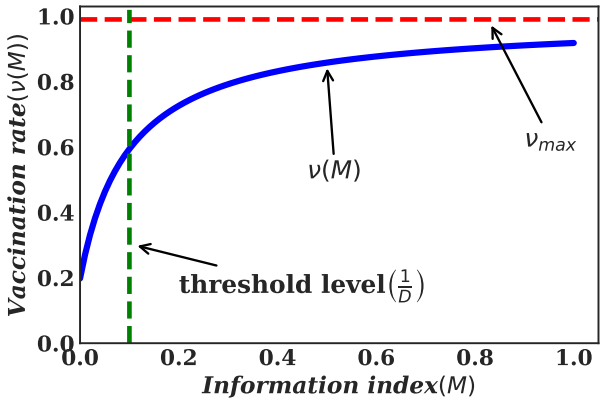

Figure 6.2: Information-dependent vaccination rate $(\nu(M))$.

ing (6.3) and (6.4), model (6.1) with information-dependent vaccination is given by:

$$\begin{cases} S' = \chi - (\nu(M) + \zeta_c + \zeta_t + \zeta_h + \mu_d)\, S + \varphi_c V_c + \gamma_c R_{ct} \\ V_c' = \nu(M) S - (\sigma_c \zeta_c + \zeta_t + \zeta_h + \Theta_1) V_c \\ I_c' = \zeta_c S + \sigma_c \zeta_c V_c - (\zeta_t + \zeta_h + \Theta_2)\, I_c \\ I_t' = \zeta_t (S + V_c) - (\zeta_c + \zeta_h + \Theta_3)\, I_t \\ C_{ct}' = \zeta_c I_t + \zeta_t I_c - (\zeta_h + \Theta_4)\, C_{ct} \\ R_{ct}' = \theta_c I_c + \theta_t I_t + \theta_{ct} C_{ct} - \Theta_5 R_{ct} \\ I_h' = \zeta_h (S + V_c) + \eta_t C_{th} + \phi_c C_{ch} - (\zeta_c + \zeta_t + \Theta_6)\, I_h \\ C_{ch}' = \zeta_c I_h + \zeta_h I_c + \alpha_t A - (\zeta_t + \Theta_7)\, C_{ch} \\ C_{th}' = \zeta_t I_h + \zeta_h I_t + \omega_c A - (\zeta_c + \Theta_8)\, C_{th} \\ A' = \zeta_c C_{th} + \zeta_t C_{ch} + \zeta_h C_{ct} - \Theta_9 A \\ M' = a(\kappa I - M) \end{cases}, \tag{6.5}$$

where $\Theta_1 = \varphi_c + \mu_d$, $\Theta_2 = \theta_c + \delta_c + \mu_d$, $\Theta_3 = \theta_t + \delta_t + \mu_d$, $\Theta_4 = \theta_{ct} + \delta_{ct} + \mu_d$, $\Theta_5 = \gamma_c + \mu_d$, $\Theta_6 = \delta_h + \mu_d$, $\Theta_7 = \phi_c + \delta_{ch} + \mu_d$, $\Theta_8 = \eta_t + \delta_{th} + \mu_d$ and $\Theta_9 = \alpha_t + \omega_c + \delta_a + \mu_d$

6.3 Model Analysis

In this section we perform sub-models and triple infection model analysis.

6.3.1 Positivity and Boundedness of the Solutions

Theorem 6.3.1. *The solutions of the model equation (6.5) with nonnegative initial data will remain nonnegative for all time $t \geq 0$ and the region*

$$\mathcal{D} = \left\{ (S,\, V_c,\, I_c,\, I_t,\, C_{ct},\, R_{ct},\, I_h,\, C_{ch},\, C_{th},\, A,\, M) \in \mathbb{R}_+^{11} |\; 0 \leq N \leq \frac{\chi}{\mu_d},\, 0 \leq M \leq \frac{\kappa\chi}{\mu_d} \right\}$$

is positively invariant and globally attracting for system (6.5).

Proof. Let

$$\begin{aligned} \tilde{t} = \sup\{t > 0 : S(t) > 0,\, V_c(t) > 0,\, I_c(t) > 0,\, I_t(t) > 0,\, C_{ct}(t) > 0, R_{ct}(t) > 0, \\ I_h(t) > 0,\, C_{ch}(t) > 0,\, C_{th}(t) > 0,\, A(t) > 0,\, M(t) > 0\}. \end{aligned}$$

Since the initial conditions are nonnegative, $\tilde{t} > 0$. If $0 < \tilde{t} < \infty$, applying the integrating-factor method on the first equation of the system (6.5) yields

$$S(\tilde{t}) = \left(S(0) + \int_0^{\tilde{t}} (\chi + \varphi_c V_c + \gamma_c R_{ct}) e^{\int_0^t f(u)du} ds \right) \times e^{-\int_0^{\tilde{t}} f(u)du}, \text{where } f(t) = \nu(M) + \zeta_c + \zeta_t + \zeta_h + \mu_d. \tag{6.6}$$

Thus, (6.6) implies that $S(\tilde{t}) > 0$. Similarly, this is true for the other variables as well. This contradicts the fact that $\tilde{t}$ is the supremum, because at least one of the variables should be equal to zero at $\tilde{t}$. Therefore, $\tilde{t} = \infty$ by definition of $\tilde{t}$, which implies that solutions of model (6.5) are all positive for all $t > 0$.

Moreover, adding all the equations in model (6.5), the total populations, N, fulfills the following equations.

$$\frac{dN}{dt} = \chi - \mu_d N - \delta_c I_c - \delta_t I_t - \delta_h I_h - \delta_{ct} C_{ct} - \delta_{ch} C_{ch} - \delta_{th} C_{th} - \delta_a A \leq \chi - \mu_d N.$$

For $N > \frac{\chi}{\mu_d}$, $\frac{dN}{dt} < 0$ and we can see that $\frac{dN}{dt}$ is bounded above by $\chi - \mu_d N$. Following Standard Comparison Theorem (Birkhoff, Garrett and Rota, Gian-Carlo, 1978), we have $0 \leq N(t) \leq \frac{\chi}{\mu_d} + \left(N(0) - \frac{\chi}{\mu_d} \right) e^{-\mu_d t}$. This implies $0 \leq N(t) \leq \frac{\chi}{\mu_d}$ for all $t \geq 0$ if $N(0) \leq \frac{\chi}{\mu_d}$. Similar procedures can be followed to show that $0 \leq M \leq \frac{\kappa\chi}{\mu_d}$. Thus, every solution of the model (6.5) with initial conditions in $\mathcal{D}$ remains there for $t > 0$. Thus, $\mathcal{D}$ is positively-invariant and attract all

solutions in $\mathbb{R}^{11}_{+}$. In this region, the model can be considered well-posed epidemiologically and mathematically (Hethcote, 2000). □

6.3.2 Analysis of Single Disease Models

When $I_c \neq 0$. $I_t = 0$ and $I_h = 0$ the following COVID-19-only sub-model is obtained.

$$\begin{cases} S' = \chi - (\nu(M) + \zeta_c + \mu_d) S + \varphi_c V_c + \gamma_c R_{ct}, \\ V_c' = \nu(M) S - (\sigma_c \zeta_c + \Theta_1) V_c \\ I_c' = \zeta_c S + \sigma_c \zeta_c V_c - \Theta_2 I_c, \\ R_{ct}' = \theta_c I_c - \Theta_5 R_{ct}, \\ M' = a(\kappa I_c - M) \end{cases} \tag{6.7}$$

with total human population $N_c = S + V_c + I_c + R_{ct}$ and $\zeta_c = \frac{\pi_c I_c}{N_c}$.

When $I_c = 0$. $I_t \neq 0$ and $I_h = 0$ the following TB-only sub-model is obtained.

$$\begin{cases} S' = \chi - (\nu_0 + \zeta_t + \mu_d) S + \varphi_c V_c \\ V_c = \nu_0 S - (\zeta_t + \Theta_1) V_c \\ I_t' = \zeta_t (S + V_c) - \Theta_3 I_t, \\ R_{ct}' = \theta_t I_c - \mu_d R_{ct}, \end{cases} \tag{6.8}$$

with total human population $N_t = S + V_c + I_t + R_{ct}$ and $\zeta_t = \frac{\pi_t I_t}{N_t}$.

Similarly, for $I_c = 0$, $I_t = 0$ and $I_h \neq 0$ the following HIV-only sub-model is obtained.

$$\begin{cases} S' = \chi - (\nu_0 + \zeta_h + \mu_d) S + \varphi_c V_c, \\ V_c = \nu_0 S - (\zeta_h + \Theta_1) V_c \\ I_h' = \zeta_h (S + V_c) - \Theta_6 I_h, \end{cases} \tag{6.9}$$

with $N_h = S + V_c + I_h$ and $\zeta_h = \frac{\pi_h I_h}{N_h}$.

The sub-model systems (6.7), (6.8) and (6.9) will be studied in the regions

$$\mathcal{D}_c = \left\{ (S,\, V_c,\, I_c,\, R_{ct},\, M) \in \mathbb{R}^5_+ : S + V_c + I_c + R_{ct} \leq \frac{\chi}{\mu_d},\, 0 \leq M \leq \frac{\kappa\chi}{\mu_d} \right\},$$

$$\mathcal{D}_t = \left\{ (S,\, V_c,\, I_c,\, R_{ct}) \in \mathbb{R}^4_+ : S + V_c + I_t + R_{ct} \leq \frac{\chi}{\mu_d} \right\} \text{ and}$$

$$\mathcal{D}_h = \left\{ (S,\, V_c,\, I_h) \in \mathbb{R}^3_+ : S + V_c + I_h \leq \frac{\chi}{\mu_d} \right\}$$

, respectively.

Following the same procedure as in Section 6.3.1 it can be easily shown that the solutions of the sub-models are positive for $t \geq 0$, that the regions $\mathcal{D}_c$, $\mathcal{D}_t$ and $\mathcal{D}_h$ are positively invariant, and that solutions starting in these regions remain there for $t > 0$.

Analysis of the COVID-19-only sub-model

In this section, qualitative analysis of the steady-state, time-independent, solution of (6.7) will be performed to investigate the long-term behavior of the disease. Because these solutions do not depend on time, we set $S'(t) = 0,\ V_c'(t) = 0, I_c{}'(t) = 0,$ and $R_{ct}'(t) = 0$. That is,

$$\chi - (\nu(M) + \zeta_c + \mu_d)\, S + \varphi_c V_c + \gamma_c R_{ct} = 0 \tag{6.10a}$$

$$\nu(M) S - (\sigma_c \zeta_c + \Theta_1) V_c = 0 \tag{6.10b}$$

$$\zeta_c S + \sigma_c \zeta_c V_c - \Theta_2 I_c = 0 \tag{6.10c}$$

$$\theta_c I_c - \Theta_5 R_{ct} = 0 \tag{6.10d}$$

$$a(\kappa I_c - M) = 0 \tag{6.10e}$$

Setting $I_c = 0$ in system (6.10) we obtain the COVID-19-free equilibrium given by $E_c = \left(\frac{\Theta_1 \chi}{\mu_d(\Theta_1 + \nu_0)}, \frac{\nu_0 \chi}{\mu_d(\Theta_1 + \nu_0)}, 0, 0, 0 \right)$. The reproduction number can be established by employing the next-generation matrix method (Appendix A.2), on system (6.7). Indeed, I_c and R_{ct} are considered to be the infected compartments. Taking the infected compartments and their dynamics into account, the appearance of new infection, $\mathcal{F}_c$, and the rate of transfer of individuals in these compartments, $\mathcal{V}_c$, is defined as follows:

$$\mathcal{F}_c = \begin{pmatrix} \zeta_c (S + \sigma_c V_c) \\ 0 \end{pmatrix} \quad \textit{and} \quad \mathcal{V}_c = \begin{pmatrix} \Theta_2 I_c \\ \Theta_5 R_{ct} - \theta_c I_c \end{pmatrix},$$

respectively.

The Jacobian matrix of $\mathcal{F}_c$ and $\mathcal{V}_c$, at E_c are

$$\mathcal{F}_c(E_c) = F_c = \begin{pmatrix} \frac{\pi_c(\nu_0 \sigma_c + \Theta_1)}{\Theta_1 + \nu_0} & 0 \\ 0 & 0 \end{pmatrix} \quad \textit{and} \quad \mathcal{V}_c(E_c) = V_c = \begin{pmatrix} \Theta_2 & 0 \\ -\theta_c & \Theta_5 \end{pmatrix}.$$

Therefore, we have

$$F_c V_c^{-1} = \begin{pmatrix} \frac{\pi_c(\nu_0\sigma_c+\Theta_1)}{\Theta_2(\Theta_1+\nu_0)} & 0 \\ 0 & 0 \end{pmatrix}.$$

The corresponding eigenvalues are $\frac{\pi_c(\nu_0\sigma_c+\Theta_1)}{\Theta_2(\Theta_1+\nu_0)}$ and 0. Hence, The basic reproduction number, $\mathcal{R}_0^c$, which is defined as the expected number of secondary cases produced by a single (typical) infection in a completely susceptible population, becomes

$$\mathcal{R}_0^c = \frac{\pi_c\left(\nu_0\sigma_c+\Theta_1\right)}{\Theta_2\left(\Theta_1+\nu_0\right)}. \tag{6.11}$$

Solving (6.10) for state variables with the assumption $\mathcal{R}_0^c > 1$ gives the endemic equilibrium(EE) denoted by $\tilde{E}_c = (S^*, V_c^*, I_c^*, R_{ct}^*, M^*)$. Thus, using $\zeta_c^* = \frac{\pi_c I_c^*}{N_c^*}$, I_c^* can be written as a function of ζ_c^*. That is,

$$I_c^* = \frac{\chi\zeta_c^*}{\mu_d\pi_c + \delta_c\zeta_c^*}. \tag{6.12}$$

Moreover, using (6.10a), (6.10b), (6.10d), (6.10e) and (6.12) , we can write S^*, V_c^*, R_{ct}^* and M^* as

$$R_{ct}^* = \frac{\theta_c I_c^*}{\Theta_5} = A_1 I_c^* \tag{6.13a}$$

$$M^* = \kappa I_c^* \tag{6.13b}$$

$$S^* = \frac{\left(D\kappa I_c^*+1\right)\left(A_1 I_c^*\gamma_c+\chi\right)\left(\zeta_c^*\sigma_c+\Theta_1\right)}{Dh\kappa I_c^*\left(\zeta_c^*\sigma_c+\mu_d\right)+\left(D\kappa I_c^*+1\right)\left(\sigma_c\left(\zeta_c^{*2}+\mu_d+\nu_0\right)+\mu_d\left(\Theta_1+\nu_0\right)+\Theta_1\right)} \tag{6.13c}$$

$$V_c^* = \frac{\left(A_1 I_c^*\gamma_c+\chi\right)\left(D\kappa I_c^*\nu_{max}+\nu_0\right)}{Dh\kappa I_c^*\left(\zeta_c^*\sigma_c+\mu_d\right)+\left(D\kappa I_c^*+1\right)\left(\zeta_c^*\left(\sigma_c\left(\zeta_c^*+\mu_d+\nu_0\right)+\Theta_1\right)+\mu_d\left(\Theta_1+\nu_0\right)\right)} \tag{6.13d}$$

A simplified form of (6.10c), after substituting (6.12), (6.13c) and (6.13d), is given by

$$a_3\zeta_c^{*3} + a_2\zeta_c^{*2} + a_1\zeta_c^* + a_0 = 0, \tag{6.14}$$

where

$$\begin{aligned} a_0 &= \pi_c\mu_d\Theta_2\left(\Theta_1+\nu_0\right)\left(1-\mathcal{R}_0^c\right) \\ a_1 &= \pi_c\mu_d\left(\nu_0\sigma_c+\Theta_1\right)\left(-A_1\gamma_c+\theta_c+\mu_d\right)+Dh\kappa\chi\mu_d\Theta_2-\pi_c Dh\kappa\chi\sigma_c\mu_d \\ &\quad +\pi_c\sigma_c\mu_d^2\left(\Theta_2-\pi_c\right)+\left(1-\mathcal{R}_0^c\right)\mu_d\Theta_2\left(\Theta_1+\nu_0\right)\left(\delta_c+D\kappa\chi\right) \end{aligned}$$

$$
\begin{aligned}
a_2 &= (\theta_c + \mu_d - A_1\gamma_c)\left((\delta_c + D\kappa\chi)(\nu_0\sigma_c + \Theta_1) + \sigma_c(\pi_c\mu_d + Dh\kappa\chi)\right) \\
&\quad + (\Theta_2 - \pi_c)(D\kappa\chi\sigma_c\mu_d + \delta_c) \\
a_3 &= \sigma_c(\delta_c + D\kappa\chi\sigma_c)(\theta_c + \mu_d - A_1\gamma_c)
\end{aligned}
$$

We can see that $a_3 > 0$. Following Descartes rule of signs, the possible number of positive roots of (6.14) are illustrated in Table 6.1. Cases 1-3 in Table 6.1 suggests existence of back-

Table 6.1: Possible number of positive roots for the cases $\mathscr{R}_0^c < 1$ and $\mathscr{R}_0^c > 1$.

Cases	a_3	a_2	a_1	a_0	$\mathcal{R}_\emptyset^c$	Number of sign changes	Possible number of EE
1	+	+	−	+	<1	2	0, 2
2	+	−	+	+	<1	2	0, 2
3	+	−	−	+	<1	2	0, 2
4	+	+	−	−	>1	1	1
5	+	−	+	−	>1	3	1, 3
6	+	−	−	−	>1	1	1
7	+	+	+	−	>1	1	1

ward bifurcation. We rely on centre manifold theory to determine the existence of an endemic equilibrium when $\mathcal{R}_\emptyset^c < 1$. Center manifold theory is a powerful tool for analyzing dynamical systems' local stability and bifurcation behavior near equilibrium points, as presented in Appendix A.3. In epidemiological models, it can be used to demonstrate backward bifurcation, a phenomenon where a stable disease-free equilibrium coexists with a stable endemic equilibrium for reproduction numbers less than one. To apply center manifold theory, one must identify equilibrium points, linearize the system, calculate eigenvalues, identify the centre manifold, reduce the system to the centre manifold, analyze the reduced system, and calculate the bifurcation parameter. The signs of bifurcation parameters, a and b, dictate the bifurcation type; backward bifurcation occurs when $a > 0$.

Certainly, with the notion in Appendix A.3, we introduce the following change of variables.

$$x_1 = S,\ x_2 = V,\ x_3 = I_c\ x_4 = R,\ x_5 = M$$

Which implies,

$$\begin{cases} x_1' = \chi - (\nu(M) + \zeta_c + \mu_d)x_1 + \varphi_c x_2 + \gamma_c x_4, \\ x_2' = \nu(M)x_1 - (\sigma_c\zeta_c + \Theta_1)x_2 \\ x_3' = \zeta_c x_1 + \sigma_c\zeta_c x_2 - \Theta_2 x_3, \\ x_4' = \theta_c x_3 - \Theta_5 x_4, \\ x_5' = a(\kappa x_3 - x_5) \end{cases}$$

Choosing π_c as the bifurcation parameter, then setting $\mathcal{R}_0^c = 1$ gives $\pi_c = \pi_c^* = \frac{\Theta_2(\Theta_1+\nu_0)}{(\nu_0\sigma_c+\Theta_1)}$. The Jacobian of (6.5) at E^0 with π_c^* has a simple eigenvalue with a zero real part, and all other eigenvalues have negative real parts. Therefore, we apply the Center Manifold Theorem to analyze the dynamics of (6.5) near π_c^*. The right and left eigenvectors, $(c_1, c_2, c_3, c_4, c_5)$ and $(e_1, e_2, e_3, e_4, e_5)$, respectively, associated with the zero eigenvalue and π_c^* are given by

$$\begin{aligned} c_1 =& -\frac{w_3\left(\Theta_1\left(D\kappa\chi h - A_1\gamma_c\left(\Theta_1+\nu_0\right)\right) + \pi_c^*\left({\Theta_1}^2 + \nu_0\sigma_c\varphi_c\right)\right)}{\mu_d\left(\Theta_1+\nu_0\right)^2}, \\ c_2 =& \frac{w_3\left(\Theta_1\left(A_1\nu_0\gamma_c + D\kappa\chi h\right) + A_1\nu_0^2\gamma_c - \pi_c^*\nu_0\left(\sigma_c\mu_d + \nu_0\sigma_c + \Theta_1\right)\right)}{\mu_d\left(\Theta_1+\nu_0\right)^2}, \\ c_3 =& c_3 > 0,\ c_4 = A_1c_3,\ c_5 = \kappa w_3 \text{ and } e_1 = e_2 = e_4 = e_5 = 0,\ e_3 = e_3 > 0 \end{aligned}$$

The bifurcation coefficients a and b are calculated as follows.

$$\begin{aligned} a =& \sum_{k,i,j=1}^{9} e_k c_i c_j \frac{\partial^2 f_k}{\partial x_i \partial x_j}(E^0, \pi_c^*) \\ =& \frac{2\pi_c^* v_3 w_3^2 (P-Q)}{\chi\left(\Theta_1+\nu_0\right)^2} \\ b =& \sum_{k,j=1}^{9} e_k c_j \frac{\partial^2 f_k}{\partial x_j \partial \pi_c}(E^0, \pi_c^*) = \frac{v_3 w_3\left(\nu_0\sigma_c + \Theta_1\right)}{\Theta_1+\nu_0} > 0, \end{aligned}$$

where

$$\begin{aligned} P =& \pi_c^*\nu_0\sigma_c\mu_d\left(1-\sigma_c\right) \text{ and} \\ Q =& D\kappa\chi h\Theta_1\left(1-\sigma_c\right) - \mu_d\left(1+A_1\right)\left(\Theta_1\left(\nu_0\left(1+\sigma_c\right)+\Theta_1\right) + \nu_0^2\sigma_c\right). \end{aligned}$$

Hence, we can conclude that system (6.5) exhibit a backward bifurcation (respectively forward) at $\mathcal{R}_0^c = 1$, provided that $a > 0$ (respectively $a < 0$). Hence the following theorem is established.

Theorem 6.3.2. *System* (6.7) *exhibits a backward bifurcation at* $\mathcal{R}_\vartheta^c = 1$ *if*

$$\frac{\pi_c^* \nu_0 \sigma_c \mu_d (1-\sigma_c)}{Dh\kappa\chi\Theta_1 (1-\sigma_c) + \mu_d (1+A_1)\left(\Theta_1 (\nu_0 (1+\sigma_c) + \Theta_1) + \nu_0^2 \sigma_c\right)} > 1 \tag{6.15}$$

We can see that, from the condition of bifurcations ($a \lesseqgtr 0$), an imperfect vaccine can determine the persistence of disease in the community. That is, as a result of the imperfect vaccine ($0 < \sigma_c \leq 1$) the disease continues to exist. If the vaccine is assumed to be perfect, which is not possible (Samares, Pal et al., 2006), the bifurcation becomes forward. This implies that, contrary to backward bifurcation, it is enough to make $\mathcal{R}_\vartheta^c < 1$ for the disease to be eliminated. Moreover, even if the vaccine is imperfect, from (6.15) it can be concluded that system (6.7) exhibits a forward bifurcation whenever $D\kappa > \frac{\pi_c^* \nu_0 (1-\sigma_c)\sigma_c \mu_d - \mu_d (1+A_1)\left(\Theta_1 (\nu_0 (\sigma_c+1)+\Theta_1)+\nu_0^2 \sigma_c\right)}{h\chi\Theta_1 (1-\sigma_c)}$. That is, if the information coverage that promotes vaccination is greater than certain critical value, the persistence of the disease due to imperfect vaccination can be altered. These results revealed that an effective vaccination information campaign promoting vaccination with vaccination coverage can eliminate the disease from the community.

Theorem 6.3.3. *The disease free equilibrium* E_c *of the model* (6.7) *is locally asymptotically stable whenever* $\mathcal{R}_\vartheta^c < 1$ *and unstable if* $\mathcal{R}_\vartheta^c > 1$.

Proof. The Jacobian of system (6.7) at the disease free equilibrium E_c is

$$\begin{pmatrix} -(\mu_d+\nu_0) & \varphi_c & -\frac{\pi_c \Theta_1}{\Theta_1+\nu_0} & \gamma_c & -\frac{hD\chi\Theta_1}{\mu_d(\Theta_1+\nu_0)} \\ \nu_0 & -\Theta_1 & -\frac{\pi_c \nu_0 \sigma_c}{\Theta_1+\nu_0} & 0 & \frac{hD\chi\Theta_1}{\mu_d(\Theta_1+\nu_0)} \\ 0 & 0 & \Theta_2(\mathcal{R}_\vartheta^c - 1) & 0 & 0 \\ 0 & 0 & \theta_c & -(\gamma_c+\mu_d) & 0 \\ 0 & 0 & a\kappa & 0 & -a \end{pmatrix}. \tag{6.16}$$

It is easy to see that eigenvalues of (6.16) are all negative whenever $\mathcal{R}_\vartheta^c < 1$. This completes the proof. □

Analysis of TB only sub-model (6.8)

The TB-free equilibrium, E_t, is the state where $I_t = 0$ and is given by

$$E_t = \left(\frac{\chi\Theta_1}{\mu_d(\Theta_1+\nu_0)}, \frac{\nu_0\chi}{\mu_d(\Theta_1+\nu_0)}, 0, 0, 0\right).$$

Taking I_t and R_{ct} as infected compartment, the next generation matrix approach gives the basic reproduction number, $\mathcal{R}_0^{\mathrm{t}}$, defined as

$$\mathcal{R}_0^{\mathrm{t}} = \frac{\pi_t}{\Theta_3}. \tag{6.17}$$

For $\mathcal{R}_0^{\mathrm{t}} > 1$, the endemic equilibrium can be given by $\tilde{E}_t = (\tilde{S}^*, \tilde{I}_t^*, \tilde{R}_{ct}^*)$, where $\tilde{I}_t^* = \frac{(\mathcal{R}_0^{\mathrm{t}}-1)\chi}{\pi_t-\delta_t}$, $R_{ct}^* = \frac{\theta_t \tilde{I}_t^*}{\mu_d}$, $\tilde{S}^* = \frac{\chi(\mu_d+\theta_t)(\varphi_c(\mu_d+\theta_t)+\mu_d(\pi_t-\delta_t))}{\mu_d(\pi_t-\delta_t)((\varphi_c+\nu_0)(\mu_d+\theta_t)+\mu_d(\pi_t-\delta_t))}$ and $\tilde{V}_c^* = \nu_0\chi(\mu_d+\theta_t)^2\tilde{S}^*$. Furthermore, by employing the same methodology as in the analysis of the COVID-19-only sub-model section, the local stability of TB-free steady-state solutions can be determined. For global stability analysis we employ Lyapunove stability analysis method.

Theorem 6.3.4. *The disease-free equilibrium of system* (6.8) *is globally asymptotically stable for* $\mathcal{R}_0^{t} < 1$.

Proof. Let $L = \{(S, V_c, I_t, R_{ct}) \in \mathcal{D}_t : S, V_c > 0\} \to \mathbb{R}$ be a function defined by $L = I_t$. Then, if $\mathcal{R}_0^{\mathrm{t}} < 1$

$$L' = \zeta_t(S+V_c) - \Theta_3 I_t \leq \Theta_3 I_t(\mathcal{R}_0^{\mathrm{t}} - 1) < 0.$$

Note that $L > 0$ for $(S, V_c, I_t, R_{ct}) \neq E_c$ and $L(E_t) = 0$. Hence L is a Lyapunov function on $\mathcal{D}_t$. Furthermore, $L' = 0$ if and only if $I_t = 0$. Therefore, the set $\{(S, V_c, I_t, R_{ct}) \in \mathcal{D}_t : L'(S, V_c, I_t, R_{ct}) = 0\}$ is the singleton $\{E_t\}$. LaSalle-Liapunov theory (see Theorem A.1.6 from Appendix A.1), implies that E_t is globally stable in $\mathcal{D}_t$ for $\mathcal{R}_0^{\mathrm{t}} < 1$. □

Analysis of HIV only sub-model (6.9)

Setting the right hand side of (6.9) equal to zero, we obtain two steady state solution, the disease free equilibrium(E_h), occurs when $I_h = 0$, and endemic equilibrium($\tilde{E}_h$), for $\mathcal{R}_0^{\mathrm{h}} > 1$. These two solutions are given as follows.

$$E_h = \left(\frac{\chi\Theta_1}{\mu_d(\Theta_1+\nu_0)}, \frac{\nu_0\chi}{\mu_d(\Theta_1+\nu_0)}, 0\right) \quad \text{and}$$

$$\tilde{E}_h = \left(\frac{\chi(\varphi_c+\pi_h-\delta_h)}{(\pi_h-\delta_h)(\varphi_c-\delta_h+\pi_h+\nu_0)}, \frac{\nu_0\chi}{(\pi_h-\delta_h)(\varphi_c+\pi_h+\nu_0-\delta_h)}, \frac{(\mathcal{R}_0^{\mathrm{h}}-1)\chi}{\pi_h-\delta_h}\right)$$

where

$$\mathcal{R}_0^{\mathrm{h}} = \frac{\pi_h}{\Theta_6} \tag{6.18}$$

is the basic reproduction number of sub-model (6.9) obtained by applying next generation matrix approach with infected compartment I_h. The local and global behaviors of the equilibrium

points can be explored using the same approach as that used in the analysis of the TB-only sub-model section. They can be easily analyzed by assuming that there is no recovery for individuals recruited into the I_t compartment, i.e., by letting $\theta_t = 0$ and changing the corresponding parameters as in system (6.9). Hence, we can conclude that E_h and $\tilde{E}_h$ are locally and globally asymptotically stable.

6.3.3 Analysis of the co-infection models

From (6.5) we can consider three different cases of co-infection with any of the two diseases: COVID-19 and HIV, COVID-19 and TB, and TB and HIV. As far as we are concerned about the burden of the emergence of COVID-19 and vaccination behaviors associated with it, we make the analyses of only two cases, COVID-19 and HIV, COVID-19 and TB. Several co-infection model studies on TB and HIV with detailed analysis have been made and readers can refer to them if they want. It follows that, if we consider the case in which $I_t = C_{ct} = C_{th} = A = 0$ in (6.5), we obtain the following COVID-19-HIV co-infection model.

$$\begin{cases} S' = \chi - (\nu(M) + \zeta_c + \zeta_h + \mu_d)\, S + \varphi_c V_c + \gamma_c R_{ct} \\ V_c' = \nu(M) S - (\sigma_c \zeta_c + \zeta_h + \Theta_1) V_c \\ I_c' = \zeta_c (S + \sigma_c V) - (\zeta_h + \Theta_2)\, I_c, \\ R_{ct}' = \theta_c I_c - \Theta_5 R_{ct}, \\ I_h' = \zeta_h (S + V) + \phi_c C_{ch} - (\zeta_c + \Theta_6)\, I_h, \\ C_{ch}' = I_h \zeta_c + \zeta_h I_c - \Theta_7 C_{ch}, \\ M' = a(k(I_c + I_{ch}) - M) \end{cases} \tag{6.19}$$

with total population $N_{ch} = S + I_c + R_{ct} + I_h + C_{ch}$, $\zeta_c = \frac{\pi_c (I_c + C_{ch})}{N_{ch}}$ and $\zeta_h = \frac{\pi_h (I_h + C_{ch})}{N_{ch}}$.

Similarly, substituting $I_h = C_{ch} = C_{th} = A = 0$, in (6.5) yields COVID-19-TB co-infection

model:

$$\begin{cases} S' = \chi - (\nu(M) + \zeta_c + \zeta_t + \mu_d)\, S + \varphi_c V_c + \gamma_c R_{ct} \\ V_c' = \nu(M) S - (\sigma_c \zeta_c + \zeta_t + \Theta_1) V_c \\ I_c' = \zeta_c (S + \sigma_c V) - (\zeta_t + \Theta_2)\, I_c, \\ I_t' = \zeta_t (S + V) - (\zeta_c + \Theta_3)\, I_t, \\ C_{ct}' = I_t \zeta_c + \zeta_t I_c - \Theta_4 C_{ct}, \\ R_{ct}' = \theta_c I_c + \theta_t I_t + \theta_{ct} C_{ct} - \Theta_5 R_{ct}, \\ M' = a(k(I_c + I_{ct}) - M) \end{cases} \tag{6.20}$$

with total population $N_{ct} = S + I_c + I_t + C_{ct} + R_{ct}$, $\zeta_c = \frac{\pi_c (I_c + C_{ct})}{N_{ct}}$ and $\zeta_t = \frac{\pi_t (I_t + C_{ct})}{N_{ct}}$.

The co-infection models (6.19) and (6.20) will be studied in the regions
$\mathcal{D}_{ch} = \left\{ (S, I_c, I_h, R_{ct}, C_{ch}) \in \mathbb{R}^5_+ : S + I_c + I_h + R_{ct} + C_{ch} \leq \frac{\chi}{\mu_d} \right\}$ and
$\mathcal{D}_{ct} = \left\{ (S, I_c, I_t, R_{ct}, C_{ct}) \in \mathbb{R}^5_+ : S + I_c + I_t + R_{ct} + C_{ct} \leq \frac{\chi}{\mu_d} \right\}$, respectively.

It can be easily shown that, as in Section 5.3, the solutions of the co-infection models are positive for all $t > 0$ and that the regions $\mathcal{D}_{ch}$ and $\mathcal{D}_{ct}$ are positively invariant and solutions starting in these regions stay in the regions for $t > 0$.

Analysis of the COVID-19-HIV co-infection sub-model (6.19)

COVID-19-HIV free equilibrium, denoted by E_{ch}, is obtained by setting the right-hand side of the system of equations in (6.19) equal to zero. At disease-free equilibrium, there are no infections or recovery. That is, $I_c = I_h = C_{ch} = M = R_{ct} = 0$. Thus,

$$E_{ch} = \left(\frac{\chi \Theta_1}{\mu_d (\Theta_1 + \nu_0)}, \frac{\nu_0 \chi}{\mu_d (\Theta_1 + \nu_0)}, 0, 0, 0, 0, 0 \right).$$

To determine the basic reproduction number, the next generation matrix method is used by considering I_c, I_h, and C_{ch} as infected compartments of model (6.19). Thus,

$$\frac{d}{dt} \begin{pmatrix} I_c \\ I_h \\ C_{ch} \end{pmatrix} = \mathcal{F}_{ch} - \mathcal{V}_{ch},$$

where

$$\mathcal{F}_{ch} = \begin{pmatrix} \zeta_c(S+\sigma_c V) \\ \zeta_h(S+V) \\ \zeta_c I_h + \zeta_h I_c \end{pmatrix} \quad and \quad \mathcal{V}_{ch} = \begin{pmatrix} (\Theta_2+\zeta_h)I_c \\ (\Theta_6+\zeta_c)I_h \\ \Theta_7 C_{ch} \end{pmatrix}.$$

The Jacobian matrix of $\mathcal{F}_{ch}$ and $\mathcal{V}_{ch}$ at E_{ch} (F_{ch} and V_{ch}) are

$$F_{ch} = \begin{pmatrix} \frac{\pi_c(\nu_0\sigma_c+\Theta_1)}{\Theta_1+\nu_0} & 0 & \frac{\pi_c(\nu_0\sigma_c+\Theta_1)}{\Theta_1+\nu_0} \\ 0 & \pi_h & \pi_h \\ 0 & 0 & 0 \end{pmatrix} \quad and \quad V_{ch} = \begin{pmatrix} \Theta_2 & 0 & 0 \\ 0 & \Theta_6 & -\phi_c \\ 0 & 0 & \Theta_7 \end{pmatrix}.$$

Therefore, we have

$$F_{ch}V_{ch}^{-1} = \begin{pmatrix} \mathcal{R}_0^{\,c} & 0 & \frac{\Theta_2\mathcal{R}_0^{\,c}}{\Theta_7} \\ 0 & \mathcal{R}_0^{\,h} & \frac{(\phi_c+\Theta_6)\mathcal{R}_0^{\,h}}{\Theta_7} \\ 0 & 0 & 0 \end{pmatrix}.$$

The corresponding eigenvalues are $\mathcal{R}_0^{\,c}, \mathcal{R}_0^{\,h}$ and 0. Hence, the basic reproduction number ($\mathcal{R}_0^{\,ch}$) of COVID-19-HIV co-infection model is $\mathcal{R}_0^{\,ch} = \max\left\{\mathcal{R}_0^{\,c},\ \mathcal{R}_0^{\,h}\right\}$.

Theorem 6.3.5. *E_{ch} is locally asymptotically stable whenever $\mathcal{R}_0^{\,ch} < 1$ and unstable if $\mathcal{R}_0^{\,ch} > 1$.*

Proof. The Jacobian of (6.19) at the disease free equilibrium E_{ch} is

$$\begin{pmatrix} -\mu_d-\nu_0 & \varphi_c & -\frac{\pi_c\Theta_1}{\Theta_1+\nu_0} & \gamma_c & -\frac{\pi_h\Theta_1}{\Theta_1+\nu_0} & -\frac{\Theta_1(\pi_c+\pi_h)}{\Theta_1+\nu_0} & -\frac{Dh\chi\Theta_1}{\mu_d(\Theta_1+\nu_0)} \\ \nu_0 & -\varphi_c-\mu_d & -\frac{\pi_c\nu_0\sigma_c}{\Theta_1+\nu_0} & 0 & -\frac{\pi_h\nu_0}{\Theta_1+\nu_0} & -\frac{\nu_0(\pi_c\sigma_c+\pi_h)}{\Theta_1+\nu_0} & \frac{Dh\chi\Theta_1}{\mu_d(\Theta_1+\nu_0)} \\ 0 & 0 & \Theta_2(\mathcal{R}_0^{\,c}-1) & 0 & 0 & \frac{\pi_c(\nu_0\sigma_c+\Theta_1)}{\Theta_1+\nu_0} & 0 \\ 0 & 0 & \theta_c & -\gamma_c-\mu_d & 0 & 0 & 0 \\ 0 & 0 & 0 & 0 & \Theta_6(\mathcal{R}_0^{\,h}-1) & \phi_c+\pi_h & 0 \\ 0 & 0 & 0 & 0 & 0 & -\Theta_7 & 0 \\ 0 & 0 & a\kappa & 0 & 0 & a\kappa & -a \end{pmatrix}. \tag{6.21}$$

The eigenvalues of (6.21) are: $-\mu_d$, $-a$, $-(\Theta_1+\nu_0)$, $-\Theta_5$, $\Theta_2(\mathcal{R}_0^{\,c}-1)$, $\Theta_6(\mathcal{R}_0^{\,h}-1)$ and $-\Theta_7$. Since $\mathcal{R}_0^{\,c},\ \mathcal{R}_0^{\,h} \leq \mathcal{R}_0^{\,ch}$, eigenvalues of (6.21) are all negative whenever $\mathcal{R}_0^{\,ch} < 1$. Hence, E_{ch} is locally asymptotically stable. □

To investigate the global stability of E_{ch} , we employ the method described in Chavez, C Castillo et al. (2002). Adopting the notion in Section 4.2.4, we write system (6.19) in the form

$$\frac{d\mathbf{X}}{dt} = F(\mathbf{X},\mathbf{I})$$
$$\frac{d\mathbf{I}}{dt} = G(\mathbf{X},\mathbf{I}),\ G(\mathbf{X},\mathbf{0}) = \mathbf{0}$$

where $\mathbf{X} = (S, V_c, R_{ct}, M)$ and $\mathbf{I} = (I_c, I_h, C_{ch})$ denotes uninfected and infected population respectively. $U_0 = (\mathbf{X}^*, \mathbf{0})$ denotes the disease-free equilibrium of system (6.19). Furthermore, suppose

H1: For $\frac{d\mathbf{X}}{dt} = F(\mathbf{X},\mathbf{0})$, $\mathbf{X}^*$ is globally asymptotically stable,

H2: $G(\mathbf{X},\mathbf{I}) = A\mathbf{I} - \hat{G}(\mathbf{X},\mathbf{I}),\ \hat{G}(\mathbf{X},\mathbf{I}) \geq 0$ for $(\mathbf{X},\mathbf{I}) \in \mathcal{D}_{ch}$,
where $A = D_{\mathbf{I}}G(\mathbf{X}^*,\mathbf{0})$ is an M-matrix (the off-diagonal elements of A are nonnegative).

If the model (6.19) met $H1$ and $H2$ then the following theorem holds:

Theorem 6.3.6. *$U_0 = (\mathbf{X}^*,\mathbf{0})$ is a globally asymptotic stable equilibrium of (6.19) provided that $\mathcal{R}_0^{ch} < 1$ and that assumptions (Hl) and (H2) are satisfied.*

Proof. To look into $H1$ and $H2$, we write

$$F(\mathbf{X},\mathbf{0}) = \begin{pmatrix} \chi - (\nu_0 + \mu_d)S + \varphi_c V_c + \gamma_c R_{ct} \\ \nu_0 S - \Theta_1 V_c \\ -\Theta_5 R_{ct} \\ -aM \end{pmatrix},$$

$$A = \begin{pmatrix} -\Theta_2(1-\mathcal{R}_0^{c}) & 0 & \Theta_2\mathcal{R}_0^{c} \\ 0 & -\Theta_6(1-\mathcal{R}_0^{h}) & \pi_h + \phi_c \\ 0 & 0 & -\Theta_7 \end{pmatrix}$$

and

$$\hat{G}(\mathbf{X},\mathbf{I}) = \begin{pmatrix} \left(\Theta_2\mathcal{R}_0^{c} - \frac{(S+\sigma_c V_c)\pi_c}{N_{ch}}\right)(I_c + C_{ch}) + \zeta_h I_c \\ \pi_h C_{ch}\left(1 - \frac{S+V_c}{N_{ch}}\right) + I_h(\Theta_6\mathcal{R}_0^{h} - \frac{(S+V_c)\pi_h}{N_{ch}}) + \zeta_c I_h \\ -\zeta_c I_h - \zeta_h I_c \end{pmatrix}.$$

As we can see from the above, all rows of $\hat{G}(\mathbf{X},\mathbf{I})$ are not non negative for all $(\mathbf{X},\mathbf{I}) \in \mathcal{D}_{ch}$. So assumption $H2$ is not satisfied. Hence, the disease-free equilibrium E_{ch} may not be globally stable, and backward bifurcation may occur in the system (6.19) like in the case of COVID-19 only sub-model (5.1). That is, the co-infection may persist even if the dominant reproduction

number ($\mathcal{R}_0^{ch}$) is less than unity. The existence of backward bifurcation in system (6.19) can be proved by the same steps as in the COVID-19-only model, so it is omitted. However, the following theorem is proved to show the non occurrence of backward bifurcation whenever the COVID-19 vaccine is perfect, whereby everybody who is vaccinated is completely protected. □

Theorem 6.3.7. *If we have a perfect COVID-19-vaccine* ($\sigma_c = 0$)*, E_{ch} is globally asymptotically stable for* $\mathcal{R}_0^{ch} < 1$.

Proof. System (6.19) implies,

$$\begin{aligned}
(I_c + I_h + C_{ch})' =& \zeta_c S + \zeta_h (S+V) - \Theta_2 I_c - \Theta_6 I_h - (\delta_{ch} + \mu_d) C_{ch} \\
\leq& \pi_c I_c + \pi_h I_h - \Theta_2 I_c - \Theta_6 I_h + (\pi_c + \pi_h - \delta_{ch} - \mu_d) C_{ch} \\
=& (\pi_c - \Theta_2) I_c + (\pi_h - \Theta_6) I_h + (\pi_c + \pi_h - \delta_{ch} - \mu_d) C_{ch} \\
=& \Theta_2 \left(\frac{\pi_c}{\Theta_2} - 1 \right) I_c + \Theta_6 (\mathcal{R}_0^{h} - 1) I_h \\
&+ (\delta_{ch} + \mu_d) \left(\frac{\pi_c + \pi_h}{\delta_{ch} + \mu_d} - 1 \right) C_{ch} \\
\leq& \Upsilon (I_c + I_h + C_{ch})
\end{aligned}$$

That is,

$$(I_c + I_h + C_{ch})' \leq \Upsilon (I_c + I_h + C_{ch}), \tag{6.22}$$

where $\Upsilon = \max \left\{ \Theta_2 \left(\frac{\pi_c}{\Theta_2} - 1 \right), \Theta_6 (\mathcal{R}_0^{h} - 1), (\delta_{ch} + \mu_d) \left(\frac{\pi_c + \pi_h}{\delta_{ch} + \mu_d} - 1 \right) \right\}$.

After, solving (6.22) and evaluating it as time tends to infinity, we obtain $I_c + I_h + C_{ch} = 0$ for $\max \left\{ \frac{\pi_c}{\Theta_2}, \mathcal{R}_0^{h}, \frac{\pi_c + \pi_h}{\delta_{ch} + \mu_d} \right\} < 1$. Since $0 \leq I_c, I_h, C_{ch}$, each must approach zero in the limit. Therefore, as $t \to \infty$, the solutions $I_c, I_h, C_{ch} \to 0$. Substituting $I_c, I_h, C_{ch} = 0$ in model (6.19), implies, as $t \to \infty$, R_{ct}, $M \to 0$, $S \to \frac{\chi \Theta_1}{\mu_d (\Theta_1 + \nu_0)}$ and $V_c \to \frac{\nu_0 \chi}{\mu_d (\Theta_1 + \nu_0)}$. Hence, we can conclude that E_{ch} is globally asymptotically stable $\mathcal{R}_0^{ch} < 1$. The global stability of the disease-free equilibrium E_{ch} for $\mathcal{R}_0^{ch} < 1$ claim non existence of backward bifurcation. That is, the diseases persist only if $\mathcal{R}_0^{ch} > 1$. □

Analysis of the co-infection of COVID-19-TB co-infection model (6.20)

Considering $I_c = I_t = C_{ct} = R_{ct} = M = 0$ and setting systems of equations in (6.20) in to zero, we obtain the disease free equilibrium (E_{ct}) given by $E_{ct} = \left(\frac{\chi \Theta_1}{\mu_d (\Theta_1 + \nu_0)}, \frac{\nu_0 \chi}{\mu_d (\Theta_1 + \nu_0)}, 0, 0, 0, 0, 0 \right)$.

The same procedure can be followed as in COVID-19-HIV co-infection model to obtain the reproduction number ($\mathcal{R}_0^{ct}$) of COVID-19-TB co-infection model and to investigate the stability of steady state solutions. Hence, $\mathcal{R}_0^{ct} = \max\left\{\mathcal{R}_0^{c}, \mathcal{R}_0^{t}\right\}$. Furthermore, one can easily prove that E_{ct} is both locally and globally (when $\sigma_c = 0$) asymptotically stable whenever $\mathcal{R}_0^{ct} < 1$.

6.3.4 Analysis of COVID-19, HIV and TB Triple Infection Model

The disease free equilibrium(E^0), the state in which the population is completely free from the three diseases, is given by

$$E^0 = \left(\frac{\chi\Theta_1}{\mu_d(\Theta_1+\nu_0)}, \frac{\nu_0\chi}{\mu_d(\Theta_1+\nu_0)}, 0,0,0,0,0,0,0,0,0\right).$$

To obtain the basic reproduction number($\mathcal{R}_0$) of the model (6.5), we apply the next-generation matrix approach. Indeed, the infected compartments of the model (6.5) consist of $I_c, I_t, I_h, C_{ct}, C_{ch}$, C_{th} and A classes. The dynamics of these infected compartments can be written as a difference of two matrices, $\mathcal{F}$ and $\mathcal{V}$. That is,

$$\mathcal{F} = \begin{pmatrix} \zeta_c(S+\sigma_c V_c) \\ \zeta_t(S+V_c) \\ \zeta_c I_t + \zeta_t I_c \\ \zeta_h(S+V_c) \\ \zeta_c I_h + \zeta_h I_c \\ \zeta_t I_h + \zeta_h I_t \\ \zeta_c C_{th} + \zeta_t C_{ch} + \zeta_h C_{ct} \end{pmatrix} \quad and \quad \mathcal{V} = \begin{pmatrix} (\zeta_t+\zeta_h+\Theta_2)I_c \\ (\zeta_c+\zeta_h++\Theta_3)I_t \\ (\zeta_h+\Theta_4)C_{ct} \\ (\zeta_c+\zeta_t+\Theta_6)I_h - \eta_t C_{th} - C_{ch}\phi_c \\ (+\zeta_t+\Theta_7)C_{ch} - \alpha_t A \\ (\zeta_c+\Theta_8)C_{th} - A\omega_c \\ \Theta_9 A \end{pmatrix}.$$

The Jacobian matrix of $\mathcal{F}$ and $\mathcal{V}$ at E^0, denoted by $\tilde{F}$ and $\tilde{V}$, respectively, are computed as

$$\tilde{F}\tilde{V}^{-1} = \begin{pmatrix} \mathcal{R}_0^{c} & 0 & 0 & \frac{\Theta_2\mathcal{R}_0^{c}}{\Theta_4} & \frac{\Theta_2\mathcal{R}_0^{c}}{\Theta_7} & 0 & \frac{\xi_3\Theta_2\mathcal{R}_0^{c}}{\Theta_7\Theta_9} \\ 0 & \mathcal{R}_0^{t} & 0 & \frac{\pi_t}{\Theta_4} & 0 & \frac{\pi_t}{\Theta_8} & \frac{\xi_4\pi_t}{\Theta_7\Theta_9} \\ 0 & 0 & \mathcal{R}_0^{h} & 0 & \frac{\xi_1\mathcal{R}_0^{h}}{\Theta_7} & \frac{\xi_2\mathcal{R}_0^{h}}{\Theta_7} & \frac{\mathcal{R}_0^{h}(\Theta_7(\xi_5\Theta_6+\eta_t\xi_4)+\alpha_t\xi_1\Theta_8)}{\Theta_7\Theta_8\Theta_9} \\ 0 & 0 & 0 & 0 & 0 & 0 & 0 \\ 0 & 0 & 0 & 0 & 0 & 0 & 0 \\ 0 & 0 & 0 & 0 & 0 & 0 & 0 \\ 0 & 0 & 0 & 0 & 0 & 0 & 0 \end{pmatrix},$$

where $\xi_1 = \phi_c + \Theta_6$, $\xi_2 = \Theta_6 + \eta_t$, $\xi_3 = \Theta_7 + \alpha_t$, $\xi_4 = \Theta_8 + \omega_c$, and $\xi_5 = \omega_c + \mu_d + \delta_{th}$.

Which implies, $\mathcal{R}_0 = \max\left\{\mathcal{R}_0^{\mathrm{c}},\ \mathcal{R}_0^{\mathrm{t}},\ \mathcal{R}_0^{\mathrm{h}}\right\}$.

Theorem 6.3.8. *E^0 is locally asymptotically stable whenever $\mathcal{R}_0 < 1$.*

Proof. The Jacobian of system (6.5) at E^0 is

$$\begin{pmatrix}
\beta_1 & \varphi_c & \beta_2\Theta_1 & \beta_3\Theta_1 & \gamma_{\mathrm{ct}} & \beta_4\Theta_1 & \beta_6\Theta_1 & \beta_7\Theta_1 & \beta_8\Theta_1 & \beta_9\Theta_1 & -\beta_{10}\Theta_1 \\
\nu_0 & -\Theta_1 & \beta_2\nu_0\sigma_c & \beta_3\nu_0 & 0 & \beta_4\nu_0 & \beta_{11}\nu_0 & \beta_{12}\nu_0 & \beta_8\nu_0 & \beta_{13}\nu_0 & \beta_{10}\Theta_1 \\
0 & 0 & \beta_{14} & 0 & 0 & 0 & \Theta_2 r_c & \Theta_2 r_c & 0 & \Theta_2 r_c & 0 \\
0 & 0 & 0 & \beta_{15} & 0 & 0 & \pi_t & 0 & \pi_t & \pi_t & 0 \\
0 & 0 & \theta_c & \theta_t & -\Theta_5 & 0 & \theta_{\mathrm{ct}} & 0 & 0 & 0 & 0 \\
0 & 0 & 0 & 0 & 0 & \beta_{16} & 0 & \phi_c + \pi_h & \pi_h + \eta_t & \pi_h & 0 \\
0 & 0 & 0 & 0 & 0 & 0 & -\Theta_4 & 0 & 0 & 0 & 0 \\
0 & 0 & 0 & 0 & 0 & 0 & 0 & -\Theta_7 & 0 & \alpha_t & 0 \\
0 & 0 & 0 & 0 & 0 & 0 & 0 & 0 & -\Theta_8 & \omega_c & 0 \\
0 & 0 & 0 & 0 & 0 & 0 & 0 & 0 & 0 & -\Theta_9 & 0 \\
0 & 0 & a\kappa & 0 & 0 & 0 & a\kappa & a\kappa & 0 & a\kappa & -a
\end{pmatrix},$$

where $\beta_1 = -(\mu_d + \nu_0)$, $\beta_2 = -\frac{\pi_c}{\Theta_1+\nu_0}$, $\beta_3 = -\frac{\pi_t}{\Theta_1+\nu_0}$, $\beta_4 = -\frac{\pi_h}{\Theta_1+\nu_0}$, $\beta_5 = -\frac{\sigma_c\pi_c}{\Theta_1+\nu_0}$, $\beta_6 = \beta_2 + \beta_3$, $\beta_7 = \beta_2 + \beta_4$, $\beta_8 = \beta_3 + \beta_4$, $\beta_9 = \beta_2 + \beta_3 + \beta_4$, $\beta_{10} = -\frac{hD\chi}{\mu_d(\Theta_1+\nu_0)}$, $\beta_{11} = -\beta_3 + \beta_5$, $\beta_{12} = -\beta_4 + \beta_5$, $\beta_{13} = -\beta_3 + \beta_4 + \beta_5$, $\beta_{14} = \Theta_2(\mathcal{R}_0^{\mathrm{c}} - 1)$, $\beta_{15} = \Theta_3\left(\mathcal{R}_0^{\mathrm{t}} - 1\right)$ and $\beta_{16} = \Theta_6\left(\mathcal{R}_0^{\mathrm{h}} - 1\right)$.

It is easy to see that all eigenvalues are negative if and only if $\mathscr{R}_0 < 1$. Therefore, E^0 is locally asymptotically stable whenever $\mathscr{R}_0 < 1$. □

The backward bifurcation analysis, which is exhibited due to imperfect vaccination, can be made with the same procedure as in Section 6.3.2 by taking the bifurcation parameter as π_c (that is by letting $\mathscr{R}_0 = \mathscr{R}_0^{\mathrm{c}}$).

6.4 Parametric Estimation

This study fits the suggested model to the retrieved data and fits some of the unknown parameters using WHO reports. Ethiopia, located in East Africa, has a high burden of HIV and TB cases (World Health Organization, 2024a), with reports indicating the emergence of triple infections involving COVID-19, TB, and HIV (Bizuneh, Fassikaw et al., 2024), making it a prime candidate for parametric estimation. To estimate parameters associated with COVID-19, monthly cumulative data from March 2020, the month in which COVID-19 was introduced in Ethiopia, to December 2023 is considered (WHO, 2024b). The parameters associated with

TB are estimated using notified case reports from 2000 to 2022 (World Health Organization, 2024b), while parameters associated with HIV are fitted based on WHO's new case estimations for the country from 2000 to 2022 (World Health Organization, 2024c). In order to fit the model to actual data, we used the *lmfit* Python library, which is specifically designed for nonlinear least-squares fitting (Newville, Matt et al., 2021). The remaining parameter values were obtained from the existing literature. In cases where data were unavailable, we estimated certain parameters within acceptable ranges. To maintain consistency and prevent calculation errors, all the estimated and fitted parameters in the model are standardized to a common dimension of $month^{-1}$. The total population was estimated to be $126,\ 527,\ 060$ with a life expectancy of 66 years (World Bank, 2022). It follows that $\mu_d = \frac{1}{66*12}$ and $\chi = \mu_d * N = 159756$ per month. The maximum vaccination rate ($\nu_{\max}$) is assumed to be 0.99 per month, with a baseline vaccination rate of $20\%(0.2 * \nu_{\max})$. Multiple studies have indicated that the effectiveness of COVID-19 vaccines ranges from 82% to 95% (Caifang Zheng et al., 2022; Nasreen, Sharifa et al., 2022), suggesting an ineffectiveness of 5% to 18%. Therefore, we estimated σ_c to be 13%. Furthermore, based on studies revealing that the minimum and maximum incidence rates of COVID-19 reinfection were 0.001% and 0.65% (Alimohamadi, Yousef et al., 2023), we estimate γ_c to be 0.01%. The remaining parameters are assumed to have values in Table 6.2. The solution curve in comparison with the actual data is shown in Figure 6.3. The figure presents the fitting of model (5.1) to real data for COVID-19, TB, and HIV. In Figure 6.3a, the model fitting to COVID-19 cases is displayed over 45 months, showing good agreement with the observed data. The model captures the rise and plateau in infections. Figure 6.3b illustrates the fit for TB cases over 22 years, where the model successfully follows the peak and subsequent decline in cases. Moreover, Figure 6.3c shows the fit of the estimated new HIV infections over the same 22 year period. The model captures the decline in HIV infection, suggesting a strong fit. The model output in all three subplots aligns well with the observed data, demonstrating that the model provides a reasonably good representation of the epidemiological dynamics of these diseases. The Python code utilized for parameter estimation can be found in Appendix B.1.

6.5 Numerical Simulations and Results

In this section, numerical results verifying the analytical findings and showing the effect of some parameter values are presented. Unless it is stated, the parameter values in Table 6.2 and the initial conditions $S(0) = 125775247$, $V_c(0) = 0$, $I_c(0) = 16$, $I_t(0) = 112597$, $C_{ct}(0) = 0$, $R_{ct}(0) = 8000$, $I_h(0) = 630000$, $C_{ch}(0) = 0$, $C_{th}(0) = 1200$, $A(0) = 0$ and $M(0) = 3.2(0.2 * I_c(0))$ are used to perform numerical simulations.

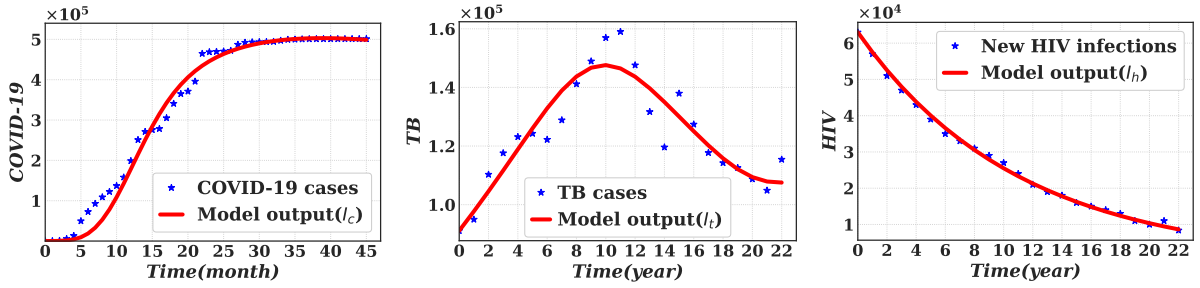

(a) COVID-19 data (b) TB data (c) HIV data

Figure 6.3: The fit of model (6.5) to the actual data.

6.5.1 The Role of HIV and TB on the Persistence of COVID-19

In this section, we analyze the impact of HIV and TB on the transmission of COVID-19. This will be accomplished by expressing the reproduction number of COVID-19 in terms of the reproduction number of HIV and TB with the help of μ_d. From (6.17) and (6.18), we have

$$\mu_d = \frac{\pi_t - \delta_t \mathcal{R}_0^{\mathrm{t}} - \theta_t \mathcal{R}_0^{\mathrm{t}}}{\mathcal{R}_0^{\mathrm{t}}} \tag{6.23}$$

$$\mu_d = \frac{\pi_h - \delta_h \mathcal{R}_0^{\mathrm{h}}}{\mathcal{R}_0^{\mathrm{h}}} \tag{6.24}$$

Substituting (6.23) in $\mathcal{R}_0^{\mathrm{c}}$ yields $\mathcal{R}_0^{\mathrm{c}} = \frac{\pi_c \mathcal{R}_0^{\mathrm{t}} \left(\pi_t + \mathcal{R}_0^{\mathrm{t}} (\nu_0 \sigma_c + \varphi_c - \delta_t - \theta_t)\right)}{\left(\pi_t + \mathcal{R}_0^{\mathrm{t}} (\delta_c + \theta_c - \delta_t - \theta_t)\right)\left(\pi_t + \mathcal{R}_0^{\mathrm{t}} (\varphi_c + \nu_0 - \delta_t - \theta_t)\right)}$. Similarly, substituting (6.24) in $\mathcal{R}_0^{\mathrm{c}}$ gives $\mathcal{R}_0^{\mathrm{c}} = \frac{\pi_c \mathcal{R}_0^{\mathrm{h}} \left(\pi_h + \mathcal{R}_0^{\mathrm{h}} (\nu_0 \sigma_c + \varphi_c - \delta_h)\right)}{\pi_h + \left(\mathcal{R}_0^{\mathrm{h}} (\delta_c + \theta_c - \delta_h)\right)\left(\pi_h + \mathcal{R}_0^{\mathrm{h}} (\varphi_c + \nu_0 - \delta_h)\right)}$. If $\frac{\partial \mathcal{R}_0^c}{\partial \mathcal{R}_0^{\mathrm{t}}}, \frac{\partial \mathcal{R}_0^c}{\partial \mathcal{R}_0^{\mathrm{h}}} > 0$, it can be concluded that an increase in TB and HIV transmission would result in an increase in COVID-19 transmission as well.The role played by both HIV and TB in the spread of COVID-19 is explored by writing $\mathcal{R}_0^c$ as a function of $\mathcal{R}_0^t$ and $\mathcal{R}_0^h$. Indeed, we add (6.23) and (6.24) and solve for μ_d as follows:

$$\mu_d = \frac{\pi_t \mathcal{R}_0^h + \pi_h \mathcal{R}_0^t - (\delta_t + \delta_h + \theta_t) \mathcal{R}_0^t \mathcal{R}_0^h}{2 \mathcal{R}_0^t \mathcal{R}_0^h}. \tag{6.25}$$

Thus, by substituting (6.25) into (6.11) we can describe $\mathcal{R}_0^c$ as

$$\mathcal{R}_0^c = \frac{2\pi_c \mathcal{R}_0^t \mathcal{R}_0^h \left(\pi_h \mathcal{R}_0^t + \mathcal{R}_0^h \pi_t + \mathcal{R}_0^t \mathcal{R}_0^h (2\nu_0 \sigma_c + 2\varphi_c - \delta_h - \delta_t - \theta_t)\right)}{\left(\pi_h \mathcal{R}_0^t + \mathcal{R}_0^h \left(\pi_t + \mathcal{R}_0^t \psi_1\right)\right)\left(\pi_h \mathcal{R}_0^t + \mathcal{R}_0^h \left(\pi_t + \mathcal{R}_0^t \psi_2\right)\right)},$$

Table 6.2: Description of parameters of the triple infection model Equation (6.5).

Parameters	Description	Values	Source
χ	Recruitment rate	159756	Calculated
δ_a	COVID-19, TB and HIV induced death rate	0.62	Estimated
θ_t	TB Recovery rate for I_t	0.06533	Fitted
δ_{ch}	COVID-19 and HIV induced death rate	0.18852	(see Table 4.3)
φ_c	Covid-19 vaccine waning rate	0.01282	Estimated
γ_c	Reinfection rate for COVID-19	0.0833	Estimated
η_t	TB recovery for C_{th}	0.0001	Estimated
π_h	HIV transmission rate	0.01033	Fitted
θ_c	Recovery rate for population in I_c	0.3474	Fitted
ν_{max}	Maximum vaccination rate	0.99	Estimated
ν_0	Baseline vaccination rate	$0.2 * \nu_{max}$	Estimated
σ_c	Vaccine inefficacy	0.13	Estimated
ϕ_c	COVID-19 recovery for C_{ch}	0.1	Fitted
δ_c	COVID-19 induced death rate	0.031	Fitted
π_t	TB transmission rate	0.07131	Fitted
δ_h	HIV induced death rate	0.01824	Fitted
θ_{ct}	Recovery rate from C_{ct}	0.2	Estimated
δ_{ct}	COVID-19 and TB induced death rate	0.5	Estimated
δ_t	TB induced death rate	$2 * 10^{-5}$	Fitted
π_c	COVID-19 transmission rate	2.402	Fitted
δ_{th}	TB and HIV induced death rate rate	0.39732	Estimated
ω_c	COVID-19 recovery rate for A	0.25	Estimated
α_t	TB recovery rate for A	0.02083	Estimated
μ_d	Natural death rate	0.00126	(World Bank, 2022)
D	Reactivity factor	$3.9517 * 10^{-6}$	Estimated
κ	Information coverage	0.2	Estimated
a	Inverse of the average information delay	0.2	Estimated

where $\psi_1 = (2\delta_c + 2\theta_c - \delta_h - \delta_t - \theta_t)$ and $\psi_2 = (2\varphi_c - \delta_h + 2\nu_0 - \delta_t - \theta_t)$.

The epidemiological consequences of HIV and TB on the transmission of COVID-19 are illustrated in Figure 6.4. This figure indicates the relationship between the reproduction number of diseases. It can be inferred that when the reproduction number of HIV and TB increases, that is, when each infected person is likely to infect others, it leads to an increase in the reproduction number of COVID-19 as well. In simple terms, the spread of the two diseases can influence the spread of COVID-19, resulting in a potentially more widespread outbreak. This implies that it is important to closely monitor the reproduction numbers of all diseases to ensure effective control measures are put in place to prevent further spread and potential health risks.

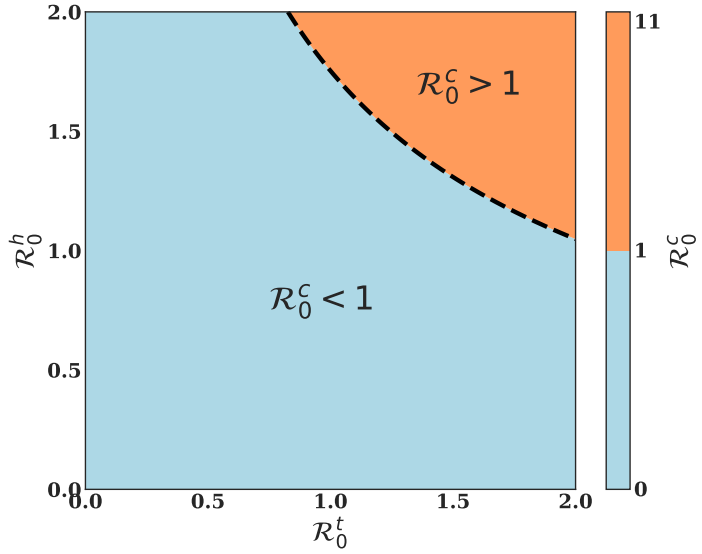

Figure 6.4: Simulation of $\mathcal{R}_0^c$ as a function of $\mathcal{R}_0^t$ and $\mathcal{R}_0^h$.

6.5.2 Effects of Reinfection

Recent studies have highlighted the significant impact of waning immunity and reinfection on COVID-19 dynamics. Both natural and vaccine-induced immunity decreases over time, leading to increased reinfection rates (Yair Goldberg et al., 2021; Zelong Li, 2023). The potential for reinfection is particularly concerning, as it could lead to increased co-infection rates and further strain healthcare systems (Teran, Ricardo et al., 2023). Figures 6.5 to 6.7 clearly supports these findings. Figure 6.5 illustrates the impact of COVID-19 reinfection rates (γ_c) on the co-dynamics of COVID-19, TB, and HIV. In the figure, we observe the interaction between COVID-19, HIV and TB co-infections (C_{ct}) for three reinfection rates: $0.01, 0.03$ and 0.35. As the reinfection rate increased, the peak co-infection level rises, with the highest value of $\gamma_c = 0.35$ producing the sharpest peak. The analysis clearly shows that an elevated COVID-19 reinfection rate intensifies the co-infection burden across all cases, contributing to longer-lasting and more severe outcomes.

6.5.3 Effects of Key Behavioral Parameters

In this section, the effects of key behavioral parameters are investigated based on figures that illustrate the interplay between waning immunity, vaccine ineffectiveness, baseline vaccination rate, level of information and information-dependent vaccination in shaping the co-dynamics of the three diseases. Figures 6.6 and 6.7 illustrates the impact of waning immunity(φ_c), with comparisons to a critical waning immunity threshold, $\varphi^* = \varphi_c = \frac{\Theta_2(\mu_d+\nu_0)-\pi_c*(\mu_d+\nu_0*\sigma_c)}{(\pi_c-\Theta_2)}$, which is

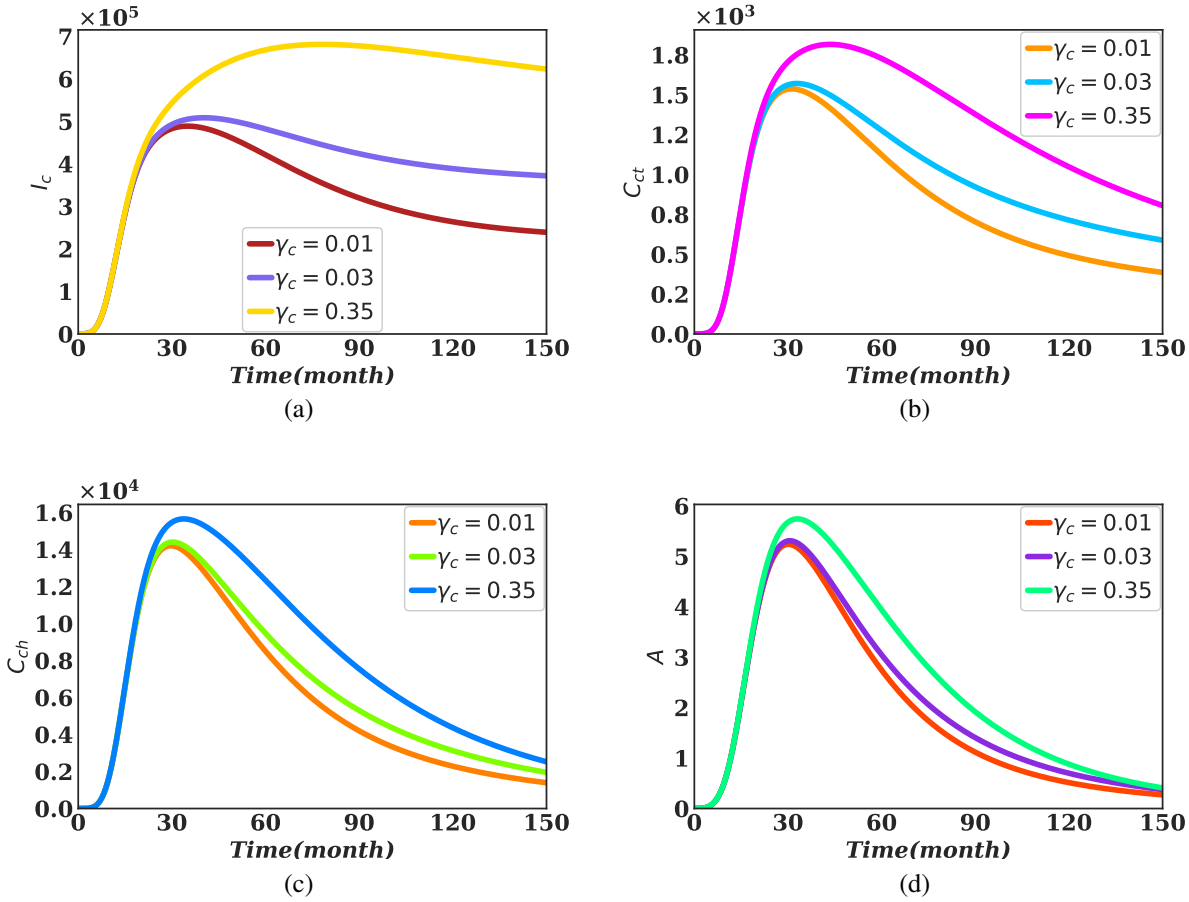

Figure 6.5: Simulations showing the impact of COVID-19 reinfection rate (γ_c).

obtained by solving (6.11) for φ_c after setting $\mathcal{R}_0^c = 1$. Using the parameter values in Table 6.1, we find that φ^* is equal to 0.00534. The two figures compare the impact of waning immunity (φ_c) on disease progression in the absence ($D = 0$) and presence ($D \neq 0$) of information-dependent vaccinations. Without information-dependent vaccination (Figure 6.7), I_c, C_{ct}, C_{ch} and A are more sensitive to the variations in φ_c. As φ_c increases beyond the critical waning immunity rate ($\varphi_c > \varphi^*$), the peak values of I_c and the other compartments increase significantly, indicating a larger disease burden. Conversely, when $\varphi_c < \varphi^*$, disease progression is slower, and the total number of cases is lower. In contrast, Figure 6.6 shows the effect of information-driven vaccination, in which individuals adjust their behavior based on disease prevalence. Here, the peaks for each compartment are generally lower than those in Figure 6.7, indicating that information-dependent vaccination helps to stop the persistence of COVID-19 and its co-infections with others. Even with higher waning immunity ($\varphi_c > \varphi^*$), the compartments show a more controlled progression, and the peaks are noticeably suppressed compared with the scenario without information. This indicates that when information is incorporated into vaccination behavior, it

effectively counteracts the detrimental effects of increased waning immunity.

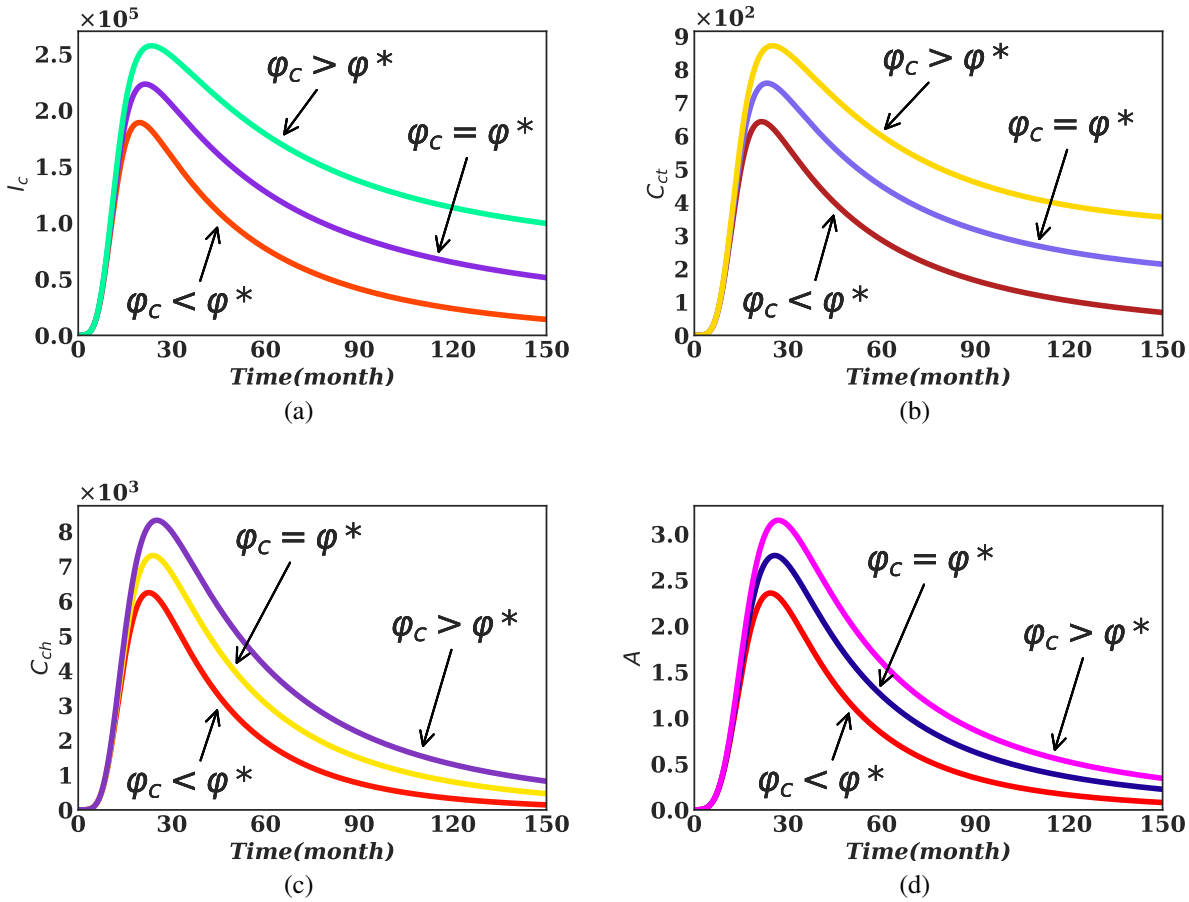

Figure 6.6: The impact of waning immunity (φ_c) for $D \neq 0$.

Figures 6.8 and 6.9 illustrate the relationship between vaccine ineffectiveness and baseline vaccination rate with and without information dependent vaccination behavior, respectively. In both figures, it is evident that even if the baseline vaccination rate is increases, a decrease in vaccine effectiveness increases the number of infection cases. This is important in showing that vaccine coverage alone may not suppress the COVID-19 cases and the associated co-infections. Figure 6.8 demonstrates that incorporating information-dependent behavior significantly mitigates infection rates, leading to lower peaks and slower growth. Conversely, Figure 6.9 shows higher infection rates across all four scenarios (I_c, C_{ct}, C_{ch}, and A). That is, the infection rates increased more rapidly and reached higher peaks, indicating that without information-dependent behavior, the baseline vaccination rate and vaccine ineffectiveness had a more pronounced negative impact on controlling the infections. This contrast highlights the importance of adaptive vaccination strategies that respond to real-time information, effectively reducing the spread of infections even when vaccine effectiveness is compromised.

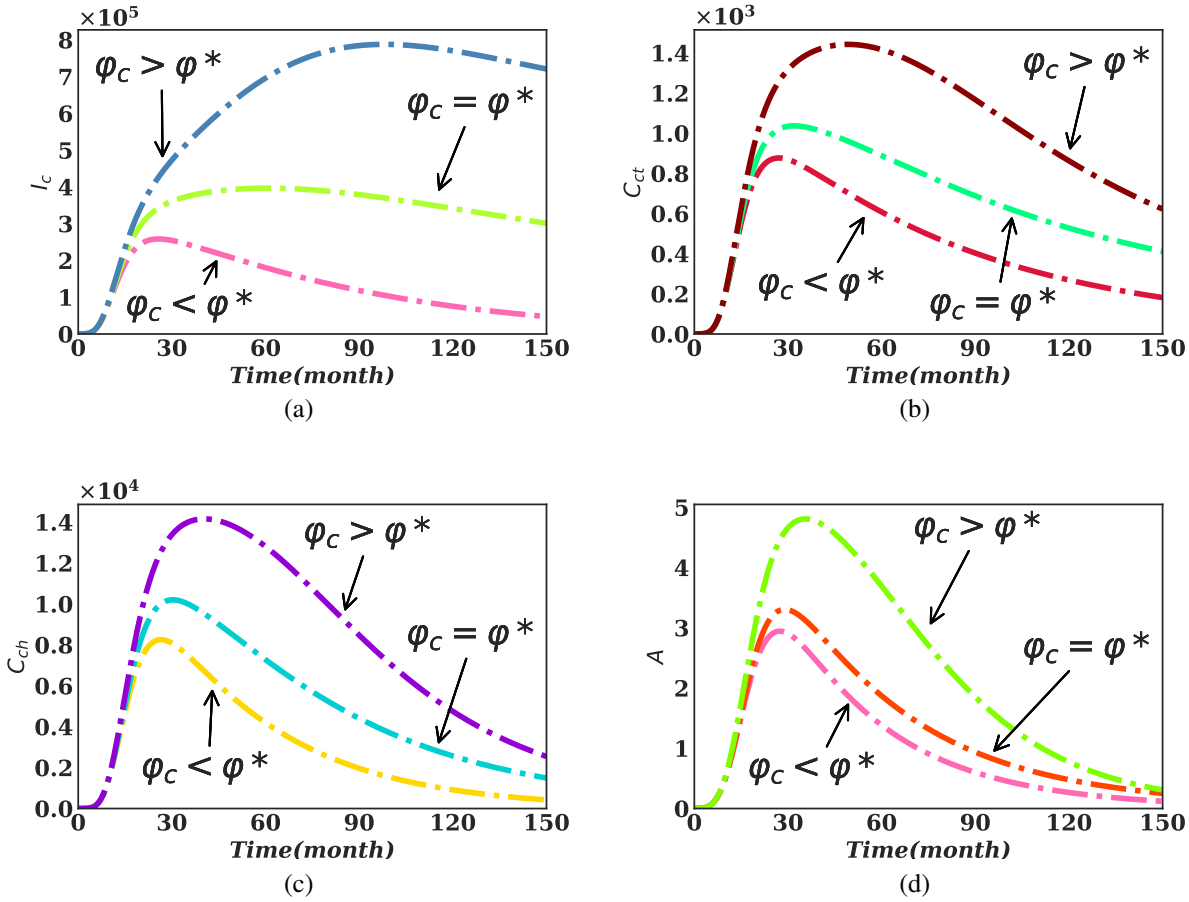

Figure 6.7: The impact of waning immunity(φ_c) for $D = 0$.

The effect of the level of information coverage(κ) on the number of COVID-19 transmission and co-infection cases is illustrated in Figure 6.10. As κ increases from 0.15 to 0.3, we observe a significant reduction in the peak values of all compartments(I_c, C_{ct}, C_{ch} and A) across the subplots. Specifically, higher levels of information lead to lower peaks of infected individuals. This demonstrates the beneficial effect of increasing information levels in curbing the spread of infection by promoting more effective and timely vaccination. This figure underscores the importance of a higher κ in reducing both the magnitude and duration of outbreaks, highlighting that better information dissemination plays a crucial role in mitigating the impact of co-infection.

Figure 6.11 presents four subplots showing the cumulative deaths over time in the absence and presence of information-dependent vaccination behavior. In Figures 6.11a to 6.11d, the curves demonstrate that information-driven vaccination ($D > 0$) significantly reduces cumula-

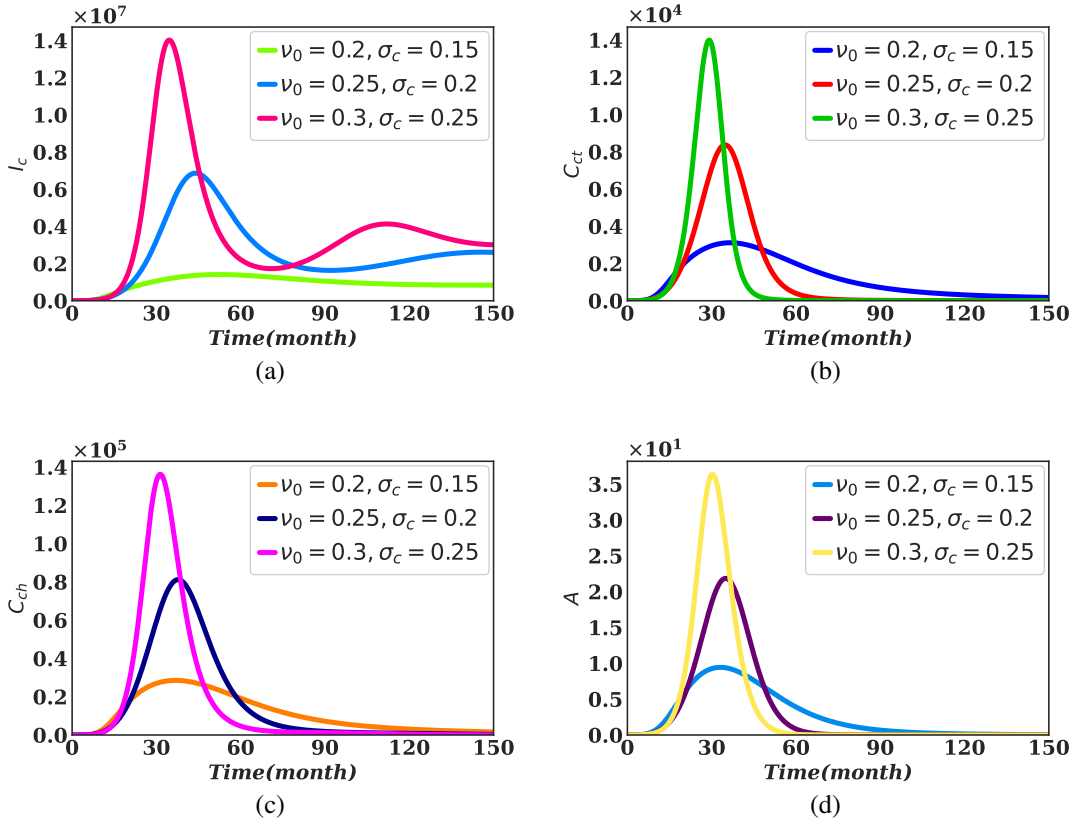

Figure 6.8: The impact of vaccine ineffectiveness factor (σ_c) and baseline vaccination rate (ν_0) in the presence of information-dependent vaccination($D \neq 0$).

tive deaths compared to the scenario where $D = 0$. For instance, in Figure 6.11a, the cumulative deaths in the COVID-19 infected compartment(I_c) without information dependent vaccination behavior grow rapidly over time, reaching around 8.7 million, while with information, deaths are considerably lower, plateauing at about 1.8 million. A similar pattern is observed across the other compartments: C_{ct}, C_{ch}, and A, where information-dependent vaccination behavior delays and reduces the number of deaths over time, indicating the crucial role of information in mitigating the spread of the infection. The results highlight the crucial role of information-dependent vaccination in minimizing the deadly consequences of the infection. The results underscore the vital role of information dependent vaccination behavior in reducing the severe outcomes of COVID-19 infection, including COVID-19-HIV and COVID-19-TB co-infection, and COVID-19-HIV-TB triple infection.

The contour plots displayed in Figure 6.12 showcase the behavior of I_c, C_{ct}, C_{ch} and A over specific time ($t = 35, 50, 60$) as functions of two parameters, κ (level of information) and a

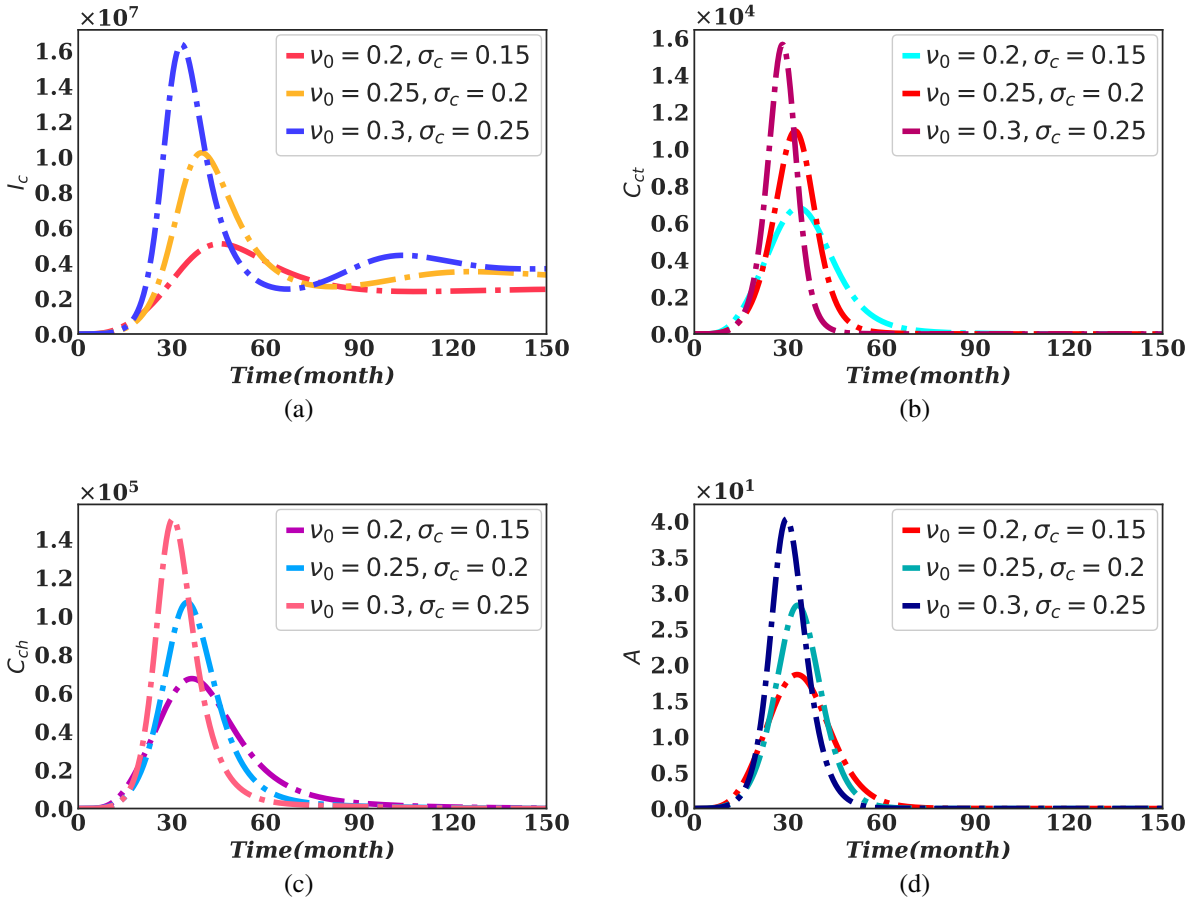

Figure 6.9: The impact of vaccine ineffectiveness factor(σ_c) and baseline vaccination rate (ν_0) in the absence of information-dependent vaccination ($D = 0$).

(inverse of the average time delay) for $D = 0.0001$. Each row corresponds to a different variable, and within each row, the columns represent the variable's evolution at three different time points. The figures suggest that for COVID-19, a shorter time delay in information dissemination (higher a) can lead to increased co-infection cases, especially when information coverage is low (smaller κ). This implies that while timely information is crucial for mitigating the spread of COVID-19, it must be accompanied by comprehensive and accurate information to be effective. A balance between these two factors is essential to ensure individuals have the knowledge and understanding needed to make informed decisions and take appropriate actions to protect themselves and others. Without sufficient context or understanding, timely information can inadvertently contribute to the spread of the disease due to factors such as misinformation or delayed responses.

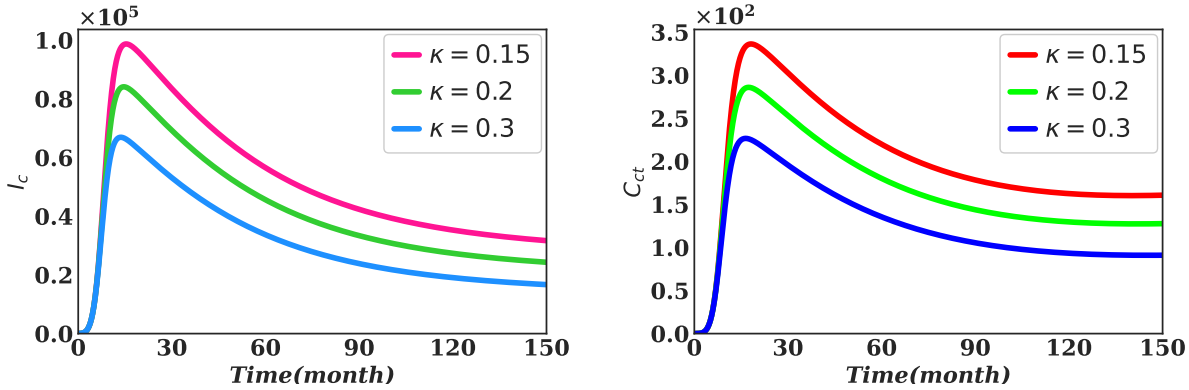

(a)

(b)

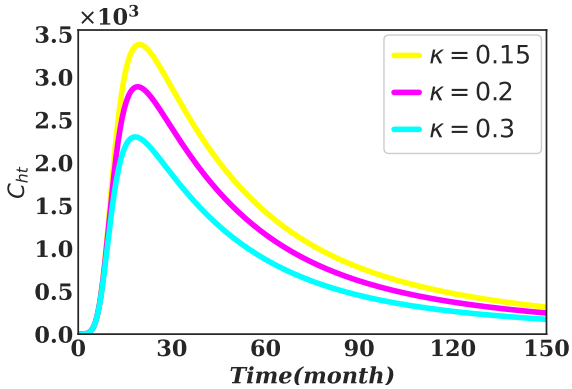

(c)

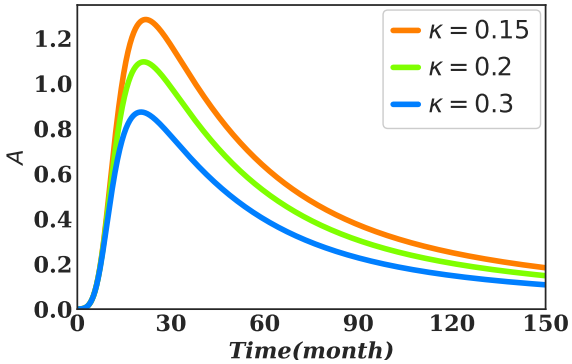

(d)

Figure 6.10: The impact of the level of information (κ)

.

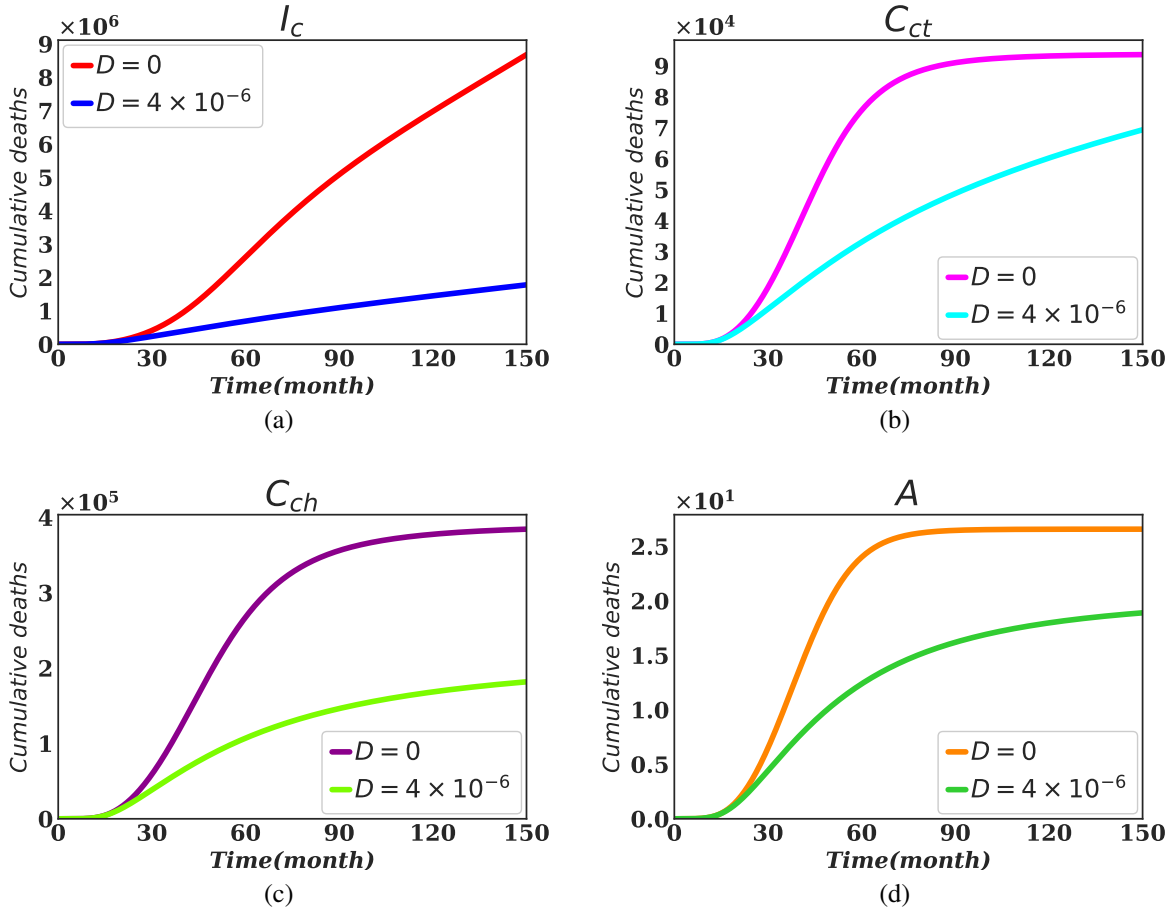

Figure 6.11: Vaccination-dependent behaviors and cumulative deaths.

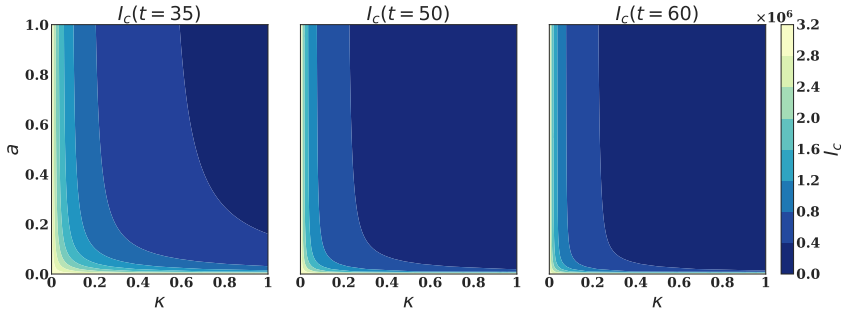

(a) COVID-19 infected

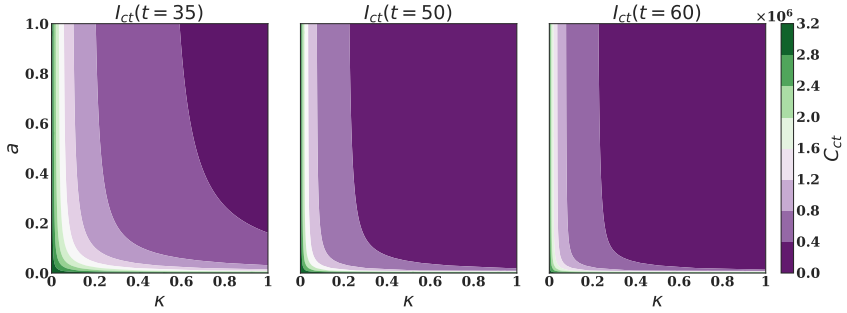

(b) COVID-19-TB co-infected

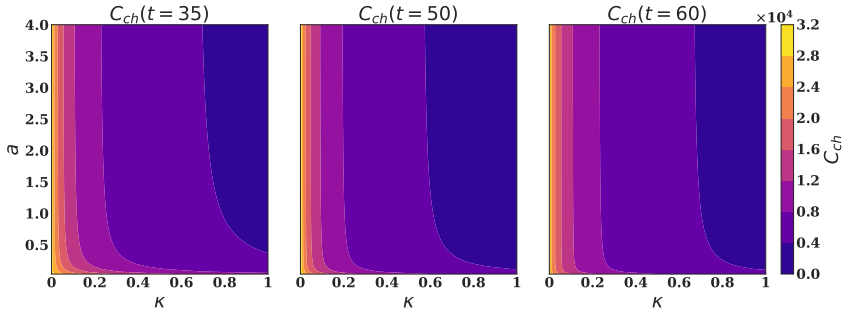

(c) COVID-19-HIV infected

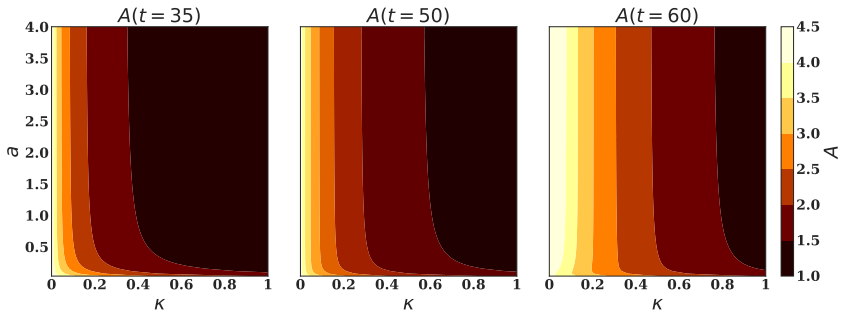

(d) COVID-19, HIV and TB triple infected

Figure 6.12: Effect of the average time delay (a).

CHAPTER 7

SUMMARY, CONCLUSIONS AND RECOMMENDATIONS

This chapter offers a concise overview of the research findings, presents key conclusions, and proposes recommendations based on the study. It also discusses potential areas for future research to build upon the existing knowledge and address identified gaps.

7.1 Summary and Conclusions

Although COVID-19 is under control with an incredible global public health effort, the impact of the disease in the community continues. People who have HIV/AIDS are among those affected by COVID-19. The mathematical models have been very beneficial in providing various reasons for the dynamics of disease and designing practical control strategies. In this dissertation, we provide co-infection models that govern the transmission dynamics of COVID-19 and HIV/AIDS in order to assess the impacts of COVID-19 among PLHIV and identify control strategies. Moreover, because TB is the number one risk factor of death for HIV patients and COVID-19 imposes another burden, the triple infection dynamics of COVID-19, HIV, and TB are investigated. Deterministic models with different numbers of compartments are used to describe the co-dynamics of COVID-19, HIV/AIDS, and TB. The basic properties of the models, positivity and boundedness of the solutions, are examined. That is, wellposedeness of the co-infection models is established. Equilibria and reproduction numbers are determined to examine the qualitative behaviors of the models and analyze the epidemiological implications. Based on sensitivity analysis, parameters are identified to extend the co-infection model into an optimal control problem, which emphasizes identifying the most cost-effective strategy to mitigate the spread and impact of COVID-19 and HIV co-infection. Numerical simulations support and clarify the analytical results and show how different parameters affect the co-infected population. The results revealed key parameters that determine the transmission dynamics of the diseases.

It is found that transmission rates of the disease are the most important parameters that determine the dynamics of diseases. Figures 4.7 and 4.8 shows that the number of people co-infected with COVID-19 and HIV/AIDS cannot be reduced unless the rate of their transmission is made as low as possible. This demonstrates that the ongoing efforts to stop the two diseases must be stepped up. The same result has also been found in other similar studies (Teklu, S. W. and Kotola, B. S., 2023). This observation is in direct agreement with mitigation approaches that aim at minimizing the transmission rate, primarily through self-protective measures (such as taking

the vaccine and wearing masks for COVID-19, and abstinence, faithfulness, and protection for HIV). HIV patients' risk of transmitting the disease or contracting another disease depends on their viral load. Following their compromised immunity, PLHIV may have an increased risk for severe disease from COVID-19 as well as hospitalizations (Squillace, Nicola et al., 2021). This can be realized from Figures 4.9 and 4.10. For people with HIV, when the ability to transmit the disease decreases, the number of co-infected people also decreases, and when it increases, the number of co-infected people rises. The same is true for the risk of exposure to other diseases. Along with this, if we look at Figure 4.10, we can clearly understand that immunity has a significant contribution to the number of co-infected people. This is consistent with existing research and shows that more attention is needed for these people. Additionally, it can be understood that the weakening of the immune system of HIV patients increases the death rate caused by COVID-19 and HIV/AIDS co-infection. These findings underscore the necessity to intensify efforts to provide HIV/AIDS patients with treatments such as antiretroviral therapy, which serves two purposes: preventing HIV transmission and reducing HIV/AIDS patients' vulnerability to other diseases. The World Health Organization considers safe and effective vaccines to be a game-changing tool in controlling the COVID-19 pandemic (WHO, 2024a). This role of the vaccine is illustrated in Figures 4.11 and 4.12. From the figure, we observe that COVID-19 vaccination has a significant role in reducing the population of infected individuals, especially by reducing the risk of death due to these diseases. This result reinforces the WHO recommendation to prioritize HIV/AIDS patients during COVID-19 vaccine administration (WHO, 2021b). Moreover, Figure 4.12 and Figure 4.13 show that COVID-19 treatment also plays a vital role in reducing the risk of death due to co-infection.

In addition to exploring the role of different control parameters, this study illustrates the efficacy and cost-effectiveness of control strategies: prevention and treatment. This point is especially crucial in countries with high HIV prevalence rates (Han, Xueya et al., 2022). A comprehensive cost-effectiveness analysis, grounded in established theories, is conducted to identify the most economically viable strategy for curbing HIV and COVID-19 co-infections. The analysis reveals that a synergistic approach involving COVID-19 vaccination and treatment is the most efficient and cost-effective strategy for reducing the prevalence of co-infected individuals, as shown in Figures 5.4h, 5.5j and 5.6h. These findings provide valuable insights for policymakers, guiding them to prioritize preventive measures to reduce the incidence of co-infection cases and associated fatalities.

Moreover, this thesis offers additional insights into the impact of COVID-19 on PLHIV during the post-vaccination period. It delves into the effects of waning immunity, reinfection rates, and behavioral factors such as information-driven vaccination. Furthermore, it considers

the impact of TB, which is the most infectious disease among PLHIV. Reproduction numbers were determined and used as a threshold value to examine stability analyses of equilibria and investigate how one disease affects another. Their analyses show that more secondary infections of HIV and TB disease translate into more COVID-19 disease. This result is consistent with existing studies that have discussed how the increasing number of HIV-TB co-infection cases can lead to a higher incidence of COVID-19 (Jacques Tamuzi et al., 2020). It is illustrated that an increase in the reproduction numbers of HIV and TB can elevate the reproduction number of COVID-19, highlighting the importance of monitoring multiple diseases. Results on the impact of waning immunity and reinfection rates on the dynamics of COVID-19, HIV and TB show that higher reinfection rates lead to greater peaks in co-infections as well as triple infections. The role of key parameters, such as baseline vaccination rates, vaccine ineffectiveness, and information-dependent vaccination, is explored to demonstrate their influence on infection control. It is revealed that without information-driven vaccination, waning immunity exacerbates the burden of co-infections, while incorporating information-dependent behavior reduces disease peaks. Additionally, the study underscores the critical role of effective information dissemination in lowering infection rates, suggesting that better-informed populations exhibit better disease control outcomes. Furthermore, the dynamic interplay between information levels and response delays is examined, highlighting the necessity for timely and accurate information in managing the spread of COVID-19 and its co-infections.

In conclusion, this dissertation provides a comprehensive mathematical investigation into the transmission dynamics and control of COVID-19, HIV/AIDS, and TB co-infections. By developing and analyzing various deterministic models, we have identified the crucial role of transmission rates, immunity, and co-morbid infections in shaping disease dynamics. Our findings emphasize that lowering transmission rates, strengthening immunity through treatment and vaccination, and prioritizing preventive strategies are critical for controlling co-infections, especially among vulnerable populations like PLHIV. The study also highlights the significant impact of TB on COVID-19 outcomes among HIV-positive individuals, the effects of waning immunity and reinfection, and the role of information-dependent vaccination behavior in mitigating disease spread. Moreover, through optimal control and cost-effectiveness analyses, we establish that a combined strategy of vaccination and treatment offers the most practical and economically sound approach for reducing co-infection prevalence and mortality. These results offer valuable insights for policymakers and health authorities, underscoring the need for integrated, sustained, and informed intervention efforts to effectively manage the interconnected epidemics of COVID-19, HIV/AIDS, and TB.

7.2 Recommendations

To effectively control the transmission of COVID-19 and HIV/AIDS, it is crucial to intensify efforts aimed at reducing transmission rates, as these are key determinants of disease dynamics. Protective measures such as vaccination and preventive behaviors must be emphasized, especially among high-risk populations like people PLHIV. Prioritizing HIV/AIDS patients for COVID-19 vaccination, as recommended by the World Health Organization (WHO), is essential since vaccination significantly reduces the risk of severe illness and death from co-infection. Furthermore, providing antiretroviral therapy (ART) to HIV/AIDS patients serves a dual purpose: it prevents HIV transmission and mitigates the effects of compromised immunity, which can exacerbates the severity of COVID-19 and other infections. In terms of resource allocation, a comprehensive cost-effectiveness analysis should guide policymakers in identifying the most economically viable strategies for combating co-infections, especially in regions with high HIV prevalence. Evidence suggests that a synergistic approach combining COVID-19 vaccination with treatment is the most efficient and cost-effective strategy to reduce the prevalence of co-infected individuals. Additionally, in the post-vaccination period, waning immunity and reinfection rates must be carefully monitored, as higher reinfection rates can lead to more severe peaks in co-infection cases. The role of information-driven vaccination strategies also cannot be overstated—without them, waning immunity and vaccine ineffectiveness exacerbate the burden of co-infections, whereas effective dissemination of information helps reduce disease transmission. Timely and accurate information is therefore critical in managing the spread of COVID-19 and its co-infections, as better-informed populations consistently demonstrate improved control outcomes. Ultimately, focusing on these strategies will lead to more effective disease mitigation, particularly in vulnerable communities like PLHIV.

7.3 Future Work

There are several ways this study can be extended. Future research could explore the incorporation of more complex stochastic elements to account for real-time variations in infection rates and healthcare interventions. Further analysis of the triple co-infection dynamics of COVID-19, HIV, and TB with varying environmental factors (for instance, climate influence on TB transmission) could provide more robust predictions. The model does not consider COVID-19 asymptotic individuals who transmit the disease while contacting susceptible populations, so including their impact makes the model more representative. Self-protective measures are crucial in preventing the spread of viruses like HIV/AIDS, as they cannot be cured. However, the specific contribution of self-protective measures is not taken into account in this study. Therefore, models that incorporate specific self-protective measures may be considered for advancing

this research. Furthermore, the inflow of infected people due to the vertical transmission of HIV/AIDS and age structures can be considered in the areas of research for the future. Drug resistance poses a critical challenge in HIV infection. The study's outcomes could be significantly enhanced by incorporating drug resistance into the proposed models. Apart from these, our study may help policymakers develop better ways to control the combined effects of these diseases. This study offers information on the variables that increase the likelihood of COVID-19, TB, and HIV co-and triple-infection cases and what can be done to lessen their impact. Furthermore, this work can serve as basis for modeling studies that consider the occurrence of these infections.

Contribution of the Dissertation

The dissertation reports original results that contribute knowledge to the scientific advancement in mathematics. Two of the contributions were published in peer reviewed journals indexed in Web of Science and Scopus.

Batu, T. D., Obsu, L. L., & Deressa, C. T. (2023). *Co-infection dynamics of COVID-19 and HIV/AIDS*. Scientific Reports, 13(1), 18437.

Available at: https://doi.org/10.1038/s41598-023-45520-6

Batu, T. D., & Obsu, L. L(2024). *Optimal Control Strategies for HIV and COVID-19 Co-infection: A Cost-Effectiveness Analysis*. Frontiers in Applied Mathematics and Statistics, 10, 1439284.

Available at: https://doi.org/10.3389/fams.2024.1439284

Batu, T. D., & Obsu, L. L. (2025). *Co-dynamics of COVID-19, HIV and TB with information-dependent vaccination behavior and waning immunity*. Scientific African, 28, e02680.

Available at: https://doi.org/10.1016/j.sciaf.2025.e02680

References

Abiodun, Oluwakemi et al. (2023). Mathematical modeling and optimal control strategies of hiv/aids with haart. In *2023 international conference on science, engineering and business for sustainable development goals (seb-sdg)* (Vol. 1, p. 1-9). (doi: https://doi.org/10.1109/SEB-SDG57117.2023.10124496)

Ahmed. M. Elaiw et al. (2022). Global analysis of within-host sars-cov-2/hiv coinfection model with latency. *European Physical Journal plus*, *137*. (doi: https://doi.org/10.1140/epjp/s13360-022-02387-2)

Ajao, Saheed et al. (2023). Understanding the transmission dynamics and control of hiv infection: A mathematical model approach. *Journal of the Nigerian Society of Physical Sciences*, 1389–1389. (doi: https://doi.org/10.46481/jnsps.2023.1389)

Al-Ahdal, Mohammed et al. (2012). Coronavirus respiratory illness in Saudi Arabia. *The Journal of Infection in Developing Countries*, *6*(10), 692–694. (doi: https:///doi.org/10.1038/s41598-021-82862-5)

Aldila, Dipo et al. (2020). A mathematical study on the spread of COVID-19 considering social distancing and rapid assessment: The case of Jakarta, Indonesia. *Chaos, Solitons & Fractals*, *139*, 110042. (doi: https://doi.org/10.1016/j.chaos.2020.110042)

Ali, Mohsin et al. (2020). The role of asymptomatic class, quarantine and isolation in the transmission of COVID-19. *Journal of Biological Dynamics*, *14*(1), 389–408. (doi: https://doi.org/10.1080/17513758.2020.1773000)

Alimohamadi, Yousef et al. (2023). Sars-cov-2 reinfection rate: A systematic review and meta-analysis. *Infection Epidemiology and Microbiology*, *9*(1). (doi: http://dx.doi.org/10.52547/iem.9.1.63)

Aniefiok John et al. (2023). The covid-19, tuberculosis and hiv/aids: Ménage à trois. *Frontiers in Immunology*, *14*. (doi: https://doi.org/10.3389/fimmu.2023.1104828)

Atalan, A. (2020). Is the lockdown important to prevent the COVID-19 pandemic? Effects on psychology, environment and economy-perspective. *Annals of medicine and surgery*, *56*, 38–42. (doi: https://doi.org/10.1016/j.amsu.2020.06.010)

Awoke, Temesgen D. and Kassa, Semu M. (2018). Optimal control strategy for TB-HIV/AIDS Co-infection model in the presence of behaviour modification. *Processes*, *6*(5), 48. (doi: https://doi.org/10.3390/pr6050048)

Ayele, Tigabu et al. (2021). Mathematical modeling of hiv/aids with optimal control: a case study in ethiopia. *Results in Physics*, *26*, 104263. (doi: https://doi.org/10.1016/j.rinp.2021.104263)

Bahrami, A. and Ferns, G. (2020, 08). Genetic and pathogenic characterization of SARS-CoV-2: A review. *Future Virology*, *15*. (doi: https://doi.org/10.2217/fvl-2020-0129)

Bandekar, S. R., & Ghosh, M. (2022). A co-infection model on tb-covid-19 with optimal control and sensitivity analysis. *Mathematics and Computers in Simulation*, *200*, 1–31. (doi: https://doi.org/10.1016/j.matcom.2022.04.001)

Belela Samuel Kotola et al. (2023). Bifurcation and optimal control analysis of hiv/aids and covid-19 co-infection model with numerical simulation. *PLOS ONE*, *18*. (doi: https://doi.org/10.1371/journal.pone.0284759)

Ben Ashby and Alex Best. (2021). Herd immunity. *Current Biology*, *31*(4), R174-R177. (doi: https://doi.org/10.1016/j.cub.2021.01.006)

Bertagnolio, Silvia et al. (2022). Clinical features of, and risk factors for, severe or fatal covid-19 among people living with hiv admitted to hospital: analysis of data from the who global clinical platform of covid-19. *The Lancet HIV*, *9*(7), e486–e495. (doi: https://doi.org/10.1016/S2352-3018(22)00097-2)

Bianchi, Arianna et al. (2019). *The Dynamics of Biological Systems* (Vol. 4). Springer. (doi: https://doi.org/10.1007/978-3-030-22583-4)

Birkhoff, Garrett and Rota, Gian-Carlo. (1978). *Ordinary differential equations* (Vol. 4). Wiley New York.

Bizuneh, Fassikaw et al. (2024). Tuberculosis-associated mortality and risk factors for hiv-infected population in ethiopia: a systematic review and meta-analysis. *Frontiers in Public Health*, *12*, 1386113.

Bo Yang et al. (2022). The impact of vaccination on the spread of covid-19: Studying by a mathematical model. *Physica A: Statistical Mechanics and its Applications*, *590*, 126717. (doi: https://doi.org/10.1016/j.physa.2021.126717)

Brauer, Fred et al. (2019). *Mathematical Models in Epidemiology*. Springer. (doi: https://doi.org/10.1007/978-1-4939-9828-9)

Buonomo, B. (2020). Effects of information-dependent vaccination behavior on coronavirus outbreak: insights from a SIRI model. *Ricerche di Matematica*, *69*, 483–499. (doi: https://doi.org/10.1007/s11587-020-00506-8)

Caifang Zheng et al. (2022). Real-world effectiveness of covid-19 vaccines: a literature review and meta-analysis. *International Journal of Infectious Diseases*, *114*, 252-260. (doi: https://doi.org/10.1016/j.ijid.2021.11.009)

Cain, John W and Reynolds, Angela M, y. (n.d.). *Ordinary and Particial Differential Equations: An Introduction to Dynamical Systems*. Virginia Commonwealth University Mathematics.

Castillo-Chavez, C. and Song, Baojun. (2004). Dynamical models of tuberculosis and their applications. *Mathematical Biosciences & Engineering*, *1*(2), 361. (doi: 10.3934/mbe.2004.1.361.PMID:20369977.)

Centers for Disease Control and Prevention and others. (2018). Evidence of HIV treatment and viral suppression in preventing the sexual transmission of HIV. *Department of Health & Human Services*, *10*.

Chathappady House et al. (2021). Corona Viruses: A Review on SARS, MERS and COVID-19. *Microbiology Insights*, *14*, 11786361211002481. (doi: https://doi.org/10.1177/11786361211002481)

Chavez, C Castillo et al. (2002). On the computation of $\mathcal{R}_0$ and its role on global stability. *Mathematical Approaches for Emerging and Re-emerging Infection Diseases: An Introduction*, *125*, 31–65.

Daniel Eike et al. (2022). How the covid-19 pandemic alters the landscapes of the hiv and tuberculosis epidemics in south africa: A case study and future directions. *Epidemiologia*, *3*, 297 - 313. (doi: https://doi.org/10.3390/epidemiologia3020023)

Danwang, Celestin et al. (2022). Outcomes of patients with hiv and covid-19 co-infection: a systematic review and meta-analysis. *AIDS research and therapy*, *19*(1), 1–12. (doi: https://doi.org/10.1186/s12981-021-00427-y)

Darmawati, Darmawati et al. (2022). Sensitivity, optimal control, and cost-effectiveness analysis of intervention strategies of filariasis. *Jambura Journal of Mathematics*, *4*(1), 64–76. (doi: https://doi.org/10.34312/jjom.v4i1.11766)

Deressa, C. T., & Duressa, G. F. (2021). Modeling and optimal control analysis of transmission dynamics of covid-19: The case of ethiopia. *Alexandria Engineering Journal*, *60*(1), 719-732. (doi: https://doi.org/10.1016/j.aej.2020.10.004)

Diekmann, Odo et al. (1990). On the definition and the computation of the basic reproduction ratio $\mathscr{R}_0$ in models for infectious diseases in heterogeneous populations. *Journal of Mathematical Biology*, *28*(4), 365–382. (doi: https://doi.org/10.1007/BF00178324)

Donnelly, Christl A et al. (2019). Worldwide reduction in MERS cases and deaths since 2016. *Emerging infectious diseases*, *25*(9), 1758. (doi: https://doi.org/10.3201/eid2509.190143)

Du, Wenjun et al. (2020). Epidemic update of COVID-19 in Hubei Province compared with other regions in China. *International Journal of Infectious Diseases*. (doi: https://doi.org/10.1016/j.ijid.2020.04.031)

Ejaz, Hasan et al. (2020). COVID-19 and comorbidities: Deleterious impact on infected patients. *Journal of infection and public health*. (doi: https://doi.org/10.1016/j.jiph.2020.07.014)

Eka D.A.Ginting et al. (2024). A deterministic compartment model for analyzing tuberculosis dynamics considering vaccination and reinfection. *Healthcare Analytics*, *5*, 100341. (doi: https://doi.org/10.1016/j.health.2024.100341)

Elezkurtaj, Sefer et al. (2021). Causes of death and comorbidities in hospitalized patients with COVID-19. *Scientific Reports*, *11*(1), 1–9. (doi: https://doi.org/10.1038/s41598-021-82862-5)

EPHI. (2022a). *Covid-19 pandemic preparedness and response in ethiopia.* (Retrieved April 5, 2022, from https://ephi.gov.et/download/pheoc/)

EPHI. (2022b). *Hiv related estimates and projections in ethiopia for the year 2021–2022.* Ethiopian Public Health Institute Addis Ababa.

Executive Board, 113. (2004). *Severe acute respiratory syndrome (sars): report by the secretariat* (Governing body document). Geneva, Switzerland: World Health Organization. (Executive Board 113th session, provisional agenda item 8.3)

Flacco, Maria Elena et al. (2022). Covid-19 vaccines reduce the risk of sars-cov-2 reinfection and hospitalization: Meta-analysis. *Frontiers in Medicine*, *9*. (doi: https://doi.org/10.3389/fmed.2022.1023507)

Fleming, Wendell H and Rishel, Raymond W. (2012). *Deterministic and stochastic optimal control* (Vol. 1). Springer Science & Business Media. (doi: https://doi.org/10.1007/978-1-4612-6380-7)

Gatechompol, Sivaporn et al. (2021). COVID-19 and HIV infection co-pandemics and their impact: a review of the literature. *AIDS Research and Therapy*, *18*(1), 1–9. (doi: https://doi.org/10.1186/s12981-021-00335-1)

Gelaw, Yalemzewod Assefa et al. (2019). Hiv prevalence among tuberculosis patients in sub-saharan africa: a systematic review and meta-analysis. *AIDS and Behavior*, *23*, 1561–1575. (doi: https://doi.org/10.1007/s10461-018-02386-4)

Getachew B. B. and Eshetu D. G. (2021). Mathematical model of the transmission dynamics of novel corona virus (covid-19) pandamic disease with optimal control. *International Journal of Mathematical Models and Methods in Applied Sciences*. (doi: 10.46300/9101.2021.15.27)

González-Domenech et al. (2021a). A Pandemic within Other Pandemics. When a Multiple Infection of a Host Occurs: SARS-CoV-2, HIV and Mycobacterium tuberculosis. *Viruses*, *13*(5), 931. (doi: https://doi.org/10.3390/v13050931)

González-Domenech et al. (2021b). A pandemic within other pandemics. when a multiple infection of a host occurs: Sars-cov-2, hiv and mycobacterium tuberculosis. *Viruses*, *13*(5), 931. (doi: 10.3390/V13050931)

Govere-Hwenje, Sabina et al. (2022). Willingness to accept covid-19 vaccination among people living with hiv in a high hiv prevalence community. *BMC Public Health*, *22*(1), 1239. (doi: https://doi.org/10.1186/s1288902213623w)

Group, T. T.-. G. S. (2022). Tuberculosis and covid-19 co-infection: description of the global cohort. *European Respiratory Journal*, *59*(3). (doi: 10.1183/13993003.02538-2021)

Guido, Giacomo et al. (2023). Recovery from triple infection with sars-cov-2, rsv and influenza virus: A case report. *Journal of Infection and Public Health*, *16*(7), 1045–1047. (doi: https://doi.org/10.1016/j.jiph.2023.05.001)

Gumel, A. (2012). Causes of backward bifurcations in some epidemiological models. *Journal of Mathematical Analysis and Applications*, *395*(1), 355–365. (doi: https://doi.org/10.1016/j.jmaa.2012.04.077)

Gupta Parakriti et al. (2024). Triple burden: The incorrigible threat of tuberculosis, hiv, and covid-19. *Infectious Disorders - Drug Targets*, *24*(4), 1-7. (doi: https://doi.org/10.2174/0118715265259959231031104820)

Han, Xueya et al. (2022). Significant association between hiv infection and increased risk of covid-19 mortality: a meta-analysis based on adjusted effect estimates. *Clinical and Experimental Medicine*, 1–12. (doi: https://doi.org/10.1007/s10238-022-00840-1)

Hethcote, H. W. (2000). The mathematics of infectious diseases. *SIAM review*, *42*(4), 599–653. (doi: https://doi.org/10.1137/S0036144500371907)

Höft, Maxine A. et al. (2024). The immune response to sars-cov-2 in people with hiv. *Cellular & Molecular Immunology*, *21*(2), 184-196. (doi: https://doi.org/10.1038/s41423-023-01087-w)

Hou, Lulu et al. (2021). The relationship between quarantine length and negative affect during the COVID-19 epidemic among the general population in China: The roles of negative cognition and protective factors. *Frontiers in psychology*, *12*. (doi: https://doi.org/10.3389/fpsyg.2021.575684)

Hussaini, N. et al. (2016). Mathematical analysis of a model for avl–hiv co-endemicity. *Mathematical biosciences*, *271*, 80–95. (doi: https://doi.org/10.1016/j.mbs.2015.10.008)

Jacques Tamuzi et al. (2020). Implications of covid-19 in high burden countries for hiv/tb: A systematic review of evidence. *BMC Infectious Diseases*, *20*. (doi: https://doi.org/10.1186/s12879-020-05450-4)

Jin, Yuefei et al. (2020). Virology, epidemiology, pathogenesis, and control of COVID-19. *Viruses*, *12*(4), 372. (doi: http://dx.doi.org/10.3390/v12040372)

Joachim O. Osur et al. (2022). Determinants of covid-19 vaccine behaviour intentions among the youth in kenya: a cross-sectional study. *Archives of Public Health*, *80*. (doi: https://doi.org/10.1186/s13690-022-00904-4)

Kanwugu, Osman N. and Adadi, Parise. (2021). HIV/SARS-CoV-2 coinfection: A global perspective. *Journal of medical virology*, *93*(2), 726–732. (doi: https://doi.org/10.1002/jmv.26321)

Karia, Rutu et al. (2020). COVID-19 and its modes of transmission. *SN Comprehensive Clinical Medicine*, 1–4. (doi: https://doi.org/10.1007/s42399-020-00498-4)

Kassa, Semu M et al. (2020). Analysis of the mitigation strategies for COVID-19: from mathematical modelling perspective. *Chaos, Solitons & Fractals*, 109968. (doi: https://doi.org/10.1016/j.chaos.2020.109968)

Kassahun et al. (2022). Optimal control analysis for the coinfection of covid-19 and tb. *Arab Journal of Basic and Applied Sciences*, *29*(1), 175–192. (doi: https://doi.org/10.1080/25765299.2022.2085445)

Kassahun, G. M. and Legesse, L. O. (2022). Mathematical modeling and analysis for the co-infection of covid-19 and tuberculosis. *Heliyon*, *8*(10). (doi: https://doi.org/10.1016/j.heliyon.2022.e11195)

Kelley, Walter G. and Peterson, Allan C. (2010). *The Theory of Differential Equations: Classical and Qualitative*. Springer Science & Business Media. (doi: https://doi.org/10.1007/978-1-4419-5783-2)

Kifle, Z. S. and Obsu, L. L. (2023). Co-dynamics of covid-19 and tb with covid-19 vaccination and exogenous reinfection for tb: An optimal control application. *Infectious Disease Modelling*, *8*(2), 574–602. (doi: https://doi.org/10.1016/j.idm.2023.05.005)

Kitaro, Damtew et al. (2023). Modeling and bifurcation analysis of tuberculosis with the multidrug-resistant compartment incorporating chemoprophylaxis treatment. *Frontiers in Applied Mathematics and Statistics*, *9*, 1264201. (doi: https://doi.org/10.3389/fams.2023.1264201)

Klompas, M. (2021, 11). Understanding Breakthrough Infections Following mRNA SARS-CoV-2 Vaccination. *JAMA*, *326*(20), 2018-2020. (doi: https://doi.org/10.1001/jama.2021.19063)

Kuate, Marius et al. (2022). Sars-cov-2, hiv, and tb triple co-infection. *Authorea Preprints*. (doi: https://doi.org/10.1002/ccr3.6018)

Layek, G. (2015). *An Introduction to Dynamical Systems and Chaos*. Springer. (doi: https://doi.org/10.1007/978-81-322-2556-0)

LeBien, T. W. and Tedder, T. F. (2008). B lymphocytes: how they develop and function. *Blood, The Journal of the American Society of Hematology*, *112*(5), 1570–1580. (doi: https://doi.org/10.1182/blood-2008-02-078071)

Lenhart, S. and Workman, J. T. (2007). *Optimal Control Applied to Biological Models*. Chapman and Hall/CRC. (doi: https://doi.org/10.1201/9781420011418)

Li, Michael Y. (2018). *An introduction to mathematical modeling of infectious diseases* (Vol. 2). Springer. (doi: https://doi.org/10.1007/978-3-319-72122-4)

Lynch, S. (2018). *Dynamical Systems with Applications using Python*. Springer. (doi: https://doi.org/10.1007/978-3-319-78145-7)

Maartens, Gary et al. (2014). HIV infection: epidemiology, pathogenesis, treatment, and prevention. *The Lancet*, *384*(9939), 258–271. (doi: https://doi.org/10.1016/S0140-6736(14)60164-1)

Manfredi, P. and D'Onofrio, A. (2013). *Modeling the interplay between human behavior and the spread of infectious diseases*. Springer Science & Business Media. (doi: https://doi.org/10.1007/978-1-4614-5474-8)

Martcheva, M. (2015). *An Introduction to Mathematical Epidemiology* (Vol. 61). Springer. (doi: https://doi.org/10.1007/978-1-4899-7612-3)

Mayanja, Edison et al. (2020). Mathematical Modelling of HIV-HCV Coinfection Dynamics in Absence of Therapy. *Computational and Mathematical Methods in Medicine*, *2020*. (doi: https://doi.org/10.1155/2020/2106570)

Mediawati, Ati Surya et al. (2020). The routes of COVID-19 transmission: A literature review. *Journal of critical reviews*, *7*(6), 722–724.

Mekonen, Kassahun et al. (2022). Mathematical modeling and analysis of tb and covid-19 coinfection. *Journal of Applied Mathematics*, *2022*, 1–20. (doi: https://doi.org/10.1155/2022/2449710)

Melese, Z. T. and Alemneh, H. T. (2021). Enhancing reservoir control in the co-dynamics of HIV-VL: from mathematical modeling perspective. *Advances in Difference Equations*, *2021*(1), 1–20. (doi: https://doi.org/10.1186/s13662-021-03584-6)

Mirzaei, Hossein et al. (2021). COVID-19 among people living with HIV: a systematic review. *AIDS and Behavior*, *25*(1), 85–92. (doi: https://doi.org/10.1007/s10461-020-02983-2)

Mishina et al. (2021). New coronoviral infection (covid-19) combined with tuberculosis in patients at late stages of hiv infection with immunodeficiency. *HIV Infection and Immunosuppressive Disorders*. (doi: 10.22328/2077-9828-2021-13-1-80-87)

Mishra, Ajay et al. (2020). Tuberculosis and covid-19 co-infection: An updated review. *Acta Bio-Medica: Atenei Parmensis*, *92*(1), e2021025–e2021025. (doi: https://doi.org/10.23750/abm.v92i1.10738)

Mohd, M. H. and Sulayman, F. (2020). Unravelling the Myths of $\mathscr{R}_0$ in Controlling the Dynamics of COVID-19 Outbreak: a Modelling Perspective. *Chaos, Solitons & Fractals*, 109943. (doi: https://doi.org/10.1016/j.chaos.2020.109943)

Morison, L. (2001). The global epidemiology of HIV/AIDS. *British Medical Bulletin*, *58*(1), 7–18. (doi: https://doi.org/10.1093/bmb/58.1.7)

Mumbu, A. J. and Hugo, A. K. (2020). Mathematical modelling on COVID-19 transmission impacts with preventive measures: a case study of Tanzania. *Journal of biological dynamics*, *14*(1), 748–766. (doi: https://doi.org/10.1080/17513758.2020.1823494)

Mwalili, Samuel et al. (2020). SEIR model for COVID-19 dynamics incorporating the environment and social distancing. *BMC Research Notes*, *13*(1), 1–5. (doi: https://doi.org/10.1186/s13104-020-05192-1)

Nainggolan, Jonner et al. (2023). Sensitivity analysis and optimal countermeasures control of model of the spread of covid-19 co-infection with hiv/aids. *Commun. Math. Biol. Neurosci.*. (doi: https://doi.org/10.28919/cmbn/8161)

Nasreen, Sharifa et al. (2022). Effectiveness of covid-19 vaccines against symptomatic sars-cov-2 infection and severe outcomes with variants of concern in ontario. *Nature microbiology*, *7*(3), 379–385. (doi: https://doi.org/10.1038/s41564-021-01053-0)

Ndairou, Faical et al. (2020). Mathematical modeling of COVID-19 transmission dynamics with a case study of Wuhan. *Chaos, Solitons & Fractals*, 109846. (doi: https://doi.org/10.1016/j.chaos.2020.109846)

Newville, Matt et al. (2021). *lmfit/lmfit-py (version 1.0.2)*. Zenodo. (https://doi.org/10.5281/zenodo.12785036)

Norman and MacDonald. (2008). *Biological delay systems: linear stability theory*. Cambridge University Press. (doi: https://doi.org/10.2307/2532182)

Notice, Ringa et al. (2022). Hiv and covid-19 co-infection: A mathematical model and optimal control. *Informatics in Medicine Unlocked*, *31*, 100978. (doi: https://doi.org/10.1016/j.imu.2022.100978)

OECD. (2020). *The territorial impact of COVID-19: managing the crisis across levels of government.* Organisation for Economic Co-operation and Development Paris.

Ogidi, Odangowei Inetiminebiet al. (2021). Covid-19 vaccination: the pros and cons. *World Journal of Biology Pharmacy and Health Sciences*, *7*(1), 015–022. (doi: https://doi.org/10.30574/wjbphs.2021.7.1.0072)

Olayiwola, M. O. and Adedokun, K. A. (2023). A novel tuberculosis model incorporating a caputo fractional derivative and treatment effect via the homotopy perturbation method. *Bulletin of the National Research Centre*, *47*(1), 121. (doi: https://doi.org/10.1186/s42269-023-01091-0)

Oluyori, D. A. and Adebayo, H. O. (2020). Global Analysis of an SEIRS Model for COVID-19 Capturing Saturated Incidence with Treatment Response. *medRxiv*. (doi: https://doi.org/10.1101/2020.05.15.20103630)

Omame, A. and Okuonghae, D. (2021). A co-infection model for oncogenic human papillomavirus and tuberculosis with optimal control and cost-effectiveness analysis. *Optimal Control Applications and Methods*, *42*(4), 1081–1101. (doi: https://doi.org/10.1002/oca.2717)

Omame, Andrew et al. (2020). Analysis of COVID-19 and comorbidity co-infection model with optimal control. *Optimal Control Applications and Methods*. (doi: https://doi.org/10.1002/oca.2748)

Omame, Andrew et al. (2023). The optimal strategies to be adopted in controlling the co-circulation of covid-19, dengue and hiv: Insight from a mathematical model. *Axioms*, *12*(8), 773. (doi: https://doi.org/10.3390/axioms12080773)

Otoo, Dominic et al. (2024). Stability analysis for co-dynamics of covid-19 and hiv-aids with public sensitization and education as controls. *Contemporary Mathematics*, 2877–2912. (doi: https://doi.org/10.37256/cm.5320243232)

Pal, D. et al. (2020). Mathematical Analysis of a COVID-19 Epidemic Model by using Data Driven Epidemiological Parameters of Diseases Spread in India. *medRxiv*. (doi: https://doi.org/10.1134/S0006350922020154)

Pan, Xiaoyu et al. (2013). Restrictions to HIV-1 replication in resting CD4+ T lymphocytes. *Cell research*, *23*(7), 876–885. (doi: https://doi.org/10.1038/cr.2013.74)

Pontryagin, L. S. (1987). *Mathematical theory of optimal processes* (1st ed.). London: Routledge. (doi: https://doi.org/10.1201/9780203749319)

Prem, Kiesha et al. (2020). The effect of control strategies to reduce social mixing on outcomes of the COVID-19 epidemic in Wuhan, China: a modelling study. *The Lancet Public Health*. (doi: https://doi.org/10.1016/S2468-2667(20)30073-6)

Priya, Singh et al. (2024). Impact of covid-19 vaccination: a global perspective. *Frontiers in Public Health*, *11*. (doi: https://doi.org/10.3389/fpubh.2023.1272961)

Rajendran, Dinesh et al. (2020). Systematic literature review on novel corona virus SARS-CoV-2: a threat to human era. *VirusDisease*, 1–13. (doi: https://doi.org/10.1007/s13337-020-00604-z)

Ren, Xiangying et al. (2022). Reinfection in patients with covid-19: a systematic review. *Global health research and policy*, *7*(1), 12. (doi: https://doi.org/10.1186/s41256-022-00245-3)

Rivas, Neyla et al. (2020). Case report: Covid-19 recovery from triple infection with mycobacterium tuberculosis, hiv, and sars-cov-2. *The American journal of tropical medicine and hygiene*, *103*(4), 1597. (doi: https://doi.org/10.4269/ajtmh.20-0756)

Rodrigues, Paula et al. (2014). Cost-effectiveness analysis of optimal control measures for tuberculosis. *Bulletin of mathematical biology*, *76*, 2627–2645. (doi: https://doi.org/10.1007/s11538-014-0028-6)

Samares, Pal et al. (2006). Role of standard incidence in an eco-epidemiological system: A mathematical study. *Ecological Modelling*, *199*(3), 229-239. (doi: https://doi.org/10.1016/j.ecolmodel.2006.05.030)

scipy.org. (2021). *scipy.optimize.curve_fit*. (Retrieved September 9, 2023, from https://docs.scipy.org/doc/scipy/reference/generated/scipy.optimize.curve_fit.html)

Sharma, M. (2024). Diagnostic dilemma of tuberculosis among hiv-positive patients: Challenges and advances. *Z H Sikder Women's Medical College Journal*. (doi: https://doi.org/10.47648/zhswmcj.2024.v0602.11)

Shereen, Muhammad et al. (2020). COVID-19 infection: Origin, transmission, and characteristics of human coronaviruses. *Journal of advanced research*, *24*, 91. (doi: https://doi.org/10.1016/j.jare.2020.03.005)

Simon, Viviana et al. (2006). HIV/AIDS epidemiology, pathogenesis, prevention, and treatment. *The Lancet*, *368*(9534), 489–504. (doi: https://doi.org/10.1016/S0140-6736(06)69157-5)

Song, Wan-mei et al. (2021). Covid-19 and tuberculosis coinfection: an overview of case reports/case series and meta-analysis. *Frontiers in medicine*, *8*, 657006. (doi: https://doi.org/10.3389/fmed.2021.657006)

Squillace, Nicola et al. (2021). HIV and SARS-CoV-2 Co-Infection: What are the Risks? *Infection and Drug Resistance*, *14*, 3991. (doi: https://doi.org/10.2147/IDR.S277899)

Ssentongo, Paddy et al. (2021). Epidemiology and outcomes of COVID-19 in HIV-infected individuals: a systematic review and meta-analysis. *Scientific reports*, *11*(1), 1–12. (doi: https://doi.org/10.1038/s41598-021-85359-3)

Suwanwongse, Kulachanya and Shabarek, Nehad. (2020). Variation in mortality of HIV/SARS-CoV-2 co-infected patients in the Bronx, New York City. *Journal of medical virology*. (doi: https://doi.org/10.1002/jmv.26370)

Tanne, J. (2022, 11). Us faces triple epidemic of flu, rsv, and covid. *BMJ (Clinical research ed.)*, *379*, o2681. (doi: http://dx.doi.org/10.1136/bmj.o2681)

Teklu, S. W. and Kotola, B. S. (2023). A dynamical analysis and numerical simulation of covid-19 and hiv/aids co-infection with intervention strategies. *Journal of Biological Dynamics*, *17*(1), 2175920. (doi: https://doi.org/10.1080/17513758.2023.217592)

Teran, Ricardo et al. (2023). Sars-cov-2 reinfection risk in persons with hiv, chicago, illinois, usa, 2020–2022. *Emerging Infectious Diseases*, *29*(11), 2257–2265. (doi: https://doi.org/10.3201/eid2911.230577)

Tilahun, G. T. (2019). Modeling co-dynamics of pneumonia and meningitis diseases. *Advances in Difference Equations*, *2019*(1), 1–18. (doi: https://doi.org/10.1186/s13662-019-2087-3)

Tolossa, Tadesse et al. (2021). Survival from a triple co-infection of COVID-19, HIV, and tuberculosis: a case report. *International Medical Case Reports Journal*, *14*, 611. (doi: https://doi.org/10.2147/IMCRJ.S326383)

Tseng, Alice et al. (2015). The evolution of three decades of antiretroviral therapy: challenges, triumphs and the promise of the future. *British journal of clinical pharmacology*, *79*(2), 182–194.

UNAIDS. (2023). *The path that ends aids: Unaids global aids update.* Retrieved from https://www.unaids.org/en/resources/documents/2023/global-aids-update (Report. Licence: CC BY-NC-SA 3.0 IGO)

UNAIDS. (2024). *What people living with hiv need to know about hiv and covid-19.* (Retrieved September, 2024, from https://www.unaids.org/en/covid19)

Van den Driessche, P. and Watmough, J. (2002). Reproduction numbers and sub-threshold endemic equilibria for compartmental models of disease transmission. *Mathematical biosciences*, *180*(1-2), 29–48. (doi: https://doi.org/10.1016/S0025-5564(02)00108-6)

Vos, Theo et al. (2020). Global burden of 369 diseases and injuries in 204 countries and territories, 1990-2019: a systematic analysis for the Global Burden of Disease Study 2019. *The Lancet*, *396*(10258), 1204–1222.

Waheed, Ahmad et al. (2021). Mathematical analysis for the effect of voluntary vaccination on the propagation of corona virus pandemic. *Results in Physics*, *31*, 104917. (doi: https://doi.org/10.1016/j.rinp.2021.104917)

Wang, X. (2004). A simple proof of descartes's rule of signs. *The American Mathematical Monthly*, *111*(6), 525. (doi: https://doi.org/10.1080/00029890.2004.11920108)

Wang, Jingzhou et al. (2021). Covid-19 reinfection: A rapid systematic review of case reports and case series. *medRxiv*. (doi: 10.1101/2021.03.22.21254081)

Weike Zhou et al. (2022). The resurgence risk of covid-19 in china in the presence of immunity waning and ade: A mathematical modelling study. *Vaccine*, *40*(49), 7141-7150. (doi: https://doi.org/10.1016/j.vaccine.2022.10.043)

WHO. (2003). *Summary of probable SARS cases with onset of illness from 1 November 2002 to 31 July 2003.* (Retrieved January 24, 2020, from https://bit.ly/309CrNS)

WHO. (2020). *Coronavirus disease (COVID-19): Herd immunity, lockdowns and COVID-19.* (Retrieved December 31, 2020, from https://bit.ly/3rbE87i)

WHO. (2021a). *Clinical features and prognostic factors of COVID-19 in people living with HIV hospitalized with suspected or confirmed SARS-CoV-2 infection, 15 July 2021* (Technical documents). Geneva, Switzerland: World Health Organization.

WHO. (2021b). *Episode 48: HIV and COVID-19.* (Retrieved November 10, 2021, from https://bit.ly/3wLbZqp)

WHO. (2021c). *HIV data and statistics.* (Retrieved November 13, 2021, from https://bit.ly/3HmxDpQ)

WHO. (2021d). *Noncommunicable diseases.* https://bit.ly/3flWjlt.

WHO. (2023). *HIV and AIDS.* (Retrieved October 13, 2024, from https://bit.ly/4eRfxwp)

WHO. (2024a). *COVID-19 advice for the public: Getting vaccinated.* (Retrieved January 24, 2024, from https://bit.ly/3FwysKm)

WHO. (2024b). *Global situation.* (Retrieved January 24, 2024, from https://covid19.who.int/)

WHO. (2024c). *Tuberculosis.* (Retrieved October, 2024, from https://www.who.int/news-room/fact-sheets/detail/tuberculosis)

WHO. (2024d). *Vaccine efficacy, effectiveness and protection.* (https://www.who.int/news-room/feature-stories/detail/vaccine-efficacy-effectiveness-and-protection)

Wiggins, S. (2003). *Introduction to Applied Nonlinear Dynamical Systems and Chaos* (Vol. 2). Springer Science & Business Media.

William Ogilvie Kermack and À. G. Mckendrick. (1927). A contribution to the mathematical theory of epidemics. *Proceedings of The Royal Society A: Mathematical, Physical and Engineering Sciences*, *115*, 700-721. (doi: https://doi.org/10.1098/rspa.1927.0118)

Williams, Chukwu et al. (2020). A mathematical model for co-dynamics of listeriosis and bacterial meningitis diseases. *Commun. Math. Biol. Neurosci.*. (doi: https://doi.org/10.28919/cmbn/5060)

World Bank. (2022). *Population ethiopia.* (Retrieved February 20, 2022, from https://data.worldbank.org/indicator/SP.POP.TOTL)

World Health Organization. (2024a). *Country Disease Outlook: Ethiopia, 2023.* https://www.afro.who.int/publications. (Accessed 29 October 2024)

World Health Organization. (2024b). *Global tuberculosis programme: Data.* https://www.who.int/teams/global-tuberculosis-programme/data. (Accessed 19 May 2024)

World Health Organization. (2024c). *Hiv data and statistics.* https://www.who.int/teams/global-hiv-hepatitis-and-stis-programmes/hiv/strategic-information/hiv-data-and-statistics. (Accessed 19 May 2024)

World Health Organization. (2024d). *Tuberculosis & hiv.* (Retrieved September, 2024, from https://www.who.int/teams/global-hiv-hepatitis-and-stis-programmes/hiv/treatment/tuberculosis-hiv)

Xue, Ling et al. (2023). Modelling the transmission dynamics and optimal control strategies for hiv infection in china. *Journal of Biological Dynamics*, *17*(1), 2174275. (doi: https://www.doi.org/10.1080/17513758.2023.2174275)

Yair Goldberg et al. (2021). Protection and waning of natural and hybrid covid-19 immunity. *Thenew england journal of medicine*. (doi: https://doi.org/10.1101/2021.12.04.21267114)

Yang, C. and Wang, J. (2020). A mathematical model for the novel coronavirus epidemic in Wuhan, China. *Mathematical Biosciences and Engineering*, *17*(3), 2708–2724. (doi: 10.3934/mbe.2020148)

Yang, Rongrong et al. (2021). Clinical characteristics of COVID-19 patients with HIV coinfection in Wuhan, China. *Expert Review of Respiratory Medicine*, *15*(3), 403–409. (doi: https://doi.org/10.1080/17476348.2021.1836965)

Yavuz, Mehmet et al. (2021). A new mathematical modeling of the COVID-19 pandemic including the vaccination campaign. *Open Journal of Modelling and Simulation*, *9*(3), 299–321. (doi: https://doi.org/10.4236/ojmsi.2021.93020)

Yunihastuti, Evy et al. (2022). Incidence and severity prediction score of covid-19 in people living with hiv (scovhiv): experience from the first and second waves of the pandemic in indonesia. *AIDS Research and Therapy*, *19*(1), 47. (doi: https://doi.org/10.1186/s12981-022-00472-1)

Zein, Abdulrahman R. et al. (2022). Most common concurrent infections with covid-19. *International Journal Of Community Medicine And Public Health*, *9*(2), 1108–1112. (doi: https://doi.org/10.18203/2394-6040.ijcmph20220079)

Zelong Li. (2023). Evaluating the impact of waning antibodies on covid-19 reinfection and the importance of vaccines using a household epidemic model. *Proceedings of the International Conference on Mathematics and Machine Learning*. (doi: https://doi.org/10.1145/3653724.3653766)

Zeru, M. A. (2021). Prevalence and associated factors of hiv-tb co-infection among hiv patients: a retrospective study. *African health sciences*, *21*(3), 1003–1009. (doi: https://dx.doi.org/10.4314/ahs.v21i3.7)

Zviiteyi Chazuka et al. (2024). Modelling and analysis of an hiv model with control strategies and cost-effectiveness. *Results in Control and Optimization*, *14*, 100355. (doi: https://doi.org/10.1016/j.rico.2023.100355)

APPENDIX A

MATHEMATICAL PRELIMINARIES

Based on the references (Cain, John W and Reynolds, Angela M, n.d.; Kelley, Walter G. and Peterson, Allan C., 2010; Layek, 2015; Lynch, 2018; Martcheva, 2015; Wiggins, 2003), this appendix establish the mathematical foundation for disease modeling conducted in this dissertation. The tools covered—well-posedness (existence, uniqueness, positivity and boundedness of solutions), stability analysis, and optimal control—are essential for investigating the transmission dynamics of diseases, studying stability, and designing optimal control strategies like vaccination or treatment.

A.1 Basics of Dynamical Systems

Ordinary Differential Equations (ODEs) are widely used to model biological systems, including disease transmission. Let t be a real scalar; let D be an open set in $\mathbb{R}^{n+1}$ with an element of D written as (t,x); let $f : D \to \mathbb{R}^n$ be continuous and let $\dot{x} = \frac{dx}{dt}$. A differential equation is a relation of the form

$$\dot{x}(t) = \mathbf{f}(t,\mathbf{x}(t)), \quad \text{or} \quad \dot{x} = \mathbf{f}(t,\mathbf{x}(t)). \tag{A.1}$$

An ODE in which the independent variable does not occur explicitly is called autonomous ODE. If equation (A.1) is autonomous it is often written as:

$$\mathbf{x}' = \mathbf{f}(\mathbf{x}). \tag{A.2}$$

Definition A.1.1. *We say* $\mathbf{x}$ *is a solution of* (A.1) *in an interval* $I \subseteq \mathbb{R}$ *if* $\mathbf{x}$ *is a continuously differentiable function defined on* I, $(t,\mathbf{x}(t)) \in D$ *for all* $t \in I$, *and* x *satisfies* (A.1) *on* I. *We refer to* f *as a vector field in* D.

Definition A.1.2. *(Initial Value Problem): The initial value problem for an ordinary differential equation involves finding a function* $\mathbf{x}(t)$ *that satisfies*

$$\begin{aligned} \mathbf{x}' &= \mathbf{f}(t,\mathbf{x}(t)) \\ \mathbf{x}(t_0) &= \mathbf{x}_0 \ . \end{aligned} \tag{A.3}$$

In initial value problem (IVP), we look for solutions that lie within a given interval that

contains t_0, so that the solution curves passes through the point $(t_0, \mathbf{x}(t_0))$.

Well-posedness

Theorem A.1.1. *(Peano Existence Theorem). If f is continuous in D, then for any $(t_0, x_0) \in D$, there is at least one solution of* (A.3) *passing through (t_0, x_0).*

Definition A.1.3. *A function $f(t,x)$ defined on a domain D is said to be locally Lipschitzian in x if for any closed bounded set U in D there is L such that*

$$|f(t,x) - f(t,y)| \leq L|x-y|$$

for $(t,x),(t,y) \in U$. If $f(t,x)$ has continuous first partial derivatives with respect to x in D, then $f(t,x)$ is locally Lipschitzian in x.

Theorem A.1.2. *(Picard-Lindelöf). If $f(t,x)$ is continuous in D and locally Lipschitzian with respect to x in D, then for any $(t_0, x_0) \in D$, there exists a unique solution $x(t, t_0, x_0)$, $x(t_0, t_0, x_0) = x_0$, of* (A.1) *passing through (t_0, x_0).*

Definition A.1.4. *(Flow). Consider System* (A.3). *The flow, $\phi(t, x_0)$, of* (A.3) *represents the solution of* (A.3) *over time given an initial condition, provided that the solutions to the differential equation exist and are unique.*

Definition A.1.5. *(Invariant set). A set $M \subset \mathbb{R}^n$ is said to be an invariant set under the flow ϕ if for any point $x_0 \in M$, $\phi(t, x_0) \in M$ for all $t \in \mathbb{R}$: The set M is said to be positively invariant if $\phi(t, x_0) \in M$ for $t \geq 0$.*

Definition A.1.6. *(Well-posedness): System* (A.3) *is well-posed if solutions exist, are unique, and for systems describing populations, remain bounded and nonnegative for all nonnegative initial conditions.*

In establishing well-posedness, positivity plays a crucial role in ensuring that model solutions maintain physical meaning, specifically non-negative populations. On the other hand, boundedness guarantees that the solution values do not grow infinitely over time, which is essential for maintaining realistic model solutions. In epidemiology, population sizes are naturally limited by the total population, and unbounded solutions would lead to unrealistic scenarios, such as an infected population growing infinitely.

Stability analysis

Definition A.1.7. *(Equilibrium point): An equilibrium point (Equilibrium solution) of* (A.2) *is a point* $\mathbf{x}^*$ *such that* $\mathbf{f}(\mathbf{x}^*) = 0$.

As a point $\mathbf{x}^*$ satisfies $(\mathbf{x}^*)' = \mathbf{f}(\mathbf{x}^*) = 0$, so the solution is constant when $\mathbf{x} = \mathbf{x}^*$. That is, $\mathbf{x}^*$ is time-independent solution, solution that is constant in time. Terms such as fixed point, stationary point, singularity point, critical point and steady state are another name for equilibrium point.

An equilibrium point is stable if all solutions starting at nearby points stays near by; otherwise it is unstable. It is asymptotically stable if all solutions starting at nearby points not only stays near by but it tends to the equilibrium point as time approaches to infinity. The formal definition is given as follows:

Definition A.1.8. *(Stable and unstable equilibrium point): Let* $\phi(t)$ *be the flow of* (A.2)*, assumed to be defined for all* $t \in \mathbb{R}$*. An equilibrium solution* $\mathbf{x}^*$ *of* (A.2) *is said to be locally stable if for all* $\varepsilon > 0$*, there exists* $\delta = \delta(\varepsilon) > 0$ *such that for all* $\mathbf{x} \in N_\delta(\mathbf{x}^*)$ *and* $t \geq 0$*,* $\phi_t(\mathbf{x}) \in N_\delta(\mathbf{x}^*)$*. The equilibrium point is unstable if it is not stable.*

Definition A.1.9. *(Asymptotically stable equilibrium point): Let* $\phi(t)$ *be the flow of* (A.2)*. An equilibrium solution* $\mathbf{x}^*$ *is (locally) asymptotically stable if there exists* $\delta > 0$ *such that for all* $\mathbf{x} \in N_\delta(\mathbf{x}^*)$ *and* $t \geq 0$*, there holds*

$$\lim_{t\to\infty} \phi(t) = \mathbf{x}^*.$$

Definition A.1.10. *Given a set* $\mathbf{y} = \mathbf{f}(\mathbf{x})$ *of n equations in n variables* $x_1, ..., x_n$*, written explicitly as*

$$\begin{cases} y_1 = f_1(x_1, ..., x_n), \\ y_2 = f_2(x_1, ..., x_n), \\ \quad \vdots, \\ y_n = f_n(x_1, ..., x_n). \end{cases}.$$

The Jacobian matrix(sometimes simply called "the Jacobian"), denoted by $D\mathbf{f}$*, is defined by*

$$D\mathbf{f} = \begin{pmatrix} \frac{\partial f_1}{\partial x_1} & \frac{\partial f_1}{\partial x_2} & \cdots & \frac{\partial f_1}{\partial x_n} \\ \frac{\partial f_2}{\partial x_1} & \frac{\partial f_2}{\partial x_2} & \cdots & \frac{\partial f_2}{\partial x_n} \\ \vdots & \vdots & \ddots & \vdots \\ \frac{\partial f_n}{\partial x_1} & \frac{\partial f_n}{\partial x_2} & \cdots & \frac{\partial f_n}{\partial x_n} \end{pmatrix}.$$

Definition A.1.11. *A function* $\mathbf{f}$ *is said to be continuously differentiable on the open set E, denoted by* $C^1(E)$*, if the elements of* $D\mathbf{f}$ *are continuous on E.*

Definition A.1.12. *If* $\mathbf{f} \in C^1(E)$*, then the linearization of* (A.2) *at the equilibrium* $\mathbf{x}^* \in E$ *is given by*

$$\mathbf{x}' = D\mathbf{f}(\mathbf{x}^*)\mathbf{x}.$$

Definition A.1.13. *An equilibrium* $\mathbf{x}^*$ *of* (A.2) *is called isolated if there exists a positive number* ε *such that the open ball* $B(\mathbf{x}^*, \varepsilon)$ *contains no equilibria other than* $\mathbf{x}^*$.

Theorem A.1.3. *(Hartman-Grobman): Suppose* $\mathbf{x}^*$ *is an isolated equilibrium of a nonlinear system* $\mathbf{x}' = \mathbf{f}(\mathbf{x})$*. Then in the vicinity of* $\mathbf{x}^*$*, the linearization* $\mathbf{x}' = D\mathbf{f}(\mathbf{x}^*)(\mathbf{x} - \mathbf{x}^*)$ *about that equilibrium has the same qualitative behavior as the original nonlinear system.*

Hartman-Grobman justifies very important result in the local qualitative theory of a dynamical system. It can be used to determine the stability of equilibrium in system (A.2) without finding explicit solutions.

Definition A.1.14. *Let* $\mathbf{x}^*$ *be an equilibrium point of the autonomous system* (A.2)*, where* $\mathbf{f} \in C^1$ *(once continuously differentiable) in a neighborhood of* $\mathbf{x}^*$.

1. *If all the eigenvalues of* $D\mathbf{f}(\mathbf{x}^*)$ *have negative real part, then* $\mathbf{x}^*$ *is a locally asymptotically stable equilibrium point.*

2. *If* $D\mathbf{f}(\mathbf{x}^*)$ *has at least one eigenvalue with positive real part, then* $\mathbf{x}^*$ *is an unstable equilibrium point.*

Theorem A.1.4. *(Routh-Hurwitz criteria): Consider the nth-degree polynomial with real constant coefficients*

$$P(\lambda) = \lambda^n + a_1\lambda^{n-1} + a_2\lambda^{n-2} + \cdots + a_{n-1}\lambda + a_n.$$

Define n Hurwitz matrices using the coefficients a_i *of the characteristic polynomial:*

$$H_1 = (a_1),\ H_2 = \begin{pmatrix} a_1 & 1 \\ 0 & a_2 \end{pmatrix},\ H_3 = \begin{pmatrix} a_1 & 1 & 0 \\ a_3 & a_2 & a_1 \\ 0 & 0 & a_3 \end{pmatrix} \text{ and, } H_n = \begin{pmatrix} a_1 & 1 & 0 & 0 & \dots & 0 \\ a_3 & a_2 & a_1 & 1 & \dots & 0 \\ a_5 & a_4 & a_3 & a_2 & \dots & 0 \\ \vdots & \vdots & \vdots & \vdots & \dots & \vdots \\ 0 & 0 & 0 & 0 & \dots & a_n \end{pmatrix}$$

where $a_j = 0$ *if* $j > n$*. All roots of the polynomial* $P(\lambda)$ *are negative or have negative real part if and only if the determinants of all Hurwitz matrices are positive:*

$$i.e.,\ \ det(H_j) > 0,\ \ j = 1, ..., n$$

Establishing global properties of a dynamical system is generally a nontrivial problem. The most successful approach to the problem is the direct Lyapunov method (Martcheva, 2015). However, the method requires an auxiliary function with specific properties, a Lyapunov function, which is not easy to find.

Theorem A.1.5. *(Lyapunov Stability Theorem): Let E be an open subset of $\mathbb{R}^n$ containing a critical point $\mathbf{x}^*$. Suppose that $\mathbf{f}$ is continuously differentiable and that there exists a continuously differentiable function, say $V(\mathbf{x})$, which satisfies the conditions:*

i $V(\mathbf{x}^*) = 0$

ii $V(\mathbf{x}) > 0$ *for* $\mathbf{x} \neq \mathbf{x}^*$ *where* $\mathbf{x} \in \mathbb{R}^n$.

Then

① *if* $\dot{V}(\mathbf{x}) \leq 0$ *for all* $\mathbf{x} \in E$, $\mathbf{x}^*$ *is globally stable.*

② *if* $\dot{V}(\mathbf{x}) < 0$ *for all* $\mathbf{x} \in E \backsim \mathbf{x}^*$, $\mathbf{x}^*$ *is globally asymptotically stable.*

③ *if* $\dot{V}(\mathbf{x}) > 0$ *for all* $\mathbf{x} \in E \backsim \mathbf{x}^*$, $\mathbf{x}^*$ *is unstable.*

Definition A.1.15. *The function $V(\mathbf{x})$ is called a Lyapunov function.*

Theorem A.1.6. *(LaSalle's Invariance Principle): Suppose that $V : E \subset \mathbb{R}^n \to \mathbb{R}$ is a Lyapunov function for the system $\mathbf{x}' = \mathbf{f}(\mathbf{x})$. If the set $\{\mathbf{x} \in E | \dot{V}(\mathbf{x}) = 0\}$ contains only one fixed point $\mathbf{x}^*$, then $\mathbf{x}^*$ is globally asymptotically stable.*

Stability analysis in epidemic modeling is a mathematical approach used to understand the long-term behavior of infectious disease spread within a population. It typically involves studying equilibrium points, such as disease-free and endemic equilibria, to determine whether small deviations from these points will die out or grow. The disease free equilibrium is the state where the population is completely free from infection; the implication is that all infected compartments are zero and the total population comprises only susceptible or immune individuals. The endemic equilibrium is the state where the infection remains in the population, so there is a positive number of infectious individuals at equilibrium. By analyzing the basic reproduction number ($\mathscr{R}_0$), which indicates the average number of secondary infections caused by an infected individual, stability analysis helps assess whether an infection will persist, die out, or oscillate over time. A disease-free equilibrium is stable if $\mathscr{R}_0 < 1$, meaning the disease will eventually die out, while an endemic equilibrium is stable when $\mathscr{R}_0 > 1$, implying persistent transmission. This analysis provides critical insights for public health interventions and understanding disease dynamics.

A.2 Reproduction Number($\mathscr{R}_0$)

Definition A.2.1. *The spectral radius of a matrix A is defined as the maximum of the absolute values of the eigenvalues of A:*

$$\rho(A) = sup\{|\lambda| : \lambda \in \sigma(A)\},$$

where $\sigma(A)$ *denotes the set of eigenvalues of A.*

The basic reproduction number, $\mathscr{R}_0$, is defined as the expected number of disease cases (secondary infections) produced by a "typical" infected individual in a wholly susceptible population over the full course of the disease outbreak (Brauer, Fred et al., 2019). The basic reproduction number is a measure of the potential for disease spread within a population and it is important to determine the stability of disease free equilibrium.

Summary for method of computing $\mathscr{R}_0$, which was introduced by Diekmann, Odo et al. (1990) and Van den Driessche, P. and Watmough, J. (2002), is given in Bianchi, Arianna et al. (2019). Following the given summary, in the general framework an epidemic model is split into two processes: new infections, expressed through an operator $\mathscr{F}$, and transition between infected compartments, expressed by an operator $\mathscr{V}$. The compartmental model can then be written in the following form:

$$\dot{x} = \mathscr{F}(x) - \mathscr{V}(x).$$

If $D\mathscr{F}$ and $D\mathscr{V}$ denote the linearizations of these operators in the disease-free equilibrium, then they have the general form

$$D\mathscr{F} = \begin{pmatrix} \mathbf{F} & 0 \\ 0 & 0 \end{pmatrix} \qquad \text{and} \qquad D\mathscr{V} = \begin{pmatrix} \mathbf{V} & 0 \\ \star & \star \end{pmatrix},$$

where $\mathbf{F}$ and $\mathbf{V}$ are matrices of dimension $m \times m$, m is the number of infected compartments, and $\star$ denote entries that are not important for the argument that we are interested in. The next generation matrix is then defined as $\mathbf{F}\mathbf{V}^{-1}$. It roughly measures the new infections that arise, while infected individuals have not yet recovered. The basic reproduction number $\mathscr{R}_0$ arises as the spectral radius of the next generation matrix:

$$\mathscr{R}_0 = \rho(\mathbf{F}\mathbf{V}^{-1}).$$

A.3 Bifurcation Analysis

Bifurcations arise in dynamical systems when a small variation of a model parameter(the bifurcation parameters) causes qualitatively different behavior in the corresponding dynamical system. Bifurcation analysis can be carried out by employing the center manifold theory as in (Castillo-Chavez, C. and Song, Baojun, 2004) on the given system of differential equations.

consider a general system of ODEs with a parameter ϕ:

$$\frac{dx}{dt} = f(x,\phi), \quad f : \mathbb{R}^n \times \mathbb{R} \text{ and } f \in C^2(\mathbb{R}^n \times \mathbb{R}). \tag{A.4}$$

Without loss of generality, it is assumed that 0 is an equilibrium for system (A.4) for all values of the parameter ϕ.

Theorem A.3.1. *(Castillo-Chavez, C. and Song, Baojun, 2004). Assume*

A1: $A = Df(0,0) = \frac{\partial f_i}{\partial x_i}(0,0)$ *is the linearization matrix of system (A.4) around the equilibrium 0 with* φ *evaluated at 0. Zero is a simple eigenvalue of A and all other eigenvalues of A have negative real parts;*

A2: Matrix A has a non-negative right eigenvector w and a left eigenvector v corresponding to the zero eigenvalue.

Let f_k *be the kth component of* f *and*

$$a = \sum_{k,i,j=1}^{6} v_k w_i w_j \frac{\partial^2 f_k}{\partial x_i \partial x_j}(\varepsilon_0, \beta_1^*)$$
$$b = \sum_{k,j=1}^{6} v_k w_j \frac{\partial^2 f_k}{\partial x_j \partial \beta_1}(\varepsilon_0, \beta_1^*)$$

The local dynamics of (A.4) around 0 are totally determined by a and b.

i. $a > 0,\ b > 0$. *When* $\varphi < 0$ *with* $|\varphi| \ll 1$, *0 is locally asymptotically stable, and there exists a positive unstable equilibrium; when* $0 < \varphi \ll 1$, *0 is unstable and there exists a negative and locally asymptotically stable equilibrium;*

ii. $a < 0,\ b < 0$. *When* $\varphi < 0$ *with* $|\varphi| \ll 1$, *0 is unstable; when* $0 < \varphi \ll 1$, *0 is locally asymptotically stable, and there exists a positive unstable equilibrium;*

iii. $a > 0,\ b < 0$. *When* $\varphi < 0$ *with* $|\varphi| \ll 1$, 0 *is unstable, and there exists a locally asymptotically stable negative equilibrium; when* $0 < \varphi \ll 1$, 0 *is stable, and a positive unstable equilibrium appears;*

iv. $a < 0,\ b > 0$. *When* φ *changes from negative to positive,* 0 *changes its stability from stable to unstable. Correspondingly a negative unstable equilibrium becomes positive and locally asymptotically stable.*

In particular, When $a > 0$ *and* $b > 0$*, the bifurcation at* $\varphi = 0$ *is sub-critical (backward).*

Remark (Martcheva, 2015): In practice, the following two observations are important.

- The equilibrium 0 is actually the disease-free equilibrium.
- φ is one of the parameters in the reproduction number, and the critical value of φ is the value of the parameter that makes the reproduction number equal to one.
- Since the disease-free equilibrium has positive entries, the right eigenvector w need not be non-negative. Components of the right eigenvector w that correspond to positive entries in the disease-free equilibrium could be negative. However, components that correspond to zero entries in the disease-free equilibrium should be nonnegative.

A backward bifurcation at the critical threshold $\mathscr{R}_0 = 1$ may be qualitatively described as follows. In the neighborhood of 1, for $\mathscr{R}_0 < 1$, a stable disease-free equilibrium coexists with two endemic equilibria: a smaller equilibrium (i.e. with a smaller number of infective individuals), which is unstable, and a larger one (i.e. with a larger number of infective individuals) which is stable. For $\mathscr{R}_0 > 1$, there are only two equilibria: the disease-free equilibrium, unstable and the larger endemic equilibrium, which is stable. Hence, in a system with a backward bifurcation at $\mathscr{R}_0 = 1$, when the bifurcation parameter $\mathscr{R}_0$ is increased so that $\mathscr{R}_0 > 1$, it is not sufficient to continuously reduce $\mathscr{R}_0$ just below 1 to eradicate the disease. To this aim, the bifurcation parameter $\mathscr{R}_0$ has to be reduced below a further bifurcation value, i.e. $\mathscr{R}_0^* = 1$, where a saddle-node bifurcation occurs and causes the disappearing of the two (respectively, stable and unstable) endemic equilibria.

A.4 Optimal Control Theory for ODE

Consider a system of ODEs

$$\begin{aligned} \mathbf{x}'(t) &= \mathbf{f}(\mathbf{x}(t)), \\ \mathbf{x}(0) &= \mathbf{x}_0, \end{aligned} \tag{A.5}$$

where the given initial condition is $\mathbf{x}_0 \in \mathbb{R}^n$, and $\mathbf{f} : \mathbb{R}^n \to \mathbb{R}^n$. The unknown state variable is $\mathbf{x} : [0,\infty) \to \mathbb{R}^n$.

Suppose that the right-hand side of (A.5) depends on a control function given by $\mathbf{u}(t) : [0,\infty) \to \mathcal{D}$, where $\mathcal{D} \subset \mathbb{R}^m$. Then state variable satisfies a differential equation which depends on the control variable:

$$\mathbf{x}'(t) = \mathbf{f}(\mathbf{x}(t), \mathbf{u}(t)).$$

The basic optimal control problem consists of finding a piecewise continuous control $\mathbf{u}(t)$ and the associated state variable $\mathbf{x}(t)$ to maximize the given objective functional, which is typically an integral expression formulated terms of the state and control variables. That is,

$$\min_{u \in \mathcal{U}} \int_0^T g(\mathbf{x}(t), \mathbf{u}(t))\, dt$$

subject to

$$\mathbf{x}'(t) = \mathbf{f}(\mathbf{x}(t), \mathbf{u}(t)),$$
$$\mathbf{x}(0) = \mathbf{x}_0 \text{ and } \mathbf{x}(T) \text{ free},$$

where $\mathcal{U}$ is a set of Lebesgue measurable functions.

By $\mathbf{x}(T)$ free, it is meant that the value of $\mathbf{x}(T)$ is unrestricted. The function $g : \mathbb{R}^n \times \mathcal{D} \to \mathbb{R}$ is given. The terminal time T is given as well. The function g is called the *running payoff*. If a control $\mathbf{u}^*(T)$ exists, it is called an optimal control. The optimal control together with the corresponding solution gives the optimal control pair $(\mathbf{x}^*, \mathbf{u}^*)$.

If an optimal pair exists, it can be found with Pontryagin's minimum principle. Let $\lambda(t)$ be a time-varying Lagrange multiplier vector and the Hamiltonian H is defined for all $t \in [0,T]$ by

$$H(\mathbf{x}(t), \mathbf{u}(t), \lambda(t)) = g(\mathbf{x}(t), \mathbf{u}(t)) + \sum_{i=1}^{n} \lambda_i(t) f_i(\mathbf{x}(t), \mathbf{u}(t)).$$

The Pontryagin first-order necessary optimality condition is given as follows.

Theorem A.4.1. *(Pontryagin's Minimum Principle) For the optimality of control* $\mathbf{x}^*$ *and corresponding trajectory* $\mathbf{x}^*$ *with* $t \in [0,T]$*, it is necessary that there exist a nonzero adjoint vector*

function $\lambda^*(t)$ *that is a solution to the adjoint system*

$$\lambda'(t) = -\frac{\partial H(\mathbf{x}(t), \mathbf{u}(t), \lambda(t))}{\partial x}$$
$$\lambda(T) = 0$$

so that

$$H(\mathbf{x}^*(t), \mathbf{u}^*(t), \lambda^*(t)) = \min_{\mathbf{u} \in \mathcal{U}} H(\mathbf{x}^*(t), \mathbf{u}(t), \lambda^*(t)).$$

Thus, the necessary conditions for optimizing the Hamiltonian are:

$$\begin{aligned}
&\frac{\partial H}{\partial u} = 0 \implies g_u + \sum_{i=0}^{n} \lambda_i (f_i)_u = 0 && \text{(optimality equation)},\\
&\lambda_i'(t) = -\frac{\partial H(\mathbf{x}(t), \mathbf{u}(t), \lambda(t))}{\partial x_i} \implies \lambda_i'(t) = -g_{x_i} + \sum_{i=0}^{n} \lambda_i (f_i)_{x_i} && \text{(adjoint equation)},\\
&\lambda(T) = 0 && \text{(transversality condition)}.
\end{aligned} \tag{A.6}$$

For minimization problem, we must also have $\frac{\partial^2 H}{\partial u^2} \geq 0$ at $\mathbf{u}^*$.

It is difficult to solve the optimality system, the state equations and the adjoint equations together with the characterization of the optimal control and the boundary conditions, analytically. Instead, we use numerical methods to approximate solutions and display results. To solve the optimality system with initial conditions for the states and final time conditions for the adjoints, an iterative scheme was used, namely forward-backward sweep method. The forward-backward sweep method is an indirect method to solve the optimal control problem. According to Lenhart, S. and Workman, J. T. (2007), the steps to perform the forward-backward sweep method are as follows. First, the model parameters must be entered to obtain the desired simulation for the disease outbreak. After that, an initial guess has to be made for the control input $u(= u_{old})$, where the initial guess $u_{old} = 0$ almost always suffices. The state equations $(\dot{x})$ must now be solved forward in time. After that, the adjoint equations (l) must be solved backwards in time. Now that the variables x and l are solved, a new optimal control u_{new} can be calculated based on the optimality equation. The calculated u_{new} and the initial guess u_{old} must be updated with a update policy to obtain control input u_{update}. A common update policy is to calculate the average value of the two u's, $\frac{u_{new}+u_{old}}{2}$. Ultimately, it must be examined whether convergence can be achieved. Convergence is achieved when the variables of the current iteration compared to the previous iteration are within a certain tolerance. That is,

$$\frac{\|u_{update} - u_{old}\|}{\|u_{update}\|} \leq \delta$$

where δ is the accepted tolerance. If the outcome is not within the accepted tolerance, the updated $u(u_{update})$ must replace the old $u(u_{old})$, and the forward-backward sweep method must be performed again. The method stops when u_{update} is within the accepted tolerance. If the latter is the case, then these are the final values, and the optimal control has been determined. It should be noted that convergence can also occur with the variables x and l, meaning that once these variables achieve convergence, the method stops as well. Below is the pseudocode summarizing the iterative scheme serves as the basis for the Matlab code we have constructed.

Algorithm 1 Forward-Backward Sweep Method

Result: The optimal solution u^* that solves the optimal control problem.

Initialization: Set M the number of subdivisions, h the step size, $t = [0, t_f]$, tolerance δ, $u_{\text{old}} = u_0$, $l_{\text{old}} = l(t_f) = 0$. Set the error:

$$err = \frac{\|u_{update} - u_{old}\|}{\|u_{update}\|}$$

while $(err < \delta)$ **do**

$u_{\text{old}} \leftarrow u$;

$x_{\text{old}} \leftarrow x$;

$l_{\text{old}} \leftarrow l$;

for $i = 1$ to N **do**

Solve the **state equation** forward in time (using a 4th-order Runge-Kutta scheme):

$\dot{x}(t) = f(x,u,t)$, with $x(0) = x_0$;

Using the **transversality condition** $l(T) = 0$ and the stored values for u, x,

solve the **adjoint equation** backward in time (using a 4th-order Runge-Kutta scheme):

$\dot{l}(t) = -\frac{\partial H}{\partial x}(x,u,l,t)$;

end

Update the control:

$u \leftarrow \frac{u_{\text{old}}+u}{2}$;

$l \leftarrow l_{\text{old}}$;

Compute error: $err = \frac{\|u_{update}-u_{old}\|}{\|u_{update}\|}$

end

Output: Optimal control u^*

APPENDIX B

PYTHON CODES

Below are Python scripts used for performing simulations.

B.1 Parametric Estimation

```
'''This code serves as a representative example of the codes
   utilized for parametric estimation. It is designed for the
   parametric estimation of COVID-19 related parameters within
   the COVID-19, HIV and TB co-dynamics model.'''

# Importing relevant modules
import numpy as np
from scipy.integrate import odeint
import matplotlib.pyplot as plt
from lmfit import Model
from matplotlib.ticker import ScalarFormatter
import matplotlib.style

# Figure styles and figures text fonts
matplotlib.style.use('seaborn-white')
plt.rcParams['axes.prop_cycle'] = plt.cycler(color=["blue", "
   lime", "cyan"])

# COVID-19 monthly data from march 2020 to December 2023
data=np.array([16, 122, 1063, 5570, 13248, 49654, 72700, 92858,
108930, 122413, 137021, 158058, 198794, 250955, 271200, 275881,
278446, 305077, 340845, 364960, 371177, 395750, 464754, 468625,
469611, 470417, 472232, 487212, 492194, 493132, 493505, 493939,
494462, 497096, 499466, 499959, 500436, 500831, 500890, 500920,
500946, 500991, 501060, 501077, 501104, 501117])

# Time points
t=np.arange(0,len(data),1)
```

```
25
26 # Parameters assigned to be fixed
27 chi=159756
28 mu_d=1/(66*12)
29 nu_m=0.99
30 nu_0=nu_m*0.2
31 D=500/(66*12*159756)
32 a=0.2
33 kappa=0.2
34 sigma_c=0.13
35 pi_t=0.85572872/12
36 delta_t=2.8000e-04/12
37 theta_t=0.78399616/12
38 pi_h=0.124/12
39 delta_h=0.21886958/12
40 varphi_c=1/(6.5*12)
41 gamma_ct=1/40
42 delta_th=0.39732
43 eta_t=0.0001
44 alpha_t=1/(4*12)
45 delta_ct=0.5
46 theta_ct=0.2
47 delta_ch=0.1885189
48 phi_c=0.1
49 delta_a=0.062
50 omega_c=1/4
51
52 # Triple infection model ODE system
53 def model_odes(y,t,pi_c,theta_c,delta_c):
54
55       # Assigning initial values
56       S,V_c,I_c,I_t,C_ct,R_ct,I_h,C_ch,C_th,A,M=y
57
58       # Force of infections
59       zeta_c=pi_c*(I_c+C_ct+C_ch+A)/N
60       zeta_t=pi_t*(I_t+C_ct+C_th+A)/N
```

```
61        zeta_h=pi_h*(I_h+C_ch+C_th+A)/N
62
63        # Model systems
64        dS=chi-(nu_0+(nu_m-nu_0)*D*M/(1+D*M)+zeta_c+zeta_t+ zeta_h
              +mu_d)*S+varphi_c*V_c+gamma_ct*R_ct
65        dV_c=(nu_0+(nu_m-nu_0)*D*M/(1+D*M))*S- (sigma_c*zeta_c+
              zeta_t+zeta_h+varphi_c+mu_d)*V_c
66        dI_c=zeta_c*S+sigma_c*zeta_c*V_c-(delta_c+theta_c+zeta_t+
              zeta_h+mu_d)*I_c
67        dI_t=zeta_t*(S+V_c)-(delta_t+theta_t+zeta_c+ zeta_h+mu_d)*
              I_t
68        dC_ct=zeta_c*I_t+zeta_t*I_c-(delta_ct+theta_ct+ zeta_h+
              mu_d)*C_ct
69        dR_ct=theta_c*I_c+theta_t*I_t+theta_ct*C_ct- (gamma_ct+
              mu_d)*R_ct
70        dI_h=zeta_h*(S+V_c)+eta_t*C_th+phi_c*C_ch- (delta_h+zeta_c
              +zeta_t+mu_d)*I_h
71        dC_ch=zeta_c*I_h+zeta_h*I_c+alpha_t*A- (delta_ch+zeta_t+
              mu_d+phi_c)*C_ch
72        dC_th=zeta_t*I_h+zeta_h*I_t+omega_c*A- (delta_th+eta_t+
              zeta_c+mu_d)*C_th
73        dA=zeta_c*C_th+zeta_t*C_ch+zeta_h*C_ct- (delta_a+alpha_t+
              mu_d+omega_c)*A
74        dM=a*(kappa*(I_c+C_ct+C_ch+A)-M)
75        return[dS,dV_c,dI_c,dI_t,dC_ct,dR_ct,dI_h,dC_ch,dC_th,dA,
              dM]
76
77  #Integrate the model equations over time
78  def solve_model(t,pi_c,theta_c,delta_c):
79
80        # Initial values
81        N=126527060
82        V_c0=0
83        I_c0=16
84        I_t0=112597
85        C_ct0=0
```

```
86        R_ct0=8000
87        I_h0=630000
88        C_ch0=0
89        C_th0=1200
90        A0=0
91        M0=0.04*I_c0
92        S0=N-V_c0-I_c0-I_t0-C_ct0-R_ct0-I_h0-C_ch0-C_th0-A0
93
94        # Initial conditions vector
95        y0=[S0,V_c0,I_c0,I_t0,C_ct0,R_ct0,I_h0,C_ch0,C_th0,A0,M0]
96        result=odeint(model_odes,y0,t,args=(pi_c,theta_c,delta_c))
97        return result[:,2] # ReturnI_c as the fitting target
98
99  #Define the lmfit model
100 co-infection_model=Model(solve_model)
101
102 #Initial parameter guesses
103 params=co-infection_model.make_params(pi_c=1.2125,theta_c=1,
       delta_c=0.015)
104
105 #Setting parameter bounds
106 params['pi_c'].set(min=0,max=3)
107 params['theta_c'].set(min=0,max=1)
108 params['delta_c'].set(min=0,max=0.031)
109
110 #Fitting the model to the data
111 result=co-infection_model.fit(data,params,t=t,nan_policy='raise
       ',method='least_squares')
112
113 #Printing the fit report
114 print(result.fit_report())
115 result.params.pretty_print()
116
117 #Plot format for axes
118 class ScalarFormatterClass(ScalarFormatter):
119       def _set_format(self):
```

```
            self.format="%1.0f"
ax=plt.gca()
yScalarFormatter=ScalarFormatterClass(useMathText=True,)
yScalarFormatter.set_powerlimits((0,0))
ax.yaxis.set_major_formatter(yScalarFormatter)

#Fitting plot
plt.plot(t,data,'*',color='blue',label=r'COVID-19cases',
   markersize=7)
plt.plot(t,result.best_fit,'r-',lw=4,label=r'Modeloutput($I_c$)
   ')
plt.ylabel(r'COVID-19',ha='center',family='serif',style='italic
   ',size=18,weight='bold')
plt.xlabel(r'Time(month)',ha='center',family='serif',style='
   italic',size=18,weight='bold')
labelsx=ax.get_xticklabels()
plt.setp(labelsx,size=16,family='serif',weight='bold')
ax.set_xticks([0,5,10,15,20,25,30,35,40,45])
ax.set_yticks([100000,200000,300000,400000,500000])
labelsy=ax.get_yticklabels()
plt.setp(labelsy,size=16,family='serif',weight='bold')
plt.xlim(0,47)
plt.ylim(0,5.4e+5)
plt.legend(loc='lowerright',fancybox=True,framealpha=0.75,
   frameon=True,handlelength=1.25,prop={'family':'serif','
   weight':'bold','size':18})

# Modifying axes font properties
offset_text=ax.yaxis.get_offset_text()
offset_text.set_fontsize(16)
offset_text.set_fontweight('bold')
offset_text.set_fontfamily('serif')
plt.grid(True,linestyle='dotted',alpha=10**(-30))
```

B.2 Python Scripts for Stability Analysis and Simulation

```
'''This code is an example of stability analysis. It generates
   Figure 5. We modify it to demonstrate the local stability of
    equilibria and to illustrate the existence of backward
   bifurcation in the models.'''

#Importing relevant modules
import numpy as np
from scipy.integrate import odeint
import matplotlib.pyplot as plt
import sympy as s
from matplotlib.ticker import ScalarFormatter

# parameter values
Lambda=32998
mu=1/(67*52)
sigmma=0.01
tau=1.22
gamma_h=0.00502
xi=0.19
omega=0.15
delta_h=0.016
rho=0.25
epsilon=1.38500

# An array of initial conditions
N=114963583
V0=[12000,61936000]
Ih0=[201905,413333]
Ia0=[150740,206666]
S0=[0,0]
y0=[0,0]
foriinrange(0,len(Ih0)):
      S0[i]=N-V0[i]-Ih0[i]-Ia0[i]
      y0[i]=S0[i],V0[i],Ih0[i],Ia0[i]

```

```
33 # Time points
34 t=np.linspace(0,200,1600)
35
36 # The HIV only model
37 def HIV_only_model(y,t,N,Lambda,gamma_h,epsilon,rho,mu,xi,
      omega,delta_h):
38       D_1=mu+xi;D_4=mu+omega;D_5=mu+delta_h;
39       S,V,Ih,Ia=y
40       lh=gamma_h*(Ih+epsilon*Ia)/(S+V+Ih+Ia)
41       dS=(1-rho)*Lambda-(D_1+lh)*S
42       dV=rho*Lambda+xi*S-(mu+lh)*V
43       dIh=(S+V)*lh-D_4*Ih
44       dIa=omega*Ih-D_5*Ia
45       return dS,dV,dIh,dIa
46
47 # Solving the system for different values of psi
48 ret=odeint(HIV_only_model,y0[0],t,args=(N,Lambda,gamma_h,
      epsilon,rho,mu,xi,omega,delta_h))
49 ret1=odeint(HIV_only_model,y0[1],t,args=(N,Lambda,gamma_h,
      epsilon,rho,mu,xi,omega,delta_h))
50 # Solitions of the system
51 S,V,Ih,Ia=ret.T
52 S1,V1,Ih1,Ia1=ret1.T
53
54 # Ploting the projection of state variables
55 plt.figure(figsize=(10,8))
56
57 # Format for axes
58 class ScalarFormatterClass(ScalarFormatter):
59       def _set_format(self):
60             self.format="%1.1f"
61 ax=plt.gca()
62 yScalarFormatter=ScalarFormatterClass(useMathText=True)
63 yScalarFormatter.set_powerlimits((0,0))
64 ax.yaxis.set_major_formatter(yScalarFormatter)
65
```

```
66 # The plot of state varibles S and V (Figue 4.5a)
67 # plt.plot(t,V,label='$V:S_0=112823418,V_0=1530000,$\n$I_{H0
       }=519425,I_{A0}=90740$',color='y',linestyle='--',linewidth
       =4)
68 # plt.plot(t,V1,label='$V:S_0=114598938,V_0=12000,$\n$I_{H0
       }=201905,I_{A0}=150740$',color='r',linestyle='--',linewidth
       =4)
69 # plt.plot(t,S,label='$S:S_0=112823418,V_0=1530000,$\n$I_{H0
       }=519425,I_{A0}=90740$',linestyle='-',color='m',linewidth=3)
70 # plt.plot(t,S1,label='$S:S_0=114598938,V_0=12000,$\n$I_{H0
       }=201905,I_{A0}=150740$',color='darkgreen',linestyle='-',
       linewidth=4)
71
72 # Legends and Labels
73 # plt.legend(loc='centerright',handlelength=2,handletextpad
       =0.3,borderpad=0.2,prop={'weight':'bold','size':20})
74 # plt.ylabel(r'Population',family='Serif',ha='center',style='
       italic',fontsize=18,fontweight='bold')
75
76 #The plot of state varibles I_H and I_A (Figue 4.5b)
77 plt.plot(t,Ia,label='$I_A:S_0=114598938,V_0=12000,$\n$I_{H0
       }=201905,I_{A0}=150740$',color='g',linestyle='--',linewidth
       =4)
78 plt.plot(t,Ia1,label='$I_A:S_0=112823418,V_0=1530000,$\n$I_{H0
       }=519425,I_{A0}=90740$',color='maroon',linestyle='--',
       linewidth=4)
79 plt.plot(t,Ih,label='$I_H:S_0=114598938,V_0=12000,$\n$I_{H0
       }=201905,I_{A0}=150740$',linewidth=4)
80 plt.plot(t,Ih1,label='$I_H:S_0=112823418,V_0=1530000,$\n$\I_{H0
       }=519425,I_{A0}=90740$',linewidth=4)
81
82 # Legends and Labels
83 plt.legend(loc='upperright',handlelength=1.5,handletextpad=0.1,
       borderpad=0.,prop={'weight':'bold','size':18})
84 plt.ylabel(r'Population',family='Serif',ha='center',style='
       italic',fontsize=18,fontweight='bold')
```

```
85
86 # x and y axes limits, ticks and formats
87 plt.xlim(0,200)
88 plt.ylim(0,)
89 plt.xticks(fontsize=20,fontweight='bold')
90 plt.yticks(fontsize=20,fontweight='bold')
91 plt.rc('ytick',labelsize=20)
92 plt.xlabel('Time(inMonths)',family='Serif',ha='center',style='
      italic',fontsize=18,fontweight='bold')
93 plt.show()
```

B.3 Python Scripts Demonstrating Parameter Effects

```
1 ''' This code generates a simulation illustrating the impact of
      different parameter values. It is employed to simulate
    figures 7.7 and 7.8, which demonstrate the effect of nu_0
    and sigma_c. It is adapted to showcase the impact of other
    parameters.'''
2
3 # Importing relevant modules
4 from scipy.integrate import odeint
5 import numpy as np
6 import matplotlib.pyplot as plt
7 from mpl_toolkits.mplot3d import Axes3D
8 from matplotlib.ticker import ScalarFormatter
9 import matplotlib.style
10
11 # Plotting style
12 matplotlib.style.use('seaborn-white')
13
14 # Parameters
15 chi=159756
16 mu_d=1/(66*12)
17 nu_m=0.99
18 nu_0=nu_m*0.2
19 D=500/(66*12*159756)#D=0togenerateFigure6.7
```

```
a=0.2
kappa=0.2
sigma_c=0.13
pi_c=2.402
delta_c=0.031
theta_c=0.3474
pi_t=0.85572872/12
delta_t=2.8000e-04/12
theta_t=0.78399616/12
pi_h=0.124/12
delta_h=0.21886958/12
varphi_c=1/(6.5*12)
gamma_ct=1/40
delta_th=0.39732
eta_t=0.0001
alpha_t=1/(4*12)
delta_ct=0.5
theta_ct=0.2
delta_ch=0.1885189
phi_c=0.1
delta_a=0.062
omega_c=1/4

# The Triple infection model ODE system
def model_odes(y,tf,N,nu_0,nu_m,sigma_c,d,pi_c,theta_c,delta_c,
    pi_t,delta_t,theta_t,pi_h,delta_h,chi,mu_d,varphi_c,gamma_ct
    ,delta_ct,theta_ct,delta_ch,phi_c,delta_th,eta_t,delta_a,
    alpha_t,omega_c,kappa,a):

      # Assigning initial values
      S,V_c,I_c,I_t,C_ct,R_ct,I_h,C_ch,C_th,A,M=y

      # Force of infections
      zeta_c=pi_c*(I_c+C_ct+C_ch+A)/N
      zeta_t=pi_t*(I_t+C_ct+C_th+A)/N
      zeta_h=pi_h*(I_h+C_ch+C_th+A)/N
```

```
53
54        # Mdel systems
55        dS=chi-(nu_0+(nu_m-nu_0)*D*M/(1+D*M)+zeta_c+zeta_t+zeta_h+
              mu_d)*S+varphi_c*V_c+gamma_ct*R_ct
56        dV_c=(nu_0+(nu_m-nu_0)*D*M/(1+D*M))*S-(sigma_c*zeta_c+
              zeta_t+zeta_h+varphi_c+mu_d)*V_c
57        dI_c=zeta_c*S+sigma_c*zeta_c*V_c-(delta_c+theta_c+zeta_t+
              zeta_h+mu_d)*I_c
58        dI_t=zeta_t*(S+V_c)-(delta_t+theta_t+zeta_c+zeta_h+mu_d)*
              I_t
59        dC_ct=zeta_c*I_t+zeta_t*I_c-(delta_ct+theta_ct+zeta_h+mu_d
              )*C_ct
60        dR_ct=theta_c*I_c+theta_t*I_t+theta_ct*C_ct-(gamma_ct+mu_d
              )*R_ct
61        dI_h=zeta_h*(S+V_c)+eta_t*C_th+phi_c*C_ch-(delta_h+zeta_c+
              zeta_t+mu_d)*I_h
62        dC_ch=zeta_c*I_h+zeta_h*I_c+alpha_t*A-(delta_ch+zeta_t+
              mu_d+phi_c)*C_ch
63        dC_th=zeta_t*I_h+zeta_h*I_t+omega_c*A-(delta_th+eta_t+
              zeta_c+mu_d)*C_th
64        dA=zeta_c*C_th+zeta_t*C_ch+zeta_h*C_ct-(delta_a+alpha_t+
              mu_d+omega_c)*A
65        dM=a*(kappa*(I_c+C_ct+C_ch+A)-M)
66        return [dS,dV_c,dI_c,dI_t,dC_ct,dR_ct,dI_h,dC_ch,dC_th,dA,
              dM]
67
68  # Initial conditions
69  N=126527060
70  V_c0=0
71  I_c0=16
72  I_t0=112597
73  C_ct0=0
74  R_ct0=8000
75  I_h0=630000
76  C_ch0=0
77  C_th0=1200
```

```
78  A0=0
79  M0=0.04*I_c0
80  S0=N-V_c0-I_c0-I_t0-C_ct0-R_ct0-I_h0-C_ch0-C_th0-A0
81  y0=[S0,V_c0,I_c0,I_t0,C_ct0,R_ct0,I_h0,C_ch0,C_th0,A0,M0]
82
83  # Time points
84  t=np.linspace(0,100,10000)
85
86  # Plots to show impact of sigma_c and nu_0 (Figures 6.7 and
        6.8)
87  # --Colors---
88  ccD=['#FF2800','#00C100','#0000F7'] # Ic(D!=0)
89  # ctD=['#0000FF','#FF0000','#00C500'] # Cct(D!=0)
90  # chD=['#FF7D00','#000087','#FF00FF'] # Cch(D!=0)
91  # caD=['#008BEC','#6B006F','#FFE855'] # A(D!=0)
92
93  # cc=['#7EFF00','#0080FF','#FF007D'] # Ic(D=0)
94  # ct=['#00FFFF','#FF0000','#B90068'] # Cct(D=0)
95  # ch=['#B900B4','#00A5FF','#FF6080'] # Cch(D=0)
96  # ca=['#FF0000','#00ABAE','#000087'] # A(D=0)
97
98  # The three diffrent values of nu_0 and sigma_c
99  nu_0=[0.2,0.25,0.3]
100 sigma_c=[0.15,0.2,0.25]
101 for cn,nu_0,sigma_cinzip(ccD,nu_0,sigma_c):
102       ret=odeint(model_odes,y0,t,args=(N,nu_0,nu_m,sigma_c,d,
              pi_c,theta_c,delta_c,pi_t,delta_t,theta_t,pi_h,delta_h,
              chi,mu_d,varphi_c,gamma_ct,delta_ct,theta_ct,delta_ch,
              phi_c,delta_th,eta_t,delta_a,alpha_t,omega_c,kappa,a))
103       S,V_c,I_c,I_t,C_ct,R_ct,I_h,C_ch,C_th,A,M=ret.T
104
105       plt.plot(t,I_c,lw=4,linestyle='-',color=cn,label=r'$\nu_0
              ={},\sigma_c={}$'.format(nu_0,sigma_c))
106       # plt.plot(t,C_ct,lw=4,linestyle='-',color=cn,label=r'$\
              nu_0={},\sigma_c={}$'.format(nu_0,sigma_c))
```

```
107         # plt.plot(t,C_ch,lw=4,color=cn,label=r'$\nu_0={},\sigma_c
              ={}$'.format(nu_0,sigma_c))
108         # plt.plot(t,A,lw=4,linestyle='-',color=cn,label=r'$\nu_0
              ={},\sigma_c={}$'.format(nu_0,sigma_c))
109
110 # x and y labeles (which can be changed based on the state
      variables)
111 plt.ylabel(r'$A$',ha='center',family='serif',style='italic',
      size=16,weight='bold')
112 plt.xlabel(r'Time(month)',ha='center',family='serif',style='
      italic',size=16,weight='bold')
113 labelsx=ax.get_xticklabels()
114 plt.setp(labelsx,size=16,family='serif',weight='bold')
115 labelsy=ax.get_yticklabels()
116 plt.setp(labelsy,size=16,family='serif',weight='bold')
117
118 # legend
119 plt.legend(loc='best',fancybox=True,framealpha=0.75,frameon=
      True,handlelength=0.7,handletextpad=0.2,borderaxespad=0.2,
      prop={'family':'serif','weight':'bold','size':18})
120
121 # Font properties and limits for the axes
122 offset_text=ax.yaxis.get_offset_text()
123 offset_text.set_fontsize(16)
124 offset_text.set_fontweight('bold')
125 offset_text.set_fontfamily('serif')
126 plt.xlim(0,100)
127 plt.ylim(0,)
128 plt.show()
```